POLITECNICO DI MILANO

Thesis for the degree of Doctor of Philosophy

Catalytic removal of NO_x and soot from mobile sources

NANCY ARTIOLI

Tutor Prof. Pio Forzatti

Advisor Prof. Luca Lietti

Department of Energy
POLITECNICO DI MILANO
Milan, Italy 2012

to my family

'You've got to find what you love. And that is as true for your work as it is for your lovers. Your work is going to fill a large part of your life, and the only way to be truly satisfied is to do what you believe is great work. And the only way to do great work is to love what you do. If you haven't found it yet, keep looking. Don't settle.'

Steve Jobs

Thesis for the degree of Doctor of Philosophy

Catalytic removal of NO_x and soot from mobile sources

NANCY ARTIOLI

Department of Energy
POLITECNICO DI MILANO
Milan, Italy 2012

Abstract

Commercial vehicles and diesel passenger cars will be subjected in a near future to very stringent emission regulations regarding nitrogen oxides (NO_x) and particulate. To handle these limits the use of exhaust after-treatment technologies is required. Different strategies have been proposed for lean-burn engines; one such strategy is the Diesel Particulate NO_x Reduction (DPNR) system that accomplishes the simultaneous removal of NO_x and particulate. In this thesis work the behavior of a model $PtBa/Al_2O_3$ and PtK/Al_2O_3 NSR catalyst in both NO_x storage/reduction and soot oxidation is investigated.

It is found that the presence of soot reduces the NOx storage capacity of the catalyst, evaluated in presence of water and CO_2 in the feed stream in the range 200–350 °C and with different values of the NO inlet concentration. Besides the presence of soot favors the decomposition and the reduction of the stored nitrates, while soot is being oxidized. A direct reaction between the stored nitrates and soot is suggested, that has been explained on the basis of the surface mobility of the adsorbed nitrates. This soot oxidation pathway involves surface species and parallels the NO_2-soot oxidation that occurs in the presence of gas-phase NO_2. This has also been confirmed by dedicated TPD and TPO experiments. However the presence of soot does not appreciably affect the behavior of the catalysts in the reduction by H_2 or CO of the stored nitrates, being in all cases N_2 the major reaction product along with minor amounts of ammonia.

Mechanistic aspects involved in the formation of N_2 and of N_2O during the reduction of gas-phase NO and of NO_x stored over $PtBa/Al_2O_3$ catalyst are also investigated using unlabelled ammonia and labelled NO. It appears that N_2 formation occurs primarily through the statistical coupling of N-atoms formed by dissociation of NO_x- and NH_3-related surface intermediates, although an SCR-pathway (involving the coupling of NH_3- and NO-derived ad-species) is also likely to occur. It appears as well that the formation of nitrous oxide involves either the coupling of two adsorbed NO molecules or the recombination of an adsorbed NO molecule with an adsorbed NH_x fragment.

Mecanicistic aspects of NO oxidation reaction are also investigated with other catalytic systems of interest like Rh and Co-based catalysts. It is shown that NO oxidation on RhO_2 and Co_3O_4 is limited by O_2 activation at vacancies on oxygen-saturated surfaces, as also found on Pt and PdO. Oxygen binding energies set vacancy densities and turnover rates. One electron reductions accessible to RhO_2 and Co_3O_4 facilitate O_2 activation and allow faster $^{16}O_2$-$^{18}O_2$ exchange and NO oxidation than expected from their oxygen binding strengths.

Keywords

Soot oxidation, Diesel particulate filter, 4-Ways catalysts, Lean deNOx, NOx trap promotion, LNT systems, Pt–Ba/Al_2O_3 catalyst, Pt–K/Al_2O_3 catalyst, Combined soot–NOx removal, DPNR, Lean NOx traps, NO_x storage and reduction, Structure sensitivity

List of Pubblications

This thesis is based on the work contained in the following paper s referred to by roman numerals (I-VIII) in the text

I. *Study of DPNR catalysts for combined soot oxidation and NOx reduction*
Lidia Castoldi, Nancy Artioli, Roberto Matarrese, Luca Lietti, Pio Forzatti
Catalysis Today 157 (2010) 384–389

II. *Effect of soot on the storage-reduction performances of LNT PtBa/Al_2O_3 catalyst*
Nancy Artioli, Roberto Matarrese, Lidia Castoldi, Luca Lietti, Pio Forzatti
Catalysis Today 169 (2011) 36-44

III. *Interaction between soot and stored NO_x during operation of LNT Pt-Ba/Al_2O_3 catalysts*
R. Matarrese, N. Artioli, L. Castoldi, L. Lietti, P. Forzatti, Catal. Today, (2011) in press
doi:10.1016/j.cattod.2011.11.026

IV. *Diesel soot and NO_x abatement on Pt-K/Al_2O_3 LNT catalyst: influence of temperature and ageing*
R. Matarrese, N. Artioli, L. Castoldi, L. Lietti,E. Finocchio, P. Forzatti
in preparation

V. *The NO_x reduction by CO on Pt-K/Al_2O_3 Lean NO_x Trap Catalyst*
L. Castoldi, L. Lietti, R. Bonzi, N. Artioli, P. Forzatti, S. Morandi, G.Ghiotti
Journal of Physical Chemistry C 115 (2011)1277–1286

VI. *FT-IR study of the surface redox states on platinum-potassium-alumina catalysts*
T. Montanari, R. Matarrese, N. Artioli ,G. Busca
Applied Catalysis B: Environmental 105 (2011) 15–23

VII. *Pathways for N_2 and N_2O formation during the reduction of NO_x over Pt-Ba/Al_2O_3 LNT catalysts investigated by labelling isotopic experiments*
L. Lietti, N. Artioli, L. Righini, L. Castoldi, P. Forzatti
Industrial & Engineering Chemistry Research (2012)
DOI: 10.1021/ie2021976

VIII. *Catalytic NO Oxidation Pathways and Redox Cycles on Dispersed Oxides of Rhodium and Cobalt*
Brian M. Weiss, Nancy Artioli, Enrique Iglesia,
ChemCatChem (2012) in press

Contents

1. Introduction

1.1 Background

Diesel-equipped vehicles are considered as one of the primary sources of NO_x and particulate (soot) emissions in industrialized countries. Accordingly regulations to limit their emission are becoming very strict. In Europe, the current Euro 5 rules limit NO_x and soot emissions from light-weight diesel vehicles (up to 2500 kg) at 0.18 and 0.005 g/km, respectively, but a more drastic reduction is required for NO_x emissions in the upcoming Euro 6 regulations (0.08 g/km).

The soot removal relies on the use of diesel particulate filters (DPFs): these devices, usually made by cordierite or SiC, remove a significant fraction of the particulate by filtration. The filters must be periodically regenerated to remove the entrapped soot, thus avoiding excessive pressure drops at the exhaust: moreover the filter may by catalyzed to promote soot combustion at lower temperatures (DOC, Diesel Oxidation Catalyst).

Concerning NO_x, either Selective Catalytic Reduction (SCR) or Nitrogen Storage Reduction (NSR), also quoted as Lean NO_x Trap (LNT), represent the top contenders for reducing NO_x concentrations in the exhausts from diesel and lean burn gasoline engines. The SCR technique is based on the reaction between NO and NH_3, which is produced by hydrolysis of an aqueous urea solution injected into the exhausts from an on-board tank:

$$4\ NO + 4\ NH_3 + O_2 \rightarrow 4\ N_2 + 6\ H_2O \qquad (1)$$

Metal-substituted zeolites or vanadia-tungsta-titania catalysts are generally used as catalytic materials, although the former are generally preferred in view of their better high-temperature durability when the SCR catalyst is placed downstream the DPF.

On the other hand the NSR catalysts make no use of any external reductant and operate the NO_x reduction under cyclic conditions by alternating long lean phases during which NO_x emitted in the exhaust gases are adsorbed on the catalyst, with subsequent short rich periods (typically in the order of few seconds) in which the stored NO_x are reduced by H_2, CO and Hydrocarbons (HC) present in the flue gases to produce nitrogen. LNT catalysts are generally made by a high surface area support (such as γ-Al_2O_3), alkaline/alkaline-earth metal oxides (such as K_2O and BaO) and precious metals like Pt, Rh, Pd; other components are also present in fully formulated catalysts (e.g. CeO_2).

While the SCR technique is generally used in heavy vehicles (mini-van and trucks), NSR catalysts are generally preferred for small engines. Hybrid NSR + SCR configurations have also been proposed, since they guarantee higher NO_x removal efficiencies.

De-NO_x devices are used together with De-soot devices, along with Diesel Oxidation Catalyst (DOC) as well to respect the complex emission standards. The optimal design of the aftertreatment exhaust system is still a matter of debate: the DOC is generally placed upstream the DPF and SCR/LNT converters, while different solutions have been proposed for the DPF and the DeNO_x catalyst. In fact the DPF may be placed downstream the deNO_x catalyst (to prevent hot gases generated upon regeneration of the DPF to reach the LNT/SCR catalysts), but in this case the DeNO_x catalysts must manage the presence of soot in the exhausts. Integrated (or one-pot) solutions have also been proposed, like Catalyzed Diesel Particulate Filters (CDPFs) which act as DOC but also remove soot, or the DPNR (Diesel Particulate-NOx Reduction) technology which has been recently proposed by the Toyota group. The DPNR technique has the unique capacity to remove simultaneously soot and NO_x and is based on the use of a catalyzed filter on which a NSR catalyst is deposited. In this way soot is removed by the filter while NO_x are reduced according to the NSR technology. Soot oxidation occurs during the lean phase, possibly involving NO_2 (formed upon NO oxidation) and/or adsorbed NOx species. In view of this, the catalytic NO oxidation to NO_2 is an important issue.

This reaction has been largely studied in the literature in a wide range of operative conditions and using various catalytic systems. Among them, Rh and Co represent a valid alternative to thePt and Pd catalytic system. In the case of Co-based catalysts, the rate of NO oxidation has been correlated with the reducibility of CoO_x clusters, suggesting that chemisorbed oxygen atoms O* binding and the availability of vacancies determines turnover rates on Co-based catalysts.

1.2 Objectives

Concerning the study of DPNR systems, the aim of the work is to provide new insights on the pathways involved in the NO_x storage-reduction and soot oxidation over model $PtBa/Al_2O_3$ and PtK/Al_2O_3 LNT catalyst on the interactions among the related catalyst functions. For this purpose, a systematic study has been performed on the DPNR selected catalyst samples in which the reactivity in the NO_x storage-reduction and in the soot oxidation has been investigated in a wide temperature range (150-350°C) and at different NO inlet concentrations with Isothermal step concentration (ISC) experiments.

The interaction between soot and the stored NO_x species has been further studied by Temperature Programmed Methods under inert flow (TPD) and in the presence of oxygen (TPO) in which the stability/reactivity of the stored NO_x species has been analyzed both in the presence and in the absence of

soot. The experiments have also been carried out over a Platinum-free catalyst in order to assess the role of Pt in the stability/reactivity of adsorbed nitrates as well.

Mechanistic aspects of the reduction of stored NO_x and the pathways involved in the formation of N_2 and N_2O during regeneration of Ba based NSR catalyst have been also investigated. Experiments have been carried out with different reductants (H_2 and CO) and by means of isotopic labeling experiments as well. The results collected over the Pt-Ba/Al_2O_3 catalyst have been compared with those collected in the case of a Pt-K/Al_2O_3 catalyst in order to highlight possible similarities and differences.

Concerning the catalytic NO oxidation reaction, the elementary steps involved in the NO oxidation on Rh and Co catalysts and their kinetic relevance and site requirements were probed using isotopic tracers and the kinetic effects of NO, O_2, and NO_2 pressures on turnover rates have been investigated.

2. Diesel emissions and abatement technologies

Pollution has become a subject of central concern due to increasing mobility [1]: in the last sixty years, motor vehicles increased from 40 to 700 million and their number raised up to 920 million in 2010 because of the growing demand in developing countries [2].

In particular, vehicles powered by internal combustion engines are some of main responsible for the production Nitrogen Oxides (NO_x), Carbon Oxides (CO_x), Volatile Organic Compounds (VOCs) and Particulate Matter (PM) (Figure 2.1).

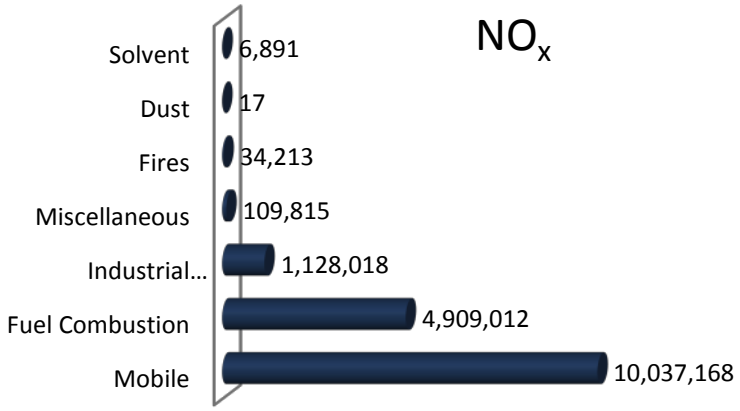

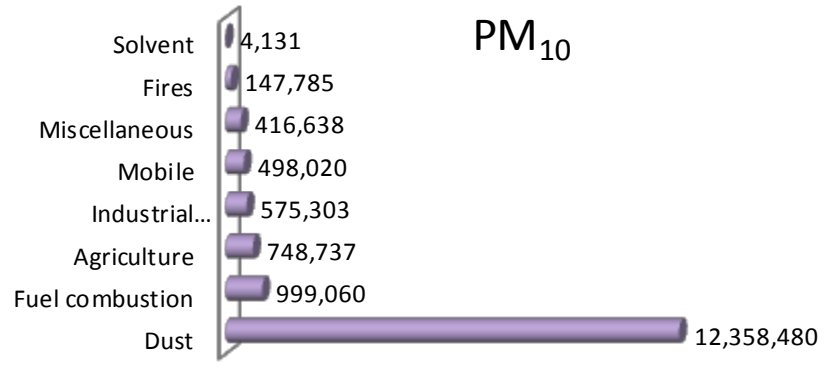

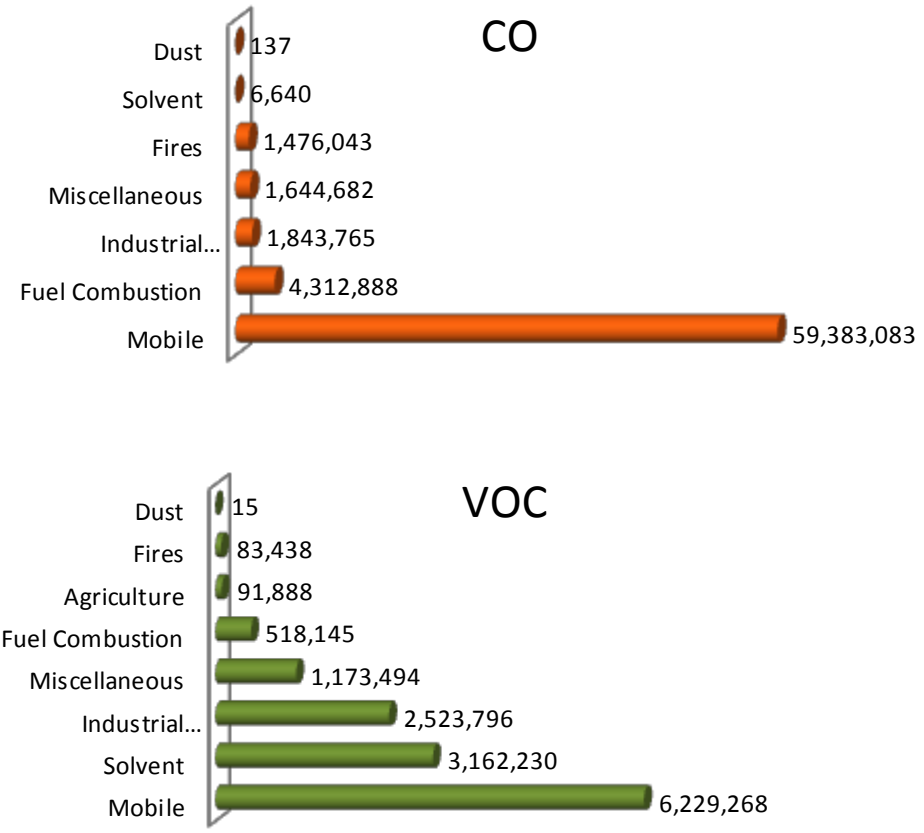

Figure 2.1 - USA pollutants emission by sources [3]

Emissions control regulations have been introduced in all the industrialized countries in order to reduce the emissions from both gasoline and Diesel engines.

In particular Diesel vehicles are increasing more their worldwide penetration, starting from European countries (Figure 2.2) where Diesel motorisation in 2008 reached gasoline one [4].

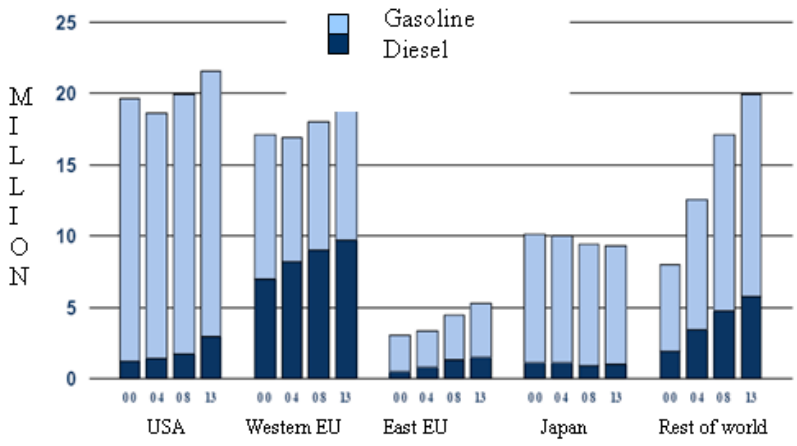

Figure 2.2 - Share market: gasoline and Diesel

To comprehend this market change it is useful to analyze some differences between the two kinds of engine, summarized in Table 2.1:

	Diesel	Gasoline
Vehicle weight	More	Less
Noise and vibration	High	Low
Starting	Quite instant	Instant
Air/fuel ratio	>14.7 (Lean condition)	14.7(Stoichiometric)
Fuel consumption	Less	More
Compression ratio	15/24	9/12
Efficiency	35%	Less 30%
Turbocharging	Applied	Not used

Table 2.1 - Diesel vs gasoline features [5]

The lower fuel consumption is one of the main reasons of the increasing diffusion of Diesel engines equipped vehicles. This is due to a higher engine efficiency, that is also enhanced by turbocharging, which allows a better fuel combustion [5]. Furthermore the life of Diesel engine is generally about twice as long as gasoline one, also thanks to the better fuel lubrication properties [6]. Last but not least, lean-burn engines offer the prospect of reducing the emissions of CO_2 (Figure 2.3).

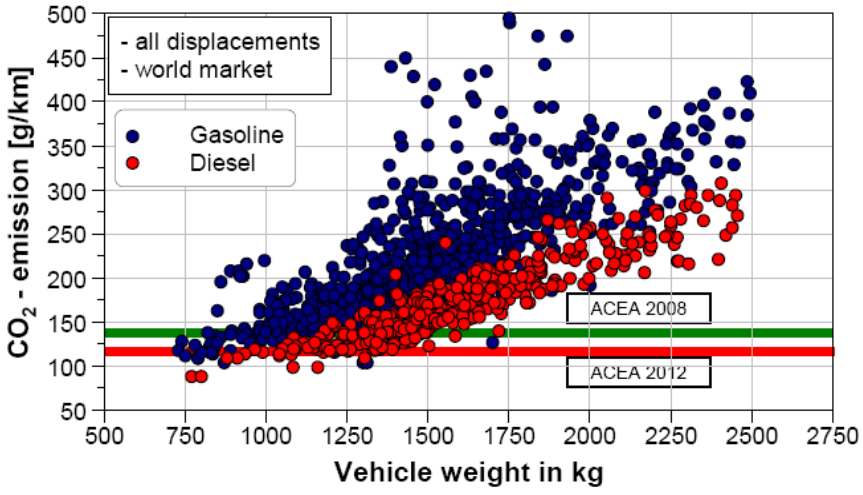

Figure 2.3 - Gasoline vs Diesel: CO_2 emissions [7]

However, Diesel engines produce higher emissions of NO_x and PM (Figure 2.4) which have negative effects both on mankind and environment.

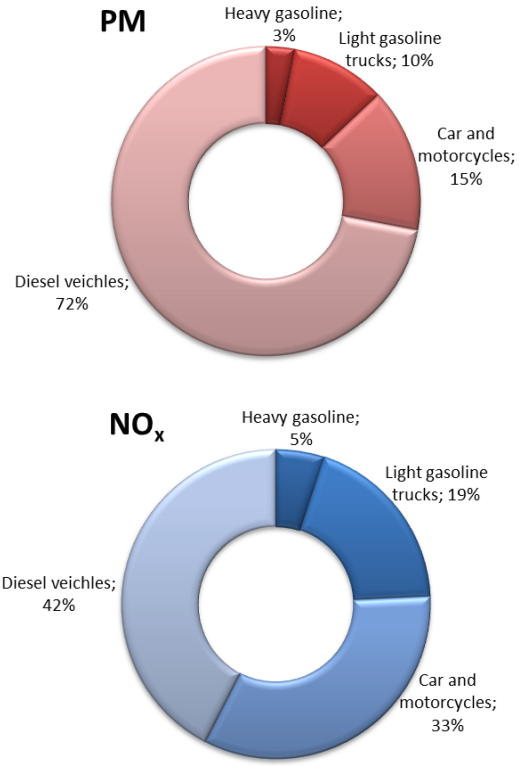

Figure 2.4 - Diesel and gasoline PM and NO_x emissions [3]

In particular most of the nitrogen oxides are irritant for eyes, skin, and respiratory tract [8]. Nitrogen dioxide (NO_2) is more acutely toxic (about 30 times more toxic) than nitric oxide (NO), except at lethal concentrations when nitric oxide may kill more rapidly. Acute effects in a healthy subject can be seen for very high NO_2 concentrations (>1990 $\mu g/m^3$ [9]). From 400-500 $\mu g/m^3$ some alterations of respiratory functions can be observed in asthmatic people. For a long period exposure it is recommended a maximum NO_2 concentration equal to 40 $\mu g/m^3$ as yearly average in order to prevent collateral damages.

Furthermore NO_x are responsible for the diminishing of photosynthetic activity, the soil acidification, the reduction of visibility and the so-called acid rain. They also contribute to the photochemical smog: acid nitric production, formation with VOCs of peroxyacyl nitrate (PANs), aldehydes and ozone. Finally, nitrous oxide (N_2O) is considered one of the major greenhouse gases which, for some researchers [10], are responsible for the global warming (actually a phenomena not yet scientifically demonstrated).

Particulate matter, as well, leads to the above-mentioned negative effects on environment; in addition it causes the monuments fouling. On mankind, the main problem is connected to respiratory system: a constant and long exposure could be responsible for a lung cancer.

Therefore it is obvious why limits on the emissions of these pollutants become more and more stringent.

II.

Diesel emissions and abatement technologies

In the following sections legislative aspects about NO_x and PM regulations will be presented. Furthermore, abatement technologies (applied or which research focuses on, to reach the required standards), with particular regard to Diesel engines, will be introduced.

2.1 Emission standards

All over the world, emissions legislation has become increasingly stringent and this encourages new research projects. Several sets of standards have already been defined in the past two decades for different types of vehicles. Tier 1 standards were published in 1991 in the U.S. and progressively phased-in between 1994 and 1997. Then, Tier 2 standards were adopted in 1999 with a phase-in implementation schedule from 2004 to 2009. Tier 1 standards were applied to light-duty vehicles, while Tier 2 regulation introduced more stringent numerical emission limits relative to the previous Tier 1 requirements, and a number of additional changes were made that are more stringent for larger vehicles. Similar emission limits were adopted for all vehicles regardless of the fuel consumption including gasoline, diesel, or alternative fuels. The sulfur levels in gasoline were required to be reduced by 30 ppm with an 80 ppm sulfur cap in 2006. Diesel fuel of maximum sulfur level of 15 ppm was made available for highway use beginning in 2006. Tier 4 standards designed for the period of 2008-2015 require that emissions of particulate matter and NO_x be further reduced by about 90%. Sulfur was recommended to be reduced to 15 ppm (ultralow sulfur diesel) as of June 2010 for nonroad fuel and in June 2012 for locomotive and marine fuels. Such emission reductions can be achieved only through the use of control technologies—including advanced exhaust gas after-treatment systems, catalytic particulate filters, and NO_x adsorbers.[I]

As shown in Table 2.2, progress in European standard regulations also highlights more stringent emission limits especially for NO_x emissions within the Euro 6 standard regulations.

	gasoline engine				diesel engine			
standard regulation[a]	CO	HC	NO_x	HC + NO_x	CO	NO_x	HC + NO_x	particulates
Euro 1 (1993)	2.72			0.97	2.72		0.97	0.14
Euro 2 (1996)	2.20			0.5	1.00		0.90	0.10
Euro 3 (2000)	2.30	0.20	0.15		0.64	0.50	0.56	0.05
Euro 4 (2005)	1.00	0.10	0.08		0.50	0.25	0.30	0.025
Euro 5 (2009)	1.00	0.10	0.06		0.50	0.18	0.25	0.005
Euro 6 (2014)	1.00	0.10	0.06		0.50	0.08	0.17	0.005

[a] Measured from New European Driving Cycle (g/km).

Table 2.2 – EURO emission standard for light-duty veichles

European legislation concerns only some kinds of pollutants: CO, HC (Hydrocarbons), PM and NO_x. On the contrary CO_2 is not officially regulated, but EU and automotive manufactures came to a voluntary agreement few years ago [13].

Furthermore, starting from the EURO 3 stage, vehicles must be equipped with an *On Board Diagnostic* (OBD) system for emissions control [14]. Driver must be notified in case of a malfunction or deterioration of the emission system that would cause emissions to exceed mandatory thresholds.

Moreover since Euro 5, a particle number emission limit, in addition to the mass-based limits, has been introduced. This to prevent the emission of ultra fine particles, which are more dangerous for human health, because of their major ability to penetrate in respiratory system. To measure particle number a

new method is adopted: PMP (*Particulate Matter Protocol*). One of the main concern about a number particle limit emission is the difficulty and the reliability of measure, but current system has been demonstrated to be repeatable and reproducible between laboratories [14].

Actually, every country has its own emission standards, but it is worth of note that European legislation is followed also by all but three Asian countries (the exception are Japan, South Korea and Taiwan). To put it in another way a population of 3 billion people follows the European standards. Precisely the delay in implementation of EU standards is three or four years. Hence this gives European legislators a special responsibility: the earlier we introduce standards in EU, the more perspective there is for cities in China, India and elsewhere to improve their appalling air quality [14]. Nevertheless European regulations are not the strictest ones: Japan and USA have traditionally harsher environment policies. There has been much talk in recent years about the need to harmonise global emission standards. In particular, the car industry has always been keen on this topic, in fact a car that just has to pass one emissions test could then be sold everywhere: Asia, Europe and USA [14]. Indeed some of the USA federal states (California, New York, Massachusetts, Maine, Vermont) have adopted more stringent standards.

The technological development is obviously close to issued laws; Figure 2.5 shows the strategies adopted by automobile industry in order to respect the required standards for both PM and NO_x:

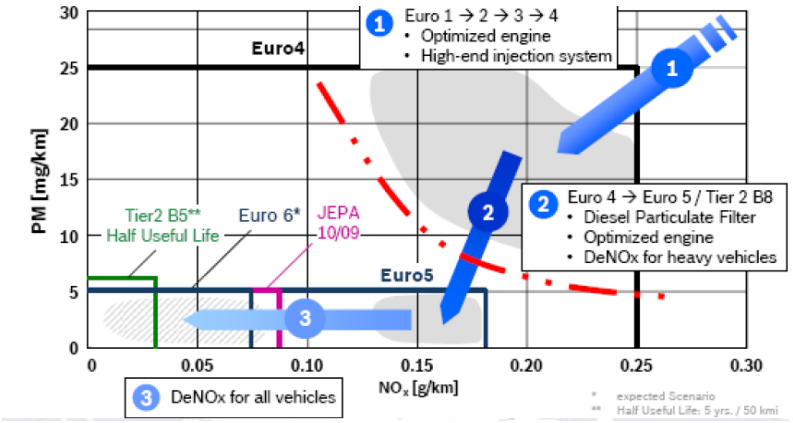

Figure 2.5 - Measures to achieve emission levels for Diesel equipped vehicles [15]

In the passage from EURO 1 to EURO 3, the optimization of engine and injection system were required, as well as the use of an oxidation catalyst (DOC) in order to abate particulate matter.

With EURO 3, NO_x limits were introduced for Diesel engines and issued standards for both the pollutants were respected with a further optimization of engine, injection system, combustion and fuel. This, since EURO 4 has not ever been possible: for the engine out-emission there is a well-known trade-off between the two pollutants mentioned above. Over a period of time, thanks to the so-called *primary techniques* the trade-off curve moved to lower values of both NO_x and PM. However this is not enough to join the limit emission of further legislation for both the pollutants, therefore *secondary techniques* are required.

In particular, the passage from EURO 4 to EURO 5 saw the DPF system as compulsory for particulate matter abatement and a deNO_x after-treatment technology as necessary on heavier vehicles which are

equipped with an always more complex abatement technology. Eventually, only applying deNO_x system EURO 6, US and Japanese NO_x limits will be respected.

In next paragraph, some of the main primary and secondary techniques (applied on vehicles or still under study) will be presented.

It is worth of note that, to obtain the required standards, several technologies have to be put together. Actually, the performances of commercial catalytic post-treatment systems are not optimized to fulfill the forthcoming U.S. standard legislation and those that will be implemented in Europe near 2014, particularly the low limit of NO_x emissions from diesel engines.

2.2 Abatement technologies

In order to reduce both NO_x and PM are necessary:

- *primary* techniques which limit pollutant formation;
- *secondary* techniques which work on flue gases, purifying them through chemical or mechanical treatments.

Primary techniques are not sufficient to reach the required standards because of the so-called trade-off: operative conditions influence in opposite way the pollutant formation. In Figure 4.28 the effect of air/fuel ratio, defined as:

$$AFR = {}^{Air}/_{Fuel} = \frac{mass\ of\ air\ used\ by\ the\ engine}{mass\ of\ fuel\ burned\ by\ the\ engine} \quad (1.1)$$

Lambda (λ = stoichiometric combustion ratio) is an alternative way to represent AFR:

$$\lambda = \frac{A/F_{effective}}{A/F_{stoichiometric}} \quad (1.2)$$

which is unitary for spark ignited engines, with AFR = 14.7.

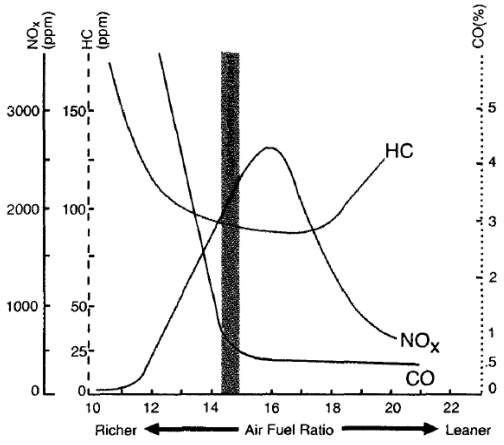

Figure 2.6 - Effect of air/fuel ratio on exhaust emissions [15]

The vertical line in Figure 2.6 separates the *rich-mixtures* (AFR < 14.7) and *lean-mixtures* (AFR > 14.7) for gasoline engines. Typically Diesel engines work in lean conditions where it is evident the opposite behavior in HC/CO (soot precursors) and NO_x production.

2.2.1 Primary techniques

Developments in fuel composition, injection systems, combustion process and engine technology allow the trade-off curve to move to lower values of both NO_x and PM.

2.2.1.1 Fuel

An improvement in fuels composition was imposed since EURO III [17]. One of the parameters strictly ruled by legislation is the sulphur content (Table 2.3).

	EURO III	EURO IV	EURO V
Sulfur ppm	**350**	**50**	**10**

Table 2.3 - Sulphur content ruled by legislation [18]

It precludes the use of the most effective PM and NO_x control technologies and it affects directly the PM emissions: for every 100 ppm reduction in sulphur, there is a particulate abatement of 0.16% for light-duty vehicles and of 0.87% for heavy-duty vehicles [18].

Cetane number is the reference index for Diesel fuels: the higher it is the better fuel qualities are. The minimum value is fixed to 51 and it depends on fuel composition; for instance a large amount of aromatics lowers it to 40-45 and this produces more difficulties in cold starting and increases combustion noise, HC and NO_x production. Furthermore the aromatic content is correlated with particulate emissions [18].

Density and viscosity are the physical properties which most affect the mass of fuel injected into the combustion chamber and, thus, the AFR [18] and the consequent pollutants formation.

At present, researchers are interest in the formulation of alternative fuels:

- Bio - Diesel, in particular the RME (Rape Methyl Ether) which affects pollutants emissions as listed in Table 2.4

Emission [g/kWh]	**Diesel fuel**	**RME**
NO_x	17.9	19.6
PM	0.8	0.5
CO	2.5	1.9
HC	0.6	0.5

Table 2.4 - Emissions of RME vs Diesel Fuel [4]

The major NO_x production is connected to higher oxygen content in Bio - Diesel.

- Synthetic Diesel obtained by Fischer - Tropsch process. It is evident (Figure 2.7) the reduction of all the main pollutants.

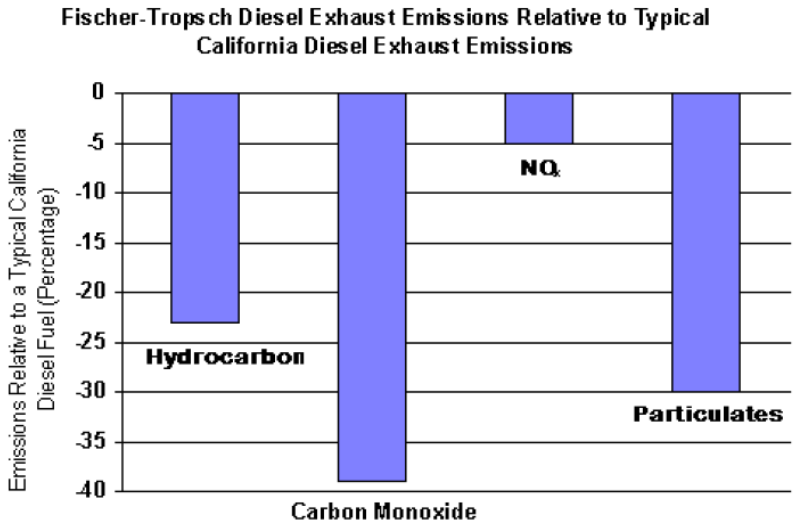

Figure 2.7 - Reduction of emissions with a synthetic fuel [4]

2.2.1.2 *Injection system and strategies*

Fuel atomization, thus the ignition and combustion process, depends on injection system. It is possible to distinguish:

- *Indirect injection*: fuel is injected into a small prechamber which is connected to the cylinder by a narrow opening. The initial combustion takes place in this prechamber. This has the effect of slowing the rate of combustion, which tends to reduce audible noise [21];
- *Direct injection* fuel is injected directly into the cylinder; the piston incorporates a depression which is where initial combustion takes place [21].

Direct injection system is used for both gasoline and Diesel engines, on the contrary, indirect injection is typical for Diesel. However, it is not so applied to modern cars because of its lower efficiency compared to direct systems: the reduced material volume of the direct injection Diesel engines decreases heat losses, therefore cold starting is easier and with a less production of pollutants. A particular kind of direct injection is the TDI (T*urbocharged Diesel Injection*), commercialized by Volkswagen Group, which is a gas compressor used for forced-induction of an internal combustion engine. Like a supercharger, the purpose of a turbocharger is to increase the density of air entering the engine to create more power. However, a turbocharger differs in that the compressor is powered by a turbine driven by the engine's own exhaust gases [22]. Another very famous system is *Multijet,* introduced by FIAT in 2002. It is a *common rail* system, characterized by five injectors that allow a slower combustion and permit a better control of the engine during the cold start [23].

Furthermore there are several injection strategies:

- air staging which consists of air fed at different stages;

- fuel staging which consists of air and fuel fed at different stages;
- early injection [13] which consists of a mixing between fuel and gas before the ignition. This avoid the condition for soot formation;
- late injection [13] which consists of a simultaneously mixing and burning of the charge using a swirl;
- EGR which works by recirculating a portion of the engine's exhaust gas back to the combustion chamber. Recirculated exhaust gas consists of inert gas (CO_2 and H_2O) which dilutes the incoming air reducing a possible oxygen excess and lowering the adiabatic flame and peak combustion temperature, responsible for the formation of *thermal* NO_x. In modern Diesel engines, the EGR gas is cooled by a heat exchanger which allows the introduction of a great mass of recirculated gas (Figure 2.8).

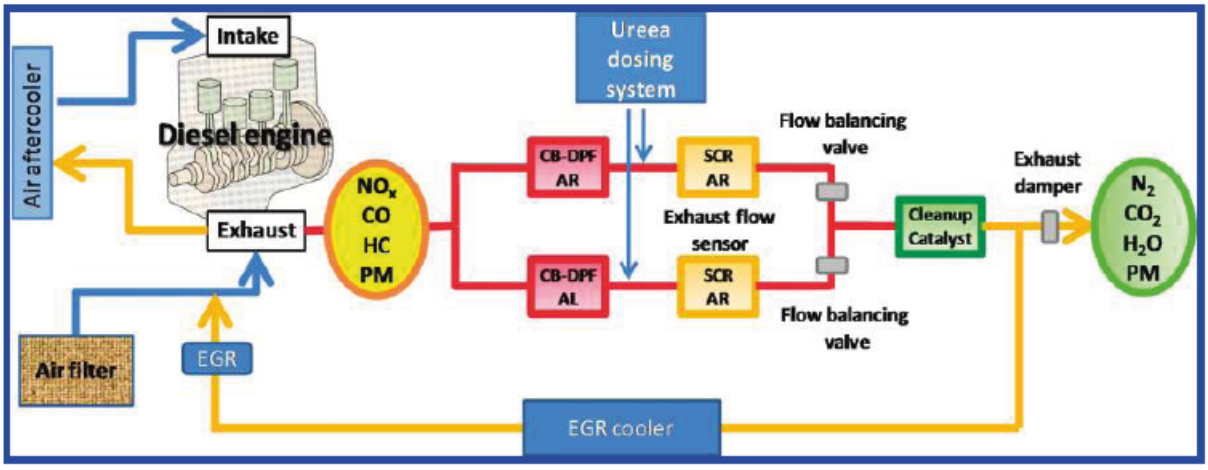

Figure 2.8 - EGR diagram

Diesel engines operate with an excess of air and they benefit from EGR rate as high as 50% in controlling NO_x emissions, but an increase in particulate matter production is present due to the reduction of the specific heat ratio of the combustion gases in the power stroke. Even if the combination of good mixing and high EGR helps to reduce soot and NO_x [13] a particulate matter abatement technology is required, typically DPF (*Diesel Particulate Filter*).

2.2.2 Secondary techniques

With primary techniques the trade-off curve was lowered (Figure 2.9) but, to cope with the emissions standard, secondary techniques are necessary: in particular a DPF system to abate particulate matter and a deNO_x catalyst to reduce nitrogen oxides emissions.

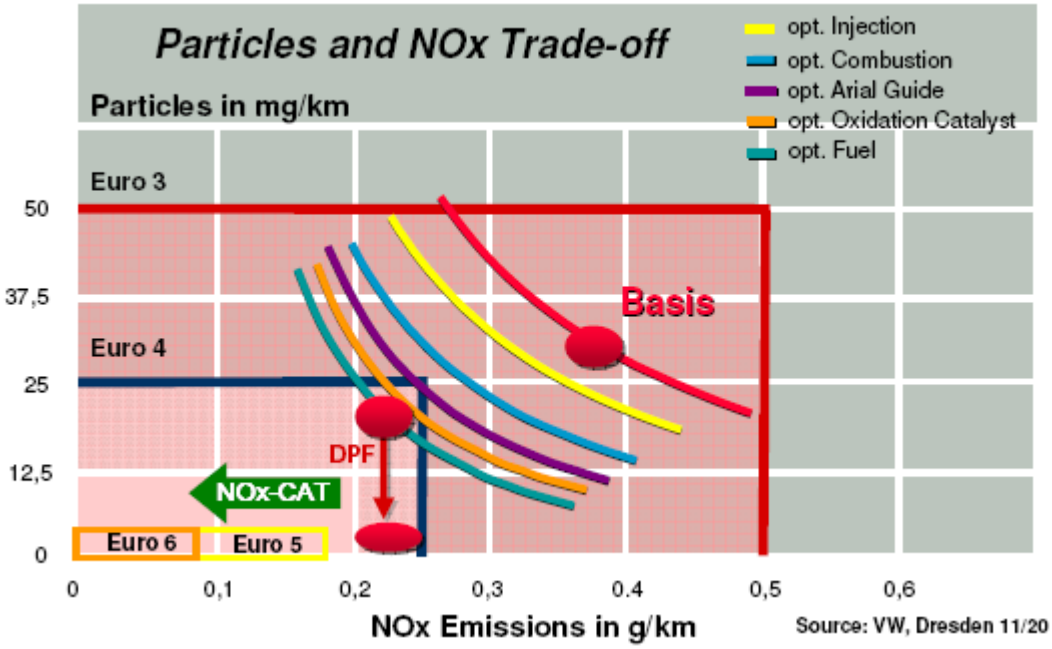

Figure 2.9 - Trade-off curve [25]

2.2.2.1 *Particulate matter*

In order to respect the PM and HC/CO limit emissions imposed by EURO IV the introduction of DOC (*Diesel Oxidation Catalyst*) was critical. It is a flow-through device that consists of a stainless steel canister containing a honeycomb-like structure or substrate (Figure 2.10).

Figure 2.10 - DOC system [26]

The substrate has a large surface area coated with a catalyst layer containing a small, well dispersed amount of precious metals such as platinum or palladium [27].

The DOC is also called 2-way oxidation catalyst because, as the exhaust gases pass through the catalyst, CO and unburned compounds are oxidized according to the following reactions:

$$4\,HC + 5\,O_2 \rightarrow 2H_2O + 4\,CO_2 \quad (1.3)$$

$$2\,CO + O_2 \rightarrow 2\,CO_2 \quad (1.4)$$

Diesel oxidation catalyst removes up to 90% of carbon monoxide and hydrocarbons. It can also reduce Diesel particulate matter by up to 30%, though typically it is in the region of 8-10% [26].

Actually the used catalysts lead to the oxidation of NO to NO_2, which is more dangerous for human health but which is very useful to improve the performances of downstream devices:

- DPF regeneration (CRT® – *Continuously Regeneration Trap)*;
- NH_3 - SCR nitrogen oxides reduction at low temperature.

Nowadays, in order to submit PM limit emissions, almost all the Diesel vehicles are equipped with a DPF. (Diesel Particulate Filter). It is a wall-flow ceramic monolith, derived from the flow-through supports used for catalytic converters. The adjacent channels are alternatively plugged at each end in order to force the Diesel aerosol through the porous substrate wall, which acts as a mechanical filter. The particulates are not able to flow through the wall and is deposited in the channel walls (Figure 2.11).

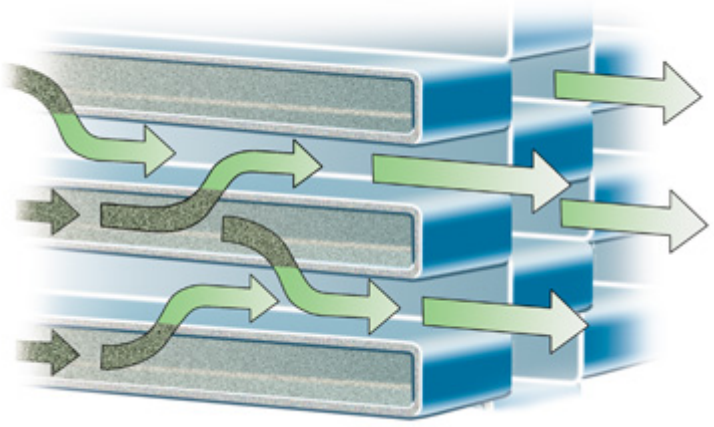

Figure 2.11 - DPF filter structure [28]

The main advantage of the wall-flow particulate filter is the high surface area per unit volume which, combined with the high collection efficiency (over 95%), makes this technique very attractive. The filter walls have a porous structure that is carefully controlled during the manufacturing process: typical values of material porosity are 45 - 50% and medium pore size is 10 - 20 µm [28].

Two kinds of filter materials are commonly used: *cordierite* and *silicon carbide*. The first one is a synthetic ceramic developed for flow-through catalyst substrates and then adapted to filter; silicon carbide has been recently introduced as filter material, because of its better durability in high thermal stress applications, but, due to its weight and high cost, the market is still dominated by cordierite [13].

Actually other materials are studied, for example aluminium titanate whose properties are impressive compare to SiC materials: low thermal expansion and high strength; in fact no cracks in the filter material were observed even after a long run of severe regeneration cycles. Further, a tight control of pore size reduces the typical backpressure on filter with soot presence [29].

The particulate collection mechanism is governed by:

- Depth filtration (particles with diameter size lower than the filter porosity are deposited inside the porous material);
- Cake filtration (particles are deposited on the channel as show in Figure 2.12).

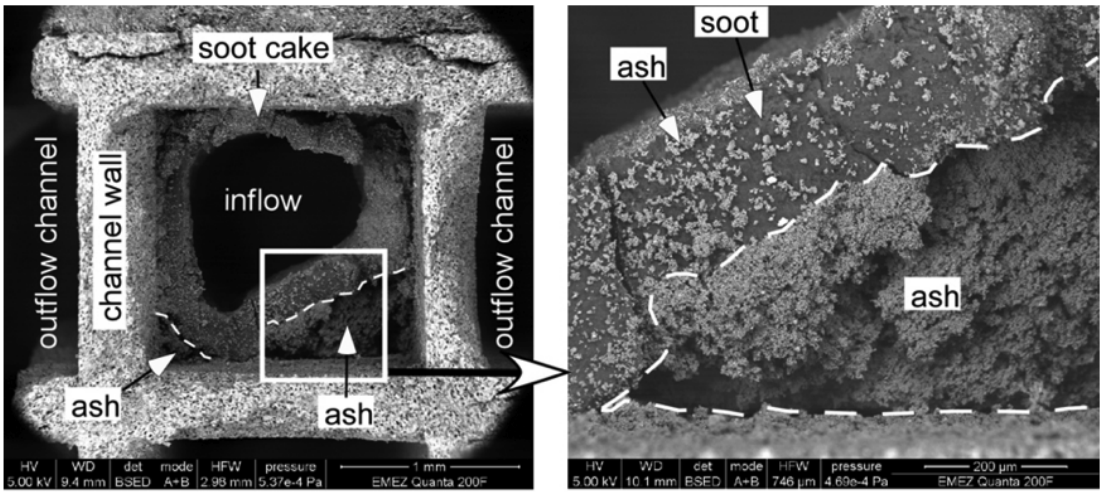

Figure 2.12 - SEM-image of a DPF section showing the soot accumulation on a channel (left) and distinguishing the soot from the ash layer (middle and right) [28]

Obviously when filter collects the particulate matter from the exhaust gas an increase in filter backpressure is present. This provokes higher fuel consumption and reduces available torque [30]. Moreover the capacity of the filter is not infinite and it has to be regenerated. The regeneration process can be classified as *active* or *passive*.

Active methods

The *active* methods consist of burning off the collected particulate. Under the conditions met in Diesel exhaust systems regarding flow and oxygen concentration, the required reaction rates for complete regeneration are attained at temperatures above 550 °C, which are scarcely reached at urban driving conditions. Thus several regeneration techniques have been suggested over the last 20 years, the most simple and effective based on catalysts: coated filter [31] or fuel doping [32].

The soot combustion temperature is lowered by doping fuel with catalytic additives(Fuel Borne Catalyst), typically organometallic compounds: the organic part is oxidized in the engine combustion chamber, while the metallic part is well dispersed in soot. A lot of metals have been proposed: cerium [33] and iron [34] for their low cost and low toxicity. Actually copper [35] and molybdenum [36] have a higher activity but they have a negative influence on men health.

Although the oxidation rate of soot is significantly increased, additional heating is necessary due to the low exhaust gas temperatures under all operating conditions. PSA Peugeot-Citroen was the first car manufacturer that commercialized system represented in Figure 2.13 - Schematic representation of an active regeneration system [37]

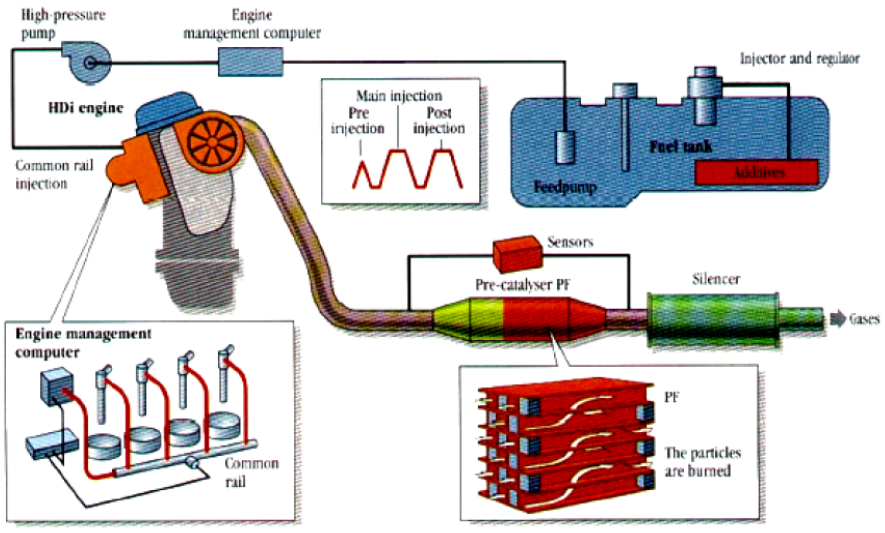

Figure 2.13 - Schematic representation of an active regeneration system [37]

The system consists of a wall-flow SiC filter, an oxidation catalyst in front of the filter, a dosing filter for fuel additive and a number of sensors associated with a specific engine software which allows the regeneration process and guaranties system diagnosis. During the regeneration mode, occurring every 400-500 km, three injections are performed:

- a pilot fuel injection to control the initiation of the heat release;
- a second injection to insure stable and late combustion;

- a third injection (post injection) to allow the necessary exhaust gas temperature.

Actually the increase of the exhaust gas temperature is obtained by the oxidation of HC of the third injection thanks to the catalyst placed in front of the filter. This contribute is much more significant at low engine load and speeds.

These filters have to mainly face the ash accumulation which makes necessary to clean or to substitute the filter itself. Furthermore the additive tank has to be refilled periodically [28].

The alternatives to this kind of filters are the washcoated ones (Catalyzed Ceramic Traps), commercially introduced in 1985 on Mercedes cars sold in California [28]. The main component of the filter is the wall-flow monolith (Figure 2.14), whose walls are coated with an active catalyst: oxides of base metals, noble metals as well as a mixture of both.

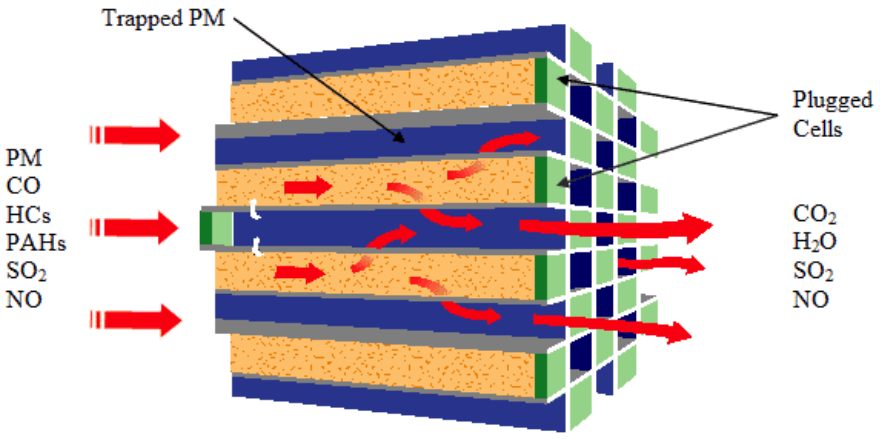

Figure 2.14 - Washcoated Filter [28]

The main disadvantage of this system is the pure contact between the catalytic coating and the soot particles: only particulate in direct contact with the catalyst can be oxidized. Moreover sulphur oxides, in exhaust gas, thanks to water can be transformed in sulphates which increase the particulate matter emissions.

Some catalytic coating may overcome the above limitation: liquid phase catalysts such as molten salts. These catalysts are based on eutectic mixtures of metal oxides that are liquid at relative low temperatures. Due to the liquid state, the soot particles may be wetting by the catalyst providing a better contact [38].

Other kinds of filter exist, for example the sintered metals or the bobbin filters.

The first consist of metal plates that can be deformed like metal sheets (Figure 2.15) in order to be finalised to cell-like structures. Their advantages are the very good heat conduction (easier active regeneration) and the low susceptibility at thermal stresses.

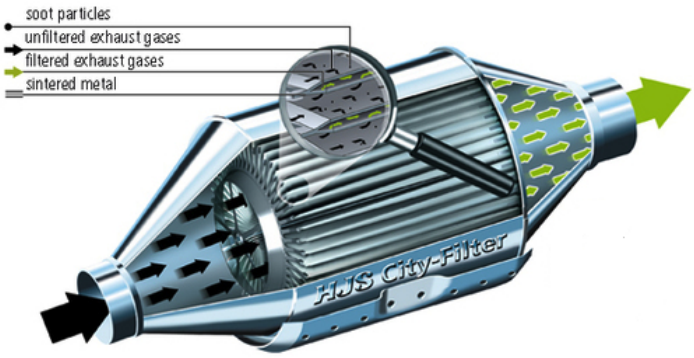

Figure 2.15 - Sintered metal filter

On the other hand, bobbin filters consist of a number of perforated cylindrical metal tubes with ceramic fibres threads woven in a diamond pattern (Figure 2.16). Their advantages are the high filtration efficiency and the low pressure drops.

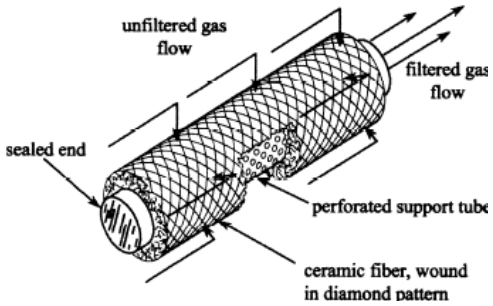

Figure 2.16 - Bobbin filter

Passive methods

As said before, the filter regeneration can be also *passive*, since additional heat is not required. One of the main applied system is CRT® (*Continuously Regeneration Trap*), patented by Johnson Matthey [40]. As presented in Figure 2.17 it consists of a Platinum catalyst and a particulate filter .

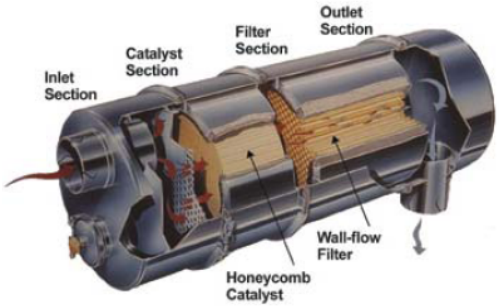

Figure 2.17 - CRT® filter system [40]

The device is made up of two chambers where the oxidation step is separated from the soot collection/combustion process. The first chamber contains a substrate coated with a highly active Platinum catalyst which allows the oxidation of a portion of NO to NO_2, which is the key to the soot burning collected by CRT filter. In fact, in presence of NO_2, soot is oxidized at lower temperatures than with oxygen: compatible with the typical exhaust gas temperatures. The filter can be uncoated or coated with Pt to enhance the soot combustion. In order to have a high system efficiency, fuel has to have a low sulphur content (30 ppm is recommended) and NO_2/PM ratio has to be at least 25 [30].

This device had a lot of success, but, in view of more stringent legislation about nitrogen oxides, its performances are not so promising.

Another system capable to reduce Diesel particulate matter at low oxidation temperature is the *Plasma* regeneration device. The soot is oxidized in air ionised by an electric arc [41]. Some reactive species, such as OH, O radicals or NO_2 facilitate the combustion. To achieve the required regeneration two configurations have been proposed:

- Two stage reactor patented by Johnson Matthey. It is made up of a plasma, which generates the oxidant species, and of a downstream DPF [42]; however, in order to reduce both particulate and nitrogen oxides a deNO_x catalyst is required;
- One stage reactor patented by AEA Technology. It utilizes a bed of ceramic pellets placed between two electrodes. A system of channels in the inner electrode directs the exhaust gas through the pellet bed (Figure 2.18);

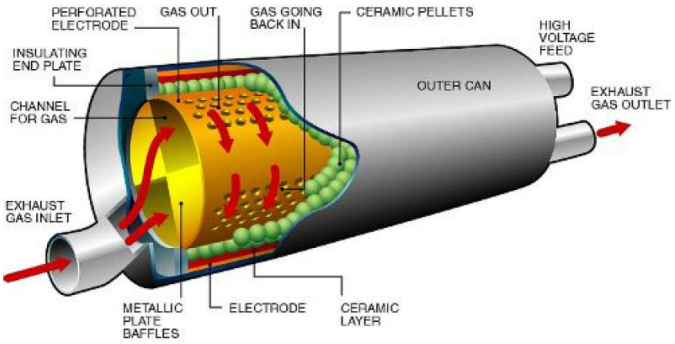

Figure 2.18 - Single stage plasma reactor [43]

In this reactor, the presence of carbonaceous particles affects the chemical reactions, in particular a less production of NO_2 is observed.

2.2.2.2 Nitrogen oxides

In order to abate NO_x several secondary techniques are available, all connected to a catalyst activity. One of the emerging is NH_3-SCR (*Ammonia-Selective Catalytic Reduction*) both for light-duty and heavy-duty applications [13]. Alternatives are mainly HC-SCR (*Hydrocarbon -Selective Catalytic Reduction*) and LNT (*Lean NOx Trap*).

Selective Catalytic Reduction of NOx with Ammonia (Urea)

The SCR process was first applied in 1970s in Japanese stationary plants for the reduction of NO_x emissions by using ammonia as reducing agent. In Europe it was introduced 1985 and today is very diffuse: from power and co-generation plants, to glass, steel and cement factories. This process is up today regarded as the most effective method for NO_x reduction [45]. It is presently considered to be also the best technology for the removal of nitrogen oxides of Diesel engines equipped vehicles. In fact it is the only one that grants an optimum compromise between low emissions and fuel consumption.

The SCR process, for stationary plants, is well represented by the so called *Standard - SCR* which follows a 1:1 stoichiometry for ammonia and NO according to reaction 1.6:

$$4NH_3 + 4NO + O_2 \rightarrow 4N_2 + 6H_2O \qquad \text{(Standard SCR)} \qquad (1.6)$$

It occurs when more than 90 % of nitrogen oxides consist of NO (usually flue gases have this composition, for that the reaction is named as *standard*). It takes place fast in the temperature range 250 - 450 °C.

However, to describe SCR process applied on mobile systems, two more reactions are necessary. They occur in presence of NO_2 that, on vehicles, comes from the oxidation of NO by DOC. When reactive system is characterized by an equimolar amount of NO and NO_2 the *Fast - SCR* occurs.

$$2NH_3 + NO + NO_2 \rightarrow 2N_2 + 3H_2O \qquad \text{(Fast SCR)} \qquad (1.7)$$

It is called *fast*, because of its higher reactivity compared to S*tandard* overall at low temperatures.
When reactive system consists of pure NO_2 the *NO_2 - SCR* occurs. Above 250 °C the process stoichiometry is as follow:

$$8NH_3 + 6NO_2 \rightarrow 7N_2 + 12H_2O \qquad \text{(NO_2 SCR)} \qquad (1.8)$$

Nowadays research is focusing on development of selective catalysts, experimenting different suitable materials. SCR techniques for stationary application are very well established but improvements are necessary to allow a wide diffusion of this technology on mobile systems, in particular Diesel engine equipped vehicles. By reactions 1.6 - 1.8 it is evident that the reducing agent is ammonia, but it has problem of toxicity, handling (it is gaseous at environment conditions) and flammability, so it cannot be used directly on mobile systems. The solution is to produce ammonia *in situ*, for example using an aqueous urea solution (it is liquid and no toxic). The commercial name of this solution, patented by BASF, is Adblue®. It is a solution with a concentration of 32.5%w/w, so at the mixture eutectic point. Actually, alternative products are studied because of the Adblue® limitations:

- high freezing point (-11 °C);
- deposition of solid matter caused by a delayed evaporation;
- low ammonia content (0.2 kg_{NH3}/kg) [46].

Urea is usually atomized into the hot exhaust gas. The first steps are the evaporation of water from droplets and the urea melting. Subsequently, urea is thermally decomposed into equimolar amounts of ammonia and isocyanic acid that is in turn hydrolyzed.

Anyway the ammonia slip has to be reduced, to this purpose an accurate control system could be installed: monitoring several parameters such has NO_x flow rate and temperature the ammonia injection is modified. Another solution, coupled with the former, could be a further oxidation step, in order to abate residual ammonia. The system described is more adapt for big Diesel engines. The greatest problem for its application on small vehicles is represented by the volume.

As said before, if *Fast-SCR* occurs, overall at low temperatures, an improvement in abatement performances is observed. It proceeds with an equimolar consumption of both the nitrogen oxides involved according to 1.7. Actually, this reaction has a complicated chemistry, which has been extensively studied on V_2O_5-WO_3/TiO_2 [48, 49, 50, 51, 52] and it is still under study for new commercial zeolites catalysts: a mechanistic pathway similar to that proposed for V_2O_5-WO_3/TiO_2 well explains data on BaNa-Y zeolite [53] and on transition metal zeolite [54] with particular regard to Fe-Zeolite [55]. Zeolites offer a number of advantages over vanadia/titania catalysts: they are active over a wider

temperature range, they are more resistant to thermal excursions, and the spent catalyst can present less of a disposal problem.

Automobile manufacturers aim to replace traditional V_2O_5-WO_3/TiO_2 with catalysts having a wider working temperature window: mainly to solve the high-temperature anatase-rutile TiO_2 deactivation, the SO_2 enhanced oxidation to SO_3 and the loss of vanadium above 650 °C. Moreover V compounds are toxic, with an increasing toxicity with the valence: pentavalent compounds, like V_2O_5, are the most dangerous, in fact it was reported to be carcinogenic for rats by inhalation [60], although the interpretation of the results has recently been disputed. Further it has not been classified as to carcinogen by the U.S. EPA (1991).

Several kinds of zeolite were proposed as nitrogen oxides reduction catalysts, overall for mobile applications, even if some stationary plants already use them [13].

Selective catalytic reduction with hydrocarbons (HC-SCR)

The selective catalytic reduction for NO_x using hydrocarbons is a technique similar to NH_3 but using unburned or injected HC as the reducing agent instead of ammonia. Since the concept of HC-SCR was first developed a vast amount of research has been undertaken and published, however a commercialisation of the system still lies in the future.
Even though a lot of effort has been paid to understand the reaction mechanism for reduction of NOx by hydrocarbons under lean conditions the reaction steps remain unclear. In the literature several reaction pathways have been proposed and they seem to be dependent on factors like the type catalyst, reducing agent, reaction conditions, presence of water and sulphur oxides in exhaust gases. Essentially three types of active catalyst have been identified, i.e zeolites, metal oxides and nobles metal. The major unsolved problems of this technique could be summarized as follows:

- Catalysts require some form of HC enrichment; HC levels in diesel exhaust, especially in modern engines, is too low for any significant NOx reduction using diesel exhaust itself (passive DeNOx).
- Even with HC enrichment, the maximum conversion efficiency at realistic HC/NOx ratios is low, on the order of 30 - 50%.
- Temperature window of known catalysts is narrow and not always corresponds to the exhaust gas temperature range at which most NOx is emitted from the engine.
- Catalyst durability needs to be improved in terms of both resistance to poisons and, in some cases, hydro-thermal durability.
- Catalysts need to be more selective towards reducing NOx to nitrogen, as opposed to nitrous oxide.

Solutions to these problems can be classified into two groups: (1) optimization of catalyst formulation and (2) optimization of the emission control system. Better catalysts could provide such benefits as

improved efficiencies, wider temperature window, or, last but not least, better durability. Even in the absence of new, breakthrough catalyst formulations, significant improvement can be achieved by system optimization. Reported ideas include using two catalysts, possibly of different formulations, optimized catalyst locations (close-coupled, underfloor), optimized HC enrichment strategies (including exhaust flow by-passes), exhaust gas cooling, and more.

Lean NO_x Trap

Lean NO_x Trap (also known as NRS NO_x storage reduction) system is generally regarded as one of the leading technologies for the control of NOx emission under lean-burn conditions. It is, nowadays, studied in depth because seen as promising for passenger cars: it is cheaper than NH_3-SCR for engines less than about 2.0 to 2.5 litres capacity as shown inFigure 2.19 [13].

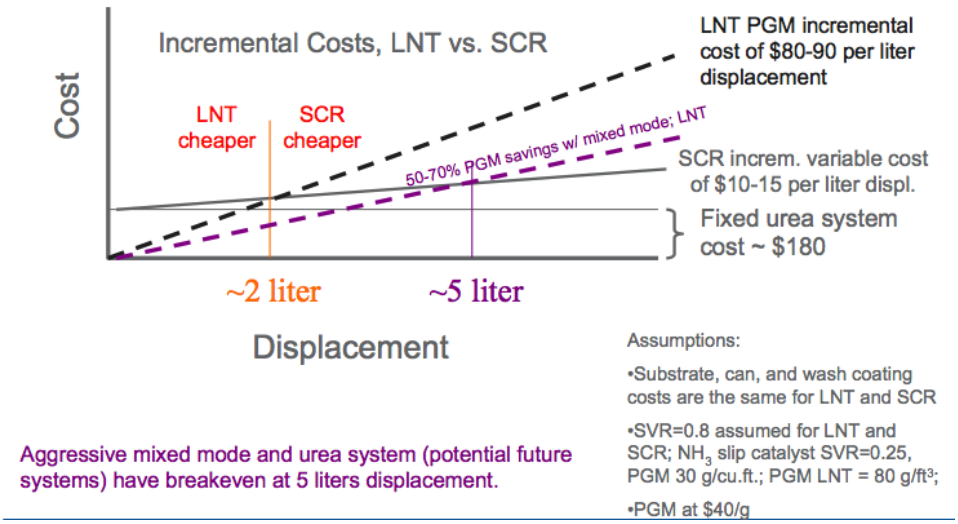

Figure 2.19 - LNT /SCR cost comparison [25]

A typical LNT catalyst consists of at least one precious metal (such as Pt, Pd or/and Rh), NO_x storage material (alkaline or alkaline-earth), and a high-surface-area support (i.e. Υ-Al_2O_3). In this approach no additional reducing agent is required. These systems cycle through two stages of operation: under lean-conditions (for about 1 min) NO is oxidized to NO_2 over precious metal and then is stored in a form of nitrate/nitrite at the surface of Ba-containing material. After changing periodically to short cycles of fuel-rich conditions (less the 1 s) the stored NO_x are reduced to N_2 by unburnt HC over noble metal catalyst, resulting in the regeneration of the catalyst. The activity of NO_x adsorbers covers a fairly wide catalyst temperature window, extending from about 200°C to 450-500°C. In diesel NO_x adsorber systems, the maximum performance typically occurs in the 350-380°C range. The lower end of the temperature window is determined by the catalyst activity in regards to the oxidation of NO to NO_2, as well as NO_x release and reduction. The upper temperature is related to the thermodynamic stability of nitrates, which undergo thermal decomposition at higher exhaust temperatures, even under lean

conditions. The NO_x adsorber temperature window is in fairly good correlation with diesel engine loads and exhaust temperatures at which most of diesel NOx generation occurs. It is this favourable position of the temperature window and the high NO_x conversion efficiency, which makes NO_x adsorbers an attractive diesel NOx control technology. However several issues still have to be answered before the LNT technology can be confirmed as an option for commercial vehicles.

The main drawback hindering the widely commercial use of the NSR catalyst for mobile lean NOx reduction is its sensitivity to sulphur poisoning. Fuel and lubricant oil are the major sources for the sulphur in the exhaust gas. Reduced sulphur species including hydrogen sulphide (H2S) and carbonyl sulphide (COS) may be also present in the gas during the rich excursions. In the presence of an oxidation catalyst, these compounds form stable sulphates with the NOx storage materials. The adsorption of sulphur is preferential over the adsorption of NOx. Stable sulphates, such as Al2(SO4)3, are also formed with washcoat materials. As a result, the catalyst performance gradually declines and fewer sites are available for NOx adsorption.

The sulfur is removed by passing a rich, hot stream (700°C) for a total of about 10 minutes every 3000 to 6000 miles (5000 to 10,000 km). Although earlier LNTs lost perhaps 50% of their capacity over 15 to 20 desulfation cycles, newer versions now lose only about 25% of the fresh NOx capacity. Further, in the past it was difficult to control desulphation temperature to within 700 to 800°C. Newer control strategies now allow this degree of control, and perhaps even better.

Given this, LNTs are effective to about 60 to 70% NOx efficiency in ‘realworld’ light-duty systems.

Finally, there has been much recent interest in combining LNTs with SCR. In this case, a downstream SCR catalyst stores ammonia that is generated in the LNT during rich operation. The ammonia can react with slipped rich NOx or lean NOx, increasing system efficiency, or decreasing the platinum group metals (pgms) loading, and hence cost at constant efficiency. A recent variant of this method employs a NOx adsorber/SCR double layer configuration. The system exhibits excellent low-temperature NOx conversion in the 200°C range, but poor high temperature conversion over 350°C. Another feature is that desulphation occurs at 500ºC, as compared with 700 to 750°C for conventional LNT systems [8].

2.2.2.3 Combined technologies

In order to comply with the more stringent limit emissions for Diesel equipped vehicles, concerning both PM and NO_x, it is necessary to design complex after-treatment systems obtained by combining some of the above described technologies. Actually the aim is not only to reduce emissions but also costs, volume and mass. Indeed vehicles, due to the presence of several after-treatment devices are heavier and this causes indirectly an increase in fuel consumption and in CO_2 production.

The amount of pollutant emissions strongly depends on vehicle size and the after-treatment systems, as well, are connected to the vehicle volume and capacity (Figure 2.20).

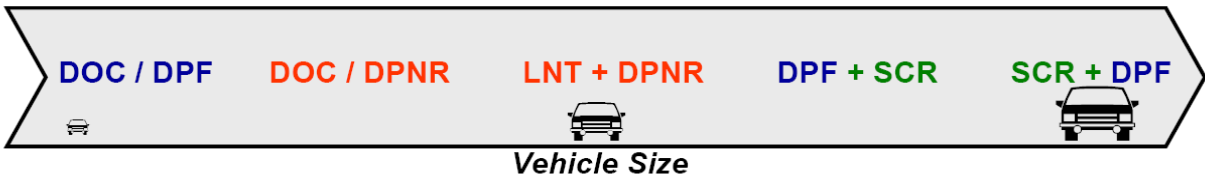

Figure 2.20 - Light duty Diesel MiNO$_x$ applications [75]

Typically, the bigger the vehicle is, the more complicated is the after-treatment system. It is worth of note that, at the present, the smallest Diesel cars need only a PM abatement technology, but with the increase of dimensions it is necessary the combination with a deNO$_x$ system.

The choice of the nitrogen oxides after-treatment system is closely dependent on vehicle size and weight (Figure 2.21):

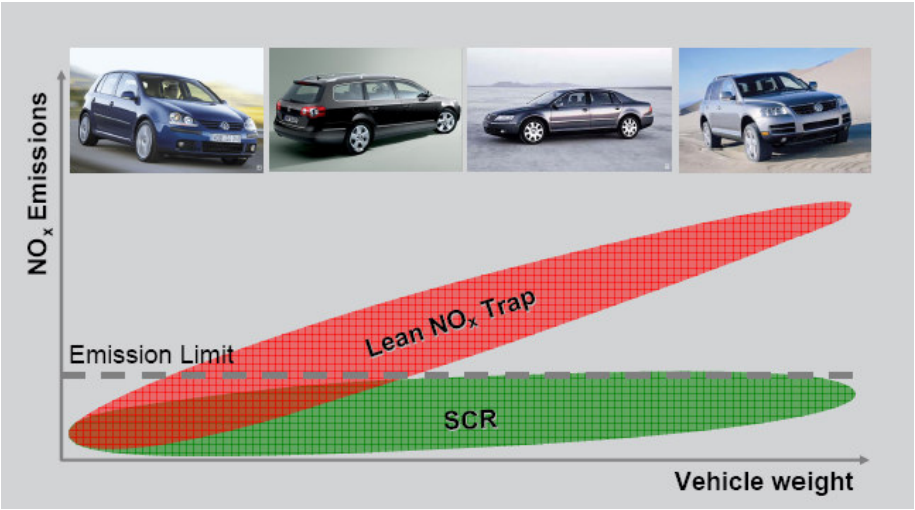

Figure 2.21 - DeNO$_x$ system required depending on vehicle weight [25]

It is worth of note that the heavier is the vehicle the higher is NO_x production and a SCR system is required to fulfil limit emissions.

Actually, to put a classic SCR system on a medium size vehicle is a problem connected to the presence of the big urea storage tank. A possible solution is an *in situ* NH_3 production, for instance, by a LNT system. This was proposed by Daimler in the *BlueTEC® I technology.*

BlueTEC® I technology

BlueTEC® is a modular exhaust treatment package that can be aligned with different vehicle and engine types to ensure the most stringent emission limits both of NO_x and PM.

The first element of this technology consists of engine and combustion optimization measures designed to achieve the lowest possible raw emissions during cylinder combustion.

The second *BlueTEC®* component is the oxidizing catalytic converter which reduces carbon monoxide and unburned hydrocarbons emissions.

Component number three is the maintenance-free particulate filter. This filter, which reduces particulate emissions by up to 98 percent and its emission levels are on a par with the limits specified in EURO V standards. Actually this device, in *BlueTEC® I* technology, is interposed between LNT and SCR catalytic converters (Figure 2.22).

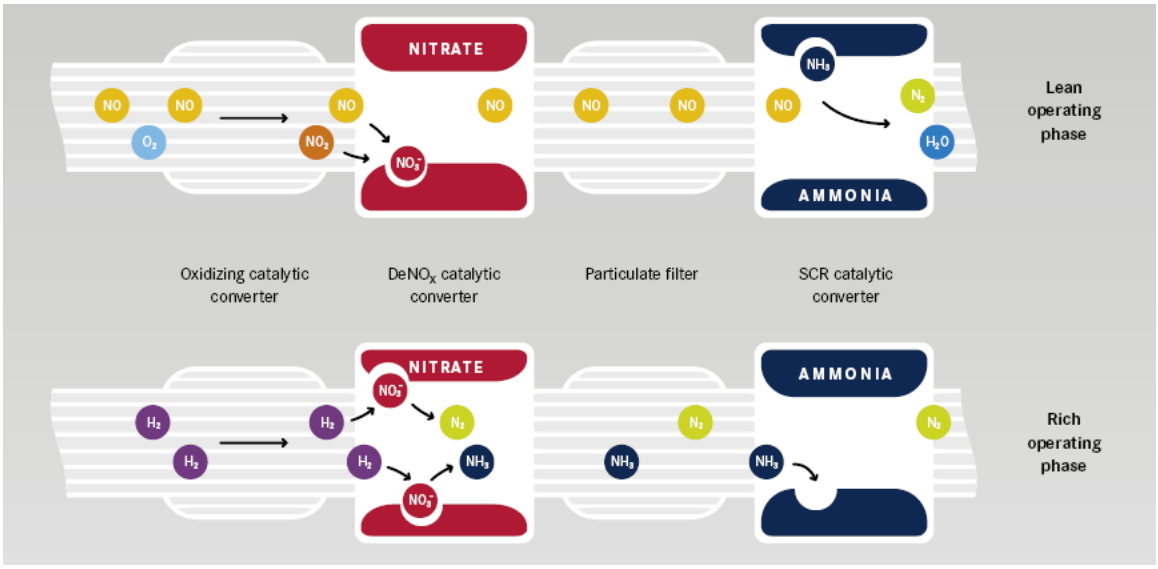

Figure 2.22 - BlueTEC® I technology scheme [79]

Thus NO_x reduction takes place in two stages: first by the LNT and second by the SCR catalyst, supported by ammonia from the LNT. The system shows a discontinuous behavior: during the rich phase LNT is regenerated and the ammonia produced is stored by SCR catalyst; during the lean phase LNT and SCR abate NO_x. Furthermore the SCR deNO_x activity makes up for the loss in LNT performance over time due to fuel sulfur poisoning.

It is evident that the above after-treatment systems take up a lot of space and research focuses on more compact systems. For example, to reduce the occupied volume, LNT and SCR could be put together in a single device, like proposed by Honda. In 2006, they announced the launch of a new Diesel car equipped with a NO_x reduction catalyst, combining NO_x adsorber catalyst (NAC) and a SCR catalyst in a two-layer structure: one adsorbs NO_x and generates ammonia during the regeneration, the other adsorbs the ammonia and uses it for a SCR reaction to further reduce NO_x [82].

SCRT® *technology*

Other companies like Eminox and Johnson-Matthey propose a configuration that conbines CRT® (*Continuously Regenerating Trap*) technology with SCR to reduce nitrogen oxides (NO_x). The combination of these technologies in SCRT® provides a system which reduces all legislated Diesel engine emissions in Figure 2.23.

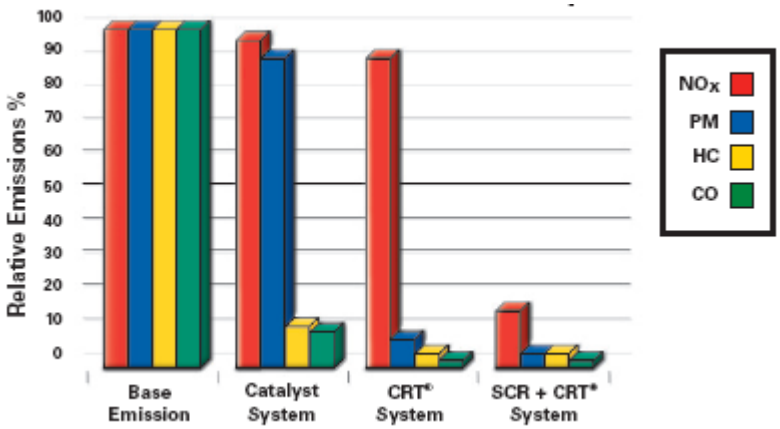

Figure 2.23 - Emission reduction capability [83]

As already said, the SCRT® system combines two major components, the CRT® and the SCR, integrated into a single compact unit, as shown in Figure 2.24.

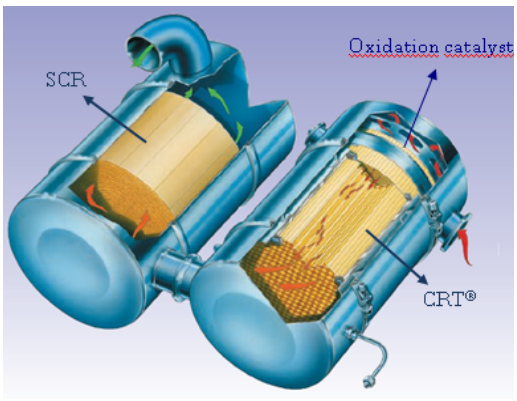

Figure 2.24 - Eminox SCRT® after-treatment system layout [83]

At the CRT® outlet flow, gas consists of CO_2, H_2O, NO e NO_2. In fact, in upstream section platinum catalyst allows the reactions (1.3)-(1.4) and the following:

$$NO + \frac{1}{2}O_2 \rightarrow NO_2 \qquad (1.24)$$

Some of the NO_2 continuously oxidizes particulate matter collected in DPF according to:

$$C + 2NO_2 \rightarrow CO_2 + 2NO \qquad (1.25)$$

The exhaust gas goes through SCR section, which consists of two chambers, one to mix the urea with the exhaust gas and the second, containing a coated monolith developed to realized the deNO_x activity.

It is very important to dose exactly the amount of required urea, otherwise all the nitrogen oxides will not be consumed and ammonia could be emitted from the tail pipe. In order to avoid the first problem a nitrogen oxide and temperature sensors provide to an ECU (*Electronic Control Unit*) the necessary information to be able to dose the urea accurately. On the other hand, to abate possible unconverted ammonia, a *slip catalyst* (an oxidation catalyst) is placed downstream.

Even if SCRT® is considered as a compact system, actually it consists of three or four catalyst bricks (oxidation catalyst, particulate filter, SCR monolith and ammonia slip catalyst). Thus, the occupied-space problem is not completely solved. Moreover, the gas flowing through the SCR section has a larger amount of NO, than NO_2; that means a lower efficiency of deNO_x activity, overall during low speed and engine load. The solution to this problem could be a different after-treatment configuration: putting SCR section upstream of DPF.

At present, the proposed layouts are mainly two: DOC + SCR + DPF and DOC + DPF + SCR. It is worth of note that in both the configurations DOC is in first position, upstream of the other devices. In fact, in this way, it allows greater system durability at high temperatures, contributing to convert, thanks to oxidation reactions, CO and unburned hydrocarbons to CO_2 and H_2O. As the reactions occurring in DOC are exothermic, they generate the necessary heat for the thermal DPF regeneration. Moreover this device supplies an extra amount of NO_2, useful to passively regenerate the DPF and to enhance the NO_x conversion in the SCR section (mostly at low temperatures thanks to the *Fast*-SCR).

DPNR® *technology*

If LNT process is sufficient in order to fulfil limit emissions, it may be coupled with a particulate matter abatement system in a single device: the DPNR. It was proposed by Toyota and commercialized in large scale, for the first time, on Avensis in year 2002. This system is a combination of a highly porous wall-flow ceramic particulate filter coated with a NO_x absorber catalyst (Figure 2.25) which contains both precious metals (Pt, Rh), in order to oxidize NO to NO_2 and reduce NO_x, and a storage component containing alkaline or earth alkaline metals.

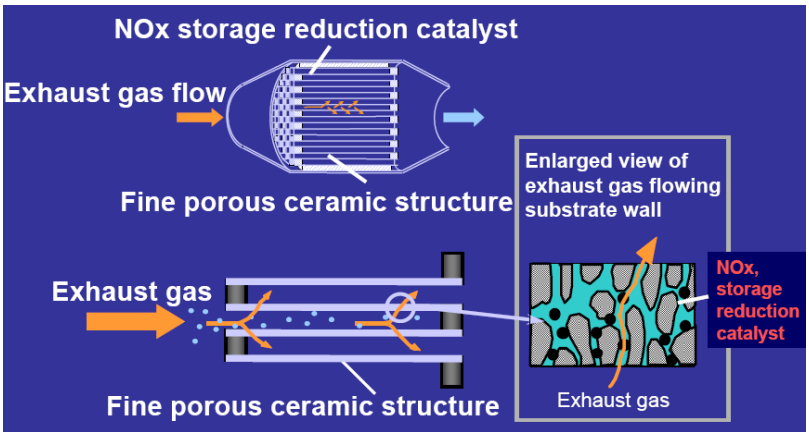

Figure 2.25 - DPNR catalyst [77]

This device works in an alternative way (lean/rich conditions) as show in

This device works under cyclic conditions, alternating a lean phase during which the NOx produced by the engine are adsorbed on the alkaline or earth-alkaline metal oxide component (with nitrate species formation), with a short rich phase, during which the stored nitrate species are reduced to nitrogen. This cyclic process is reported in Figure 2.26.

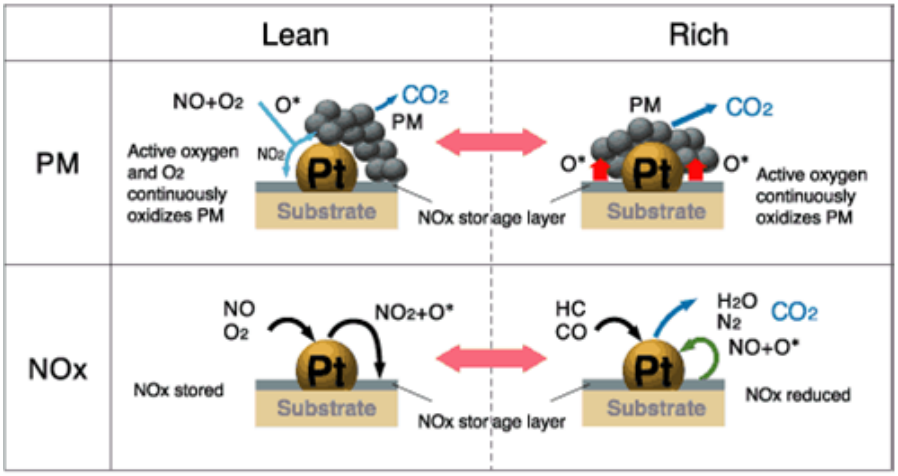

Figure 2.26 - DPNR process scheme

This catalytic system allows continuous soot oxidation at exhaust temperature as low as 250°C, achieved by a pre-turbo fuel injection upstream the DPNR catalyst. One of the problem of this system is the sulfur poisoning. To prevent it, when the sulfur accumulated in DPNR catalyst reaches a certain level, the

catalyst's bed temperature is increased in order to release the sulfur. Nowadays Toyota is developing a sulfur trap catalyst, placed upstream of the DPNR: the trap reduces sulfur accumulation on the catalyst and it also reduces the thermal deterioration caused by the earlier method of sulfur discharge [78]. Furthermore, to reduce the thermal deterioration of the catalyst, Toyota is now looking at a new ceria-based catalyst which is effective for suppression of Pt sintering.

The described system is one of the first examples of a compact devices, but it can be applied only on small vehicles because its efficiency, at present, does not meet the limit emissions for heavier vehicles, in particular concerning NO_x emissions. Furthermore this system, at the present state of the art, will not be able to fulfil future legislation limits also for light-duty vehicles.

References

1. U. G. Alkemade, B. Schumann, *Engines and Exhaust After Treatment Systems for Future Automotive Applications,* Solide State Ionics 177, (2006), 2291-2296
2. J. C. Guibet, E. Faure-Birchem, *Fuels and Engines: Technology, Energy, Environment,* vol. 1, Editions Technip, Paris, (1999), 1-385
3. http://www.epa.gov/air/emission/data/
4. F. E. Corcione, *Il Ruolo dei Combustibili nella Problematica Ambientale,* XVII Convegno Tecnico ACI, Roma, 16-17 February 2006
5. C. Sousa, *Alternative fuels and vehicles*
6. http://en.wikipedia.org/wiki/Diesel_engine/
7. Sommer, 3rd MinOx conference presentation (2008).
8. ATSDR (Agency for Toxic Substances & Disease Registry), *Medical Management Guidelines (MMGs) for Nitrogen Oxides (NO, NO2, and others)*, website (September 2007)
9. WHO (World Health Organization), website.
10. J. T. Kiehl, K. E. Trenberth, Earth's Annual Global Mean Energy Budget, *Bulletin of the American Meteorological Society*, Vol. 78, No. 2, (1997), 197-208
11. http://www.dieselnet.com/standards/eu/
12. http://www.dieselnet.com/standards/cycles/ece_eudc.html
13. T. Johnson, *Diesel Engine Emissions and Their Control,* Platinum Metals Rev., 2008, 23-27.
14. *EURO 5 and 6 emissions standards for cars and vans,* Position Paper, September 2006, European Federation for Transport and Environment
15. J. B. Dementhon, T. Seguelong, *Solutions to the Remaining Obstacles to the Full Deployment of the AdBlue®-Based SCR-Technology*, Aaqius & Aaqius S.A., 2nd MiNOx Conference, 20th June 2008
16. Toyota Motor Sales, USA, Emissions – Combustion Chemistry, website
17. http://www.unionepetrolifera.it/Repository/-1435117574/-1091923124/318967663/1089536976
18. http://www.tamoil.it/Prodotti/Carburanti+e+combustibili/Gasolio+autotrazione/
19. *Policy guidelines for reducing vehicle emissions in Asia,* 2006,14-23
20. http://en.wikipedia.org/wiki/Indirect_injection
21. http://www.indopedia.org/Direct_injection_vs_indirect_injection.html
22. http://en.wikipedia.org/wiki/Turbocharged_Direct_Injection
23. http://it.wikipedia.org/wiki/Motore_multijet
24. P. Granger, V. I. Parvulescu*, Catalytic NOx Abatement Systems for Mobile Sources: FromThree-Way to Lean Burn after-Treatment Technologies, Chem. Rev. 2011, 111, 3155–3207*
25. V. B. Baça, E. Rohart, M. Allain, *Designed Materials to Fulfill Euro 6 DeNO$_x$ LNT and NH$_3$-SCR Catalysts,* MiNO$_x$, 2008
26. http://www.eminox.com/products/doc.shtml
27. *Diesel Oxidation Catalyst*, Washington State University Extension Energy Program

28. G. A. Stratakis, *Exeperimetal Investigation of Catalytic Soot Oxidation and Pressure Drop Characteristics in Wall-Flow Diesel Particulate Filter,* (2004), Valos

29. R. Dorenkamp *et al., Application af a New Filter Material in Volkswagen's Diesel Particulate Filter System,* Dresden Conference *Emission Control 2006,* Technical University, Dresden, Germany, 18th-19th May, 2006

30. A.M. Stamatelos, *A Review of the Effect of Particulate Traps on the Efficincy of Vehicle Diesel Engines,* Energy Conversion & Management, Vol. 38,1997, 83-89

31. J.A.P., Neeft, M. Makkee, J.A. Moulijin, *Catalyst fot the Oxidation of Soot from Diesel Exhaust gases, An Explorative study,* Applied Catalyst B: Environmental 8, (1996), 57-58

32. M. Kasper, K. Sattler, K. Siegamann, U. Matter, H.C. Siegmann, *The Influence of Fuel Additive on the Formation of Carbon During Combustion,* Journal of Aerosol Science, Vol. 30, February 1999, 217-225

33. K. Pattas, Z. Samaras, A. Roumbos, J. Lemaire, W. Mustel, P. Ruveirolles, *Regeneration of DPF at Low Temperatures with the use of a Cerium Based Fuel Additive,* SAE paper 960135, 1996

34. J. Zangh, C. M. Megaridis, *Soot Supression by Ferrocene in Liminar Ethilen_Air Non premixed Flames,* Combustion and Flames 105: 528-540 (1996)

35. A. Gantawar, C. Opris, J. Johnson, *A Study of the Regeneration Characteristics of Silicon Carbide and Cordierite Diesel Particulate Filter Using a Copper Fuel Additive,* SAE paper 970187

36. M. Hasan, M. Zaki, K. Kumari, L. Pasupulety, *Soot Deep Oxidation Catalyzed by Molybdena and Molibdates: a Thermogravimetric Investigation,* Thermochimica Acta, Vol. 320, 1998, 23-32

37. O. Salvat, P. Marez, G. Belot, *Passenger Car Serial Application of a Particulate Filter System on a Common Rail Direct Injection Diesel Engine,* SAE paper 2000-01-0473

38. G. Saracco, N. Russo, M. Ambrogio, C. Badini, V. Specchia, *Diesel Particulate Abatement Via Catalytic Traps,* Catalyst Today, Vol. 60, 1-2, 10 July 2000, 33-41

39. C. van Gulijik, *Rational Design of a Robust Diesel Particulate Filter,* PhD Thesis TU, Delft, 2002

40. B. J. Copper, H. J. Jung, J. E. Thoss, *Treatment of Diesel Exhaust Gas,* US Patent 4,902, 487, 1990

41. Y. Levendis, C. Larsen, *Use of Ozone-Enriched Air for Diesel Particulate Trap Regeneration,* SAE paper 1999-01-0114

42. M.V. Twigg, *System and Method for Purifying Exhaust Gases*, US patent 6,557, 340, May 6, 2003

43. S. Thomas, *Non Thermal Plasma Aftertreatment of Particulate – Theoretical Limits and Impact on Reactor Design,* SAE paper 2000-01-1926

44. M. Iwamoto, H. Hamada, Catalyst Today, 10, (1991), 57

45. P. Forzatti, L. Lietti, Heter. Chem. Rev. 3 (1996), 33

46. E. Jacob*, Prospektiven der mobilen SCR-Technik,* Aachener Kolloquium Fahrzeug

47. V. Fracassetti, P. Viganò, *Analisi sperimentale e modellistica della reattività SCR su catalizzatori zeolitici per l'abbattimento di NO_x da sorgenti mobile: effetto della geometria del supporto*, Thesis in Chemical Engineering, Politecnico di Milano, A.A. 2006/2007

48. G. Madia, M. Koebel, M. Elsener, A. Wokaun, *The Effect of an Oxidation Precatalyst on the NOx Reduction by Ammonia SCR*, Ind. Eng. Chem. Res. 41 (2002), 3512

49. M. Koebel, M. Elsener, G. Madia, *Reaction Pathways in the Selective Catalytic Reduction Process with NO and NO2 at Low Temperatures*, Ind. Eng. Chem. Res. 40 (2001), 52

50. M. Koebel, G. Madia, F. Raimondi, A. Wokaun, *Enhanced Reoxidation of Vanadia by NO2 in the Fast SCR Reaction*, J. Catal. 209 (2002), 159

51. M. Koebel, M. Elsener, G. Madia, *Selective catalytic reduction of NO and NO2 at low temperatures*, Catal. Today 73, (2002), 239

52. C.Ciardelli, I. Nova, E. Tronconi, D. Chatterjee, T. Burkhardt, M. Weibel, Chem. Eng. Sci., 62, (2007), 5001

53. Y.H. Yeom, J. Henao, M.J. W.M.H. Sachtler; E. Weitz, J. Catal. 231, (2005), 181

54. O. Kröcher, *Proceeding of Congress NO_x-Minimisation of NO_x Emissions through Aftertreatment,* Berlin, February 1-2, 2007, Paper H030-02-286-7

55. A. Grossale, I. Nova, E. Tronconi, D. Chatterjee, M. Weibel, *The Chemistry of the NO/NO_2-NH_3 "fast" SCR reaction over Fe-ZMS-5 investigated by transient reaction analysis,* Journal of Catalysis, 256, (2008), 312-322

56. S.Agnello, F.Riboldi, *Studio della reattività SCR su catalizzatore a base di Vanadio in polvere ed in forma di monolita*, Thesis in Chemical Engineering, Politecnico di Milano, AA. 2005/2006

57. J. Eng, C.H. Bartholomew, J. Catal., 171, (1997), 27

58. J. Eng, C.H. Bartholomew, J. Catal., 161, (1996), 14

59. S. A., Stevenson, J. C. Vartuli, C. F. Brooks, J. Catal., 190, (2000), 89

60. Ress et al., 2003

61. R. M. Milton, CS Symp. Ser., 398, (1989), 1

62. M. Devadas, *Selective Catalytic Reduction (SCR) Nitrogen Oxides with ammonia over Fe-ZSM5*, Thesis at Swiss Federal Instutute of Technology Zurich, 2006

63. K. R. Tolonen, T. Maunula, M. Lomma, M. Huuhtanen, R. L. Keiski, *The effect of NO2 on the activity of fresh and aged zeolite catalysts in the NH3-SCR reaction*, Catalysis Today 100, (2005), 217–222

64. R. Q. Long, R. T. Yang, Jour. Catal., 188, (1992), 332

65. K. Krishna, G. B. F. Seijger, C. M. Van den Bleek, M. Makkee, G. Mul, H. P.A. Calis, Catal. Lett. 86, (2003), 121

66. G. Delahay, D. Valade, A. G. Vargas, B. Coq, Appl. Catal B, 55, (2005), 149

67. M. Huuhtanen, *Zeolite Catalysts in the Reduction of NOx in Lean Automotive Exhaust Gas Conditions,* Thesis in Process and Environment Engineering at University of Oulu, 2006

68. G. I. Panov, A. K. Uriarte, M. A. Rodkin, V. J. Sobolev, Catal. Today 41 (1998) 365.

69. V. I. Sobolev, G. Panov, A. Kharitonov, V. Romannikov, A. Volodin, K. Ione, J. Catal. 139 (1993) 435.

70. X. Feng, W. K. Hall, J. Catal. 166 (1997) 368.

71. H. Y. Chen, W. M. H. Sachtler, Catal. Today 42 (1998) 73.

72. W. K. Hall, X. Feng, J. Dumesic, R. Watwe, Catal. Lett. 52 (1998) 13.

73. T. V. Voskoboinikov, H. Y. Chen, W. M. H. Sachtler, Appl. Catal. B 19 (1998) 279.

74. R. Joyner, M. Stockenhuber, J. Phys. Chem. B 103 (1999) 5963.

75. A.M Freay, S Mert, J. Due-Hansen, R. Fehrmann, C. H. Christensen, *Fe-BEA Zeolite Catalyst for NH_3-SCR of NO_x,* Catal. Lett, (2009), 130, 1-8

76. R. Bals, et al*, Assessment of 3rd generation SCR system for Potential Future Applications*, 2nd MiNOx Conference, 20th June 2008

77. S. Watanabe, S. Itabashi, K. Niimi, *An Improvement of Diesel PM and NOx Reduction System*, DEER 2005

78. http://www.greencarcongress.com/2007/08/toyota-enhancin.html

79. Daimler HighTech Report (HTC) 2007

80. Eaton, *Hybrid LNT/SCR System for 2010 NOx Emissions Requirements*, Green Car Congress (2006)

81. J. McCarthy, W. Taylor III, *LNT + SCR Aftertreatment for Medium-Heavy Duty Applications: A Systems Approach*, DOE DEER Conference (2007)

82. DieselNet website

83. Eminox SCRT® System, Eminox leale

84. C. Lambert, G. Cavataio, Y. Cheng, D. Dobson, J. Girard, P. Laing, J. Patterson, S. Williams, *Urea SCR and DPF System for Tier 2 Diesel Light-Duty Trucks*, DEER (2006)

85. D. N. Tsinoglou, O. A. Haralampous, G. C. Koltsakis, Z. C. Samaras, *Model-based optimisation methods of combined DPF+SCR systems,* SAE paper 2007-24-0098

86. B. Oladipo, O. Bailey, K. Price, N. Balzan, S. Kaul, *Simplification of Diesel Emission Control System Packaging Using SCR Coated on DPF*, 14th Diesel Engine-Efficiency and Emissions Research (DEER) Conference (2008)

87. T. Mizutani, Y.Watanabi, K. Yuuki, S. Hashimoto, T. Hamanaka, J. Kawashima, *Soot Regeneration Model for SiC -DPF System Design,* SAE Tech. Pap. 2004, 2004-01-0159

88. M. Mali, M. Claussen, O. Carlowitz, P. Kroner, N. Ranalli, S. Schimdt, *Influence of the nItrogen Dioxides Based Regeneration on Soot distribution,* SAE Tech. Pap. 2004, 2004-01-0823

89. J. F. Knoth, A. Drochner, H. Vogel, J. Gieshoff, M.Kögel, M. Pfeifer, M. Votsmeier, *Transport and recation in catalytic wall-flow filters,* Catalysis Today, 105, (2005), 598-604

3. Research approach and scientific methods

The behavior of $PtBa/Al_2O_3$ and PtK/Al_2O_3 NSR catalyst in both the NO_x storage/reduction and soot oxidation is investigated in this thesis work. For this purpose model catalysts have been prepared and carachterized in line with the procedure outilined in section 3.1. In section 3.2 thus the configurations of the experimental setup and methods have been briefly descibed.

3.1 Preparation and characterization of the catalysts

The model $PtBa/Al_2O_3$ (1/20/100 w/w) catalyst used in this study has been prepared by incipient wetness impregnation with dinitro-diammine platinum (Strem Chemicals, 5%) and then with barium acetate of an Al_2O_3 support, obtained by calcination at 700 °C of a commercial alumina (Versal 250 from UOP). After each impregnation steps, the powders was dried overnight in air at 80 °C and calcined at 500 °C for 5 h. The selected impregnation order (first Pt and then Ba) has been adopted in order to ensure a good dispersion and stability of the noble metal on the alumina support, in line with the recipes of Toyota patents [1]. The Pt-free sample (Ba/Al_2O_3, 20/100 w/w) was also prepared by impregnation of alumina with an aqueous solution of barium acetate (Sigma Aldrich, 99%), followed by drying overnight in air at 80 °C and calcination at 500 °C for 5 h. Surface area and pore size distribution of the prepared catalyst samples were determined by N_2 adsorption–desorption with the BET method using a Micromeritics TriStar 3000 instrument. The specific surface area of the ternary $PtBa/Al_2O_3$ sample is near 160 m^2g^{-1}; a lower surface area value was determined for the Ba/Al_2O_3 sample (105 m^2g^{-1}). The surface area contraction is accompanied by a slight reduction of the pore volume, from 0.80 cm^3/g for the $PtBa/Al_2O_3$ catalyst down to 0.63 cm^3/g for the binary Ba/Al_2O_3 sample. The Pt dispersion of the $PtBa/Al_2O_3$ sample was also estimated by hydrogen chemisorption at 0°C (TPD/R/O 1100 Thermo Fischer Instrument). The measured Pt dispersion value was near 60%.

The Ba/Al_2O_3 and $PtBa/Al_2O_3$ catalysts were characterized by XRD analysis (Brüker D8 Advanced Instrument equipped with graphite monochromator on the diffracted beam). The XRD patterns showed both the monoclinic (JCPDS 78-2057) and orthorhombic (Whiterite, JCPDS 5-378) polymorphic forms of $BaCO_3$, in addition to microcrystalline γ-Al_2O_3 (JCPDS 10-425).

The K/Al_2O_3 and $Pt\text{-}K/Al_2O_3$ catalysts were also prepared by the incipient wetness impregnation method, using aqueous solutions of CH_3COOK (Sigma Aldrich, 99%) and $Pt(NH_3)_2(NO_2)_2$ (Strem

Chemicals, 5% Pt in ammonium hydroxide) to impregnate the γ-alumina support calcined at 700°C (Versal 250 from UOP, surface area of 207 m^2/g and pore volume of 0.96 cm^3/g). In the case of the Pt-K/Al_2O_3 catalyst the impregnation was carried out in sequential manner: the alumina support was first impregnated with the Pt dinitrodiammine solution, and then with the K acetate solution. After each impregnation step the catalysts were dried at 80°C overnight and then calcined at 500°C for 5 h. The final loading was 5.4/100 w/w for the K/Al_2O_3 catalyst and 1/5.4/100 w/w for the Pt-K/Al_2O_3 catalyst. The following surface areas and pore volumes were measured by N_2 adsorption-desorption at 77K: 179 m^2/g and 0.84 cm^3/g for the K/Al_2O_3 sample; 176 m^2/g and 0.9 cm^3/g for the Pt-K/Al_2O_3 sample. The Pt dispersion, as determined by H_2 chemisorption at 0°C, was ~ 65 %. Mean Pt particle size measured by HRTEM was 1.5 nm [2], in good agreement with the mean Pt particle sizes (d_{Pt}) calculated from the empirical relationship often used for monometallic catalysts, d_{Pt}(nm) = 1.1/(H/Pt), where H/Pt is the Pt dispersion measured from H_2 chemisorption.

Printex-U (Degussa), whose properties are well addressed in literature [3],was used as model soot. It presents a surface area of 95 m^2/g and a carbon content higher than 90%. The ash content is negligible, as common for synthetic soot. Catalyst-soot mixtures were prepared by gently mixing in a vial the catalyst powder (74-105 μm) with the soot, thus realizing a loose contact which is representative of the soot/catalyst contact mode occurring in the DPNR system where soot is entrapped in the filter pores [4]. A soot loading (w_{soot}/w_{cat}) near 11 % has been typically employed.

The Rh and Co catalysts used to study the elementary steps and site requirements of NO oxidation have been prepared by using as supports γ-Al_2O_3 (Sasol, SBa-200, 180 $m^2\ g^{-1}$) and SiO_2 (Davisil, Grade 646, 300 $m^2\ g^{-1}$) respectively. Both supports were heated to 750°C at 0.07 °C s^{-1} in flowing dry air (Praxair, Extra Dry, 1 $cm^3\ s^{-1}\ g^{-1}$) and held for 4 h. $Rh(NO_3)_3 \bullet H_2O$ (Sigma Aldrich) or $Co(NO_3)_2 \bullet (H_2O)_6$ (Sigma-Aldrich) were added to de-ionized distilled water (Barnstead, Nanopure) and the solution was added dropwise to γ-Al_2O_3 or SiO_2 to the incipient wetness point (0.45 g solution (g $Al_2O_3)^{-1}$, 0.9 g solution (g $SiO_2)^{-1}$) to prepare samples with 0.8% and 2.4% wt. Rh and 10% wt. Co. Impregnated supports were heated in ambient air at 120°C for 4 h and then in flowing dry air (Praxair, extra dry, 1 $cm^3\ s^{-1}\ g^{-1}$) for 4 h by heating at 0.07 °C s^{-1} to a temperature between 400-875°C. Rh- or Co-containing samples were then heated to 600°C or 400°C K, respectively, at 0.07°C s^{-1} and held in 9% H_2/He (Praxair, 99.999% purity, 1 $cm^3\ s^{-1}\ g^{-1}$) for 5 h. Materials were treated with 0.5% O_2/He (Praxair, 99.999% purity, 1 $cm^3\ s^{-1}\ g^{-1}$) at 22°C for 1 h before exposure to ambient air.

3.2 Experimental setup and method

3.2.1 TPD, TPO, TPSR and Transient experiments

All reactivity tests were performed in a flow-reactor apparatus consisting of a quartz tube reactor (7 mm i.d) heated by a tubular furnace controlled by a PID regulator (Eurotherm 2408). The temperature of the catalyst was measured and controlled by a K-type thermocouple (outer diameter 0.5 mm) directly immersed in the catalyst bed. Cooling down of the reactor was realised with compressed air.The flow rates of the gases were measured and controlled by mass-flow controllers (Brooks 5850 TR), and the gases were mixed in a single stream before entering the reactor. The helium line pass through a saturator allowing co-feeding of water. The reactor outlet was connected to a mass spectrometer (Omnistar 200, Pfeiffer Vacuum)for the on-line analysis of the outlet gases. The following mass-to-charge ratios (m/e) have been used to follow the reaction products: H_2 (m/e=2),N_2 (m/e=28), NN(m/e=29), N_2 (m/e=30),NO(m/e=30), NO(m/e=31),N_2O(m/e= 44), ^{15}NNO (m/e = 45), $^{15}N_2O$ (m/e = 46), H_2O (m/e = 18), NH_3 (m/e = 15), NO_2 (m/e = 46), $^{15}NO_2$ (m/e = 47), and $^{15}NH_3$ (m/e = 16).The mass-spectrometer data were quantitatively analysed using the fragmentation patterns and the response factors determined experimentally from calibration gases. Relevant interferences in the mass-to-charge signals were taken into account in determining the products composition. A gas chromatograph (micro GC Agilent 300A) equipped with a Poraplot Q and a 5 Å molecular sieve capillary column was used for the online analysis of CO_2, N_2O, and H_2O, and of O_2, N_2, and CO respectively. Furthermore a UV analyzer(Limas 11HW, ABB) was also used in continuous to detect simultaneously NH_3, NO, and NO_2.

Transient Response Method (TRM) experiments

The NO_x storage and reduction activity of the catalytic system has been studied in the presence and in the absence of soot by performing lean-rich cycles at constant temperature. In a typical run, a stream of He + 3% O_2(100 cm^3/min) was fed to the reactor and the catalyst temperature was set at the desired value. After stabilisation of the concentration signals a rectangular step feed of ^{15}NO or NO(250-1000ppm) was admitted at constant temperature, by means of a pneumatically actuated four-way valve by keeping constant the overall flow rate. The NO_x storage proceeded up to nearly steady-state, then the inlet NO concentration was stepwise decreased to zero. After a few minutes the O_2 concentration was also decreased in a stepwise manner to zero. The catalyst reduction was accomplished by imposing stepwise changes in the H_2 concentration (4000 ppm) at the reactor inlet with a second four-way valve. In each step the total gas flow was always maintained constant with He as balance. A stream of Ar was also present in the feed gases as inert tracer: accordingly the lag

time of the system could be carefully evaluated, but it has always been found negligible. Note that the lean and rich phases have been separated with a He purge in between in order to analyze separately the catalytic performances of the investigated catalyst during the lean and rich phases, and to avoid any spurious effects due to temperature variations upon lean/rich switches. 1% v/v H_2O and 0.1% v/v CO_2 are always present in the feed; even if the CO_2 and H_2O concentrations are lower than in real applications, their effects are still representative [5].

TPD, TPO and TPSR experiments

In order to analyse the interaction between soot and the stored NO_x, TPD, TPO and TPSR experiments were also performed over $PtBa/Al_2O_3$ and Ba/Al_2O_3 catalysts. Accordingly NO_x have been stored onto the catalytic surface in the absence of soot at 350°C with NO or ^{15}NO(1000 ppm v/v) in He + O_2 (3% v/v) + H_2O (1% v/v) + CO_2 (0,1% v/v); then the catalyst has been cooled at room temperature in He, extracted from the reactor and mixed with soot (11 % w/w). TPD and TPO experiments have been carried by heating the so-prepared catalyst-soot mixture at a rate of 10°C/min in He + H_2O (1% v/v) + CO_2 (0.1% v/v) in the absence and in the presence of 3% v/v O_2, respectively, from room temperature to 500°C.

In the case of TPSR experiments, a rectangular step feed of NH_3 (1000 ppm in He) or H_2 (4000ppm in He) has been admitted to the reactor at r.t. and the catalyst temperature has been linearly increased to 400°C (heating rate 10 °C/min, hold 1 hour), while monitoring the concentration of the products exiting the reactor. The results collected with the catalyst/soot mixture have been compared with those obtained in analogous experiments performed in the absence of soot.

3.2.2 FT-IR experiments

Absorption/transmission IR spectra were run on a Perkin-Elmer FT-IR System 2000 spectrophotometer equipped with a Hg-Cd-Te cryo-detector, working in the range of wavenumbers 7200-580 cm^{-1} at a resolution of 2 cm^{-1}. For IR analysis powder samples were compressed in self-supporting discs (10 mg cm^{-2}) and placed in a commercial heated stainless steel cell (Aabspec) allowing thermal treatments *in situ* under vacuum or controlled atmosphere and the simultaneous registration of spectra at temperatures up to 600°C.

Before the NO_x storage, the K/Al_2O_3 and $Pt\text{-}K/Al_2O_3$ samples were conditioned by *i)* outgassing at 500°C for 30 min, *ii)* one or two cycles consisting of NO_2 adsorption at 350°C and reduction with H_2 at 350°C (for $Pt\text{-}K/Al_2O_3$ catalyst) or out-gassing at 500°C (for K/Al_2O_3 sample), necessary to eliminate

the carbonates present on calcined powder [2], *iii)* oxidation at 500°C for 30 min and cooling in oxygen down to the temperature requested.

NO_x storage was carried out at 350°C by admitting, on the Pt-K/Al_2O_3 disc, freshly prepared NO/O_2 mixtures (p_{NO} = 5 mbar, p_{O2} = 20 mbar) or, on the K-Al_2O_3 disc, NO_2 (p_{NO2} = 5 mbar) up to catalysts saturation (ca. 20 min), and outgassing at the same temperature. The spectra of the stored NO_x were collected at 350°C or after cooling down the discs at the chosen temperature. The reduction was accomplished in CO (P_{CO} = 10 mbar) and was performed both in isothermal conditions and at increasing temperature. The reduction in isothermal conditions was accomplished at 280°C and 350°C: at each temperature the spectra were run at increasing exposure times. For the reduction experiments at increasing temperature, the samples were cooled down at 100°C under vacuum, then heated in CO in the range 100-400°C. NO (Praxair, purity ≥ 99.0 %) was freshly distilled before use. Conversely, NO_2 (Praxair, purity ≥ 99.5 %), O_2 (Praxair, purity ≥ 99.999 %) and CO (Praxair, purity ≥ 99.9 %) were directly used.

3.2.3 NO Oxidation Rate Measurements

NO oxidation rates were measured on 0.12-0.18 mm Rh/Al_2O_3 and Co/SiO_2 aggregates. Samples were held on a porous quartz frit within a tubular reactor (10 mm). Reactants (15% O_2/He, 2% NO/He, 1% NO_2/He, and 5% CO_2/He) and He carrier (Praxair, 99.999% purity) were metered using electronic controllers (Porter Instruments) to achieve a broad range of reactant pressures (1-12 kPa O_2, 0.04-0.25 kPa NO, 0.02-0.25 kPa NO_2, 0-2 kPa CO_2). A resistively-heated furnace with a controller (Watlow, 96 series) and a K-type thermocouple were used to maintain constant temperatures (275-400°C). Inlet and outlet concentrations were measured using an infrared analyzer (MKS 2030; 2 cm^3 cell; 2 cm pathlength; 65°C). NO oxidation rates are reported as turnover rates (TOR, mol NO converted (mol Rh_s or Co_s)$^{-1}$ s^{-1}) at NO conversions below 15%.

3.2.4 Isotopic Oxygen Exchange Measurements

$^{16}O_2$-$^{18}O_2$ exchange rates were measured on Co and Rh catalyst using a gradientless batch reactor (498 cm^3 volume), in which reactants were circulated by a graphite gear pump (Micropump; 2 cm^3 s^{-1}). Gases (99.999% chemical purity) were obtained from Praxair (90% O_2/Ar, He) and Ikon Isotopes ($^{18}O_2$, 96% isotopic ^{18}O purity). Catalysts were heated to 300-380°C at 0.07 °C s^{-1} and held for 1 h in flowing 2 kPa $^{16}O_2$/Ar/He (30 cm^3 s^{-1} g^{-1}) before the reactor was evacuated and filled with an

equimolar $^{16}O_2$-$^{18}O_2$ mixture and He as balance. Isotopomer concentrations were measured by periodic pulses injected into a mass spectrometer (MKS Mini-Lab).

References

[1] N. Miyoshi, T. Tanizawa, K. Kasahara, S. Tateishi, European Patent Application 0 669 157 A1, 1995.

[2] Prinetto, F.; Manzoli, M.; Morandi, S.; Frola, F.; Ghiotti, G.; Castoldi, L.; Lietti, L.; Forzatti P. J. Phys. Chem. C **(2010)** 114, 1127-1138

[3] A. Setiabudi, M. Makee, J.A. Moulijn, Appl. Catal. B: Environ. 50 **(2004)** 185

[4] K. Nakatani, S. Hirota, S. Takeshima, K. Itoh, T. Tanaka, SAE Paper SP-1674 2002-01-0957.

[5] I. Nova, L. Castoldi, L. Lietti, E. Tronconi, P. Forzatti, Catal. Today 75 **(2002)** 431

4. Results and discussion

4.1 Study of DPNR catalysts for combined soot oxidation and NOx reduction

4.1.1 Introduction

The main pollutants emitted by diesel engine exhausts are nitrogen oxides and soot particles. For this reason, the simultaneous abatement of NO_x and particulates from diesel exhaust gas represents an outstanding issue. The current three-way technology used near stoichiometric conditions is unable to meet upcoming regulations in Europe, United States and Japan. The existing technical solutions involving an exhaust gas recirculation to get an optimal NO_x/particulates compromise by controlling the recirculated gas rate will likely be unable to fulfill the next Euro 6 standard regulation. The implementation of an optimal strategy is not an easy task because a reduction of NO_x induces an increase in particulate emission and reversibly subsequent reduction of particulate matter will induce an increase in NO_x emission. Consequently such a situation implies to reconsider the actual end-of-pipe technologies commercially available combining diesel particulate filter (DPF) and $DeNO_x$ catalysts [1].

Commercial NO_x abatement technologies are actually available. They are essentially developed for heavy-duty vehicles such as the urea selective catalytic reduction (SCR). For light vehicles a competition between SCR and NO_x storage and reduction after-treatment systems exist. In this complex technological context, the development of integrated De-NO_x and De-soot after-treatment technologies have also been proposed. One example is the Diesel Clean Advanced Technology (D-CAT) emission control system recently proposed by the Toyota group. Its Avensis model is equipped with the D-CAT package which includes the DPNR (Diesel PM and NO_x Reduction) system, a combination of a diesel particulate filter with a NO_x adsorber-catalyst [2].The DPNR converter features a newly developed, highly porous ceramic filter coated with a catalyst exclusively developed by Toyota for its NO_x storage reduction catalytic converter (NSR catalysts), initially designed for use with Toyota's lean-burn (high-oxygen) gasoline engines [3].

NSR systems or Lean NO_x traps (LNTs) [4,5,6] are based on the use of a catalyst containing precious metals such as Pt, Pd and Rh for the reduction and oxidation reactions, and alkali or alkaline-earth

metal components such as Ba or K that store NO_x as nitrite and nitrate species [7,8]. Overall, NO_x are reduced to N_2 over NSR catalyst by alternating lean and rich periods, i.e. a lean period of 30-90 s during which the NO_x emitted in the exhaust gases are stored on the catalyst surface, and a short 3-5 s rich period during which the stored NO_x are reduced to N_2 by H_2, CO and unburned hydrocarbons.

Several studies deal with the reactivity and characteristics of Ba containing catalysts (see for example Refs. [9,10,11,12]), but reports on the specific behaviour of K-based catalysts are scarce in the literature, particularly on the reduction step. The reactivity of different reducing agents (e.g. H_2, CO, C_3H_6 and C_3H_8) has been investigated in the case of Ba-containing catalysts; these studies indicate that hydrogen is the most effective reductant for lean NO_x traps [13,14,15,16,17].

In recent papers of various research groups, including ours, mechanistic aspects of the reduction of NO_x stored over Ba-based NSR catalytic systems have been reported when H_2 is used as a reductant [18,19,20]. It has been shown that the reduction by H_2 under near isothermal conditions of NO_x stored onto Pt-Ba/Al_2O_3 (and onto Pt-K/Al_2O_3 as well) is not initiated by the thermal decomposition of nitrates/nitrites ad-species with release of NO_x in the gas phase, but involves a Pt catalyzed surface pathway which is active at low temperature and leads to nitrogen [21,22]. It has also been proposed that under near isothermal conditions N_2 is formed exclusively via a consecutive reaction scheme which involves the fast reaction of H_2 with stored NO_x to give ammonia followed by the slower reaction of ammonia with residual stored NO_x to give N_2 [23]. However, it has been also pointed out that the reaction of ammonia with residual stored NO_x to give N_2 is slower over Pt-Ba/Al_2O_3 than over Pt-K/Al_2O_3.

Soot oxidation over NSR catalyst has been also investigated; various surface compounds such as nitrates and active oxygen generated during storage and reduction steps are proposed as active soot oxidation species and, thereby, decreasing the oxidation temperature. NO_2 produced over noble metals of NSR catalysts can be trapped as nitrates and can also react with soot generating NO again [24]. Under lean conditions NSR system can be expected to function as catalyzed soot filter (CSF). DPNR or NSR catalysts in this respect will have obvious advantages as it can reduce emission of both the pollutants and acts as '4-way' catalyst.

Only a few studies over '4-way' catalytic materials that can store NO_x, such as CeO_2, Ba and K-containing catalysts, for soot oxidation are reported [25]. In our previous works [26,27], it has been shown that soot oxidation occurs during the lean phase only, while NO is being oxidized to NO_2 and nitrites/nitrates are being stored on the catalyst surface. NO_2 is an efficient and well recognized oxidizing agent for soot, but surface nitrates may have a role as well according to that proposed by Makkee et al. [28].

It has been reported that K-promoted catalysts have good activity in the soot possibly due to the high mobility of some K compounds. However, the high mobility causes K to present a technological problem associated with its interaction with the monolith support, and looses due to volatilization and/or stripping by condensed water. For this reason, the stability of the Pt-K/Al_2O_3 catalyst during lean-rich cycles it is an important aspect that needs to be taken to account.

4.1.2 NO_x storage and soot oxidation on Pt-Ba/Al_2O_3 and Pt-K/Al_2O_3 catalysts

In this thesis work the reactivity of model Pt-Ba/Al_2O_3 and Pt-K/Al_2O_3 catalysts in the simultaneous removal of NO_x and soot has been investigated under a variety of experimental conditions (NO concentration, temperature, and particulate loading), performing lean-rich cycles in the presence of water and CO_2.

The results obtained during the lean-rich cycles performed at 350°C over Pt-Ba/Al_2O_3 catalyst have been reported in **Figure4.27** in the absence (A, B) and in the presence of soot (C, D) (see **Paper I**).

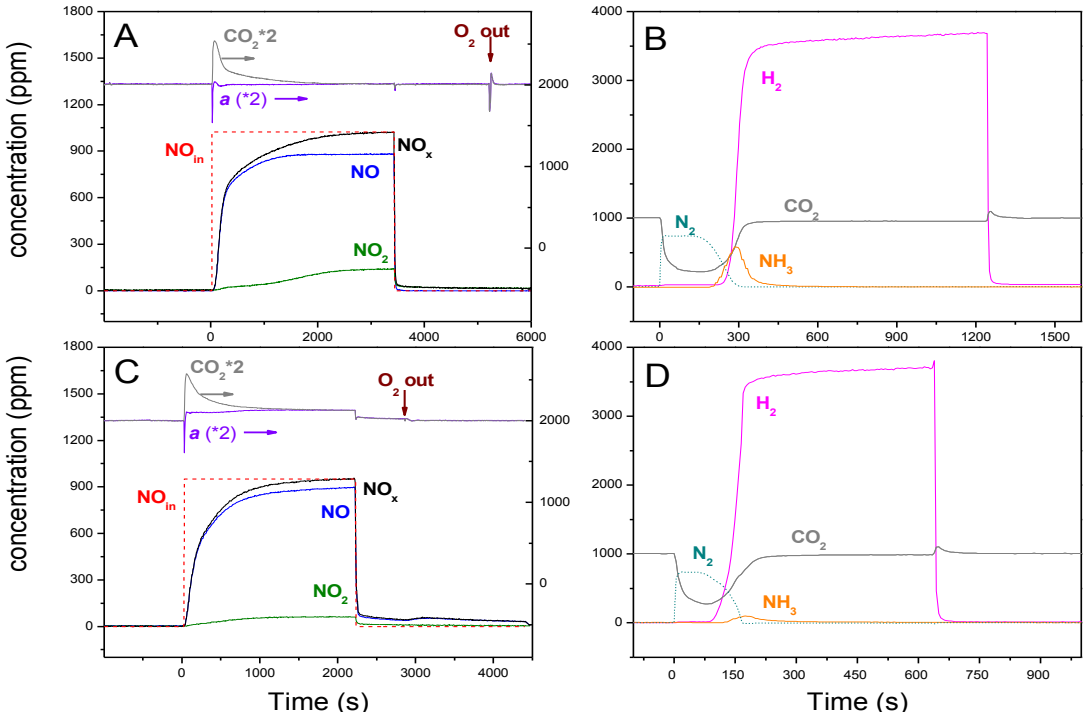

Figure4.27– Storage-reduction cycle performed at 350°C over PtBa/Al_2O_3 (A and B)and Pt–Ba/Al_2O_3-soot mixture (C and D). Trace a is the CO_2 production due to soot oxidation.

In the absence of soot (**Figure4.27**A), upon the NO step addition (at t = 0 s) the NO outlet concentration increases with time, approaching the asymptotic values corresponding to the NO inlet concentration after about 2000 s. Also NO_2 is observed due to the occurrence of the oxidation of NO by O_2 according to the stoichiometry of reaction (1):

$$NO + ½\ O_2 \leftrightarrow NO_2 \qquad (1)$$

During the NO pulse, CO_2 evolution is also observed. This is due to the formation of nitrate species upon NO_x adsorption [29,30], that replace carbonates with release of CO_2 according to the stoichiometry of reaction (2),

$$BaCO_3 + 2\ NO + 3/2\ O_2 \rightarrow Ba(NO_3)_2 + CO_2 \qquad (2)$$

In fact upon subtracting half of the adsorbed NO concentration value (i.e. ½ (NO_{IN} – NO_{out})) to the actual CO_2 concentration curve, a flat CO_2 trace is obtained (trace ***a*** of **Figure4.27**A).
Finally, upon NO shutoff, a tail is observed in the NO and NO_2 concentrations due to the desorption of weakly adsorbed NO_x species, whose release is favored by the decrease in the NO_x partial pressure.
In presence of soot (**Figure4.27**C), the evolution of NO and NO_2 are qualitatively similar to those observed for the soot-free catalyst.

An increase in the CO_2 outlet concentration is also observed. It results from two contributes: one is related to the decomposition of carbonates on the catalytic surface due to nitrates formation (in line with reactions (2)-(3)), and the other is due to soot combustion.

$$BaCO_3 + 3\ NO_2 \rightarrow Ba(NO_3)_2 + NO + CO_2 \qquad (3)$$

As in the absence of soot, upon NO shutoff, a release of NO and NO_2 takes place due to the desorption/decomposition of the NO_x species previously stored. Upon switching off the O_2 feed, additional NO_x are also desorbed. Both desorption contributions appear to be remarkable if compared to those observed in the case of the soot-free catalyst: this indicates that soot has a destabilizing effect on the nitrate species adsorbed onto the catalytic surface. The reasons for the destabilizing effect of soot on the stored nitrates are not yet fully understood; one can speculate that nitrates species, which are considered mobile on the catalytic surface [30], may directly interact with soot particles leading to its oxidation.

The results obtained during the lean NO_x adsorption over the Pt-Ba/Al_2O_3-soot mixture (Figure4.27C) showed that the presence of soot decreased the NO_x storage capacity of the catalyst; in particular the presence of roughly 10% w/w of soot decreased by nearly 30% the amounts of stored NO_x with respect to the soot-free catalyst. Moreover soot leads to an appreciable decrement of the rate of NO_x adsorption: these effects are seen also at different temperatures (200-350°C, see **Paper II**) and when different values of the NO inlet concentration (250-1000ppm, see **Paper II**) are used in the experiments, as clearly reported in**Errore. Non è stato specificato un nome segnalibro.** Figure4.2 and Figure 4.29 that show the amount of stored NOx in function of time in the absence (dotted lines)and in the presence of soot (solid lines) at the different temperature (Figure 4.28) and NO inlet concentration (Figure 4.29).

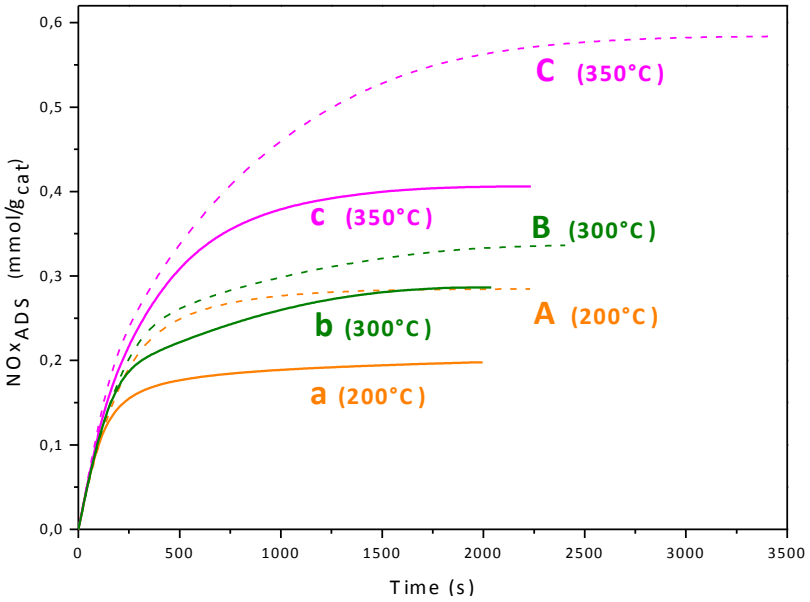

Figure 4.28 Amounts of adsorbed NOx versus time over PtBa/Al_2O_3 (dotted lines) and over PtBa/Al_2O_3/soot mixture (solid lines) at different temperatures

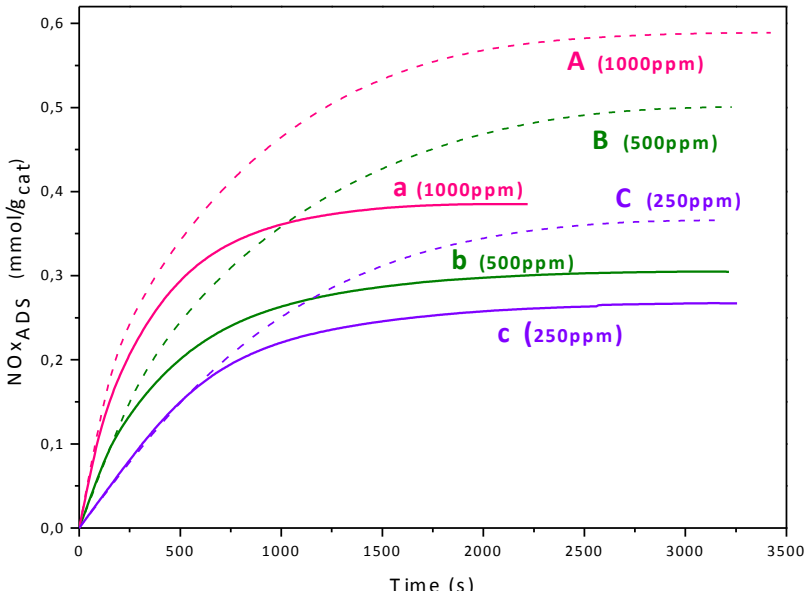

Figure 4.29 Amounts of adsorbed NOx versus time over PtBa/Al_2O_3 (dotted lines) and over PtBa/Al_2O_3/soot mixture (solid lines) at different NO inlet concentrations.

During NO_x storage (**Figure4.27** A, C), soot oxidation occurs also thanks to the presence of NO_2 formed upon NO oxidation over Pt sites. In fact the NO_2 concentration at the reactor outlet in the presence of soot is significantly lower than that observed in the absence of soot, thus pointing out the involvement of NO_2 in soot oxidation. The decrease of the NO_2 concentration may explain also the observed decline in the NO_x storage properties of the catalyst. In fact, in line with the occurrence of a "nitrate" pathway for the storage of NO_x (i.e., NO oxidation to NO_2 followed by NO_2 adsorption in the form of nitrates via a disproportion reaction), Ba and soot compete for reaction with NO_2, as suggested by Sullivan et al. [31], leading to the observed decrease in the NO_x storage properties.

The reactivity and the thermal decomposition of nitrates has been investigated by TPD (**Figure** 4.30)/TPO experiments in the presence and in the absence of soot (see **Paper I-III**).

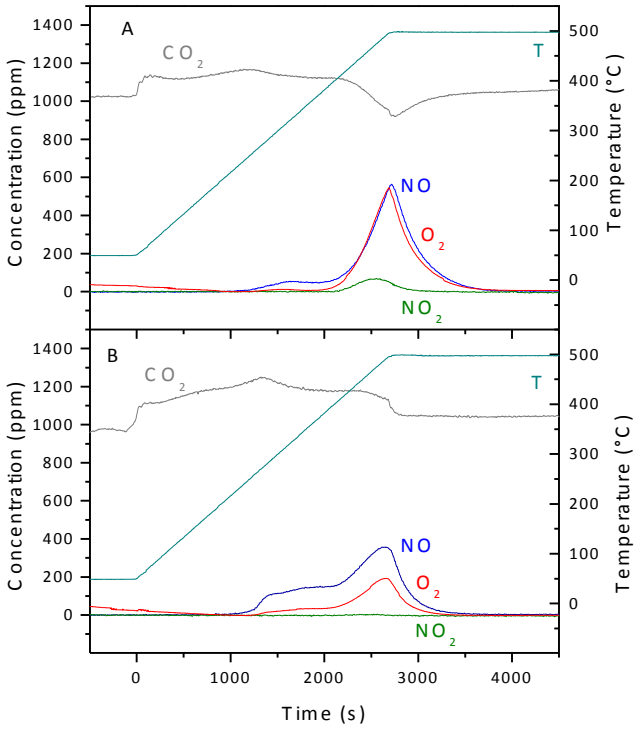

Figure 4.30. TPD run after NOx adsorption at 350 ◦C (1000ppm NO+O_2 (3%, v/v) in He+H_2O(1%, v/v) + CO_2 (0.1%, v/v)) over (A) PtBa/Al_2O_3 catalyst; (B) PtBa/Al_2O_3/soot mixture

It has been observed that the adsorbed NO_x oxidize soot at temperature well below those corresponding to their thermal decomposition originating NO_2 in the gas phase.

It has been found that the presence of soot favors the decomposition and the reduction of the stored nitrates, while soot is oxidized. In fact the presence of soot shifts the decomposition/reaction of the stored nitrates at lower temperatures, and the stoichiometry of the released products reflects the occurrence of a partial reduction of the initially stored NO_x, as well as the oxidation of soot. Hence a direct reaction between the stored nitrates and soot has been suggested, that has been explained on the basis of the surface mobility of the adsorbed nitrates, soot particles being the driving force for the process acting as reduced centers. This soot oxidation pathway involves surface species and parallels the NO_2-soot oxidation that occurs in the presence of gas-phase NO_2. . These surface reactions do not require the presence of the noble metal (Pt) that they occur also in the case of the Ba/Al_2O_3 catalyst sample as well. As expected, it is favored by the contact between the nitrates and soot. In fact when nitrates are stored onto the soot, the nitrate/soot reaction is monitored at lower temperatures (see **Paper III** for the details).

De-NO_x and De-soot activity has been also investigated over a model Pt-K/Al_2O_3 by performing lean-rich cycles at constant temperature. These results were compared to the one obtained with Pt-Ba

/Al_2O_3 catalyst in order to underline analogies and differences and asses the role of the storage component in both NO_x abatement and soot combustion (**Papers IV-V**).

The Pt-K/Al_2O_3 (Pt 1%; K 5.4% wt/wt) catalyst used for this study has been characterized in comparison with 1% Pt/Al_2O_3 catalyst (**Paper VI**). IR spectra of adsorbed CO at −140 ◦C and at room temperature allowed the detection of oxidized Pt centers and of their very strong oxidizing ability. TPD and IR spectra of adsorbed CO_2 allowed to characterize the basicity of the samples.

The data indicate that the presence of K in Pt-K/Al_2O_3 catalyst seems to increase the reducibility of Pt, whose highly oxidizing species are not observed after outgassing at 350 °C. Additionally, the basicity of K/Al_2O_3 increases the electron density on reduced Pt, as evidenced by the slightly lower CO stretching frequency of Pt carbonyls.

Pt species are located near the basic oxide species of the K/Al_2O_3 'support' and their behavior is influenced by the presence of adsorbed carbonate species.

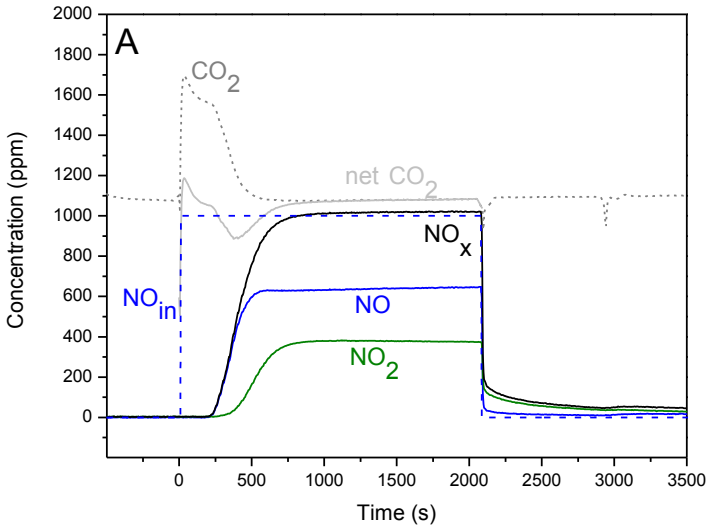

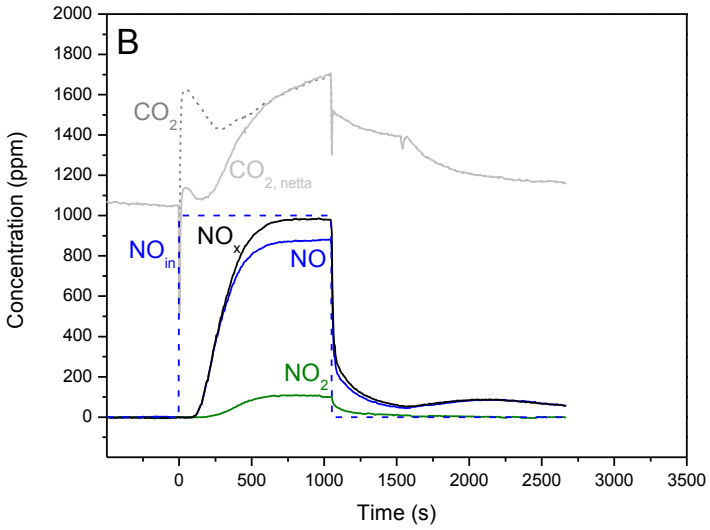

Figure 4.31 NO (100ppm)/O2(3%) adsorption over Pt-K/Al_2O_3 (A) and Pt-K/Al_2O_3/soot (B)in presence of water 1% and CO_2 0.1% at 350°C

Figure 4.5 shows the results of a typical NO_x adsorption at 350°C in the absence and in the presence of soot, respectively (Figure 4.31.A and B). In the absence of soot (Figure 4.31.A) upon NO step addition at t = 0 s the NO_x outlet concentration presents a delay of about 200 s, while the evolution of NO_2 is seen starting from 250 s. The outlet concentrations of both NO and NO_2 increase with time and eventually reach a steady state level indicating that saturation of the catalyst surface with NO_x is attained. CO_2 evolution is also observed during the lean phase, due to the formation of nitrates that replace surface carbonates.

When the NO_x storage is carried out in the presence of soot (Figure 4.31B), significant differences are apparent. The NO_x dead time is reduced (to ca. 90 s) and the amounts of NO_x stored up to steady-state are lower than those measured in the absence of soot (0.38 vs 0.58 mmol/g_{cat}) indicating a reduction in the storage capacity of the catalyst. Besides, a much higher production of CO_2 is observed, indicating the occurrence of the soot oxidation. The NO_2 concentration is significantly lower than in the absence of soot because of to the participation of NO_2 in soot oxidation. Notably, upon NO and O_2 shutoff, a release of NO_x takes place due to the desorption/decomposition of the NO_x previously stored indicating a destabilizing effect of soot on the stored NO_x.

ISC experiments have been performed in similar condition varying the reaction temperature in the range 250-350°C. It is observed that the NO_x storage behavior of the catalyst is affected by the temperature: the NO_x breakthrough and the amounts of NO_x stored up to steady state increase with temperature. Also the NO_2 concentration measured at the reactor outlet at the end of the NO_x dose

(i.e. at steady-state) increases with temperature. In fact under our experimental conditions NO_2 formation is far from chemical equilibrium and the observed increase with temperature of the NO_2 concentration is hence expected being the reaction kinetically controlled. Accordingly, the NO/NO_2 molar ratio calculated at the end of the storage phase decreases with temperature.

Temperature also affects the rate of NO_x adsorption that increases with T, as observed in the case of Pt-Ba/Al_2O_3 catalysts as well. A direct comparison between the amounts of NO_x stored at steady-state on the Pt-K/Al_2O_3 and Pt-Ba/Al_2O_3 catalyst samples is shown in **Figure 4.32**. (**Paper IV**)

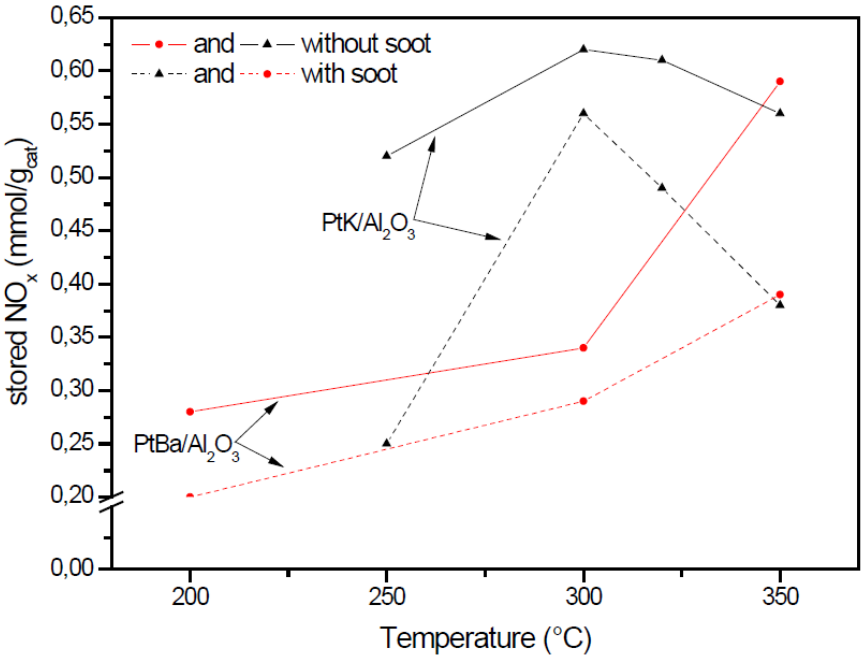

Figure 4.32 Amounts of stored NO_x versus time over Pt-K/Al_2O_3 and Pt-Ba/Al_2O_3 catalysts (A) in the absence of soot and (B) in the presence of soot

It appears that the amounts of NO_x stored on Pt-K/Al_2O_3 are higher than those on Ba-based catalyst, although at 350°C the storage capacity of the two catalysts is very similar,both in presence (solid lines) and in the absence of soot (dotted lines). Finally, the amounts of NO_x desorbed upon NO shutoff are higher over Pt-K/Al_2O_3 than over Pt-Ba/Al_2O_3. These results show that the presence of soot affects the NO_x storage capacity and the stability of the adsorbed species of both samples.

In order to investigate more in details the effect of the soot loading on the catalyst behaviour, and the stability of the Pt-K/Al_2O_3 upon repeated soot oxidation cycles, several lean-rich cycles have been carried out over the same sample. For this purpose a sequence of NO_x adsorption and reduction cycles (6-7 cycles) has been performed in the presence of soot over a fresh Pt-K/Al_2O_3 at 350°C until the complete consumption of soot (run 1); after that, the clean catalyst has been mixed

again with soot and has been again cycled under the same experimental conditions until complete soot oxidation (Run 2). This procedure has been repeated three times.

The data point out that ageing the LNT Pt-K/Al_2O_3 catalyst by repeated soot oxidation cycles, the NO_x storage capacity decreases; indeed, the amount of NO_x stored on aged Pt-K/Al_2O_3 catalyst (i.e. clean catalyst) is lower than that on the fresh catalyst.

The NO/NO_2 molar ratio strictly depends on the soot present; the amount of soot decreases the ratio decreases since NO_2 is not involved in the soot combustion. Notably, the same NO/NO_2 molar ratio is calculated on the fresh and aged catalyst, indicating the ageing process does not involve Pt sites.

The observed decrease in soot oxidation activity over aged K-containing catalyst can be attributed to the volatile nature of K-active species, like nitrates (melting point 334°C) [32,33]. The mobility of such compounds is expected to be high, leading to good contact with soot and bringing an additional activity. The degradation of catalyst should be due to the sublimation of K during soot combustion [34]. The loss of K have as consequence a lower amount of storage sites; accordingly, the storage capacity of system decreases and a lower amount of K-nitrates are available to oxidize soot.

4.1.3 NO_x reduction on Pt-Ba/Al_2O_3 and Pt-K/Al_2O_3 catalysts

The reduction of the stored NO_x on Pt-Ba/Al_2O_3 has been reported in **Figure4.27** in the absence (B) and in presence of soot (D). This process is not significantly affected by the presence of soot, although some minor changes in the N_2 selectivity (a slight increase in the presence of soot) have been observed.

In both cases, upon H_2 admission, the H_2 outlet concentration profile shows a dead time during which it is completely consumed to give at first N_2 and NH_3 later on, according to the overall stoichiometry of reactions (4) and (5):

$$Ba(NO_3)_2 + 5\ H_2 + CO_2 \rightarrow BaCO_3 + N_2 + 5\ H_2O \quad (4)$$

$$Ba(NO_3)_2 + 8\ H_2 + CO_2 \rightarrow BaCO_3 + 2\ NH_3 + 5\ H_2O \quad (5)$$

In line with the stoichiometry of reaction (4), upon admission of 4000 ppm H_2 the N_2 outlet

concentration immediately increases to the level of 800 ppm; then NH_3 formation is observed in correspondence of the decrease of the N_2 trace, at the end of the reduction. Slightly after the NH_3 breakthrough the H_2 concentration trace increases up to the inlet concentration value.

According to previous studies of our group [35,36] the reduction of stored nitrates by H_2 occurs via a two-step molecular pathway which involves a first step leading to the formation of NH_3, followed by the slower reaction of ammonia with residual nitrates to form N_2:

$$3\ Ba(NO_3)_2 + 10\ NH_3 + CO_2 \rightarrow 3\ BaCO_3 + 8\ N_2 + 15\ H_2O \quad (6)$$

The sum of reactions (4) and (5) accounts for the overall stoichiometry of reduction of nitrates with hydrogen to give N_2 (reaction 6). Notably, the temporal evolution of reduction products, with nitrogen being detected at the reactor outlet first and ammonia later, is in line with the integral behaviour of the catalytic bed [35,21]. In fact upon regeneration a hydrogen front travels along the catalyst bed. NH_3 is formed at the H_2 front upon reaction of H_2 with the stored NO_x; the formed NH_3 then reacts with NO_x stored downstream the H_2 front, leading to the formation of N_2. When the front reaches the end of the catalytic bed, there are no NO_x stored downstream and this leads to the evolution of ammonia, which follows that of N_2.

During the reduction phase, a CO_2 uptake has also been observed due to the formation of carbonates onto the Ba sites on which NO_x were previously stored; finally, after NO_x reduction, the formation of small amounts of CO is also observed due to the occurrence of the inverse water gas shift (RWGS) reaction (8):

$$CO_2 + H_2 \leftrightarrow CO + H_2O \quad (7)$$

Calculation showed that the reaction is limited by thermodynamic constraints; the relevance of this reaction appears to be limited by the presence of water in the feed [35].

Finally mechanistic aspects involved in the formation of N_2 and N_2O during the reduction of NO_x stored over the model $PtBa/Al_2O_3$ NSR catalyst have been investigated by means of isotopic labeling experiments. A combined use of MS, UV-Vis and GC analysis has been adopted allowing the complete quantitative analysis of the reaction products. The reduction of the stored labelled nitrites species (Figure4.34Figure 3.33) with $^{14}NH_3$ leads to the selective formation of N_2 since only very small amounts of nitrous oxide have been observed in the reduction of nitrites only.

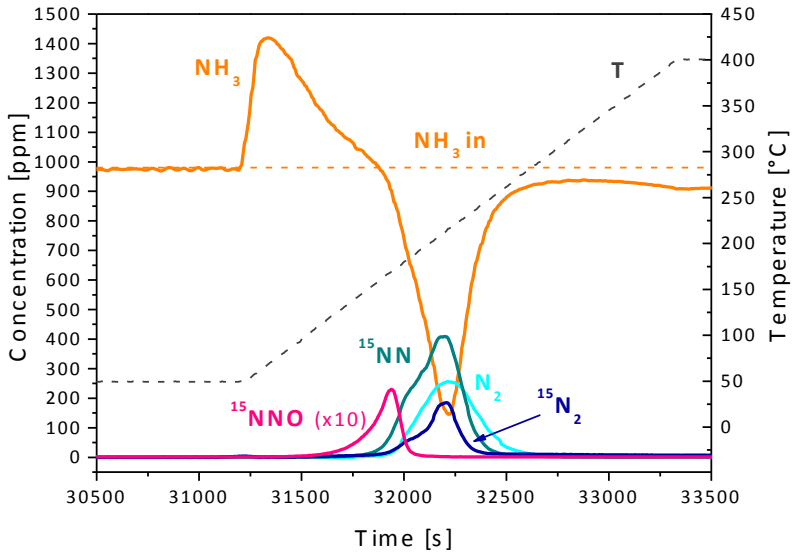

Figure 3.33 - TPSR run with NH_3 (1000ppm) after $^{15}NO_x$ adsorption at 150°C (1000 ppm ^{15}NO + O_2 3% v/v in He) over Pt-Ba/Al_2O_3 catalyst

The observed N_2 isotopic distribution includes all possible N_2 isotopes, i.e. $^{15}N_2$, $^{14}N_2$ and the mixed $^{15}N^{14}N$ species. Based on the pathway suggested for NO and NH_3 reaction on Pt-based catalysts, it has been found that the observed product distribution can be explained on the basis of the statistical coupling of ^{15}N- and ^{14}N-adatoms originated upon NH_3 and NO_x decomposition on Pt. However the simultaneous occurrence of a SCR-like pathway, involving the formation and decomposition of a NH_x-NO intermediate originating from ammonia and NO_x, and leading to the selective formation of the mixed $^{15}N^{14}N$ species is also likely. In fact at the early stages of the reduction of stored labeled nitrites with unlabeled ammonia the reduction process is selective towards the formation of the mixed $^{15}N^{14}N$ isotope, suggesting the occurrence of a SCR-like pathway.

Similar results have been obtained upon reduction of the stored labelled nitrates by $^{14}NH_3$ ((Figure 4.36). The formation of all nitrogen isotopes is seen although in this case the abundance of the double labeled $^{14}N_2$ isotope is similar to that of the $^{15}N^{14}N$ species. Hence also in the case of the stored nitrates the route for nitrogen formation involves the statistical coupling of the ^{14}N- and ^{15}N-containing reactants, along the pathways already suggested above for nitrites reduction.

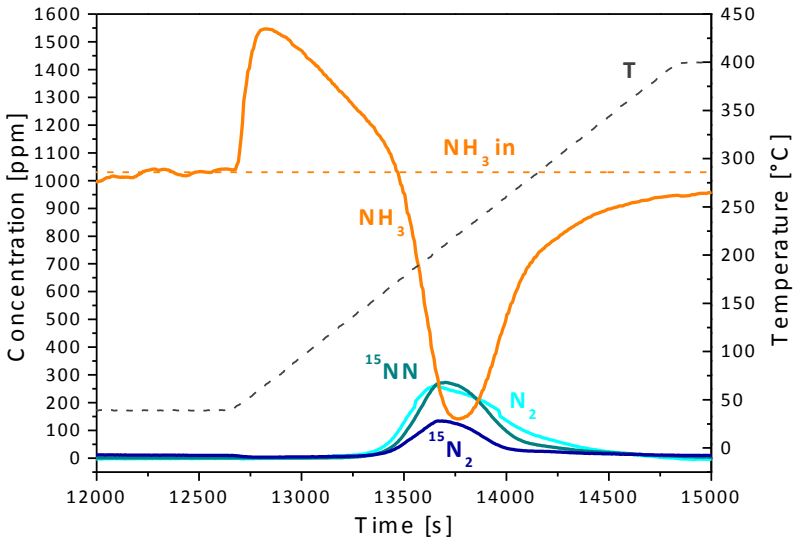

Figure4.34 TPSR run with NH_3 (1000ppm) after $^{15}NO_x$ adsorption at 350°C (1000 ppm ^{15}NO + O_2 3% v/v in He) over Pt-Ba/Al_2O_3 catalyst

Isotopic labeling experiments also provide indications on the pathways involved in the formation of N_2O. This species is formed in very limited amounts during the reduction by ammonia of stored NO_x species (nitrites and nitrates); much higher quantities have been observed during the reduction of gaseous ^{15}NO with NH_3. Since no formation of unlabeled nitrous oxide has been observed, the participation of ^{15}NO is necessary for the formation of nitrous oxide. In line with literature proposals, it has been suggested that nitrous oxide formation involves (on the Pt sites) either the coupling of two adsorbed NO molecules or the recombination of an adsorbed NO molecule with an adsorbed NHx fragment. Accordingly, N_2O formation is greatly enhanced in the presence of gas- phase NO. Temperature also drives the selectivity to nitrous oxide. This product is favored at low temperature and is likely related to the oxidation state of Pt: at high temperatures Pt is kept in a reduced state by ammonia, and this would favor NO dissociation on the Pt sites thus preventing N_2O formation. Besides, N_2O could be reduced to N_2. The presence of oxygen in the feed stream favors N_2O formation, since it increases the concentration of molecularly adsorbed NO species and inhibits N_2O reduction. The route involving the coupling of NO-ad-species is however inhibited by the presence of oxygen, and hence nitrous oxide formation involves adsorbed NO and NH_x fragments.

Furthermore the reduction of NO_x stored at 350 °C onto the Pt-K/Al_2O_3 LNT catalyst has been deeply investigated under dry conditions by using CO as reductant that allows the formation of stable intermediates useful to identify the reaction pathways.

The results collected during CO TPSR over K/Al_2O_3 and over Pt-K/Al_2O_3 highlight that, in the presence of Pt, the reduction of nitrate species by CO is faster considering that the onset temperature of the reaction is lower (~210 vs 340 °C), and the conversion of CO is higher. Besides, it appears that the reduction does not require as a first step the thermal release of NO_x in the gas phase because the reaction is seen at temperatures well below that of the thermal decomposition of adsorbed NO_x.

The results collected during the CO-ISC experiment over Pt-K/Al_2O_3 (**Figure 3.35**) are in line with the results of CO-TPSR experiments.

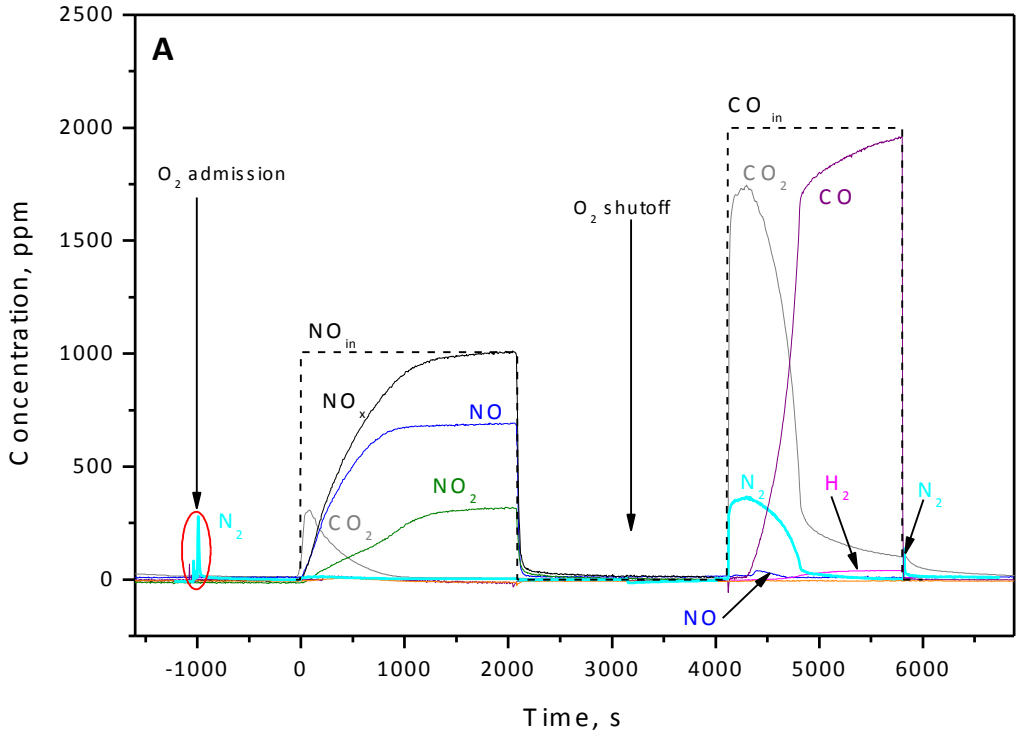

Figure 3.35 ISC experiments at 300 °C over the Pt-K/Al2O3 catalyst (storage phase, NO 1000 ppm + O2 3% v/v in He; reduction phase, CO 2000 ppm in He).

It is shown that the admission of 3% v/v O_2 causes the evolution of a small amount of N_2, produced by the oxidation of surface N-containing species that remain adsorbed at the catalyst surface after the previous reduction with CO. Upon the NO step addition (at t = 0 s), NO and NO_2 show a dead time and then their concentration rapidly increases with time, approaching the asymptotic concentrations corresponding to the NO_x feed concentration (NO + NO_2) after about 2000 s. Accordingly, significant amounts of NO_x were stored. Formation of NO_2 in the gas phase indicates that Pt is active in the NO oxidation reaction; as indicated in a dedicated FT-IR analysis, nitrates are the major adsorbed species present after adsorption in NO/O_2 at 300 °C.

Upon admission of CO, ~360 ppm N_2 and ~1730 ppm CO_2 are immediately produced, together with negligible amounts of NO (30 ppm). CO is completely consumed for about 200 s; afterward, CO is detected at the reactor outlet: its concentration increases and approaches the inlet value. After CO breakthrough, the N_2 and CO_2 concentrations (and NO production) decrease. When the nitrogen concentration is close to zero (i.e., when stored NO_x are almost depleted), H_2 production isobserved. When the CO feed is stopped (after 1700 s from the CO admission), a small amount of nitrogen is produced, along with CO_2.

The reduction by CO under nearly isothermal conditions of nitrates stored onto the Pt-K/Al_2O_3 catalyst at high temperature (300 °C) occurs according to a Ptcatalyzed surface pathway, has already demonstrated at low-temperature for the reduction by H_2 of NO_x stored over the same catalyst used in this study,leading mostly to nitrogen. Hydrogen is more effective than CO because the onset temperature of the reduction is lower (120 vs 210 °C). The same conclusions apply to a Pt-Ba/Al_2O_3 catalyst, as reported before [15,37] and this suggests that the reduction of stored NO_x with H_2 and with CO over LNT catalysts might present analogies that are worth being investigated.

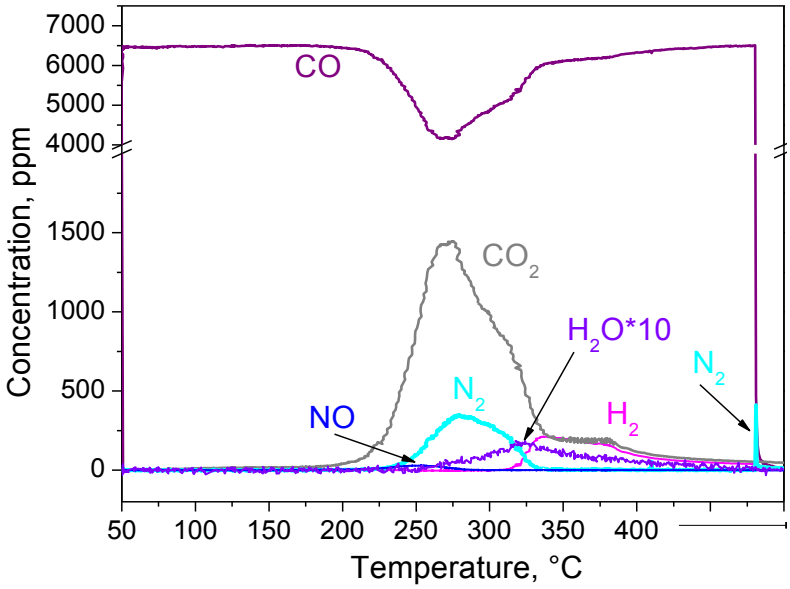

Figure 4.36 CO-TPSR (6500 ppm CO in He) after NO/O2 adsorption at 350 °C over the Pt-K/Al2O3 catalyst.

The results of CO-TPSR (**Figure 4.36**) and CO-ISC experiments over Pt-K/Al_2O_3 and of the complementary FTIR study indicate that the reduction by CO of nitrates stored onto the Pt-K/Al_2O_3 catalyst under dry conditions occurs according to the stoichiometry of the following overall reactions:

$$2KNO_3 + 5CO \rightarrow K_2CO_3 + N_2 + 4CO_2 \quad (8)$$

$$2KNO_3 + 8CO \rightarrow 2KNCO + 6CO_2 \quad (9)$$

Reactions 8 and 9 account for the consumption of CO and of nitrates, and for the formation of CO_2. In particular, reaction 9 accounts for the consumption of nitrates with the formation of isocyanates (revealed by FT-IR) and CO_2; reaction 8 accounts for the formation of N_2, CO_2, and carbonates at the catalyst surface, as revealed by FT-IR. The formation of isocyanates and carbonates at the surface explains the fact that the N balance and the C balance in the gas phase is far from 100% at the end of the CO-TPSR experiment. In particular, reaction 8 does not occur in the low-temperature range (210-250 °C) where N_2 is not detected. FT-IR spectra reveal also that bidentate nitrates stored onto the catalyst surface are reduced at first and ionic ones start to be reduced later on, i.e. the ionic nitrates result more resistant to the CO reduction.

Similar results have been obtained when H_2 was used as a reductant instead of CO; [38, 39] also, in that case, FT-IR measurements put in evidence a different reactivity between ionic and bidentate nitrates toward H_2. These features agree well with TPSR data where two contributions of reductant

(H_2 and/or CO) consumption are apparent. The data are consistent with the reaction pathway already proposed for N_2 formation in the case of Pt-Ba/Al_2O_3 [37,40]: large amounts of NCO species are left at the catalyst surface after reduction of CO under dry conditions; these species can be oxidized to give N_2 during the subsequent lean phase either by oxygen or by NO + O_2, NO_2, surface nitrites, and/or surface nitrates. N_2 is formed primarily according to an in-series two-step process, where NCO species are formed first and then are converted to nitrogen upon reaction with NO_x stored species. In analogy with the reaction pathway for the reduction by CO of nitrates stored over Pt-Ba/Al_2O_3 under dry conditions, the reduction by CO of nitrates stored onto the Pt-K/Al_2O_3 catalyst occurs according to the stoichiometry of the following overall reactions (9) and (10)

$$6KNO_3 + 10KNCO \rightarrow 8N_2 + 8K_2CO_3 + 2CO_2 \quad (10)$$

Hence, NCO species are considered intermediates in the formation of N_2, whose formation occurs exclusively according to the stoichiometry of the reactions (9) and (10) the sum giving the overall reaction(8). Besides, analogies could be found for both the catalytic systems also with the reduction of stored nitrates by H_2, where the in-series two-step molecular pathway prevously reported, has been proposed for N_2 formation [**Errore. Il segnalibro non è definito.**, 38, 40] The following overall reactions are involved:

$$2KNO_3 + 8H_2 \rightarrow 2NH_3 + KOH + 4H_2O \quad (11)$$

$$6KNO_3 + 10NH_3 \rightarrow 8N_2 + 6KOH + 12H_2O \quad (12)$$

In the case of reduction by CO, NCO ad-species play as intermediates in the reduction instead of NH_3. The reduction by CO of NO_x stored over Ba- and K containing catalysts shows slightly distinct features. Over Pt-Ba/Al_2O_3, only ionic nitrates were observed, giving during the CO reduction two FT-IR bands at 2222 and 2164 cm^{-1} related to NCO species, whereas both bidentate and ionic nitrates are present on Pt-K/Al_2O_3 and mainly the band at 2225 cm^{-1} is detected.

The CO-TPSR experiment over Pt-Ba/Al_2O_3 has shown [37, 40] that the reaction of surface nitrates to give nitrogen is slower than that responsible for the initial reduction of nitrates to give NCO species. The formation of nitrogen in this case via the reduction of nitrates by CO is explained as the sum of the reduction of nitrates by CO to give surface NCO species and the subsequent oxidation of these species by surface nitrates to give nitrogen. Also, in the case of Pt-K/Al_2O_3, the reaction of surface nitrates to give nitrogen seems to be slower than that responsible for NCO species formation. In fact, the formation of nitrogen is observed only above 250 °C, while evidence for the formation of N-

containing species from 210 °C is provided by the consumption of CO and by the simultaneous evolution in the gas phase of CO_2 with no N-containing species. Accordingly, FT-IR measurement shows that isocyanates are formed and their storage on the surface is higher at the low temperatures. However, in this case, the reaction between surface nitrates and surface NCO species to give nitrogen is faster and more efficient than over the Ba-containing system. The reason for the higher NO_x reduction efficiency to N_2 pointed out by the Pt-K/Al_2O_3 catalyst may be related to the higher mobility of the adsorbed surface species. It has been speculated that the reduction of the stored NO_x implies the surface mobility of these species toward Pt, where they are reduced by the reductant [39].In the case of CO as a reductant, isocyanate species are formed as intermediates. In the suggested pathway of the reduction of stored NO_x by CO, the ratedetermining step is the slow reaction between nitrates and isocyanates, which involves two surface species. It is known that K-nitrates have a melting point lower than that of Ba-nitrates (334 vs 592 °C). Along this line, K-nitrates might have a higher surface mobility that facilitates their spillover from the K component onto the Pt particles and, as a consequence, their reaction with K-NCO species. As a result, the CO reduction is more efficient over the Pt-K/Al_2O_3 catalyst than over the Pt-Ba/Al_2O_3 catalyst.

4.2 NO Oxidation on dispersed oxides of Rhodium and Cobalt

4.2.1 Introduction

Nitrogen oxides must be removed from combustion exhaust to meet environmental regulations, which is challenging for streams that contain O_2 and low concentrations of CO and hydrocarbons. Catalyst sites are titrated by strongly-bound chemisorbed oxygen atoms (O*) during NO decomposition in the absence of reductants. As a result, open sites on O*-saturated surfaces, required for NO dissociation, are scarce [41]. Such conditions cause low NO conversions to N_2 and favor instead NO oxidation to NO_2. NO_2, however, adsorbs on metal oxides [42] and reduces to N_2 when soot or hydrocarbons are present in exhaust streams [43,44]. These reactions provide an alternate abatement strategy for NO removal from lean-burn effluent streams, but require effective catalysts for NO oxidation to NO_2.

4.2.2 Main Results

Kinetic experiments were carried out to study the effect of NO, O_2, and NO_2 pressures on turnover rates and isotopic tracers were implied to measure the $^{16}O_2$-$^{18}O_2$ exchange rates.

It was observed that on both catalysts, NO oxidation rates were first-order in NO and O_2 and inversely proportional to NO_2 pressure, as also observed on Pt and PdO. (Fig. 9)

A

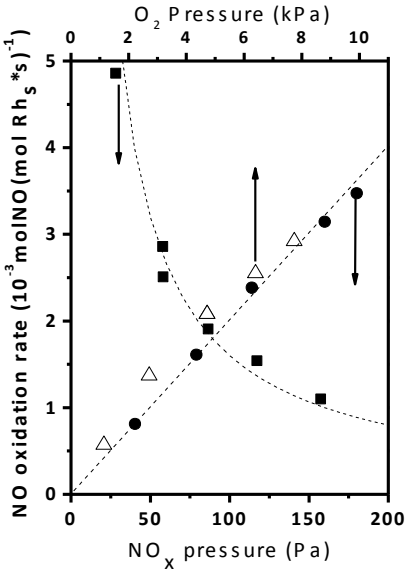

B

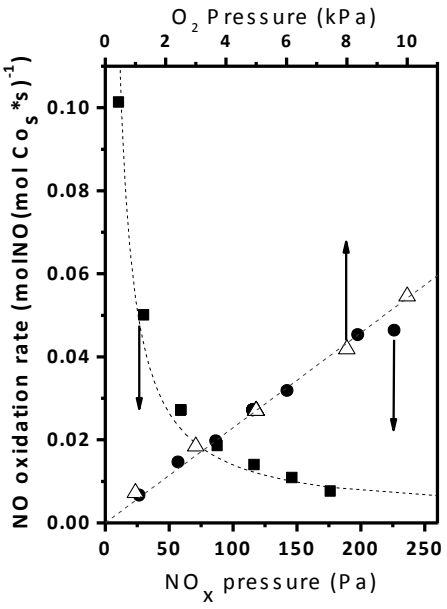

Figure 4.9. NO oxidation rates **(a)** on 2.4% wt. RhO_2/Al_2O_3 (573 K; 0.47 H / Rh) versus (●) NO pressure (at 0.055 kPa NO_2; 5 kPa O_2); (■) NO_2 pressure (at 0.11 kPa NO, 5 kPa O_2); and (△) O_2 pressure (at 0.11 kPa NO, 0.055 kPa NO_2) and **(b)** on 10% wt. Co_3O_4/SiO_2 (548 K; 0.02 H / Co_r) versus (●) NO pressure (at 0.060 kPa NO_2; 5 kPa O_2); (■) NO_2 pressure (at 0.12 kPa NO, 5 kPa O_2); and (△) O_2 pressure (at 0.12 kPa NO, 0.06 kPa NO_2).

These data suggest O_2 activation on isolated vacancies (*) on surfaces of Rh and Co oxides saturated with oxygen (O*) is the sole kinetically-relevant step. Quasi-equilibrated NO-NO_2 interconversion steps establish oxygen chemical potentials (and O* and * coverages) on these oxides during catalysis. These chemical potentials determine the oxidation state of Rh and Co clusters and are rigorously described by the prevalent O_2 virtual pressures (equals the value of the O_2 pressure that gives the same equilibrium O* coverage as a particular NO-NO_2 mixture), which are estimated using the formalism of nonequilibrium thermodynamics. RhO_2 and Co_3O_4 are the prevalent phases present during NO oxidation catalysts at relevant conditions. Turnover rates increased with increasing cluster size because vacancies, required for kinetically-relevant O_2 activation steps, are more abundant on large clusters, which delocalize electron density more effectively than small oxide clusters. NO oxidation turnover rates on RhO_2 and Co_3O_4 are higher than expected from the oxygen binding energy on Rh and Co metal surfaces or from the reduction potentials of Rh^{3+} and Co^{2+}. NO oxidation rates fall in line with those measured on Pt and PdO when one-electron reductions processes, accessible for Rh^{4+} and Co^{3+} but not for Pt^{2+} and Pd^{2+}, are used to describe the reactivity of RhO_2 and Co_3O_4. Such one-electron redox cycles also cause $^{16}O_2$-$^{18}O_2$ exchange rates to be much larger than

NO oxidation rates, in contrast with their similar values on Pt and PdO, though O_2 activation on vacancies limits both NO oxidation and O_2.

These data and their interpretation in terms of elementary steps, the role of vacancies in kinetically-relevant O_2 activation steps, and the consequent higher reactivity of larger clusters provide a common framework to describe NO oxidation and the active species on catalysts of practical interest.

[1] P. Granger, V.I. Parvulescu, Chem. Rev. 111 (2011) 3155–3207

[2] M. Hiroki, S. Tatsumasa, Y. Shunsuke, T. Masato, O. Hisashi, O. Seiji, Toyota Tech Rev 52 (2002) 66-71

[3] Toyota Patent, European Patent Application No 01107629.6 (2001)

[4] Takahashi, N.; Shinjoh, H.; Iijima, T.; Suzuki, T.; Yamazaki, K.; Yokota, K.; Suzuki, H.; Miyoshi, N.; Matsumoto, S.; Tanizawa, T.; Tanaka, T.; Tateishi, S.; Kasahara, K.; Catal. Today **1996**, 27, 63-69

[5] Epling, W.S.; Campbell, L.E.; Yezerets, A.; Currier, N.W.; Parks, J.E. Catal. Rev. – Sci. Eng. **2004**, 46, 163-245

[6] Shinojh, H.; Takahashi, N.; Yokota, K.; Sugiura, M. Appl. Catal. B: Environ. **1998**, 15, 189-201

[7] Takeuchi, M.; Matsumoto, S.I. Top. Catal. **2004**, 28, 151-156

[8] Konsolakis, M.; Yentekakis, I.V. Appl. Catal. B: Environ. **2001**, 29, 103-113

[9] Mahzoul, H.; Brilhac, J.F.; Gilot, P. Appl. Catal. B: Environ. **1999**, 20, 47-55

[10] Prinetto, F.; Ghiotti, G.; Nova, I.; Lietti, L.; Tronconi, E.; Forzatti, P. J. Phys. Chem. B **2001**, 105, 12732-12745

[11] Lietti, L.; Forzatti, P.; Nova, I.; Tronconi, E. J. Catal. **2001**, 204, 175-191

[12] Nova, I.; Castoldi, L.; Prinetto, F.; Ghiotti, G.; Lietti, L.; Tronconi, E.; Forzatti, P. J. Catal. **2004**, 222, 377-388

[13] Poulston, S.; Rajaram, R. Catal. Today **2003**, 81, 603-610

[14] Liu, Z.; Anderson, A. J. Catal. **2004**, 228, 243-253

[15] Jozsa, P.; Jobson, E.; Larsson, M. Top. Catal. **2004**, 30, 177-180

[16] James, D.; Fourre, E.; Ishii, M. Appl. Catal. B: Environ. **2003**, 45, 147-159

[17] Abdulhamid, H.; Fridell, E.; Skoglundh, M. Top. Catal. **2004**, 30, 161-168

[18] Lietti, L.; Nova, I.; Forzatti, P. J. Catal. **2008**, 257, 270-282

[19] Nova, I.; Lietti, L.; Forzatti, P. Catal. Today **2008**, 136, 128-135

[20] Forzatti, P.; Lietti, L.; Nova, I. Energ. Env. Sc, **2008**, 1, 236-247

[21] Nova, I.; Lietti, L.; Castoldi, L.; Tronconi, E.; Forzatti, P. J. Catal. **2006**, 239, 244-254

[22] Castoldi, L.; Lietti, L.; Nova, I.; Matarrese, R.; Forzatti, P.; Vindigni, F.; Morandi, S.; Prinetto, F.; Ghiotti, G. Chem. Eng. J. **2010**, 161, 416-423

[23] Castoldi, L.; Lietti, L.; Forzatti, P.; Morandi, S.; Ghiotti, G.; Vindigni, F. The NO_x storage-reduction on Pt-K/Al_2O_3 Lean NO_x Trap Catalyst, submitted to J. Catal.

[24] K. Krishna, M. Makkee, Catal. Today, 114, **2006**, 48–56

[25] V.G. Milt, C.A. Querini, E.E. Miro, M.A. Ulla, J. Catal., 220 , **2003**, 424

[26] L. Castoldi. R. Matarrese, L. Lietti, P. Forzatti, Appl. Catal. B: Environ. 64,**2006**, 25

[27] R. Matarrese, L. Castoldi, L. Lietti, P. Forzatti, Top. Cat. 42-43 , **2007**, 293

[28] A.L. Kustov, M. Makkee, Appl Catal B: Environ 88, **2009**, 263-271

[29] A. Setiabudi, M. Makee, J.A. Moulijn, Appl. Catal. B 50, **2004**, 185

[30] G.Zhou, T.Luo, R.J. Gorte, Appl. Cat. B 64, **2006**, 88

[31] J.A. Sullivan, O. Keane, A. Cassidy, Appl. Catal. B: Environ. 75, **2007**, 102.

[32] Z. Zhang, Z. Mou, P. Yu, Y. Zhang, X. Ni, Catal. Comm. 8 ,**2007**, 1621–1624

[33] L. Castoldi, R. Matarrese, L. Lietti, P. Forzatti, Appl. Catal. B: Environ. 90, **2009**, 278–285

[34] H. An, P.J. McGinn, Appl. Catal. B: Environ. 62, **2006**, 46-56

[35] I. Nova, L. Castoldi, L. Lietti, E. Tronconi, P. Forzatti, Catal. Today 75 , **2002**, 431

[36] L. Castoldi, L. Lietti, R. Matarrese, P. Forzatti, Top. Catal. 52 , **2009**, 1713

[37] Forzatti, P.; Lietti, L.; Nova, I.; Morandi, S.; Prinetto, F.; Ghiotti, G. J. Catal. **2010**, 274, 163–175.

[38] Castoldi, L.; Lietti, L.; Nova, I.; Matarrese, R.; Forzatti, P.; Vindigni, F.; Morandi, S.; Prinetto, F.; Ghiotti, G. Chem. Eng. J. **2010**, 161, 416–423

[39] Castoldi, L.; Lietti, L.; Forzatti, P.; Morandi, S.; Ghiotti, G.; Vindigni, F. J. Catal., in press. DOI:10.1016/j.jcat.2010.09.026. Published Online: Nov 4, **2010**

[40] Nova, I.; Lietti, L.; Forzatti, P.; Frola, F.; Prinetto, F.; Ghiotti, G. Top. Catal. **2009**, 52, 1757–1761.

[41] A. Amirnazmi, M. Boudart, *J. Catal.* **1975**, *39*, 383.

[42] N. Takahashi, H. Shinjoh, T. Iijima, T. Suzuki, K. Yamazaki, K. Yokota, H., Suzuki, N. Miyoshi, S. Matsumoto, T. Tanizawa, T. Tanaka, S. Tateishi K. Kasahara, *Catal. Today* **1996**, *27*, 63

[43] A. Kato, S. Matsuda, T. Kamo, F. Nakajima, H. Kuroda, T. Narita, J. Phys. Chem. 1981, 85, 4099.

[44] S. S. Mulla, N. Chen, L. Cumaranatunge, G. E. Blau, D. Y. Zemlyanov, W. N. Delgass, W. S. Epling, F. H. Ribeiro, *J. Catal.* **2006**, *241*, 389.

5. Concluding discussion

The reactivity of model DPNR catalysts such as Pt-Ba/Al_2O_3 and Pt-K/$Al_2O_3$of have been addressed both in the soot oxidation and NO_x reduction in the presence of water and CO_2.

The results obtained during the lean NO_x adsorption over the Pt-Ba/Al_2O_3-soot mixture showed that the presence of soot decreased the NO_x storage capacity of the catalyst. Moreover soot leads to an appreciable decrement of the rate of NO_x adsorption: these effects are seen also at different temperatures (200-350°C) and with different values of the NO inlet concentration (250-1000ppm). During NO_x storage, soot oxidation also occurs, thanks to the presence of NO_2 formed upon NO oxidation over Pt sites. In fact the NO_2 concentration at the reactor outlet in the presence of soot is significantly lower than that observed without soot, thus pointing out the involvement of NO_2 in soot oxidation. The decrease of the NO_2 concentration may explain also the observed decline in the NO_x storage properties of the catalyst. In fact, in line with the occurrence of a "nitrate" pathway for the storage of NO_x (i.e., NO oxidation to NO_2 followed by NO_2 adsorption in the form of nitrates via a disproportion reaction), Ba and soot compete for reaction with NO_2, leading to the observed decrease in the NO_x storage properties. On the other hand, the reduction of the stored NO_x is not significantly affected by the presence of soot, although some minor changes in the N_2 selectivity (a slight increase in the presence of soot) have been observed.

Worth to note that the adsorbed NO_x oxidize soot at temperature well below those corresponding to their thermal decomposition originating NO_2 in the gas phase. This has been shown by TPD /TPO experiments in which the reactivity / thermal decomposition of nitrates has been investigated in the presence and in the absence of soot. It has been found that the presence of soot favors the decomposition and the reduction of the stored nitrates, while soot is oxidized. In fact the presence of soot shifts the decomposition/reaction of the stored nitrates at lower temperatures, and the stoichiometry of the released products reflects the occurrence of a partial reduction of the initially stored NO_x, as well as the oxidation of soot. This reaction possibly involves the surface mobility of the stored nitrates, soot particles being the driving force for the process and acting as reduced centers.

Furthermore mechanistic aspects involved in the formation of N_2 and N_2O during the reduction of NO_x stored over the model PtBa/Al_2O_3 NSR catalyst have been investigated by means of isotopic labeling experiments. The reduction of the stored labelled nitrites species with $^{14}NH_3$ leads to the selective formation of N_2 and very small amounts of nitrous oxide.

The observed N_2 isotopic distribution includes all possible N_2 isotopes, i.e. $^{15}N_2$, $^{14}N_2$ and the mixed $^{15}N^{14}N$ species. Based on the pathway suggested for NO and NH_3 reaction on Pt-based catalysts, it has been found that the observed product distribution can be explained on the basis of the statistical coupling of ^{15}N- and ^{14}N-adatoms originated upon NH_3 and NO_x decomposition on Pt. However the simultaneous occurrence of a SCR-like pathway, involving the formation and decomposition of a NH_x-NO intermediate originating from ammonia and NO_x, and leading to the selective formation of the mixed $^{15}N^{14}N$ species is also likely.
Isotopic labeling experiments also provide indications on the pathways involved in the formation of N_2O. This species is formed in very limited amounts during the reduction by ammonia of stored NOx species (nitrites and nitrates); much higher quantities have been observed during the reduction of gaseous ^{15}NO with NH_3. Since no formation of unlabeled nitrous oxide has been observed, the participation of ^{15}NO is necessary for the formation of nitrous oxide. In line with literature proposals, it has been suggested that nitrous oxide formation involves (on the Pt sites) either the coupling of two adsorbed NO molecules or the recombination of an adsorbed NO molecule with an adsorbed NH_x fragment. Accordingly, N_2O formation is greatly enhanced in the presence of gas-phase NO.

De-NO_x and De-soot activity has been investigated also over a model Pt-K/Al_2O_3. It has been shown that the pathways for the adsorption and the reduction of NO_x are similar for the Pt-Ba/Al_2O_3 and Pt-K/Al_2O_3 catalytic system. The presence of soot affects the NO_x storage capacity and the stability of the adsorbed species of both samples.
The aspects related to the reduction of stored NO_x at 350°C onto Pt-K/Al_2O_3 catalyst have been deeply investigated using also CO as reductant. It was shown that the reduction by CO of stored nitrates occurs through a Pt catalyzed surface pathway, which does not involve the thermal decomposition of stored NO_x with release of NO_x in the gas phase and leads mainly to nitrogen and CO_2. The reaction scheme already proposed in the case of Pt-Ba/Al_2O_3 catalyst operates also in the case of Pt-K/Al_2O_3 system and implies the formation of surface isocyanate species at first and in the second step the reaction of these superficial species with residual nitrates to give nitrogen. Over Pt-K/Al_2O_3 system this last surface reaction is more efficient than over the Ba-containing catalyst, so at the end of the reduction the amount of isocyanates species present on the surface is lower for Pt-K/Al_2O_3 then Pt-Ba/Al_2O_3 catalyst. A different mobility of the surface species involved in these reactions is invoked, having K-containing species higher mobility than Ba ones.

Another important part of this thesis work was focused on the study of the elementary steps involved in NO oxidation on Rh and Co catalysts. Kinetic experiments were carried out to study the

effect of NO, O_2, and NO_2 pressures on turnover rates. It was observed that turnover rates increased linearly with NO and O_2 pressures and were inversely proportional to NO_2 pressure, as also observed on Pt and Pd catalysts. NO oxidation rates are limited by O_2 activation on isolated vacancies (*) on surfaces of Rh and Co oxides saturated with oxygen (O*). RhO_2 and Co_3O_4 as the stable active phases during NO oxidation throughout the temperature and concentration ranges relevant to catalysis. Turnover rates increase with increasing cluster size, because the formation of kinetically-relevant vacancy sites becomes more facile on larger clusters, with more coordinatively saturated surfaces. NO oxidation turnover rates on RhO_2 and Co_3O_4 are higher than expected from oxygen binding energies on the respective metals or from the two-electron reduction potentials of Rh^{4+} or Co^{3+}, but fall in line with the reactivity of Pt and PdO when one-electron reductions (accessible for Rh and Co, but not for Pt or Pd) are used to predict turnover rates.

Acknowledgments

Paper I

Study of DPNR catalysts for combined soot oxidation and NOx reduction

Lidia Castoldi, Nancy Artioli, Roberto Matarrese, Luca Lietti, Pio Forzatti
Catalysis Today 157 (2010) 384–389

Abstract

The behavior of a model $PtBa/Al_2O_3$ model NSR catalyst in both the NO_x storage/reduction and soot oxidation is investigated in this work. It is found that the presence of soot negatively influences the NO_x storage capacity of the catalyst, evaluated at 623 K in presence of water and CO_2 in the feed stream: in fact the amounts of NO_x stored in presence of soot decrease by nearly 30% in the presence of roughly 10% w/w of soot. The presence of soot has a destabilizing effect on the NO_x adsorbed species, which decompose to a large extent in the absence of gas-phase NO and oxygen. This has also been confirmed by dedicated TPD and TPO experiments. However the presence of soot does not appreciably affect the behavior of the $PtBa/Al_2O_3$ catalyst in the reduction by H_2 of the stored nitrates, being in all cases N_2 the major reaction product along with minor amounts of ammonia.

During the storage of NO_x, soot oxidation takes place. Notably, the stored NO_x participate in the soot oxidation upon release of NO_2 and O_2 which actively oxidize soot. However a direct participation of the adsorbed NO_x species in the oxidation of soot cannot be excluded.

Keywords: Soot oxidation, diesel particulate filter, 4-ways catalysts, Lean deNO_x, NO_x trap promotion, LNT systems, $Pt–Ba/Al_2O_3$ catalyst, combined soot-NO_x removal, DPNR

1. Introduction

Current and upcoming environmental legislations in the most developed countries are imposing severe limits in NO_x, hydrocarbon, CO and particulate (soot) emissions from diesel engines. While the control of soot emissions is currently accomplished by the use of the so-called Diesel Particulate Filters (DPF), suitable technologies for NO_x abatement in lean-burn engines are still under development [1]. Among these, Lean NO_x Traps (LNTs), also known as NO_x storage-reduction (NSR) systems, have been proposed. The NSR technique utilizes an unsteady state operation by switching between fuel-lean and fuel-rich conditions [2,3]. Standard NSR catalysts consist of precious metals and alkaline/alkaline-earth metal oxides, typically platinum and barium, respectively, dispersed on metal oxide supports such as alumina. During fuel-lean periods, NO_x are stored on the alkaline/alkaline-earth metal oxide; the stored NO_x are then reduced to N_2 during a short fuel-rich period [3].

To accomplish soot and NO_x removal, both de-soot and a deNO_x aftertreatment techniques must be used. In the late '90, Toyota has developed a new technology able to remove simultaneously NO_x and soot [4,5]. This system, called Diesel Particulate-NO_x Reduction (DPNR), consists of is a porous ceramic filter coated with a catalytic layer consisting of a NSR catalyst. Like the NSR technology, this system accomplishes the reduction of soot and NO_x under cyclic conditions: soot abatement occurs under lean conditions thanks to the presence of NO_x and the excess oxygen in the exhaust gas, but it is claimed to occur during the rich phase as well.

In previous works of our group the potentiality of a model $PtBa/Al_2O_3$ catalyst in the simultaneous removal of soot and NO_x has been investigated. It has been found that the $PtBa/Al_2O_3$ samples is able to oxidize soot in the presence of oxygen at temperatures above 623–673 K; the presence of NO in the gas phase significantly enhances the soot combustion activity [6,7], due to NO oxidation to NO_2 on Pt followed by the reaction of NO_2 with soot:

$$2\ NO_2 + C \rightarrow 2\ NO + CO_2 \qquad (1)$$

In reaction (1), CO_2 formation is envisaged but CO formation may occur as well. It is indeed well known that NO_2 is a better oxidant than O_2 [8 and references herein reported]; its reaction with the carbonaceous material leads to both CO and CO_2 formation [8].

Based on a comparative study of a $PtBa/Al_2O_3$ catalyst with a Pt/Al_2O_3 sample, a role of the stored NO_x species in the oxidation of soot has been suggested [9]. In a recent paper by Kustov and Makkee [10] the soot oxidation on a number of alkali-earth based catalytic systems pre-saturated with NO_x,

like $Ba(NO_3)_2/Al_2O_3$, has been investigated. The authors show that stored nitrates contribute to the soot oxidation by lowering the temperature of soot oxidation. Along similar lines, Suzuki et al. [11] noted an increased combustion activity of soot when a NO_x trap material is incorporated in the catalyst. On the other hand, Sullivan et al. [12] reported that the presence of a NO_x trapping component like BaO does not promote *per-se* the particulate combustion. However the NO_x trapping material promotes soot combustion due to the periodic localized increases in the NO_2 gas phase concentration during trap regeneration. On these bases, aim of this work was to provide new insights on the role in the soot combustion of NO_x stored onto the catalytic surface of a model $PtBa/Al_2O_3$ DPNR catalyst. Besides, we wanted to analyze the effects of the presence of soot on the behaviour of the LNT catalyst in terms of NO_x storage/reduction. For this purpose, NO_x storage/reduction experiments have been performed over a model $PtBa/Al_2O_3$ catalyst by alternating lean/rich cycles both in presence and in absence of soot. The interaction between soot and the stored NO_x species has also investigated by Temperature Programmed Methods under inert flow (TPD) or in oxygen (TPO) during which the stability/reactivity of the stored NO_x species has been analyzed both in the presence and in the absence of soot.

2. Experimental

The model catalyst studied, $PtBa/Al_2O_3$ (Pt loading near 0.8% w/w and Ba loading near 17% w/w), was prepared by the wetness impregnation technique from solutions of dinitrodiammine platinum (Strem Chemicals) and barium acetate (Strem Chemicals, as reported elsewhere [6,13]. The catalyst presents a surface area near 160 m^2/g_{cat} and pore volume of 0.8 cm^3/g_{cat} (as determined by N_2 adsorption-desorption with a Micromeritics TriStar 3000 Instrument). The Pt dispersion is close to 15% (H_2 chemisorption at 273 K, measured with a TPD/R/O 1100 Thermo Fischer Instrument). Further detail of catalyst preparation and characterization are reported in Refs.[14,15,16].

Printex-U (Degussa) was used as model soot [17,18]. Catalyst-soot mixtures were prepared by gently mixing in a vial the catalyst powder with the soot for 24 h, thus realizing a loose contact. A catalyst/soot ratio of 9/1 w/w was typically utilized in reactivity tests.

All reactivity tests were performed in a flow-reactor apparatus consisting of a quartz tube reactor (7 mm i.d) connected to a mass spectrometer (Omnistar 200, Pfeiffer Vacuum) and to a micro GC (Agilent 3000A) for the on-line analysis of the outlet gases [19]. The outlet NO, NO_2, NH_3 concentrations were also detected by a UV analyzer (Limas 11HW, ABB). 66 mg of the soot-catalyst (74-105 μm) mixture was used in each run, and the total gas flow was always set at 100 cm^3/min (at 273 K and 1 atm).

Before catalytic tests, the catalyst/soot mixture has been heated at to 773 K in He to remove any adsorbed species on the catalytic surface. The NO_x storage and reduction activity of the catalytic system has been studied in the presence and in the absence of soot by performing lean-rich cycles at constant temperature (Isothermal Step Concentration experiments, ISC). During the NO_x adsorption (lean phase, see Tab.1), a pulse of NO (1000 ppm) has been admitted to the reactor in flowing He + 3% (v/v) O_2 until catalyst saturation. Then after a He purge at the same temperature, catalyst regeneration (rich phase, see Tab.1) has been carried out with H_2 (4000 ppm in He).

	Gas composition (%v/v)			
	Lean rich cycle		**TPD**	**TPO**
	Lean phase	**Rich phase**		
O_2	3	0	0	3
NO	0.01	0	0	0
H_2	0	0.04	0	0
CO_2	1	1	0.01	0.01
He	balance	balance	balance	balance

Tab. 1. Experimental conditions of lean-rich cycles, TPD and TPO experiments. All the experiments have been carried out with a flow rate of 100cc/min (@ 0°C and 1 atm).

The catalyst samples have been conditioned by performing a few adsorption/regeneration cycles: conditioning lasted until a reproducible behaviour has been obtained, and this typically required 2-3 cycles. 1% v/v H_2O and 0.1% v/v CO_2 were always present in the feed flow during both the storage and the reduction phase (table 1). The CO_2 concentration is lower than real applications, but it is anyway representative of carbon dioxide effect on the catalytic system performance [16]. Besides such low value allows to appreciate even small changes in the CO_2 concentration during the experiments.

The selectivity to N_2 of the reduction process has also been estimated. Since the N_2 selectivity changes during the rich phase due to the variation in the product distribution with time, a time-weighted average N_2 selectivity (S_{N2}) along the entire rich step has been estimated:

$$S_{N_2} = \frac{2n_{N_2}}{2n_{N_2} + n_{NO} + n_{NH_3}} \qquad \text{(a)}$$

In eq. (a) n_{N2}, n_{NO} and n_{NH3} are the total molar amounts of N_2, NO, and NH_3, respectively, evolved during the entire reduction phase. These amounts are obtained by the integrals on time of the concentrations of the products evolved during the entire reduction phase. N_2O has not been considered in eq. (a) since formation of this species has been found to be negligible.

The thermal stability of the stored NO_x was analyzed by thermal decomposition in inert flow (Temperature Programmed Desorption, TPD). After NO_x adsorption at 623 K the sample was cooled

in He at 523 K and then heated (10 K/min) in He + H_2O (1% v/v) and CO_2 (0.1% v/v) from 523 K up to 773 K (hold 30 min) (see Tab.1). These experiments have been carried out in the presence and in the absence of soot to analyze the effect of soot on the thermal stability of the adsorbed nitrates.

Finally, the behaviour of the catalysts in the soot combustion reaction was investigated by means of temperature-programmed oxidation (TPO). Like TPD experiments, after NO_x adsorption at 623 K the catalyst was cooled in He down to 523 K and then heated (10 K/min) in He + O_2 (3%, v/v) + H_2O (1%) + CO_2 (0.1% v/v) from 523 K up to 773 K (see Tab.1). These experiments have been carried out in the presence and in the absence of stored NO_x.

Soot is progressively consuming during each test; accordingly several catalyst/soot batches have been used. All the experiments refer to a soot loading near 7-8 % of the catalyst weight.

3. Results and discussion

NO_x adsorption phase - The results obtained in the case of a rectangular step feed of NO (1000 ppm) in the presence of O_2 (3% v/v), CO_2 (0.1% v/v) and H_2O (1% v/v) at 623 K carried out on the $PtBa/Al_2O_3$ catalysts in the absence and in the presence of soot (soot loading near 8% of the catalyst weight) are shown in Figure 1A and Figure 1C, respectively. The outlet NO, NO_2 and NO_x ($NO+NO_2$) concentration curves are displayed in the Figure as a function of time, along with that of the NO inlet concentration (dotted lines). In the absence of soot (Fig. 1A), upon the NO step addition (at t = 0 s) the NO outlet concentration increases with time, approaching the asymptotic values corresponding to the NO inlet concentration after about 2000 s. Also NO_2 (140 ppm at steady-state) is observed due to the occurrence of the oxidation of NO by O_2 according to the stoichiometry of reaction (2):

$$NO + ½\ O_2 \leftrightarrow NO_2 \qquad (2)$$

The amount of NO_x that has been stored on the catalyst surface at the end of the NO pulse is near 0.58 mmol/g_{cat}. During the NO pulse, CO_2 evolution is also observed. This is due to the formation of nitrate species upon NO_x adsorption [16,19], that replace carbonates with release of CO_2 according to the stoichiometry of reaction (3),

$$BaCO_3 + 2\ NO + 3/2\ O_2 \rightarrow Ba(NO_3)_2 + CO_2 \qquad (3)$$

In fact upon subtracting half of the adsorbed NO concentration value (i.e. ½ (NO_{IN} – NO_{out})) to the actual CO_2 concentration curve, a flat CO_2 trace is obtained (trace ***a*** of Figure 1A).

Finally, upon NO shutoff near t = 3500 s, a tail is observed in the NO and NO_2 concentrations due to

the desorption of weakly adsorbed NO_x species (0.11 mmol NO_x/g_{cat} desorbed), whose release is favored by the decrease in the NO_x partial pressure. The net amount of NO_x stored before regeneration is hence is near 0.47 mmol NO_x/g_{cat}.

In presence of soot (Fig. 1C), the evolution of NO and NO_2 are qualitatively similar to those observed for the soot-free catalyst. Upon NO admission, the outlet NO concentration increases with time reaching a steady-state level after 2000 sec. The formation of NO_2 is also observed, but in lower amount (60 ppm) if compared to the soot-free catalyst. The amount of adsorbed NO_x at the end of the pulse is in this case near to 0.41mmol NO_x/g_{cat}, indicating a reduction in the storage capacity of the catalyst in presence of soot as also reported by Sullivan et al. [12].

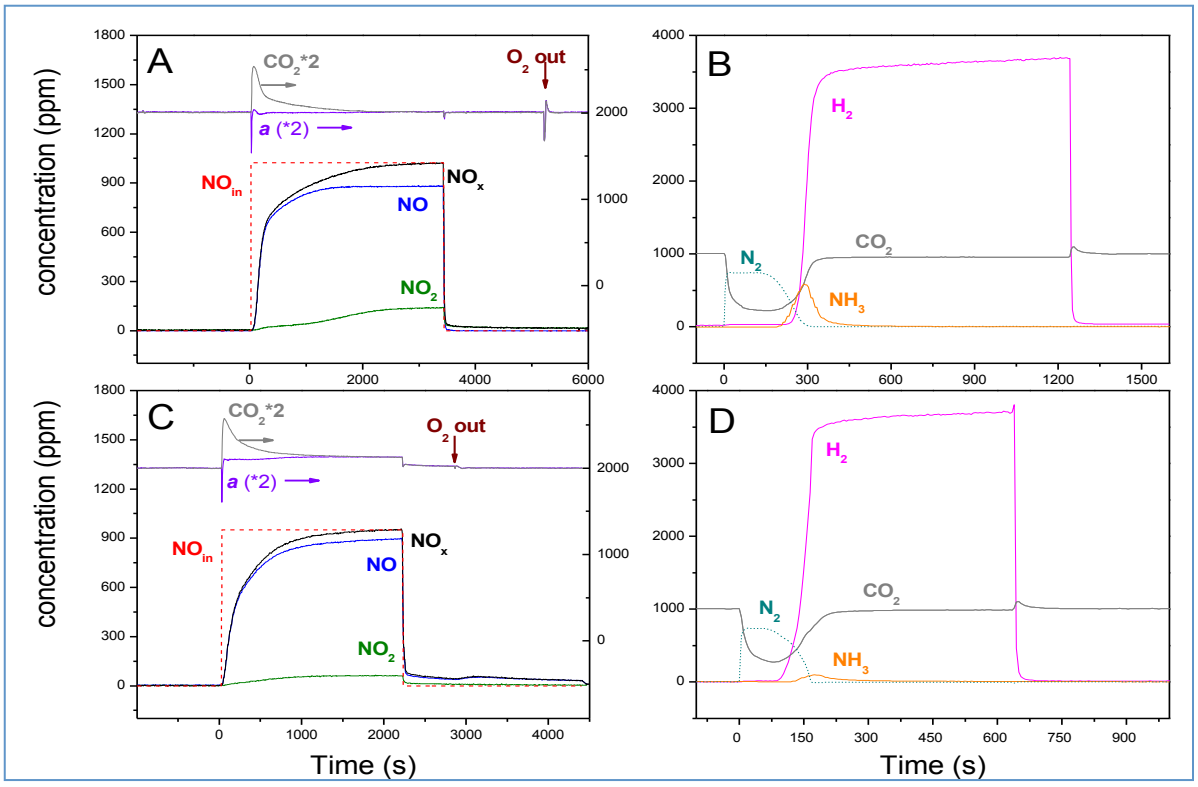

Fig. 1 – Storage-reduction cycle performed at 623K over $PtBa/Al_2O_3$ (A and B)and $Pt–Ba/Al_2O_3$-soot mixture (C and D). Trace a is the CO_2 production due to soot oxidation.

A comparison of the amounts of NO_x stored vs. adsorption time for different soot loadings (curve ***a***: soot-free catalyst; curve ***b***: soot loading 2.9% w/w; curve ***c***: soot loading 8% w/w) is shown in Figure 2.

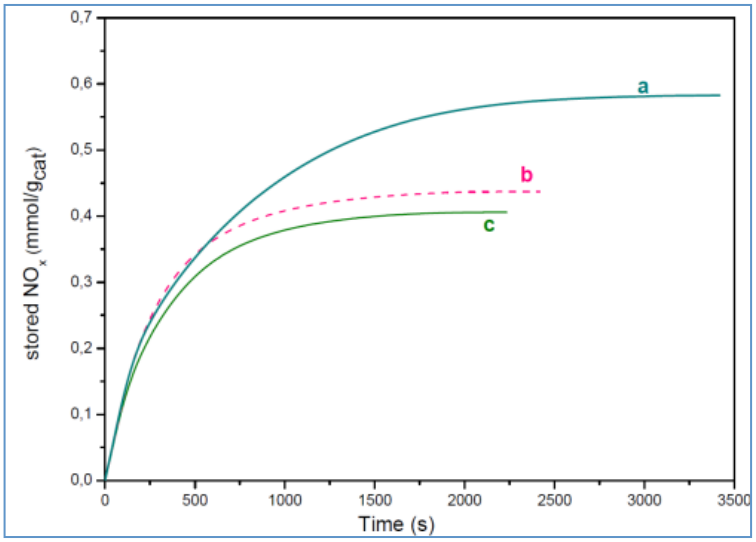

Fig. 2 - Adsorbed NOx versus time over $PtBa/Al_2O_3$ for different soot loadings: a) without soot, b) 2.9% w/w soot and c) 8%w/w soot

It clearly appears that the amount of soot present in the catalyst/soot mixture affects the NO_x storage behavior of the LNT system. In particular, the decrease of the soot loading (from curve ***c*** to curve ***a***) leads to an increase of the NO_x storage capacity, in line with the results reported by Sullivan et al. [12]. These authors pointed out that the presence of soot is detrimental to the performance of a NO_x trap since soot itself offers another reaction route for the utilisation of NO_2 rather than the desired formation of $Ba(NO_3)_2$ according to the stoichiometry:

$$BaCO_3 + 3\ NO_2 \rightarrow Ba(NO_3)_2 + NO + CO_2 \qquad (4)$$

As a matter of facts, upon comparing Figure 1A and 1C, it is noted that the presence of soot affects the NO/NO_2 ratio. Indeed the NO/NO_2 value rises from a value near 6 for the soot-free catalyst sample to roughly 15 in presence of soot. The higher NO/NO_2 ratio measured in the presence of soot is due to the participation of NO_2 in soot oxidation, according to reaction (1).

In Figure 1C, upon NO admission, CO_2 evolution is also observed above its background of 1000 ppm. The increase in the CO_2 outlet concentration results from two contributes: one is related to the decomposition of carbonates on the catalytic surface due to nitrates formation (in line with reactions (3)-(4)), and the other is due to soot combustion. In order to evaluate the net CO_2 production due to the soot combustion, the contribution of the decomposition of the surface carbonates (reaction (3)) has been subtracted from the CO_2 outlet concentration trace; the obtained

CO_2 net production curve is shown in Figure 1C (trace ***a***). During the lean phase roughly 4% of the soot initially present has been oxidized with a rate of approximately 1.08 10^{-5} mmol CO_2/s. Worth to note that at the investigated temperature soot combustion occurs only in the presence of NO. Besides, CO formation is not observed, possibly because the formed CO is further oxidized to CO_2 by O_2 on Pt sites.

Upon NO shutoff, a release of NO and NO_2 takes place due to the desorption/decomposition of the NO_x species previously stored. Upon switching off the O_2 feed, additional NO_x are also desorbed. Both desorption contributions appear to be remarkable if compared to those observed in the case of the soot-free catalyst: this indicates that soot has a destabilizing effect on the nitrate species adsorbed onto the catalytic surface. The reasons for the destabilizing effect of soot on the stored nitrates are not yet fully understood; one can speculate that nitrates species, which are considered mobile on the catalytic surface [20], may directly interact with soot particles leading to its oxidation.

The changes in the amounts of adsorbed NO_x upon NO shut off are reported in Fig. 3 as a function of time for different soot loadings (curve ***a***: soot-free catalyst; curve ***b***: soot loading 2.9% w/w; curve ***c***: soot loading 8% w/w). It appears that the higher the soot loading, the greater is the decrease of the amount of stored NO_x. After 2000 sec, the total amounts of NO_x desorbed in the presence and in the absence of soot are near 0.12 mmol/g_{cat} and 0.07 mmol/g_{cat}, respectively; these values correspond to 29 % and 12.4 % of the NO_x adsorbed species present onto the catalytic surface at saturation. This clearly points out the lower stability of nitrates in presence of soot.

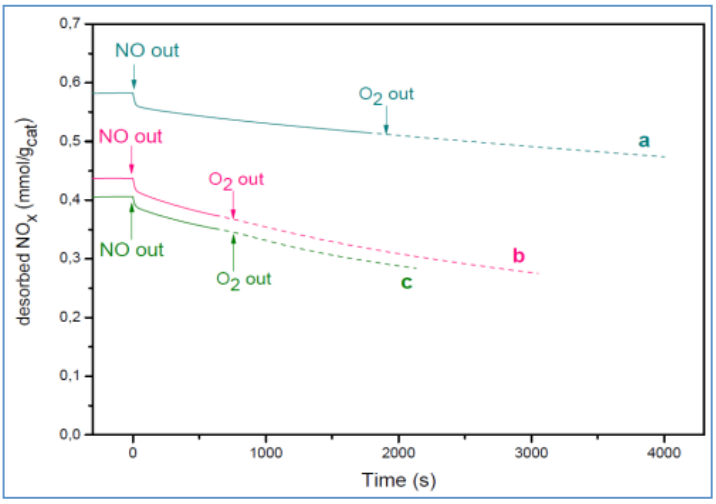

Fig. 3 - Desorbed NOx versus time after NOx storage over PtBa/Al_2O_3 for different soot loadings: a) without soot, b) 2.9% w/w soot and c) 8%w/w soot

NO_x reduction phase - The reduction of the stored NO_x has been carried out at 623 K by admission of

H_2 (rich phase, table 1). The results are shown in Figure 1B in terms of H_2, CO_2 and N_2, NH_3 outlet concentrations as a function of time in the case of the soot-free catalyst.

Upon H_2 admission (t = 0 s), the H_2 outlet concentration profile shows a dead time during which it is completely consumed to give at first N_2 and NH_3 later on, according to the overall stoichiometry of reactions (5) and (6):

$$Ba(NO_3)_2 + 5\ H_2 + CO_2 \rightarrow BaCO_3 + N_2 + 5\ H_2O \qquad (5)$$

$$Ba(NO_3)_2 + 8\ H_2 + CO_2 \rightarrow BaCO_3 + 2\ NH_3 + 5\ H_2O \qquad (6)$$

In line with the stoichiometry of reaction (5), upon admission of 4000 ppm H_2 the N_2 outlet concentration immediately increases to the level of 800 ppm; then NH_3 formation is observed in correspondence of the decrease of the N_2 trace, at the end of the reduction. Slightly after the NH_3 breakthrough the H_2 concentration trace increases up to the inlet concentration value. The integral amounts of the reduction products (0.21 mmol/g_{cat} of N_2 and 0.07 mmol/g_{cat} of NH_3) well correspond to H_2 consumption (1.46 mmol/g_{cat}), according to the stoichiometry of reactions (5) and (6). N_2O is not observed among the reduction products, as indicated by GC analyses (detection limit near 10 ppm).

According to previous studies of our group [16,21] the reduction of stored nitrates by H_2 occurs via a two-step molecular pathway which involves a first step leading to the formation of NH_3, followed by the slower reaction of ammonia with residual nitrates to form N_2:

$$3\ Ba(NO_3)_2 + 10\ NH_3 + CO_2 \rightarrow 3\ BaCO_3 + 8\ N_2 + 15\ H_2O \qquad (7)$$

The sum of reactions (6) and (7) accounts for the overall stoichiometry of reduction of nitrates with hydrogen to give N_2 (reaction 5). Notably, the temporal evolution of reduction products, with nitrogen being detected at the reactor outlet first and ammonia later, is in line with the integral behaviour of the catalytic bed [16,21]. In fact upon regeneration a hydrogen front travels along the catalyst bed. NH_3 is formed at the H_2 front upon reaction of H_2 with the stored NO_x; the formed NH_3 then reacts with NO_x stored downstream the H_2 front, leading to the formation of N_2. When the front reaches the end of the catalytic bed, there are no NO_x stored downstream and this leads to the evolution of ammonia, which follows that of N_2.

During the reduction phase, a CO_2 uptake has also been observed due to the formation of carbonates onto the Ba sites on which NO_x were previously stored; finally, after NO_x reduction, the formation of small amounts of CO is also observed due to the occurrence of the inverse water gas

shift (RWGS) reaction (8):

$$CO_2 + H_2 \leftrightarrow CO + H_2O \quad (8)$$

Calculation showed that the reaction is limited by thermodynamic constraints; the relevance of this reaction appears to be limited by the presence of water in the feed [16].

The reduction of the NO_x adsorbed species in the presence of soot (Figure 1D) does not show significant differences with respect to the soot-free catalyst (compare Figure 1B and 1D). Also in this case H_2 is immediately and completely consumed and at the beginning of the reduction phase and only N_2 is observed among the products. After 150 sec the concentration of nitrogen decreases to zero, that of H_2 progressively increases and NH_3 is observed at the reactor exit. In the presence of soot the amount of both N_2 and NH_3 which have been produced is lower if compared to the absence of soot, i.e. 0.11 mmol/g_{cat} of N_2 and 0.02 mmol/g_{cat} of NH_3. This is related to the reduced NO_x storage capacity of the catalyst in presence of soot, as shown in Figure 2 (curve ***c***). However, the N_2 selectivity calculated in the presence of soot is very similar to that measured in its absence, i.e. 86% vs. 92%.

TPD experiments - In order to analyze the stability of adsorbed NO_x species in the absence and in the presence of soot, TPD experiments have been carried out (Table 1). Figure 4A and 4B shows the results obtained in terms of NO, NO_2, and O_2 concentration traces versus time on Pt-Ba/γ-Al_2O_3 in the absence and in the presence of soot, respectively.

In the case of the soot-free Pt-Ba/γ-Al_2O_3 catalyst (Fig. 4A), no desorption peaks were observed below the adsorption temperature (623 K). This is in line with previous results [16,22,23] showing that the adsorption temperature rules the thermal stability of the adsorbed NO_x species. Decomposition of nitrates occurs above the temperature of absorption and results in the initial evolution of NO_2, followed by NO and O_2. NO, O_2, and NO_2 are likely produced through the following global reactions:

$$Ba(NO_3)_2 \rightarrow BaO + 2\ NO + 3/2\ O_2 \quad (9)$$

$$Ba(NO_3)_2 \rightarrow BaO + 2\ NO_2 + O_2 \quad (10)$$

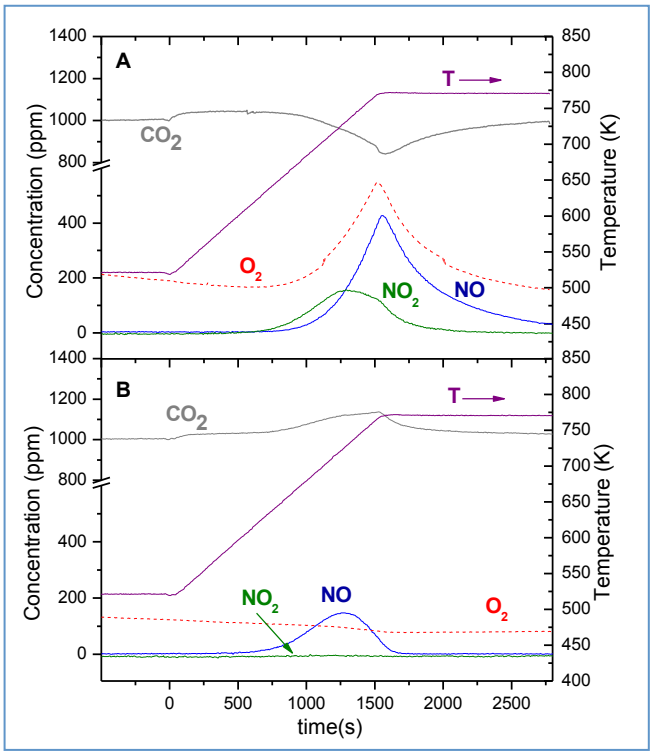

Fig. 4. TPD run after NO_x adsorption at 623K over (A) $PtBa/Al_2O_3$ catalyst; (B) $PtBa/Al_2O_3$ catalyst-soot mixture.

The process was not complete at temperatures as high as 773 K, corresponding to the maximum heating temperature; the catalyst was then kept at this temperature until desorption of nitrates was nearly complete (N-balance closes within 5.5%). After the TPD experiment a reducing treatment has been carried out with a stream of H_2 (4000 ppm in He+ H_2O+ CO_2) at 623 K to reduce the residual nitrates. During this treatment the formation of very small amounts of NH_3 (4.91 10^{-3} mmol/g_{cat}) have been detected.

In correspondence with the nitrate decomposition, a decrease of the CO_2 signal is observed, from the inlet value (1000 ppm) to a minimum of 840 ppm. This is due to the adsorption of CO_2 on Ba forming $BaCO_3$ upon decomposition of Ba nitrates. Note that the amount of CO_2 adsorbed is lower than that expected from nitrates decomposition (according to reaction (3)), possibly due to the formation of Ba oxide and/or hydroxide, along with $BaCO_3$.

TPD runs have also been performed in the presence of soot and results are shown in Fig.4B. The decomposition onset of the stored NO_x is observed about at the same temperature of adsorption (623 K) for the reasons already discussed. The amounts of desorbed species is lower than that calculated in the absence of soot (0.11 mmol/g_{cat} vs 0.48 mmol/g_{cat}), as consequence of the minor amounts of NO_x adsorbed onto the catalytic surface in the presence of soot, as already discussed. It is worth noticing that the distribution of desorbed products is different in the presence and in the

absence of soot (compare Figure 4A and 4B). Indeed in the presence of soot, NO represents the major decomposition product (Figure 4B), and no detectable amounts of NO_2 or O_2 are observed. This suggests that in the presence of soot NO_2 and O_2 produced from the nitrates decomposition are readily consumed in the soot combustion. In line with the occurrence of soot oxidation, the CO_2 concentration trace shows an increase, as opposite to what observed in the absence of soot (Figure 4A). This indicates that soot can be effectively oxidized at temperatures above the nitrate decomposition [10].

Finally, in Figure 4B it appears that the nitrates decomposition is concluded at lower temperature (near 773 K) than in the absence of soot. This indicates that the presence of soot favors the decomposition of the NO_x adsorbed species, in line with isothermal experiments reported above (see Figure 3).

TPO experiments - TPO experiments have been carried out i) in the presence of adsorbed NO_x species only, ii) in the presence of soot and iii) in the presence of both soot and adsorbed NO_x species (Figure 5A-C, respectively). In the presence of adsorbed NO_x species only (Figure 5A) the decomposition of the stored NO_x was appreciable only above 623 K, with evolution of NO_2 and NO. Comparing these data with the results of TPD experiments discussed above (Figure 4A), it appears that the products distribution is similar, with NO_2 and NO evolution above 623 K (O_2 evolution could not be detected in this case due to the high oxygen concentration in the feed stream). At the end of the heating ramp (773 K), the nitrate decomposition process was not complete; for this reason the temperature was kept at this value for several minutes. Like the TPD experiment, in correspondence of the NO_x desorption peak a decrease in the CO_2 concentration trace is observed, due to carbonates formation onto the catalytic surface. After the TPO experiment, the residual nitrates (roughly 18 % of the initially stored NO_x) were removed by a reducing treatment with H_2 at 623 K.

In the presence of both nitrates and soot (Figure 5B), the nitrates decomposition occurs at slightly lower temperatures than in the absence of soot. As already discussed in the case of the TPD run (Figure 4B), no NO_2 is detected in this case at the reactor outlet due to its involvement in the soot oxidation. A significant CO_2 evolution is observed in this case, along with O_2 consumption. At 773 K the decomposition of nitrates is already complete and the subsequent reduction doesn't show any production of reduction products: these results are in agreement with those reported above in the case of the TPD experiment.

Finally, Figure 5C shows the results of a TPO experiment carried out in the case of the soot-catalyst mixture, in the absence of pre-adsorbed nitrates. A minor CO_2 evolution is observed, produced by

soot oxidation, along with a corresponding O_2 consumption. A comparison with the experiment carried out in the presence of surface nitrates (Figure 5B) clearly points out that the presence of surface NO_x favors the soot oxidation, as pointed out by the greater amounts of evolved CO_2 in this case,. A 1.93 vs 1.36 mmol/g_{cat}.

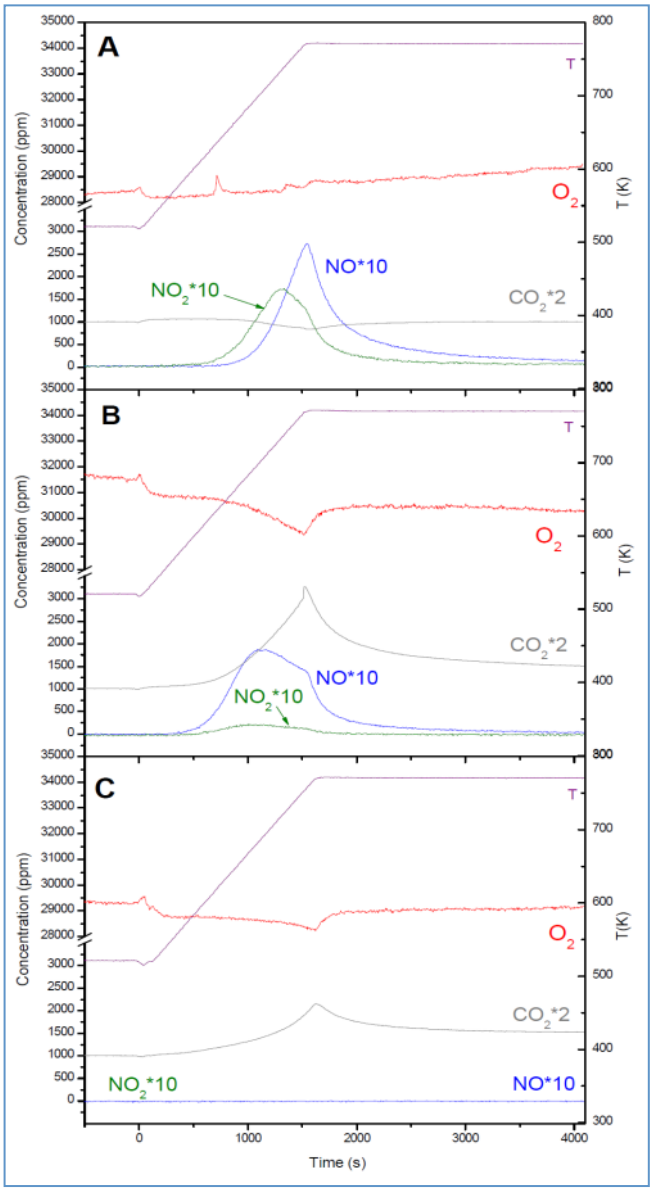

Fig. 5. TPO run after NO_x adsorption at 623K over A) $PtBa/Al_2O_3$ catalyst; B) $PtBa/Al_2O_3$ catalyst-soot mixture; C) $PtBa/Al_2O_3$ catalyst-soot mixture without nitrates pre-adsorbed onto the catalytic surface. CO_2 trace has been reported with an offset of 1000 ppm.

According to Kustov and Makkee [10] soot is oxidized in the presence of nitrates through two routes: oxidation with NO_2 and oxidation with oxygen. Oxidation with NO_2 occurs upon nitrate decomposition; according to the authors this mechanism may decrease the onset temperature for soot oxidation by some 100 K with respect to oxygen. The increase in the CO_2 concentration which is observed at the beginning of the TPO run carried out in the presence of adsorbed NO_x (compare

Figure 5B and C) may result from soot oxidation by NO_2 evolved upon decomposition of the stored nitrates. In fact only NO evolution is observed in this case upon nitrate decomposition, as opposite to what observed in the absence of soot (see Figure 5A). This clearly indicates that NO_2 which evolves upon decomposition of the stored nitrates, is involved in soot oxidation likely according to the stoichiometry of reaction (1). Notably, the increase in the CO_2 formation is much higher than that expected from the stoichiometry of reaction (1). This is due to the so-called "NO recycle", i.e. to the oxidation of NO produced according to reaction (1) to NO_2, catalyzed by Pt [24]. Besides, it has also been reported that the presence of NO_2 enhances soot oxidation by oxygen [25,26]. A specific role of the adsorbed NO_x species in the soot combustion cannot be ruled out, as also previously reported [6]. These mechanisms contribute to the significant increase in the soot oxidation which is observed when the soot combustion is carried out in the presence of adsorbed nitrates.

4. Conclusions

In this study the behavior of a model $PtBa/Al_2O_3$ model NSR catalyst in both the NO_x storage/reduction and soot oxidation has been addressed. It has been found that the presence of roughly 10% w/w of soot decreases by nearly 30% the NO_x storage capacity of the catalyst (0.58 $mmol/g_{cat}$ vs. 0.41 $mmol/g_{cat}$). The presence of soot has also a destabilizing effect on the NO_x adsorbed species, likely due to the reaction between soot particles and the nitrate species which are mobile on the surface.

The behavior of the $PtBa/Al_2O_3$ catalyst sample in the reduction by H_2 of the stored nitrates has also been investigated, in the presence and in the absence of soot. It has been found that the presence of soot does not appreciably affect the features of the reduction of the stored NO_x, being in both cases N_2 the major reaction product along with minor amounts of NH_3.

During the lean-rich cycles, and in particular during the storage of NO_x, soot oxidation takes place, pointed out by CO_2 evolution. Soot oxidation takes place only upon NO admission, and is almost negligible in the presence of O_2 only. As pointed out by TPD experiments, the stored NO_x participate in the soot oxidation upon release of NO_2 and O_2 which actively oxidize soot, although a direct participation of the stored NO_x in the oxidation of soot cannot be excluded. The participation of the adsorbed NO_x species in the soot oxidation has also been clearly pointed out by TPO experiments showing that the oxidation of soot is greatly enhanced by the presence of adsorbed NO_x species: indeed larger amounts of CO_2 are produced upon soot oxidation when the reaction is carried out in the presence of stored NO_x.

Aknowledgements - The financial support of PRIN project 2007HHCZP4 is acknowledged.

References

[1] T. Johnson, Platinum Metals Rev., 52 (2008) 23

[2] W.S. Epling, L. E. Campbell, A. Yezerets, N.W. Currier, J.E. Parks, Catal. ReV. Sci. Eng. 46 (2004) 163

[3] S. Matsumoto, Catal. Today 90 (2004) 183

[4] Toyota Patent, European Patent Application No. 01107629.6, (2001)

[5] K. Nakatani, S. Hirota, S. Takeshima, K. Itoh, T. Tanaka, SAE Paper SP-1674, 2002-01-0957 (2002)

[6] L. Castoldi, M. Matarrese, L. Lietti, P. Forzatti, Appl. Catal. B: Environ 64 (2006) 25-34

[7] A. Setiabudi, B.A.A.L. van Setten, M. Makkee, J.A. Moulijn, Appl. Catal. B 35 (2002) 159

[8] B.A.A.L. van Setten, M. Makkee, J.A. Moulijn, Catal. Reviews, 43 (2001) 489

[9] R. Matarrese, L. Castoldi, L. Lietti, P. Forzatti, Catal. Today 136 (2008) 11

[10] A.L. Kustov, M. Makkee, Appl. Catal. B, 88 (2009) 263

[11] J. Suzuki, S. Matsumoto, Top. Catal. 28 (2004) 171

[12] J.A. Sullivan, O. Keane, A. Cassidy, Appl. Catal. B, 75 (2007) 102

[13] R. Matarrese, L. Castoldi, L. Lietti, P. Forzatti, Top. Catal. 42-43 (2007) 293

[14] F. Frola, M. Manzoli, F. Prinetto, G. Ghiotti, L. Castoldi, L. Lietti, J. Phys. Chem. C 112 (2008) 2869

[15] I. Nova, L. Castoldi, L. Lietti, E. Tronconi, P. Forzatti, Catal. Today 75 (2002) 431

[16] L. Lietti, P. Forzatti, I. Nova, E. Tronconi, J Catal 204 (2001) 175

[17] A. Setiabudi, M. Makee, J.A. Moulijn, Appl. Catal. B 50 (2004) 185

[18] N. Nejar, M. Makkee, M.J. Illàn-Gómez, Appl. Catal. B 75 (2007) 11

[19] F.Frola, F. Prinetto, G. Ghiotti, L. Castoldi, I. Nova, L Lietti, P. Forzatti, Catal. Today 126 (2007) 81

[20] G.Zhou, T.Luo, R.J. Gorte, Appl. Cat. B 64(2006) 88

[21] L. Castoldi, L. Lietti, R. Matarrese, P. Forzatti, Top. Catal. 52 (2009) 1713

[22] I. Nova, L. Castoldi, L. Lietti, E. Tronconi, P. Forzatti, SAE Technical Paper, (2006) 01-1368

[23] L. Castoldi, I. Nova, L. Lietti, E. Tronconi, P. Forzatti, Top. Catal. 42-43 (2007) 189

[24] S.J. Jelles, R.R. Krul, M. Makkee, J.A. Moulijn, Catal. Today 53 (1999) 623

[25] J. Jung, J.H. Lee, S. Song, K.M. Chun, Int. J. Automotive Technology 9 (2008) 423

[26] F. Jacquot, V. Logie, J.F. Brilhac, P. Gilot, Carbon 40 (2002) 335

Paper II

Effect of soot on the storage-reduction performances of LNT PtBa/Al_2O_3 catalyst

Nancy Artioli, Roberto Matarrese, Lidia Castoldi, Luca Lietti, Pio Forzatti
Catalysis Today 169 (2011) 36-44

Effect of soot on the storage-reduction performances of LNT $PtBa/Al_2O_3$ catalyst

Abstract

The effect of soot on the storage-reduction performances of a $PtBa/Al_2O_3$ catalyst is investigated in this work. It is found that the presence of soot reduces the NO_x storage capacity of the catalyst, evaluated in presence of water and CO_2 in the feed stream in the range 200-350°C and with different values of the NO inlet concentration. Besides the presence of soot favors the decomposition and the reduction of the stored nitrates, while soot is being oxidized. A direct reaction between the stored nitrates and soot is suggested, that has been explained on the basis of the surface mobility of the adsorbed nitrates. This soot oxidation pathway involves surface species and parallels the NO_2-soot oxidation that occurs in the presence of gas-phase NO_2.

Finally, the presence of soot does not influence appreciably the behavior of the $PtBa/Al_2O_3$ catalyst in the reduction by H_2 of the stored nitrates: in all cases N_2 is the main reaction product and ammonia is observed in minor amounts.

Keywords

Soot oxidation, DPNR catalysts, simultaneous NO_x and soot removal, Diesel Particulate NO_x Reduction, NSR catalysts

1. Introduction

Diesel-equipped vehicles are considered as one of the primary sources of NO_x and particulate (soot) emissions in industrialized countries. Accordingly regulations to limit their emission are becoming very strict. In Europe, the current Euro 5 rules limit NO_x and soot emissions from light-weight diesel vehicles (up to 2500 kg) at 0,18 and 0,005 g/km, respectively, but a more drastic reduction is required for NO_x emissions in the upcoming Euro 6 regulations (0.08 g/km). This will require the use of exhaust after-treatment technologies able to reduce the NO_x emissions in addition to the soot removal technologies already set by the Euro 5 standards (the so-called Diesel Particulate Filter, DPF) [1].

The soot removal devices, usually made by a cordierite or SiC filter, provide excellent filtration efficiency but must be periodically regenerated to remove the entrapped soot in order to avoid increased pressure drop. The active regeneration is usually performed by increasing the filter temperature (at 650°C or more) by fuel injection so that the particulate is burnt by oxygen present in the exhaust. This procedure implies an extra fuel consumption; moreover, excessive heating can damage the filter.

Alternative solutions have been proposed to regenerate the filter at lower temperature. An example is the CRT (Continuously Regenerating Trap) technology, proposed by Johnson Matthey [2,3], which is constituted by a catalytic system (the pre-oxidizer) that oxidizes CO and unburned hydrocarbons (UHCs), followed by a non-catalytic wall-flow filter for the particulate. The pre-oxidizer also converts NO to NO_2, which then oxidizes at low temperature the particulate matter trapped and is back-reduced to NO:

$$NO + ½\ O_2 \rightarrow NO_2 \qquad (1)$$

$$2\ NO_2 + C \rightarrow 2\ NO + CO_2 \qquad (2)$$

Thanks to the high combustion activity of NO_2 towards soot, the wall-flow trap regeneration process is continuously performed at low temperature, without additional fuel addition. However it must be pointed out that the efficiency of this system depends on the activity in the NO to NO_2 oxidation, and on the NO concentration as well. In fact, the NO_x content of the exhaust may be not high enough to ensure the complete filter regeneration.

Integrated De-NO_x and De-soot after-treatment technologies have also been proposed. One example is the DPNR (Diesel Particulate-NO_x Reduction) concept, recently developed by the Toyota group [4,5]. This system consists of both a new catalytic filter and a new diesel combustion technology. The new catalytic converter for DPNR is a porous ceramic wall- flow filter coated with a NO_x Storage

Reduction (NSR) catalyst layer. The catalytic material is constituted by a high surface area support (e.g. γ-alumina), a noble metal (Pt), and alkaline or earth-alkaline metal oxides which present a high NO_x-storage capacity. These catalytic systems work under cyclic conditions, alternating long lean periods with short regeneration periods under rich condition. During the lean phase the NO_x produced by the engine are oxidized and adsorbed on the alkaline or earth-alkaline metal oxide component (with nitrite-nitrate species formation); during the rich phase the nitrate-nitrite species are reduced to molecular nitrogen by CO, H_2 and UHCs. The NO_x storage-reduction mechanism in the DPNR system is similar to that already proposed by Toyota for NSR systems [6,7,8,9]. Soot oxidation occurs under lean conditions thanks to the presence of NO_x and the excess of oxygen in the exhaust gas; soot removal is also claimed to occur during the rich phase as well.

Whereas the behaviour of NSR catalysts is well investigated [10,11,12,13,14,15], studies on DPNR systems are still scarce [16,17]. In particular, in previous works the performances of a model PtBa/γ-Al_2O_3 catalyst in the simultaneous NO_x and soot removal has been investigated [18,19]. It has been found that under cycling conditions, i.e. alternating lean-rich phases according to the typical DPNR operation, the Pt-Ba/Al_2O_3 sample is able to simultaneously remove soot and NO_x. It has also been shown that NO_x species stored onto the trapping component of the catalyst participate in the combustion of soot via the release of NO_x upon nitrate decomposition and/or by directly reacting with soot according to a surface reaction [18,20]. Along similar lines, Kustov et al. showed that the stored nitrates may decrease the temperature of soot oxidation when nitrate decomposition occurs in a proper temperature range, due to the release of NO_2 in the gas phase [16]. The same authors also suggested that the presence of an oxidation function (provided e.g. by Pt) is essential [21]. Along similar lines Sullivan et al. [22] reported that the presence of a NO_x trapping component like BaO in Pt/SiO_2 system does not promote *per-se* the particulate combustion, but favours soot combustion due to the increases in the NO_2 gas phase concentration upon nitrate decomposition. Accordingly there is a general consensus on the fact that the NO_x storage function of the NSR catalysts affects the combustion of soot.

Besides, soot may have a role on the NO_x storage capacity of the catalysts as well. In a recent work we have shown that the presence of soot negatively influences the NO_x storage capacity of the catalyst under representative conditions (i.e. in the presence of water and CO_2 in the feed stream) [23]. The presence of soot also decreases the stability of the NO_x adsorbed species, thus suggesting an interaction between soot and the stored NO_x.

Aim of the present work is to provide new insights on the pathways involved in the NO_x storage-reduction and soot oxidation over a model PtBa/Al_2O_3 catalyst, and on the interactions among the

related catalyst functions. For this purpose, a systematic study has been performed on the DPNR behaviour of the selected catalyst sample in which the reactivity in the NO_x storage-reduction and in the soot oxidation has been investigated in a wide temperature range (200-350°C) and at different NO inlet concentrations (250-1000 ppm). Experiments have been performed under nearly isothermal conditions, i.e. in the absence of significant temperature effects upon lean/rich switches. This has been accomplished by using a low reductant concentration (4000 ppm) and by separating the lean and the rich phases by an inert purge in between.

2. Experimental

The $PtBa/Al_2O_3$ (1/20/100 w/w) sample used in this study has been prepared by incipient wetness impregnation of a γ-Al_2O_3 calcined at 700°C (Versal 250 from UOP) with a solution of $Pt(NH_3)_2(NO_2)_2$ (Strem Chemicals, 5% Pt in ammonium hydroxide) followed by drying at 80°C and calcination at 500°C for 5 h. The obtained Pt/Al_2O_3 sample was then impregnated with an aqueous solution of $Ba(CH_3COO)_2$ (Strem Chemical, 99%), dried at 80°C and further calcined at 500 °C for 5 h to prepare the ternary $Pt\text{-}Ba/Al_2O_3$ catalyst. The selected impregnation order (first Pt and then Ba) has been adopted in order to ensure a good dispersion and stability of the noble metal on the alumina support, in line with the recipes of Toyota patents [[24]]. The obtained catalytic powder was grinded and sieved at 70-100 μm before use.

The catalyst was characterized by XRD analysis (Brüker D8 Advanced Instrument equipped with graphite monochromator on the diffracted beam), surface area and pore size distribution by N_2 adsorption-desorption at 77K (Micromeritics TriStar 3000 instrument) and Pt dispersion by hydrogen pulse chemisorption at 0°C (TPD/R/O 1100 Thermo Fischer Instrument).

The $PtBa/Al_2O_3$ sample presents a surface area near 160 m^2/g_{cat} and pore volume of 0.8 cm^3/g_{cat}, while the Pt dispersion is close to 60%. In the XRD patterns of the freshly calcined $PtBa/Al_2O_3$ catalyst both the monoclinic (JCPDS 78-2057) and orthorhombic (Whiterite, JCPDS 5-378) polymorphic forms of $BaCO_3$ were detected in addition to micro-crystalline γ-Al_2O_3 (JCPDS 10-425); no other crystalline phases were observed. Further details of catalyst preparation and characterization are reported elsewhere [[12,15,20,25,26]].

Printex-U (Degussa) was used as model soot [[27,28]]. Catalyst-soot mixtures (soot loading near 10 % w/w) were prepared by gently mixing in a vial the catalyst powder with soot, thus realizing a loose contact.

All reactivity tests were performed in a flow-reactor apparatus consisting of a quartz tube reactor (7 mm i.d) connected to a mass spectrometer (Omnistar 200, Pfeiffer Vacuum), to a micro GC (Agilent 3000A) and to a UV analyzer (Limas 11HW, ABB) for the on-line analysis of the outlet gases (NO, NO_2, N_2, O_2, CO, CO_2, N_2O and NH_3).

66 mg of the soot-catalyst mixture composed by 60 mg of catalyst and 6 mg of soot was used in each run, and the total gas flow was always set at 100 cm^3/min (at 0°C and 1 atm). When the pure catalyst was used, the sample weight was 60 mg.

Before the catalytic tests, the catalyst/soot mixture has been heated at 400°C in He in order to desorb/decompose any species weakly adsorbed on the soot/catalytic surface. The NO_x storage and reduction activity of the catalytic system has been studied in the presence and in the absence of soot by performing lean-rich cycles at constant temperature (Isothermal Step Concentration experiments, ISC) in the range 200-350°C. In a typical run, a stream of He + 3% O_2 (100 cm^3/min) was fed to the reactor and the catalyst temperature was set at the desired value. After stabilisation of the concentration signals a rectangular step feed of NO (1000 ppm) was admitted at constant temperature, by means of a pneumatically actuated four-way valve by keeping constant the overall flow rate. The NO_x storage proceeded up to nearly steady-state, then the inlet NO concentration was stepwise decreased to zero. After a few minutes the O_2 concentration was also decreased in a stepwise manner to zero. This sequence does not modify the results if compared to the simultaneous NO and O_2 removal. The catalyst reduction was accomplished by imposing stepwise changes in the H_2 concentration (0 → 4000 ppm and 4000 → 0 ppm) at the reactor inlet with a second four-way valve. In each step the total gas flow was always maintained constant with He as balance. A stream of Ar was also present in the feed gases as inert tracer: accordingly the lag time of the system could be carefully evaluated, but it has always been found negligible. Note that the lean and rich phases have been separated with a He purge in between in order to analyze separately the catalytic performances of the investigated catalyst during the lean and rich phases, and to avoid any spurious effects due to temperature variations upon lean/rich switches. 1% v/v H_2O and 0.1% v/v CO_2 are always present in the feed; even if the CO_2 and H_2O concentrations are lower than in real applications, their effects are still representative [26]. On the other hand the use of such a low CO_2 concentration allowed us to detect even small quantities of CO_2 produced by soot oxidation.

The catalyst samples have been conditioned by performing a few lean-rich cycles in order to obtain a reproducible behaviour (typically 3-4 cycles). Since soot is progressively consumed during each test, several catalyst/soot batches have been used in order to allow a proper comparison among the

various experiments. In particular all the data hereafter reported refer to a soot content near 7-8 % w/w, i.e. very close to the initial loading (10 % w/w).

Finally, in order to analyze the effect of soot on the thermal stability of the stored NO_x, TPD experiments of the stored NO_x have been performed in the presence and in the absence of soot. For this purpose NO_x have been stored onto the catalytic surface in the absence of soot, and then the NO_x-dosed catalyst has been mixed with soot. The storage phase has been carried out at 350°C with NO (1000 ppm) in He + O_2 (3% v/v), H_2O (1% v/v) and CO_2 (0,1% v/v) until a steady-state behaviour is attained; then the sample has been cooled at room temperature in He, extracted from the reactor and mixed with soot (10 % w/w) under atmospheric air. TPD experiments have been carried by heating the prepared catalyst-soot mixture at a rate of 10°C/min in He + H_2O (1% v/v) + CO_2 (0.1% v/v) from room temperature to 500°C. The results collected with the catalyst/soot mixture have been compared with those obtained in analogous experiments performed in the absence of soot.

Further details on the experimental procedure and apparatus can be found elsewhere [18,19,20].

3. Results and discussion

3.1. Effect of Temperature.

The NO_x storage–reduction over PtBa/Al_2O_3 has been investigated in the temperature range 200–350°C in the absence and in the presence of soot, and the results are shown in Figures 1 and 2, respectively.

Adsorption phase **–** The NO_x adsorption has been carried out with 1000 ppm of NO in the presence of O_2 (3 % v/v). At the lowest investigated temperature (200°C) and in the absence of soot (Fig. 1A), upon NO admission to the reactor (t = 0 s) NO is immediately observed at the reactor outlet. The NO concentration increases with time and eventually reaches the inlet NO concentration value after 1500 s. No significant NO_2 evolution is observed at this temperature. At t = 2200 s the NO inlet concentration is switched off; after the switch a tail is observed in the NO concentration profile, due to the desorption of weakly adsorbed NO_x species. The amount of NO_x stored at this temperature up to the end of the dose (steady-state) is near 0.29 mmol/g_{cat}, as apparent from Figure 3 (trace A, dotted line) which shows the amounts of NO_x stored as a function of time-on-stream. These amounts are calculated from the NO_x concentration curves showed in Figure 1A, taking into account the lag time of the apparatus which however has been found to be negligible (see experimental).

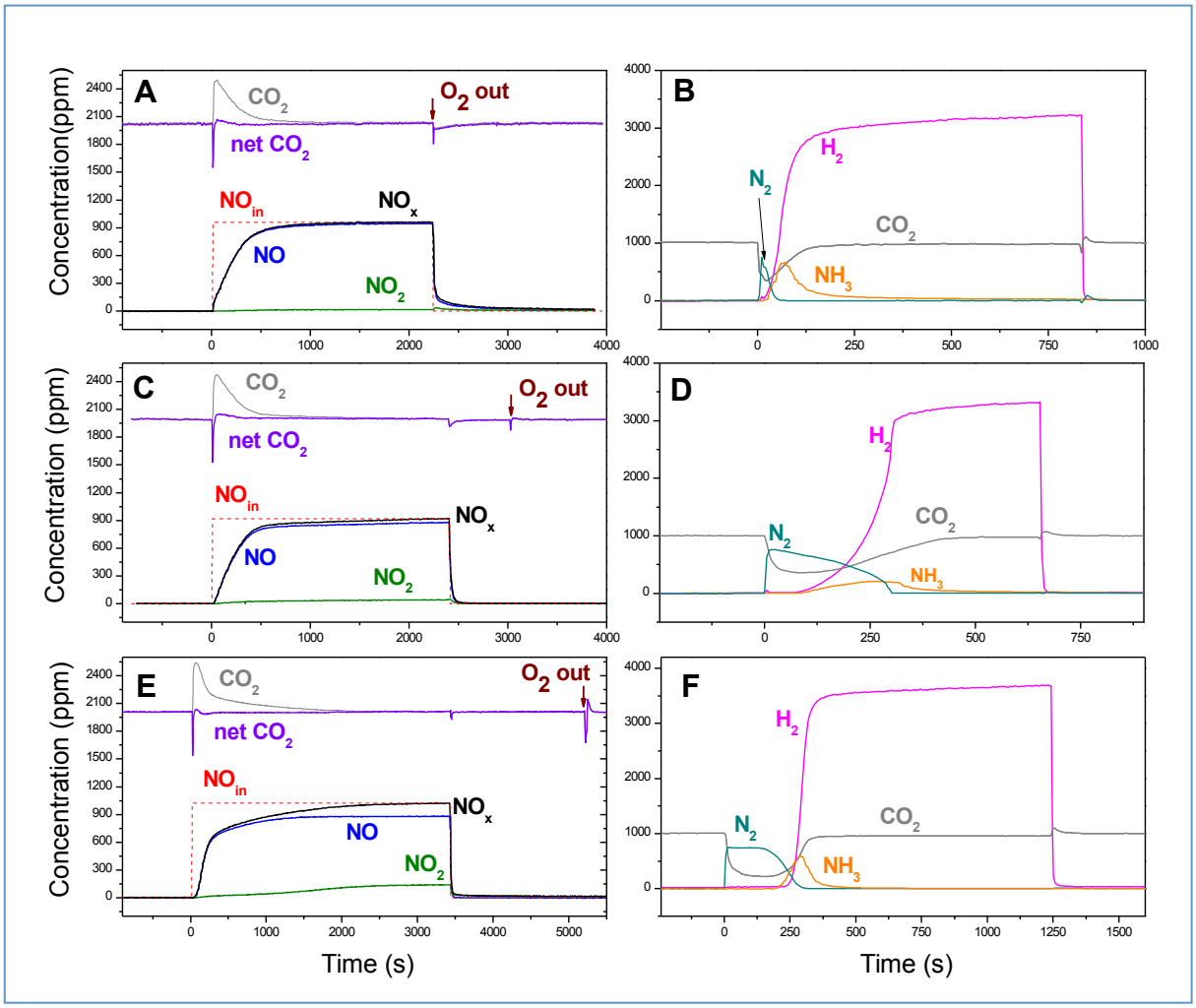

Figure 1 - Lean-rich cycles performed over Pt-Ba/Al_2O_3 in the absence of soot at different temperatures in the presence of H_2O (1% v/v) and CO_2 (0,1% v/v). Lean phase (A, C, E): 1000 ppm NO + O_2 (3% v/v) in He; rich phase (B, D, F): 4000 ppm H_2 in He. Other experimental conditions: catalyst weight 60 mg, total flow rate 100 cc/min @ 0°C and 1 atm. panels A-B: T = 200°C; panels C-D: T = 300°C; panels E-F: T = 350°C).

Upon NO admission, an increase in the CO_2 concentration is also observed, from the background level of 1000 ppm (Figure 1A). In particular a peak is initially observed; then the CO_2 concentration decreases to its background level at the end of the pulse. The increase in the CO_2 outlet concentration is due to the decomposition of surface carbonates upon NO_x uptake [12], in line with the stoichiometry of the following reaction (3):

$$BaCO_3 + 2\,NO + 3/2\,O_2 \rightarrow Ba(NO_3)_2 + CO_2 \qquad (3)$$

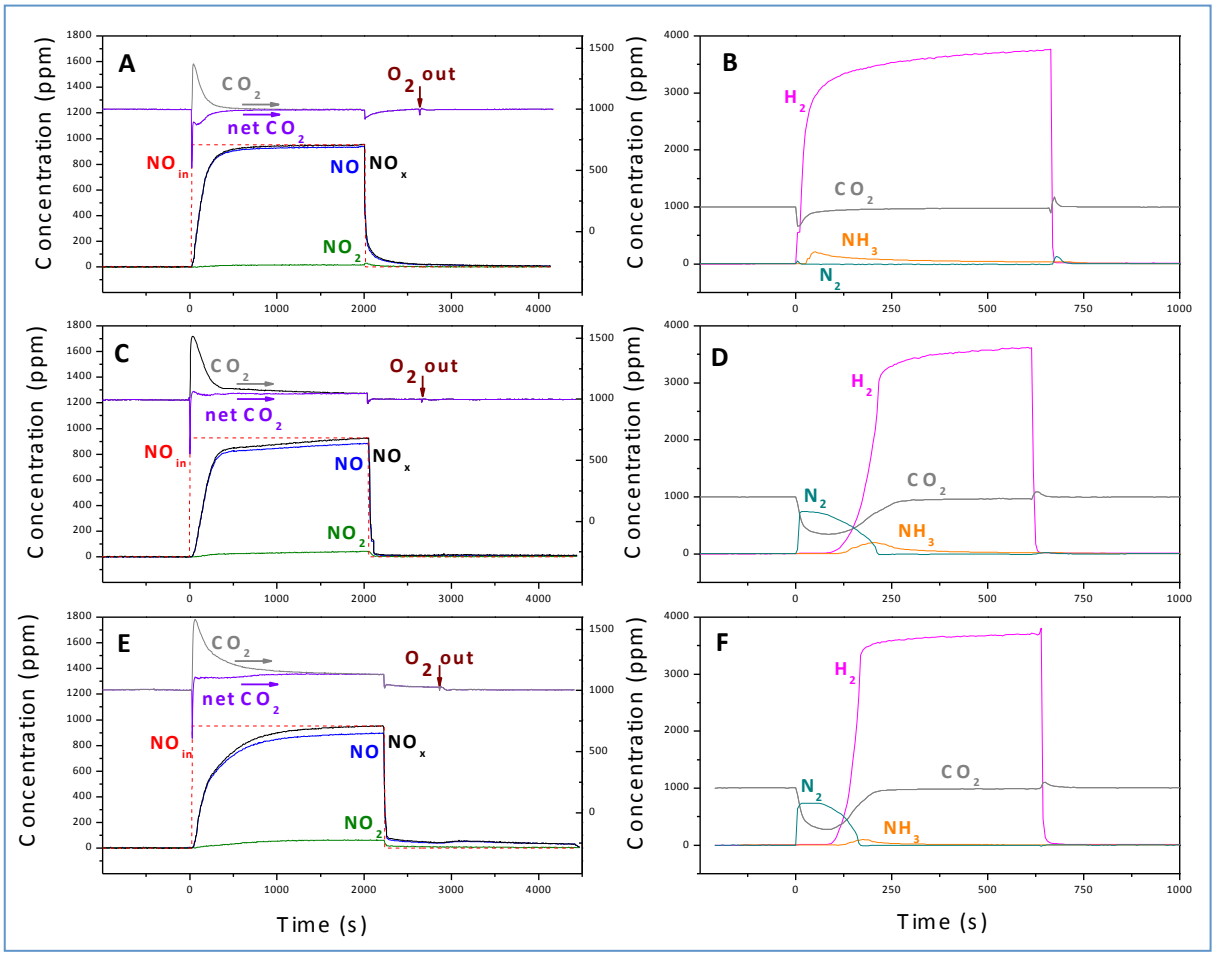

Figure 2 - Lean-rich cycles performed over Pt-Ba/Al_2O_3/soot mixture at different temperatures in the presence of H_2O (1% v/v) and CO_2 (0,1% v/v): Lean phase (A, C, E): 1000 ppm NO + O_2 (3% v/v) in He; rich phase (B, D, F): 4000 ppm H_2 in He. Other experimental conditions: 60 mg of catalyst + 6 mg of soot, total flow rate 100 cc/min @ 0°C and 1 atm. panels A-B: T = 200°C; panels C-D: T = 300°C; panels E-F: T = 350°C).

As a matter of fact, by subtracting from the CO_2 concentration trace the concentration of CO_2 estimated from the NO_x uptake according to the stoichiometry of reaction (3), a net CO_2 concentration trace is obtained (see Figure 1A) that closely resembles the inlet CO_2 concentration value (1000 ppm). This indicates that the evolution of CO_2 is uniquely related to the formation of nitrates species at the expense of carbonates, according to the stoichiometry of reaction (3). Along similar lines, after NO shutoff a small CO_2 uptake is observed, due to the occurrence of the reverse of reaction (3).

The NO_x storage behaviour of the catalyst is affected by temperature. The NO_x breakthrough increases from few seconds at 200 (Figure 1A) to 25 s at 300°C and 40 s at 350°C (Figures 1C and 1E). Besides the amounts of NO_x stored up to steady-state increase with temperature, from 0.28 mol/g_{cat} at 200°C to 0.34 mol/g_{cat} at 300°C and 0.59 mol/g_{cat} at 350°C (Figure 3 and Table 1).

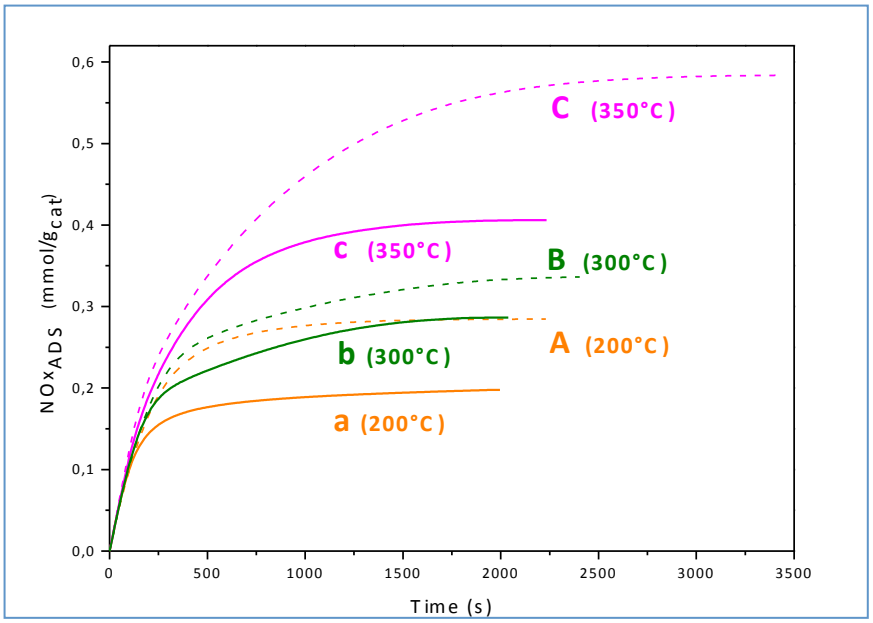

Figure 3 – Amounts of adsorbed NOx versus time over Pt-Ba/Al_2O_3 (dotted lines) and over Pt-Ba/Al_2O_3/soot mixture (solid lines) at different temperatures

Temperature °C	without soot			with soot		
	Stored NOx	Desorbed NO_x after NO shutoff	Desorbed NOx/Stored NOx	Stored NOx	Desorbed NO_x after NO shutoff	Desorbed NOx/Stored NOx
	$mmol/g_{cat}$	$mmol/g_{cat}$	%	$mmol/g_{cat}$	$mmol/g_{cat}$	%
200	0.28	0.09	34.0	0.20	0.09	43.8
300	0.34	0.02	7.2	0.29	0.06	19.6
350	0.59	0.06	10.0	0.39	0.10	27.2

Table 1. Stored NO_x, desorbed NO_x (1300s after NO_x shutoff) and percentage of desorbed NO_x / stored NO_x ratio at different temperatures, in the absence and in the presence of soot.

The NO_2 concentration at the reactor outlet measured at the end of the NO_x dose (steady-state) also increases with temperature. It has been suggested that NO_2 is precursor in the storage of NO_x, in line with the occurrence of a "nitrate" pathway for the storage of NO_x (i.e., NO oxidation to NO_2 followed by NO_2 adsorption in the form of nitrates via a disproportion reaction) [13]. Accordingly it is speculated that in the investigated temperature range the amounts of NO_x adsorbed at steady-state are in thermodynamic equilibrium with the the gas-phase NO_2 concentration, whose formation in our experimental conditions is kinetically controlled and hence increases with temperature (the reactor outlet NO_2 concentration is in all cases far from chemical equilibrium, being near 135 ppm at 350°C vs. the equilibrium value of 550 ppm at the same temperature). Accordingly in the investigated temperature range the amounts of stored NO_x increases with temperature, as opposite to what expected from the thermodynamics of adsorption which is an exothermic process.

The hypothesis of a thermodynamic control on the amounts of NO_x stored at steady state is also in line with data obtained with different inlet NO concentration (see later on). Indeed also in this case, as will be discussed below, the amount of NO_x stored at steady state are related with the NO_2 concentration. On the other hand, since other routes may be involved in the NO_x adsorption process, e.g. direct NO uptake on the catalyst surface, etc., factors other than thermodynamics may govern the amounts of NO_x stored at steady state. These aspects are still under debate and further studies are required for a better comprehension of the phenomena.

Finally, the increase in the NO_2 concentration with temperature also leads to a decrease of the NO/NO_2 ratio calculated at the end of the storage phase, from 59 at 200°C down to 6.4 at 350°C.

Temperature also affects the rate of adsorption, as expected. An indication of the average NO_x adsorption rate can be derived from the slope of the adsorption curves in Figure 3. Notably, in the initial part the curves are almost superimposed since the rate of NO_x adsorption is limited by the NO feed supply (almost complete NO uptake is initially observed at any temperature). Then the curves diverge and increase with a slope that, at fixed amounts of adsorbed NO_x, increases with temperature.

The results obtained when the same experiments have been carried out in the presence of soot are shown in Figure 2A, 2C, 2E. Also in the presence of soot the NO_x outlet concentration shows a dead time and then increases approaching the asymptotic values corresponding to the NO inlet concentration. The NO_x breakthrough increases with temperature but it is always lower than in the absence of soot. Along similar lines the amounts of NO_x stored up to steady-state (see Figure 3, solid lines) increase with temperature (from 0.20 mmol/g_{cat} at 200°C, up to 0.40 mmol/g_{cat} at 350°C), but the amounts of NO_x stored in the presence of soot are always lower than those measured in the absence. At high temperatures the NO_2 concentration measured at steady state is also lower in the presence of soot (e.g. 60 ppm vs. 140 ppm at 350°C in the presence and in the absence of soot, respectively) and accordingly higher NO/NO_2 ratios are measured.

Hence the data clearly indicates that soot reduces the NO_x storage capacity of the catalyst, in line with our previous data [23] and with results of Sullivan et al. [22] and Pieta et al. [29]. As previously suggested, the decrease in the NO_x storage capacity of the catalyst at steady state is likely related to the decrease in the NO_2 concentration.

Finally, the presence of soot also decreases the rate of NO_x adsorption, as apparent from the comparison of the slopes of the adsorption curves collected at the same temperature in the

presence and in the absence of soot at fixed amounts of stored NO_x (Figure 3). This is likely associated to the decrease in the NO_2 concentration, which hence influences the rate of the NO_x storage.

The presence of soot also influences the thermal stability of the adsorbed NO_x species. As indeed shown in Figures 1 and 2, upon NO shut off at the end of the adsorption phase (He purge) a tail is observed in the NO_x concentration and this decreases the amounts of NO_x which have been stored up to steady-state. The amounts of NO_x which have been desorbed at the various temperatures (calculated in all cases 1300 s after the NO shut off) are reported in Table 1. It is noted that in the absence of soot near 10% and 7% of the initially stored NO_x are decomposed after the NO shut off at 350 and 300°C, respectively; a higher fraction is calculated at 200°C (near 34%). In the presence of soot, the relative amounts of NO_x desorbed at 350°C and 300°C are 2-3 times higher than in its absence, being near 27.2 % (vs. 10 %) and 19.6 % (vs. 7.2 %) of those initially adsorbed, respectively. Relatively minor differences are observed at 200°C (43.8 % vs. 34%). Very similar conclusions are derived when the absolute amounts of NO_x are considered, instead of the percentage values (see table 1).

In spite of the fact that the data at 300°C seems to be slightly off-set since a minimum is observed in the absolute amounts of NO_x evolved at this temperature (see table 1), still the various effects are clearly visible. Indeed i) in all cases a significant NO_x desorption is observed, and ii) the presence of soot decreases both the amounts and the thermal stability of the NO_x adsorbed species. These points will be further discussed later in the following.

During NO_x storage in the presence of soot, the evolution of CO_2 is also observed (Figure 2). As already discussed, this is due to the decomposition of surface carbonates on the catalytic surface upon nitrates formation in correspondence of the NO admission (reaction (3)). However, in the presence of soot, CO_2 may also be formed due to soot combustion according to the stoichiometry of reactions (2) and/or (4a) and (4b):

$$NO_2 + C \rightarrow NO + CO \qquad (4a)$$

$$CO + ½\ O_2 \rightarrow CO_2 \qquad (4b)$$

where NO_2 and CO_2 are formed upon NO and CO oxidation at Pt sites, respectively. As a matter of fact, soot oxidation experiments by NO_2 carried out in the absence of the catalyst pointed out a relevant CO formation, in line with literature indications [30]. During our experiments CO formation is

not observed, likely because CO is oxidized to CO_2 by O_2 at Pt sites.

Accordingly reactions (2) and (4a-b) imply the consumption of NO_2 and a decrease of its concentration at the reactor outlet. In order to determine the amounts of CO_2 produced upon soot oxidation, the "net" CO_2 production has been calculated as previously indicated, and the results are shown in Figure 2. In the presence of soot a net CO_2 production is observed, which is negligible at 200°C (Figure 2A), but it is appreciable at 300°C and 350°C where the trace of the net CO_2 is roughly 50 ppm and 130 ppm above that of the background, respectively.

Notably, soot oxidation occurs only after NO addition to the reactor, since in the presence of oxygen alone no net CO_2 formation is observed. Hence NO_2, formed upon NO oxidation, is suggested to be the actual oxidizing agent of soot, accordingly to reactions (2) and (4a-b), and in line with many authors [16,22,31], although the participation of the stored NO_x is also likely, as will be discussed later on.

Regeneration phase **-** After NO_x adsorption and helium purge, the reduction of the stored NO_x has been carried out at the same temperature of adsorption (200, 300 and 350°C) by admission of H_2 in He in the presence of CO_2 and H_2O. The results obtained upon reduction of the stored NO_x at different temperatures in the absence and in the presence of soot are shown in Figures 1 and 2, respectively.

On the soot-free catalyst, upon the step addition of H_2 (at t = 0 s) at 200 °C (Figure 1B), the H_2 outlet concentration profile shows a dead time during which it is completely consumed and then it increases with time. During H_2 consumption, the evolution at first of N_2 and then of NH_3 is seen at the reactor outlet, together with a consumption of CO_2. No formation of other products (e.g. N_2O) has been detected in appreciable amounts. The evolution of N_2 and NH_3, and the consumption of CO_2 as well, are in line with the overall stoichiometry of the following reactions (5) and (6):

$$Ba(NO_3)_2 + 5\ H_2 + CO_2 \rightarrow BaCO_3 + N_2 + 5\ H_2O \qquad (5)$$

$$Ba(NO_3)_2 + 8\ H_2 + CO_2 \rightarrow BaCO_3 + 2\ NH_3 + 5\ H_2O \qquad (6)$$

which consider the re-adsorption of CO_2 onto the Ba sites once NO_x has been reduced to give gaseous products.

The observed temporal evolution of the reduction products (with nearly complete nitrogen selectivity at the beginning of the rich phase followed by ammonia formation) is due to the

occurrence of a two-steps in series process for the reduction of the stored NO_x by H_2 already proposed in previous studies of our group [32,33,34]. The suggested pathway involves a first fast step during which the stored NO_x react with H_2 to give NH_3, followed by the slower reaction of ammonia with residual nitrates to form nitrogen. The observed products evolution with time is due to an H_2 front which develops and travels along the reactor. Accordingly, NH_3 is formed at the H_2 front and reacts with the NO_x stored downstream the front, leading to N_2 formation, which accordingly is immediately detected at the reactor exit. When the front reaches the end of the catalytic bed, there are no NO_x stored downstream and this leads to the evolution of ammonia, which accordingly follows that of N_2.

Similar results have been obtained (in the absence of soot) at the other temperatures, i.e. 300°C and 350°C (Figure 1 D and F). However upon increasing the temperature it is observed that: i) the amounts of the evolved reduction products increase due to the larger amounts of stored NO_x with temperature (Figure 3); and ii) the nitrogen selectivity of the reduction process increases with temperature, from roughly 35% at 200°C up to 85% at 350°C. This is in line with the occurrence of the two-steps pathway previously suggested for N_2 formation [34,35,36]: by increasing the temperature the second step of the reaction which represents the r.d.s of the process (the reaction of ammonia with nitrates to give nitrogen) becomes faster and this drives the nitrogen selectivity of the reaction.

The results obtained upon reduction of the stored NO_x at the same temperatures in the presence of soot are shown in Figure 2 B, D and F. A comparison with the results obtained in the absence of soot (Figures 1 B, D and F) indicates that the presence of soot does not influences significantly the reduction of the stored NO_x, although a slight increase of the N_2 selectivity is observed in the presence of soot in same cases (e.g. from 85.7% to 94.8% at 350°C).

3.2 Effect of NO inlet concentration on the NO_x storage/reduction and soot oxidation.

Lean phase **-** The effect of the NO inlet concentration on the simultaneous NO_x and soot removal over the model PtBa/Al_2O_3 catalyst has been addressed by performing lean-rich cycles at 350°C in the presence of CO_2 (0.1% v/v) and H_2O (1% v/v) with 250, 500 and 1000 ppm of NO in the feed (NO_{in}) during the lean phase.

The results obtained in the case of 1000 ppm NO inlet concentration in the absence and in the presence of soot are shown in Figure 1E and 2E, respectively, and have been previously discussed. Figure 4 shows the results obtained at 350°C in terms of NO_x adsorbed during the lean phase as a function of time in the case of the different NO inlet concentrations both in the absence (dotted

lines) and in the presence (solid lines) of soot. As previously reported in the case of Figure 3, these amounts are calculated from the NO_x concentration curves of Figure 1 and 2.

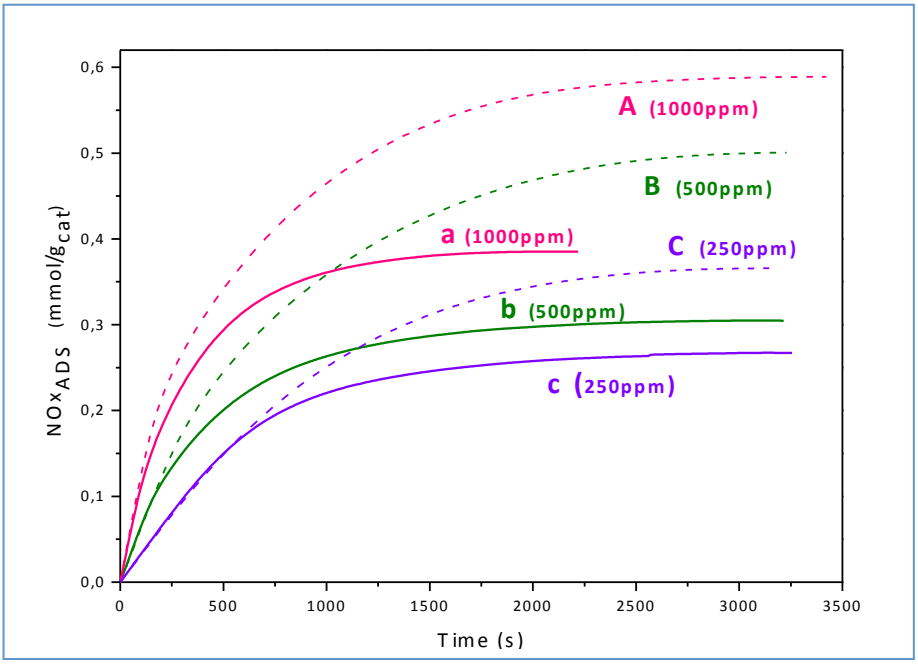

Figure 4 – Amounts of adsorbed NOx versus time over Pt-Ba/Al2O3 (dotted lines) and over Pt-Ba/Al2O3/soot mixture (solid lines) at different NO inlet concentration

As shown in Figure 4, in all cases the amounts of stored NO_x increase with time reaching an asymptotic value corresponding to the steady-state conditions. In the absence of soot (dotted lines), the amounts of stored NO_x decrease with the NO inlet concentration. A NO_x storage capacity near 0.59 mmol/g_{cat} has been measured at steady state when 1000 ppm of NO are fed to the reactor (trace A), which decreases to 0.37 mmol/g_{cat} for a NO inlet concentration value of 200 ppm (trace C). The NO_2 outlet concentration at steady-state also decreases upon decreasing the inlet NO concentration. The lower NO_x storage capacity which is observed upon decreasing the NO inlet concentration is likely related to lower concentration of NO_2 produced, as already discussed in the case of the effect of temperature. In fact, in line with the hypothesis of thermodynamic control of the NO_x storage at steady state, the amounts of stored NO_x are related to the NO_2 concentration. Also, the increase of the NO inlet concentration (and of NO_2 concentration as well) increases the rate of the NO_x adsorption, as revealed by the slopes of the adsorption curves of Figure 4 (dotted lines) in the region where the storage is not limited by the supply of NO.

Finally, upon NO and O_2 shutoff a tail in the NO_x concentration is observed, as already discussed in the case of the effect of temperature, indicating the decomposition of weakly adsorbed NO_x species. The amounts of NO_x desorbed after the NO shutoff (Table 2) decreases with the NO inlet

concentration (6 and 3 µmol/g_{cat} for NO = 1000 and 250 ppm, respectively), but are very similar if normalized to the amounts of NO_x initially stored (near 8-10%).

The presence of soot influences the storage of NO_x, as revealed by the comparison of the adsorption curves obtained in the absence and in the presence of soot (Figure 4, dotted lines vs. solid lines). In the presence of soot the amounts of adsorbed NO_x decreases upon decreasing the NO inlet concentration, from 0.39 down to 0.27 mmol NO_x/g_{cat}, and these amounts are always lower than those observed with the soot-free catalyst. The presence of soot also decreases the NO_2 concentration measured at steady-state at the exit of the reactor, if compared to the soot-free catalyst (data not shown). Accordingly in the presence of soot higher NO/NO_2 ratios are calculated at any investigated NO inlet concentration value. As previously discussed, this is related to the involvement of NO_2 in soot combustion according to reactions (2) and (4a-b). Along to the lines previously discussed, the decrease in the NO_x storage capacity of the catalyst at steady state in the presence of soot is likely explained by the lower NO_2 concentrations obtained in these cases.

The rate of NO_x adsorption also decreases upon decreasing the NO inlet concentration and upon addition of soot (compare the slopes of the adsorption curves at various NO inlet concentrations, and in the presence/absence of soot at fixed stored NO_x, respectively). Again, this is likely associated to the effect of the NO_2 concentration on the rate of NO_x adsorption.

Finally, also from these experiments it is clear that soot has a significant influence on the stability of the adsorbed NO_x. In fact near 25-30 % of the NO_x stored up to steady-state are desorbed in this case after NO shutoff (Table 2). These amounts are roughly 3 times higher than those calculated in the absence of soot.

NO inlet concentration ppm	without soot			with soot		
	Stored NO_x	Desorbed NO_x after NO shutoff	Desorbed NO_x/Stored NO_x	Stored NO_x	Desorbed NO_x after NO shutoff	Desorbed NOx/Stored NO_x
	mmol/g_{cat}	mmol/g_{cat}	%	mmol/g_{cat}	mmol/g_{cat}	%
250	0.37	0.03	8.32	0.27	0.08	30.1
500	0.50	0.04	8.14	0.31	0.07	24.1
1000	0.59	0.06	9.98	0.39	0.10	27.2

Table 2. Stored NOx, desorbed NOx (1300s after NOx shutoff) and percentage of desorbed NOx / stored NOx ratio at different NO inlet concentration, in the absence and in the presence of soot.

Regeneration phase **–** The reduction of the NO_x stored at 350°C by using different NO inlet concentration has been investigated as well. The results, here not shown for the sake of brevity, were in all cases very similar to those obtained in the case of Figure 1B (adsorption with NO = 1000 ppm at 350°C, absence of soot) and Figure 2B (adsorption with NO = 1000 ppm at 350°C, presence of soot). The results obtained in the absence and in the presence of soot point out that the presence of soot does not influence significantly the reduction of the stored NO_x.

3.3 Interaction of the stored NO_x with soot.

The results reported above pointed out that the presence of soot influences the storage of NO_x over PtBa/Al_2O_3. In fact soot i) decreases the NO_x storage capacity of the catalyst, and ii) favors the decomposition of the stored NO_x species. These conclusions apply when NO_x are stored at different temperatures and when different values of the NO inlet concentration are used. On the other hand, the reduction of the stored NO_x (i.e. catalyst regeneration) is not significantly influenced by the presence of soot, if one neglect a small increase in the N_2 selectivity. During NO_x storage, combustion of soot also takes place if the temperature is high enough, i.e. at 300°C and above. Evidence has been provided in this case for a soot oxidation pathway involving NO_2, formed upon NO oxidation, that is well recognized in the literature [16,22,31]. However, the participation of adsorbed NO_x species in the combustion of soot cannot be ruled out, as also suggested in previous papers [23]. In order to better analyze these aspects, experiments have been carried out in which the interaction of soot with NO_x adsorbed on the catalyst surface is investigated. For this purpose TPD experiments have been carried out in which the thermal stability and reactivity of NO_x species stored over the PtBa/Al_2O_3 catalyst has been studied in the presence and in the absence of soot. As previously discussed, the amounts of NO_x that are stored at steady state on the catalyst in the presence and in the absence of soot are different. Accordingly, in order to compare catalyst samples with the same amounts of stored NO_x, the NO_x have been accumulated in the absence of soot in one batch of catalyst and then the sample has been divided into two portions: one has been mixed with soot prior the TPD experiment, while the second (not mixed with soot) has been used as a reference (see experimental). NO_x have been stored by contacting the catalyst with NO/O_2 at 350°C up to steady-state; as indicated in previous studies only nitrates are formed in this case on the catalyst surface [13,35].

The results of the TPD runs (carried out in the presence of water and CO_2) are shown in Figure 5A (absence of soot) and 5B (presence of soot). In the case of the soot-free Pt-Ba/γ-Al_2O_3 catalyst (Figure 5A), decomposition of nitrates is observed starting from 260°C with the evolution of small

amounts of NO. Above 350°C (the adsorption temperature) the NO concentration rapidly increases and a maximum is observed at 500°C, i.e. corresponding to the end of the heating ramp. Accordingly this is not a genuine TPD peak but it is determined by the maximum temperature during the heating ramp. The catalyst has been kept at this temperature until complete evolution of the products.

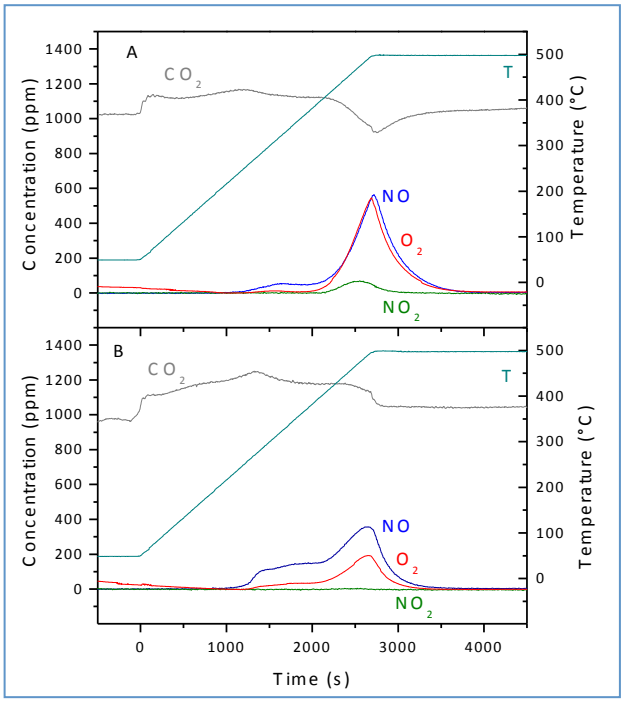

Figure 5 - TPD run after NO_x adsorption at 350°C (lean phase 1000 ppm NO + O_2 (3% v/v) in He + H_2O (1% v/v) + CO_2 (0,1% v/v)) over (A) Pt-Ba/Al_2O_3 catalyst; (B) Pt-Ba/Al_2O_3 / soot mixture

Above 350°C the NO evolution is accompanied by that of O_2 in similar amounts; minor quantities of NO_2 are also observed with peak maximum of 65 ppm at 470°C. After the TPD run, a reducing treatment has been carried out with a stream of H_2 (0.4%v/v in He + 1%v/v H_2O+ 0,1% v/v CO_2) at 350°C to reduce the residual nitrates, if any. No reaction products have been detected, thus indicating that all the adsorbed nitrate species have been decomposed during the TPD run.

The overall amounts of NO, O_2 and NO_2 evolved, estimated by integration of the TPD peaks, are well in line with the stoichiometry of the following reactions:

$$Ba(NO_3)_2 + CO_2 \rightarrow BaCO_3 + 2\ NO + 3/2\ O_2 \quad (7)$$

$$Ba(NO_3)_2 + CO_2 \rightarrow BaCO_3 + 2\ NO_2 + ½\ O_2 \quad (8)$$

with reaction (7) prevailing over reaction (8). Besides, in line with the stoichiometry of reactions (7) and (8), an uptake of CO_2 is also observed in correspondence with nitrate decomposition, due to Ba-carbonates formation at the expense of nitrates. Worth to note that the presence of CO_2 (1000 ppm)

in the flowing gases does not appreciably affects the decomposition of the surface nitrates, as pointed out by dedicated TPD experiments carried out in the presence and in the absence of CO_2. This is in line with the lower acidity of CO_2 if compared to NO_x towards adsorption onto the Ba sites.

The results of the TPD experiment of Figure 5A are very similar to those previously obtained over a similar catalyst sample, and reported elsewhere [23]. However, as opposite to the previous results, in this case a small NO evolution is observed below 350°C, i.e. below the temperature of NO_x adsorption. This is likely related to the different procedure used in this case, which involves the exposure of the nitrated catalyst to air for several hours before the TPD run, leading to water/CO_2 adsorption from the atmosphere. This may have affected the stability of the stored nitrates: in fact in several TPD runs carried out with no exposure of the catalyst to the atmosphere after NO_x adsorption, the nitrate decomposition onset was always observed very close to the temperature of adsorption. The reasons for which the thermal stability of nitrates is affected by exposure to the atmosphere are not well understood so far, although it has already been shown elsewhere that the features of the stored NO_x are affected by surface hydration already at room temperature [36].

Figure 5B shows the results of the TPD experiments carried out after mixing the catalyst with soot. A comparison with Figure 5A clearly shows that the presence of soot favors the decomposition/reduction of the stored nitrates. Indeed in this case a significant release of NO and O_2 is observed in the temperature range 260°C-350°C, i.e. below the adsorption temperature of 350°C. The decomposition of nitrates is then completed above 350°C, with a peak maximum near 485°C. Notably, a different product distribution is observed in the presence of soot, since the amounts of oxygen are markedly lower if compared to that of NO; besides, no NO_2 evolution is observed. Finally, no significant CO_2 uptake is observed.

The data shown in Figure 5 clearly indicate that the presence of soot favors the reduction of the stored nitrates, while soot is being oxidized. In fact in the presence of soot the NO evolution is shifted to lower temperatures: based on the amounts of evolved NO it appears that roughly 20 % of the initially adsorbed nitrates have been decomposed below 350°C (i.e. the temperature of adsorption) in the presence of soot, while only 7 % in the case of the soot-free sample (Figure 5A). Besides, the NO peak maximum is observed at lower temperatures, i.e. near 485°C vs. above 500°C. The oxidation of soot upon nitrate decomposition leads to $BaCO_3$ which accordingly prevents the uptake of CO_2 from the gas phase (reactions (7) and (8)).

The effect of soot on the stability of the stored nitrates has also been pointed out by the ISC experiments discussed above (Figures 1 and 2) showing that the amounts of NO_x released during the He purge, after the NO dose, are significantly higher in the presence of soot. These results imply a direct reaction between the stored nitrates and soot, which can be likely explained upon invoking a certain degree of mobility of the surface nitrates. In fact it has been suggested that nitrates, adsorbed on the Ba component of the catalyst, are rather mobile in the presence of a reducing center [16,37]. Hence it may be argued that the soot particles may behave as reducing centers towards nitrates thus activating their surface mobility. When nitrates contact a soot particle carbon is oxidized according to the following reaction:

$$C + 2\ NO_3^- \rightarrow CO_3^= + 2\ NO + \tfrac{1}{2}\ O_2 \qquad (9)$$

which results in the formation of NO and O_2, as indeed observed during the TPD experiment carried out in the presence of soot, and of carbonates species whose formation accounts for the lack of a significant CO_2 net uptake from the gas phase in the TPD experiment with the catalyst/soot mixture.

Reaction (9) obviously also implies a partial reduction of the stored nitrates. As a matter of fact, TPD data provide clear evidence for the occurrence of reduction of nitrates by soot (reaction (9)). In fact, below 350°C of the TPD run of Figure 5B (i.e. before the onset of nitrate thermal decomposition) the concentration of the evolved products obeys the stoichiometry of reaction (9), and the O/N atomic ratio in the evolved products is very close to the stoichiometric value. Besides no uptake of CO_2 is observed below 350°C (as expected from the occurrence of reactions (7) or (8)), due to CO_2 formation upon soot oxidation (reaction (9)).

Above 350°C, nitrate thermal decomposition also occurs, and hence the stoichiometry of reaction (9) is no longer respected. In fact above 350°C the evolved NO_x species give to a O/N ratio in the product higher that that expected from the stoichiometry of reaction (9). As a matter of fact, the calculated oxygen/nitrogen atomic ratio of the gaseous products evolved during the entire TPD in the presence of soot (Figure 5B) is O/N = 1.7, which is lower than the stoichiometric O/N value of 2.5 of the nitrate decomposition (reactions (7) or (8)). This value is indeed calculated from the TPD of the stored nitrates without soot (Figure 5A, O/N = 2.6).

Accordingly TPD data indicates that adsorbed nitrates are able to oxidize soot below the temperature of their thermal decomposition, following the stoichiometry of reaction (9) which implies the direct reaction of the nitrates ad-species with soot. This pathway parallels the oxidation

of soot by NO_2 that occurs in the presence of gas-phase NO_2, i.e. upon the NO_x storage during lean/rich operation of the NSR catalyst.

The suggested mechanism implying the direct interaction between nitrate adspecies and soot has analogies with the pathway proposed for nitrate reduction during lean/rich operation of NSR catalysts. Indeed in that case it has been suggested that nitrates spill over the surface towards the Pt sites where they are reduced by the reductant [38,39], the driving force for this process being the presence of a reduced Pt site. Along similar lines, the presence of soot (a reductant) is believed to be the driving force for the mobility of the nitrates which may eventually oxidize soot according to the stoichiometry of reaction (9). Notably, in the suggested mechanistic proposals concerning the nitrate-soot interaction, the role of Pt (and of Pt-Ba couples) has not yet been clarified, and work is presently in progress in our labs to elucidate such aspects.

4. Concluding remarks

The present study pointed out that the presence of soot influences the NO_x storage properties of the investigated $PtBa/Al_2O_3$ catalyst, when estimated in the presence of water and CO_2. In fact soot leads to an appreciable decrease both of the NO_x storage capacity and of the rate of NO_x adsorption. This effect is seen at different temperatures and when different values of the NO inlet concentration are used in the experiments. During NO_x storage, soot oxidation also occurs at 300°C and above, thanks to the presence of NO_2 formed upon NO oxidation over Pt sites. In fact the NO_2 concentration at the reactor outlet in the presence of soot is significantly lower than that observed in the absence of soot, thus pointing out the involvement of NO_2 in soot oxidation. The decrease of the NO_2 concentration may likely explain also the observed decline in the NO_x storage properties of the catalyst. In fact, in line with the occurrence of a “nitrate” pathway for the storage of NO_x (i.e., NO oxidation to NO_2 followed by NO_2 adsorption in the form of nitrates via a disproportion reaction), Ba and soot compete for reaction with NO_2, as suggested by Sullivan et al. [22], leading to the observed decrease in the NO_x storage properties. On the other hand, the reduction of the stored NO_x is not significantly affected by the presence of soot, although some minor changes in the N_2 selectivity (a slight increase in the presence of soot) have been observed. These aspects deserve however further investigation.

Finally, it is worth of note that the adsorbed NO_x oxidize soot at temperature well below those corresponding to their thermal decomposition originating NO_2 in the gas phase. This has been shown by TPD experiments in which the reactivity / thermal decomposition of nitrates has been

investigated in the presence and in the absence of soot. It has been found that the presence of soot favors the decomposition and the reduction of the stored nitrates, while soot is oxidized. In fact the presence of soot shifts the decomposition/reaction of the stored nitrates at lower temperatures, and the stoichiometry of the released products reflects the occurrence of a partial reduction of the initially stored NO_x, as well as the oxidation of soot. Hence a direct reaction between the stored nitrates and soot has been suggested, that has been explained on the basis of the surface mobility of the adsorbed nitrates. This soot oxidation pathway involves surface species and parallels the NO_2-soot oxidation that occurs in the presence of gas-phase NO_2.

Acknowledgements

The financial support of MUR – PRIN project 2007HHCZP4 is acknowledged.

References

[1] T. Johnson, Platinum Metals Rev. 52 (2008) 23

[2] R. Allansson, P.G. Blakeman, B.J. Cooper, H. Hess, P.J. Silcock, A.P. Walker, SAE Paper SP-1673 2002-01-428 (2002)

[3] S.J. Jelles, M. Makkee, J.A. Moulijn, Top. Catal. 16 (2001) 269

[4] Toyota Patent, European Patent Application No 01107629.6 (2001)

[5] K. Nakatani, S. Hirota, S. Takeshima, K. Itoh, T. Tanaka, SAE Paper SP-1674 2002-01-0957 (2002)

[6] N. Miyoshi, S. Matsumoto, K. Katoh, T. Tanaka, J. Harada, N. Takahashi, K. Yokota, M. Sugiura, K. Kasahara, SAE Technical Paper 950809 (1995)

[7] S. Matsumoto, Catal. Today, 29 (1996) 43

[8] N. Takahashi, H. Shinjoh, T. Iijima, T. Szuki, K. Yamazaki, K. Yokota, H. Suzuki, N. Miyoshi, S. Matsumoto, T. Tanizawa, T. Tanaka, S. Tateishi, K. Kasahara, Catal. Today 27 (1996) 63

[9] H. Shinjoh, N. Takahashi, K. Yokota, M. Sugiura, Appl. Catal. B: Environ. 15 (1998) 189

[10] S. Roy, A. Baiker, Chem. Rev. 109 (2009) 4054

[11] W.S. Epling, L.E. Campbell, A. Yezerets, N.W. Currier, J. E. Parks II, Cat. Rev. 46 (2004) 163

[12] L. Lietti, P. Forzatti, I. Nova, E. Tronconi, J. Catal. 204 (2001) 175

[13] I. Nova, L. Castoldi, L. Lietti, E. Tronconi, P. Forzatti, F. Prinetto, G. Ghiotti, J. Catal. 222 (2004) 377

[14] I. Nova, L. Lietti, L. Castoldi, E. Tronconi, P. Forzatti, J. Catal. 239 (2006) 244

[15] F. Frola, M. Manzoli, F. Prinetto, G. Ghiotti, L. Castoldi, L. Lietti, J. Phys. Chem. C 112 (2008) 12869

[16] A.L. Kustov, M. Makkee, Appl. Catal. B: Environ. 88 (2009) 263

[17] C.-N. Millet, R. Chédotal, P. Da Costa, Appl. Catal. B: Environ. 90 (2009) 339

[18] L. Castoldi, R. Matarrese, L. Lietti, P. Forzatti, Appl. Catal. B: Environ. 64 (2006) 25

[19] R. Matarrese, L. Castoldi, L. Lietti, P. Forzatti, Top. Catal. 42–43 (2007) 293

[20] R. Matarrese, L. Castoldi, L. Lietti, P. Forzatti, Catal. Today 136 (2008)11

[21] J. Suzuki, S. Matsumoto, Top. Catal. 28 (2004) 171

[22] J.A. Sullivan, O. Keane, A. Cassidy, Appl. Catal. B: Environ. 75 (2007) 102

[23] L. Castoldi, N. Artioli, R. Matarrese, L. Lietti, P. Forzatti, Study of DPNR catalysts for combined soot oxidation and NOx reduction, Catal. Today (2010), doi:10.1016/j.cattod.2010.03.022

[24] N. Miyoshi, T. Tanizawa, K. Kasahara, S. Tateishi, European Patent Application 0 669 157 A1, 1995.

[25] R. Matarrese, L. Castoldi, L. Lietti, P. Forzatti, Top. Catal. 52 (2009) 2041

[26] I. Nova, L. Castoldi, L. Lietti, E. Tronconi, P. Forzatti, Catal. Today 75 (2002) 431

[27] A. Setiabudi, M. Makee, J.A. Moulijn, Appl. Catal. B: Environ. 50 (2004) 185

[28] N. Nejar, M. Makkee, M.J. Illàn-Gómez, Appl. Catal. B: Environ. 75 (2007) 11

[29] I.S. Pieta, M. García-Diéguez, C. Herrera, M.A. Larrubia, L.J. Alemany , J. Catal. 270 (2010) 256

[30] B.A.A.L. van Setten, M. Makkee, J.A. Moulijn, Catal. Rev. 43 (2001) 489

[31] K. Krishna, M. Makkee, Catal. Today 114 (2006) 48

[32] L. Lietti, I. Nova, P. Forzatti, J. Catal. 257 (2008) 270

[33] I. Nova, L. Lietti, P. Forzatti, Catal. Today 136 (2008) 128

[34] P. Forzatti, L. Lietti, I. Nova, En. Environ. Sci. 1 (2008) 236

[35] I. Nova, L. Castoldi, L. Lietti, E. Tronconi, P. Forzatti, F. Prinetto, G. Ghiotti, SAE Technical Paper 2005-01-1085 (2005)

[36] L. Castoldi, L. Lietti, P. Forzatti, S. Morandi, G. Ghiotti, F. Vindigni, The NO_x storage-reduction on Pt-K/Al_2O_3 Lean NO_x Trap Catalyst, submitted to J. Catal.

[37] A.J. Paterson, D.J. Rosenberg, J.A. Anderson, Stud. Surf. Sc. Catal. 138 (2001) 429

[38] R.D. Clayton, M.P. Harold, V. Balakotaiah, C.Z. Wan, Appl. Catal. B: Environ. 90 (2009) 662

[39] D. Bhatia, M.P. Harold, V. Balakotaiah, Catal. Today 151 (2010) 314

Paper III

Interaction between soot and stored NOx during operation of LNT Pt–Ba/Al_2O_3 catalysts

Roberto Matarrese, Nancy Artioli, Lidia Castoldi, Luca Lietti, Pio Forzatti
Catalysis Today xxx (2011) xx–xx

Abstract

The interaction of soot with nitrates stored on a model PtBa/Al_2O_3 LNT catalyst sample is here investigated under realistic conditions, i.e. upon lean/rich cycling in the presence of water and CO_2. The presence of soot inhibits the NO_x storage capacity of the catalyst during the lean phase at different temperatures, in the range 200-350 °C, but does not affect significantly the regeneration process of the stored nitrates. Simultaneously with the NO_x storage, soot is converted to CO_2 at temperatures above 300 °C. Soot is oxidized by NO_2 formed by NO oxidation on Pt sites, but the participation of the stored nitrates in the soot oxidation is also likely, as pointed out by TPD/TPO experiments showing the occurrence of a surface reaction involving soot and the stored nitrates.

Keywords

Soot oxidation, DPNR catalysts, simultaneous NO_x and soot removal, Diesel Particulate NO_x Reduction, NSR catalysts

1. Introduction

The reduction of both soot (particulate matter) and NO_x emissions from diesel-equipped vehicles is nowadays mandatory to cope with the next coming emission standards [1]. The soot removal relies on the use of diesel particulate filters (DPFs) [2], that must be periodically regenerated to remove the entrapped soot avoiding excessive pressure drops at the exhaust. For this reason the filter may by catalyzed to promote soot combustion at lower temperatures.

Concerning NO_x, either Selective Catalytic Reduction (SCR) [3,4] or Nitrogen Storage Reduction (NSR), also quoted as Lean NO_x Trap (LNT) [5,6], represent the top contenders for reducing NO_x concentrations in the exhausts from diesel and lean burn gasoline engines [1]. While the SCR technique is based on the reaction between injected NH_3 and NO present in the flue gases on metal-substituted zeolites [1] or vanadia-tungsta-titania catalysts [8], NSR catalysts make no use of any external reductant. These catalysts operate the NO_x reduction under cyclic conditions by alternating long lean phases during which NO_x emitted in the exhaust gases are adsorbed on the catalyst, with subsequent short rich periods in which the stored NO_x are reduced by H_2, CO and Hydrocarbons (HC) present in the flue gases to produce nitrogen [5,6]. LNT catalysts are generally made by a high surface area support (such as γ-Al_2O_3), alkaline/alkaline-earth metal oxides (such as K_2O and BaO) and precious metals like Pt, Rh, Pd; other components are also present in fully formulated catalysts (e.g. CeO_2). Hybrid NSR + SCR configurations have also been proposed, since they guarantee higher NO_x removal efficiencies [3,9-14].

Exhaust after-treatment systems able to cope with the next coming strict emission standards are rather complex. De-soot and De-NO_x devices are used, along with a Diesel Oxidation Catalyst (DOC) as well. However the optimal design of the aftertreatment exhaust system is still a matter of debate: the DOC is generally placed upstream the DPF and SCR/LNT converters, while different solutions have been proposed for the DPF and the DeNO_x catalyst. Integrated (or one-pot) solutions have been proposed, like Catalyzed Diesel Particulate Filters (CDPFs) which act as DOC but also remove soot, or the DPNR (Diesel Particulate-NO_x Reduction) technology which has been recently proposed by the Toyota group [15,16]. The DPNR technique has the unique capacity to remove simultaneously soot and NO_x, and is based on the use of a catalyzed filter on which a NSR catalyst is deposited. In this way soot is removed by the filter while NO_x are reduced according to the NSR technology [15].

Despite DPNR systems are used at a commercial scale, still many aspects concerning their catalytic performances, the operating reaction mechanisms and the interactions between the De-soot and De-NO_x functions are still under debate. This has motivated in recent years a number of studies concerning the reactivity of NSR catalysts in the presence of soot [17-20]. In previous works from our

group the behavior of model PtBa/Al_2O_3 and PtK/Al_2O_3 LNT catalysts in the simultaneous removal of soot and NO_x has been investigated. It has been shown that during the lean phase NO_x are being stored on the catalyst surface, while soot oxidation occurs involving primarily NO_2, formed upon NO oxidation [21,22]. However more recent studies have shown that NO_x species, stored onto the trapping component of the catalyst, may participate in the combustion of soot by releasing gaseous NO_x upon decomposition and/or by directly reacting with soot according to a surface reaction [23-26]. Besides, it has been shown that the presence of soot depresses the NO_x storage capacity of the catalyst, in line with data obtained by Pieta et al. [27].

Along similar lines, Kustov et al. [28] showed that the stored nitrates may decrease the temperature of soot oxidation when nitrate decomposition occurs in a proper temperature range, due to the release of NO_2 in the gas phase. More recently studies carried out by Sanchez et al. [29, 30] on K/La_2O_3-based catalysts indicated that the reaction between soot and trapped NO_x can proceed before the decomposition of nitrates.

Aim of the present work is to provide additional insights on the effects of the presence of soot on the catalytic behavior of a model PtBa/Al_2O_3 LNT catalyst, and in particular to gain further insight on the interaction between soot and the stored NO_x on the de-soot and DeNO_x activity of the catalyst. For this purpose, NO_x storage/reduction experiments have been performed over the selected catalyst sample by alternating lean/rich cycles both in the presence and in the absence of soot. At variance with previous studies [21-23,25,26], in this study the absorption and reduction of the NO_x has been investigated by alternating short lean and rich phases with no inert purge in between, thus providing results closer to the transient conditions adopted under real applications.

The interaction between soot and the stored NO_x species has been further investigated by Temperature Programmed Methods under inert flow (TPD) and in the presence of oxygen (TPO) in which the stability/reactivity of the stored NO_x species has been analyzed both in the presence and in the absence of soot. The experiments have also been carried out over a platinum-free catalyst in order to assess the role of Pt in the stability/reactivity of adsorbed nitrates as well.

2. Materials and methods

A model PtBa/Al_2O_3 (1/20/100 w/w) catalyst was used in this study. The sample was prepared by incipient wetness impregnation with dinitro-diammine platinum (Strem Chemicals, 5%) and then with barium acetate of an Al_2O_3 support, obtained by calcination at 700 °C of a commercial alumina (Versal 250 from UOP). After each impregnation steps, the powders was dried overnight in air at 80 °C and calcined at 500 °C for 5 h. The selected impregnation order (first Pt and then Ba) has been

adopted in order to ensure a good dispersion and stability of the noble metal on the alumina support, in line with the recipes of Toyota patents [31]. A Pt-free sample (Ba/Al_2O_3, 20/100 w/w) was also prepared by impregnation of alumina with an aqueous solution of barium acetate (Sigma Aldrich, 99%), followed by drying overnight in air at 80 °C and calcination at 500 °C for 5 h. Finally, for comparison purposes, a sample was also prepared in which a $Ba(NO_3)_2$ solution was directly impregnated over the calcined alumina support (Ba/Al_2O_3 ratio: 20/100 w/w). After impregnation, the sample was dried at 80°C overnight. In the following, this sample will be referred as $Ba(NO_3)_2/Al_2O_3$.

Surface area and pore size distribution of the prepared catalyst samples were determined by N_2 adsorption–desorption with the BET method using a Micromeritics TriStar 3000 instrument. The specific surface area of the ternary $PtBa/Al_2O_3$ sample is near 160 m^2g^{-1}; a lower surface area value was determined for the Ba/Al_2O_3 sample (105 m^2g^{-1}). The surface area contraction is accompanied by a slight reduction of the pore volume, from 0.80 cm^3/g for the $PtBa/Al_2O_3$ catalyst down to 0.63 cm^3/g for the binary Ba/Al_2O_3 sample. The Pt dispersion of the $PtBa/Al_2O_3$ sample was also estimated by hydrogen chemisorption at 0°C (TPD/R/O 1100 Thermo Fischer Instrument). The measured Pt dispersion value was near 60%.

The Ba/Al_2O_3 and $PtBa/Al_2O_3$ catalysts were characterized by XRD analysis (Brüker D8 Advanced Instrument equipped with graphite monochromator on the diffracted beam). The XRD patterns showed both the monoclinic (JCPDS 78-2057) and orthorhombic (Whiterite, JCPDS 5-378) polymorphic forms of $BaCO_3$, in addition to microcrystalline g-Al_2O_3 (JCPDS 10-425).

Printex-U (Degussa) was used as model soot, whose properties are well addressed in literature [32]. Catalyst-soot mixtures were prepared by gently mixing in a vial the catalyst powder (74-105 μm) with the soot, thus realizing a loose contact which is representative of the soot/catalyst contact mode occurring in the DPNR system where soot is entrapped in the filter pores [15]. A soot loading (w_{soot}/w_{cat}) near 11 % has been typically employed. A sample with an intimate catalyst/soot interaction was also prepared by direct impregnation of the soot powder with aqueous solutions of Ba nitrate (“full contact” sample, [33]). After impregnation, the sample was dried overnight at 100 °C. In the following, this sample will be referred to as $Ba(NO_3)_2$/soot.

The reactivity experiments were performed in a flow micro-reactor system, consisting of a quartz tube (7 mm i.d.) equipped with a mass spectrometer (Omnistar 200, Pfeiffer Vacuum), a micro GC (Agilent 3000A) and an UV analyzer (Limas 11HW, ABB) for the on-line analysis of the reaction products. In each run 60 mg of catalyst have been used and the total flow rate was set at 100 cm^3/min (at 0 °C and 1 atm). The catalytic De-NO_x and De-soot activity was investigated by

performing lean-rich cycles at constant temperature alternating rectangular step feeds of NO (1000 ppm v/v) + 3% v/v of O_2 (lean phase) with feeds of H_2 (4000 ppm v/v, rich phase). The abrupt switches between the adsorption and the regeneration phase have been realized with the use of four-port valves. Experiments were performed in presence of 1% v/v H_2O and 0.1% v/v CO_2 at different temperatures, in the range 200 – 350 °C and with different NO inlet concentrations (500, 1000 ppm).

In order to analyse the interaction between soot and the stored NO_x, TPD and TPO experiments were also performed over PtBa/Al_2O_3 and Ba/Al_2O_3 catalysts. Accordingly NO_x have been stored onto the catalytic surface in the absence of soot at 350°C with NO or NO_2 (1000 ppm v/v) in He + O_2 (3% v/v) + H_2O (1% v/v) + CO_2 (0,1% v/v); then the catalyst has been cooled at room temperature in He, extracted from the reactor and mixed with soot (11 % w/w). TPD and TPO experiments have been carried by heating the so-prepared catalyst-soot mixture at a rate of 10°C/min in He + H_2O (1% v/v) + CO_2 (0.1% v/v) in the absence and in the presence of 3% v/v O_2, respectively, from room temperature to 500°C. The results collected with the catalyst/soot mixture have been compared with those obtained in analogous experiments performed in the absence of soot. TPD experiments have also been performed over $Ba(NO_3)_2/Al_2O_3$ (with and without soot) and over the "full contact" $Ba(NO_3)_2$/soot system.

3. Results and discussion

3.1 NO_x storage/reduction cycles in the presence of soot

In order to study the effect of soot on the catalyst activity in the NO_x adsorption and reduction, lean-rich cycles have been performed in the presence of soot over the model PtBa/Al_2O_3 NSR sample. Figure 1 shows a typical result, in term of NO, NO_2, CO_2, H_2 and N_2 outlet concentration vs. time, of a sequence of four lean-rich phases at 350 °C. For the sake of clarity, in the insert of the Figure an enlargement of the first cycle of the sequence can be seen, showing the concentrations of NO, NO_2, NO_x (= NO + NO_2), CO_2, H_2, N_2 and ammonia. Upon NO and O_2 admission (at t = 0 s, insert of Figure 1) the NO outlet concentrations shows a delay of 100 s, and then increases to a steady level near 930 ppm. Also NO_2 formation is observed (with a time delay of 170 s), due to the occurrence of the oxidation of NO by O_2 at Pt sites according to the stoichiometry of reaction (1):

$$NO + ½\ O_2 \rightarrow NO_2 \qquad (1)$$

The outlet concentrations of both NO and NO_2 increase with time and eventually reach a steady state level, indicating that the maximum NO_x storage capacity of the sample has been reached. The

area included between the NO inlet and NO_x outlet concentration traces is proportional to the amount of NO_x that have been stored onto the catalyst surface (4.04 x 10^{-4} mol/g_{cat}).

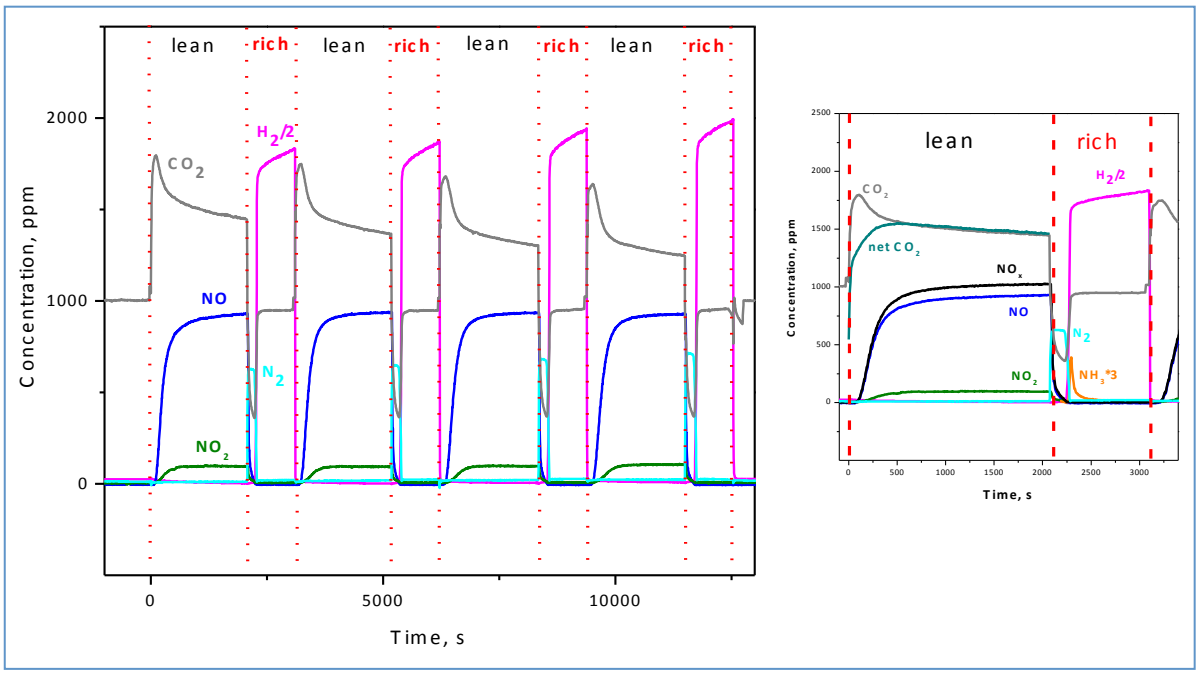

Figure 1. Lean-Rich Cycles over Pt-Ba/Al_2O_3-soot mixture. Only the first cycle is reported in the insert. Lean phase:1000 ppm NO + O_2 (3%, v/v) in He, CO_2 (0.1%, v/v) and H_2O (1%); rich phase: 4000 ppm H_2 in He, CO_2 (0.1%, v/v) and H_2O (1%).

Upon NO admission, the evolution of CO_2 is also observed. In fact the CO_2 concentration rapidly increases from its background level (1000 ppm) showing a maximum of 1800 ppm and then decreases approaching the constant value of 1450 ppm near the end of the pulse. As already reported elsewhere [21,25,26], the increase in the CO_2 outlet concentration results from two factors. One is related to the formation of Ba nitrates at the expenses of Ba-carbonates upon NO_x adsorption, as described by the stoichiometry of reaction (2):

$$BaCO_3 + 2\ NO + 3/2\ O_2 \rightarrow Ba(NO_3)_2 + CO_2 \qquad (2)$$

In reaction (2), formation of nitrates only is suggested as NO_x adsorbed species, in line with many studies showing that at this temperature only nitrates are formed upon NO/O_2 adsorption [34]. Reaction (2) is responsible for the initial CO_2 peak; then the CO_2 concentration remains above its background level due to soot combustion. As a matter of fact, by subtracting from the CO_2 concentration trace the amounts of CO_2 resulting from the NO_x uptake and calculated according to the stoichiometry of reaction (2), a net CO_2 concentration trace is obtained (see the insert) which refers uniquely to soot combustion. At the end of the lean phase, the rate of CO_2 formation due to soot combustion is near 3.35 x 10^{-8} mol/s; roughly 13% of the initial soot loading (11 % w/w) is consumed during the first lean/rich sequence. Since no appreciable CO_2 formation is seen before the

lean-rich cycles, i.e. in the presence of O_2 only, NO_x (either adsorbed or in the gas phase) are involved at the temperature of 350°C in the oxidation of soot, possibly according to the stoichiometry of reactions (3) and (4):

$$NO_2 + C \rightarrow NO + CO \quad (3)$$

$$CO + ½\ O_2 \rightarrow CO_2 \quad (4)$$

Here, NO_2 formed upon NO oxidation at Pt sites oxidizes soot with formation of CO (and possibly of CO_2); CO is then oxidized to CO_2 by O_2 at Pt sites and/or by NO_2. As a matter of facts, studies on the non-catalytic oxidation of soot by NO_2/O_2 mixtures carried out elsewhere pointed out a relevant formation of CO upon soot combustion by NO_2 in line with literature indications [35]; this indicates that Pt is involved in the CO oxidation since no appreciable CO evolution is observed at the reactor outlet. The involvement of NO_x (and more specifically of NO_2) in the oxidation of soot is also pointed out by the fact that when the NO_x storage is carried out in the absence of soot, a higher NO_2 formation is observed (see below). This points out that NO_2 is involved in the removal of soot, although the participation of the stored nitrates cannot be ruled out, as will be discussed below.

At the end of the NO_x adsorption (lean phase), the gas feed is switched to rich conditions to regenerate the catalyst surface from the stored NO_x. Accordingly, 4000 ppm of H_2 have been fed to the reactor upon NO and oxygen shutoff. H_2 is completely consumed upon admission (see the insert of Figure 1) and a simultaneous N_2 evolution is observed at the reactor outlet. The N_2 concentration reaches a level of about 800 ppm, in line with the stoichiometry of reaction (5):

$$Ba(NO_3)_2 + 5\ H_2 + CO_2 \rightarrow BaCO_3 + N_2 + 5\ H_2O \quad (5)$$

The N_2 concentration keeps almost constant for several seconds; then it decreases and a peak of NH_3 is observed, according to the stoichiometry of reaction (6):

$$Ba(NO_3)_2 + 8\ H_2 + CO_2 \rightarrow BaCO_3 + 2\ NH_3 + 5\ H_2O \quad (6)$$

In line with the stoichiometry of reactions (5) and (6), a decrease of the CO_2 inlet concentration is observed, due to the formation of Ba carbonates at the expenses of the stored nitrates. The N_2 selectivity of the regeneration process is high, being near 95 %. As detailed in previous studies [36-38], the observed sequence of reaction products has been explained on the basis of a two-step pathway involving at first the fast formation of ammonia upon reaction of nitrates with H_2 (reaction (6)), followed by the slower reaction of the so formed ammonia with the stored nitrates leading to the selective formation of N_2 (reaction (7)):

$$3\ Ba(NO_3)_2 + 10\ NH_3 \rightarrow 8\ N_2 + 3\ BaO + 15\ H_2O \quad (7)$$

As discussed elsewhere [36-38], the observed temporal evolution of products during the reduction is due to the development of an H_2 front which travels along the reactor: NH_3 is initially formed in

correspondence with the H_2 front, and reacts with NO_x stored downstream the front leading to N_2 evolution. Accordingly NH_3 evolution is observed at the reactor outlet after N_2 only when the nitrates are reduced and the H_2 front reaches the end of the catalyst bed.

The data described above clearly indicate that the catalyst system is able to simultaneously store/reduce NO_x and oxidize soot. However, considering the whole sequence of the four NO_x storage–reduction cycles (Figure 1), it appears that the behavior of the PtBa/Al_2O_3 catalyst is affected by the residual soot loading. In fact the NO_x breakthrough progressively increases during the lean/rich sequence from ~ 100 s to ~ 140 s passing from the first to the fourth cycle, respectively, i.e. upon decreasing the soot loading. The increase in the dead time is accompanied by an increase of the amounts of NO_x stored up to steady-state, from 4.04 x 10^{-4} mol/g_{cat} for the first cycle to 4.78 10^{-4} mol/g_{cat} for the fourth cycle (Figure 2).

Figure 2 also shows the amounts of soot which is oxidized during the lean phase as a function of the cycle number, estimated from the amounts of evolved CO_2. During the lean phase of the first cycle, roughly 13 % of the initial soot loading is oxidized, which reduces to 8 % during the fourth cycle. At the end of the sequence the residual soot loading is near 3.9 % w/w. In fact the CO_2 concentration measured at steady-state at the end of the lean phase decreases from 1450 ppm of the first cycle to 1250 ppm of the fourth cycle, indicating a progressive decrease of the rate of soot combustion. Of note, the NO_2 concentration is similar for all cycles during the whole experiment, as well as the NO/NO_2 ratio, although the progressive decrease of the soot combustion rate and the involvement of NO_2 in the oxidation of soot.

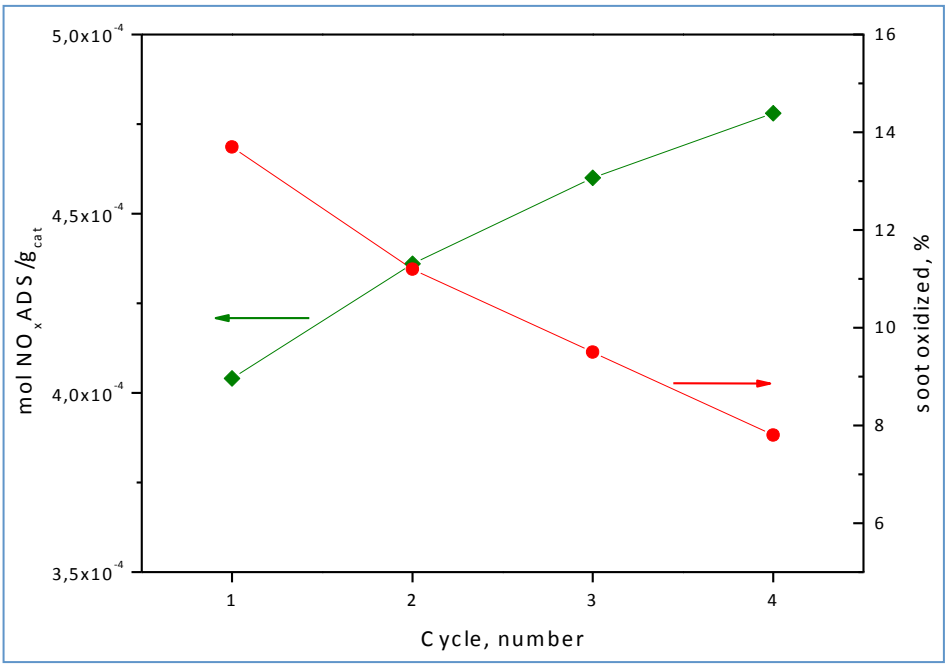

Figure 2. Amounts of stored NOx (mol/gcat) and of soot oxidized (%, w/w) during lean–rich cycles at 350 °C over PtBa/Al_2O_3-soot mixture. Exp. conditions: see caption Fig. 1.

These results are in line with our data discussed elsewhere [21] obtained during isothermal soot oxidation over PtBa/Al_2O_3 at 350 °C in presence of O_2 and NO and showing that the NO_2 concentration exhibits a remarkable increase only when the soot loading is very low (near 1 % w/w).

Finally, considering the reduction phase, no significant changes both in the products formation and in their temporal evolution are observed during the cycles. N_2 selectivity values near 95 % have been calculated in lean/rich cycles, thus indicating a negligible effect of soot on the regeneration of the stored NO_x.

A comparison of the catalytic behavior of the PtBa/Al_2O_3 catalyst during a lean-rich cycle in the presence and in the absence of soot is shown in Figures 3 A and B, respectively (a concentration of 500 ppm of NO has been used during the lean phase). In the presence of soot (6.2 % w/w in the case shown in Figure 3 A) a shorter dead time for NO_x breakthrough is observed during the lean phase (240 vs 280 s); the amounts of NO_x stored at the end of the lean phase is also lower (3.8×10^{-4} vs 4.9×10^{-4} mol/g_{cat}). Besides, a lower NO_2/NO ratio is measured in the presence of soot due to the involvement of NO_2 in the soot oxidation. On the other hand, no appreciable changes in the behavior of the sample during the rich phase are observed.

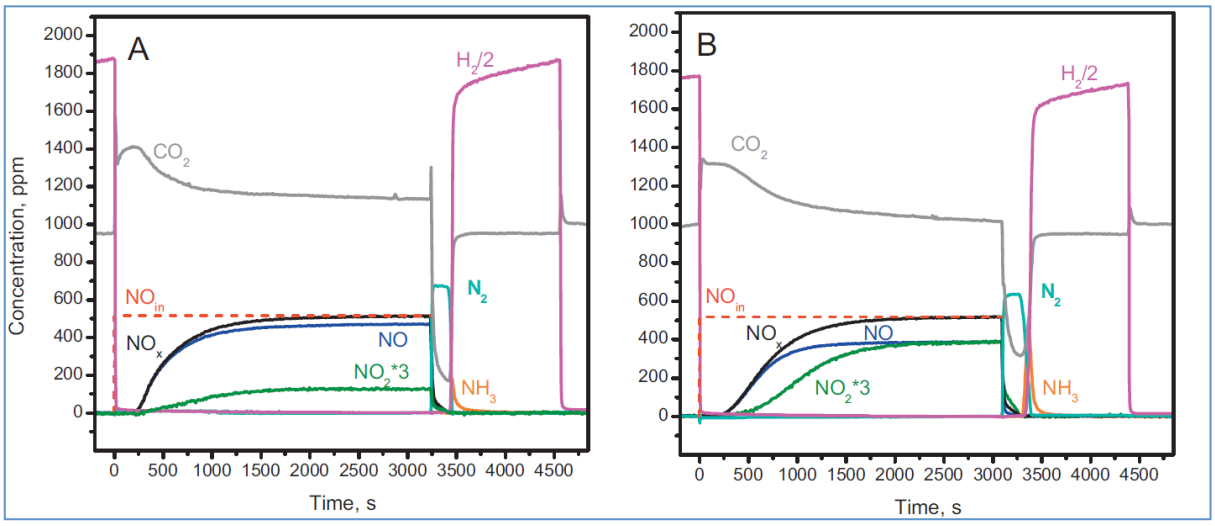

Fig. 3. Lean–rich cycles at 350 °C over PtBa/Al_2O_3 catalyst in the presence (A) and in the absence of soot (B). Lean phase: 500 ppm NO + O_2 (3%, v/v) in He, CO_2 (0.1%, v/v) and H_2O (1%); rich phase: 4000 ppm H_2 in He, CO_2 (0.1%, v/v) and H_2O (1%).

Soot is oxidized during the lean phase: as seen in figure 3 A, the steady state level of the CO_2 concentration at the end of the lean phase is higher than the inlet value (1140 ppm vs. 1000 ppm), corresponding to a rate of soot oxidation of 1.04×10^{-8} mol/s. This value is lower than that observed in the case of the run carried out with 1000 ppm NO during the lean phase likely due to the lower NO_2 concentration observed with 500 ppm of NO in the feed [26].

In conclusions the results showed in Figures 1 - 3 point out that the presence of soot affects the NO_x storage behavior of the investigated LNT system and in particular decreases the NO_x storage capacity of the catalyst, in line with the results reported in our previous works [23,25,26] and by other authors as well [27]. On the other hand the presence of soot does not impact significantly the catalyst behavior during the rich phase.

In order to investigate more in details the effect of soot on the behavior of the model PtBa/Al_2O_3 sample, lean-rich cycles have been performed at other temperatures, in the temperature range 200-350 °C, both in the absence and in the presence of soot. The results (here not reported for brevity) indicate that in the absence of soot the amounts of NO_x stored during the lean phase decrease upon decreasing the temperature from 5.6 x 10^{-4} mol/g_{cat} at 350 °C to 2.6 x 10^{-4} mol/g_{cat} at 200 °C. The presence of soot has a negative impact on the NO_x storage at all the investigated temperatures, in that it decreases the amounts of NO_x stored during the lean phase. Soot is oxidized during the lean phase, but soot oxidation is appreciable only at 300 °C and above.

Concerning the rich phase, it is noted that in the absence of soot the N_2 selectivity of the reduction process increases with temperature, as already pointed out in other studies and in line with the two-steps mechanism for NO_x reduction [36-38]. The presence of soot does not affect significantly the reduction process, as already observed at 350 °C (see above). These results parallels those obtained under different experimental conditions (lean and rich phases separated by an inert purge in between) and already reported elsewhere [26].

3.2 Soot reaction with adsorbed NO_x species: TPD experiments

3.2.1 PtBa/Al_2O_3 catalyst

To gain further insight into the effect of soot on the adsorbed NO_x species (nitrates) and in particular on their stability/reactivity, TPD experiments of the stored nitrates in the presence and in the absence of soot have been carried out. Since soot affects the NO_x storage on the PtBa/Al_2O_3 system, NO_x have been stored at 350°C in the absence of soot, and then the sample has been mixed with soot before the TPD runs (see the experimental section), thus realizing a loose contact between soot and the nitrated catalyst. A reference TPD run has also been carried without mixing with soot.

The results of the TPD runs carried out the absence and in the presence of soot (dashed and solid lines, respectively) are shown in Figure 4 in terms of NO_x, O_2 and CO_2 concentrations.

In the absence of soot (dashed lines) the nitrate decomposition is observed above 350 °C (i.e. the adsorption temperature), although very small amounts of NO_x are also seen at lower temperatures. Nitrate decomposition occurs with evolution mainly of NO (along with minor amounts of NO_2) and of

O_2. These results perfectly match those already published elsewhere [26] and confirm that the thermal stability of stored NO_x is ruled by their adsorption temperature. The nitrate decomposition is not completed at the end of the heating rate at 500 °C, but is completed during the subsequent hold at this temperature. It is noteworthy that the overall amounts of evolved NO, O_2 and NO_2, estimated by integration of the TPD peaks, are well in line with the stoichiometry of nitrates decomposition reactions (8) and (9):

$$Ba(NO_3)_2 + CO_2 \rightarrow BaCO_3 + 2\ NO + 3/2\ O_2 \qquad (8)$$

$$Ba(NO_3)_2 + CO_2 \rightarrow BaCO_3 + 2\ NO_2 + 1/2\ O_2 \qquad (9)$$

In fact the measured O/N atomic ratio in the evolved products (i.e. $(NO + 2\ NO_2 + 2\ O_2)/(NO + NO_2)$) is 2.6, very close to the theoretical value of 2.5.

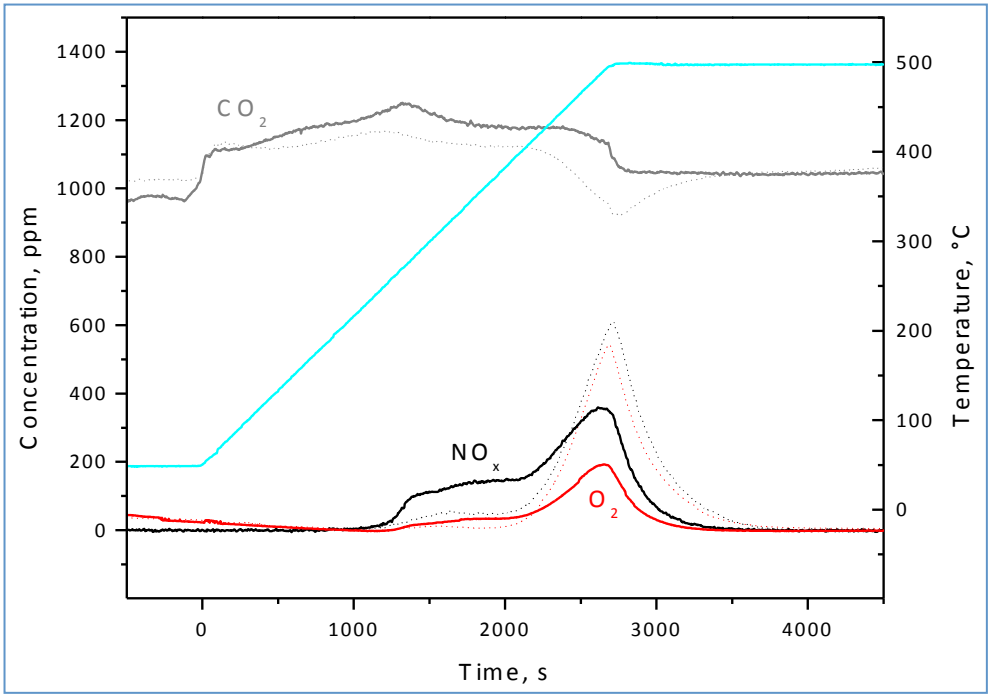

Fig. 4. TPD after NOx adsorption at 350 °C over PtBa/Al_2O_3 in the absence (dashed lines) and in the presence of soot (solid lines).

Finally, a decrease of the CO_2 concentration (contained in the feed stream with a level of 1000 ppm) is observed in correspondence with the nitrate decomposition, due to the re-adsorption of CO_2 on the Ba sites leading to the formation of Ba carbonates at the expenses of Ba nitrates (reactions (8) and (9)).

Solid lines in Figure 4 show the results of a TPD run performed in the presence of soot (i.e., after mixing the nitrated catalyst sample with soot). The decomposition of nitrates is shifted at lower temperatures if compared to the soot-free sample, in that a significant release of NO_x is observed already in the temperature range 260 – 350°C. The nitrate decomposition is then completed at

higher temperatures, with NO_x (only NO) and O_2 peaking near 485 °C. Besides, no a net CO_2 uptake is observed. It is suggested that in this case a surface reaction takes place involving nitrates and the soot particle:

$$C + Ba(NO_3)_2 \rightarrow BaCO_3 + 2\ NO + ½\ O_2 \qquad (10)$$

which results in the release of NO and O_2 and in the formation of carbonates whose formation accounts for the lack of a significant CO_2 net uptake from the gas phase in the TPD experiment with the catalyst/soot mixture.

These results clearly indicate that the presence of soot decreases the thermal stability of the stored nitrates. Moreover, if compared to the soot-free sample, a different distribution of the evolved products is also observed: in fact the calculated O/N atomic ratio of the gaseous products evolved during the entire TPD in the presence of soot is near 1.7, well below the stoichiometric O/N value of 2.5 for the nitrate decomposition. This indicates that nitrates and/or their decomposition products oxidize soot to CO_2, in line with the absence of a net CO_2 uptake (reaction (10)).

Based on the above observation, it clearly appears that soot promotes the decomposition of the NO_x adsorbed species, which is in fact observed at lower temperature if compared to the soot-free sample. This calls for the existence of a surface reaction involving the stored nitrates and the soot particles. As a matter of fact, studies on the reduction of the stored nitrates with several reductants suggested that nitrates are rather mobile on the surface [39,40], the driving force for the mobility of nitrates being the presence of reduced Pt sites (leading to nitrate decomposition/reduction). The role of the reductant in the process is to kept Pt in a reduced form. It is speculated that the soot particles, acting as reducing center for the NO_x species, provide the driving force for the process leading to nitrate reduction/decomposition (and soot oxidation). A similar nitrate destabilizing effect has been attributed to Pt in PtBa/Al_2O_3 catalysts, in order to explain the decrease in the decomposition temperature of nitrates which is observed upon Pt addition to Ba/Al_2O_3 [41].

3.2.2 Ba/Al_2O_3 catalyst

TPD runs over nitrated samples **-** In order to check whether Pt has a role in the soot-nitrate surface reaction, TPD experiments have been carried out over the binary Ba/Al_2O_3 catalyst in the absence and in the presence and of soot after NO_2 adsorption at 350 °C. The obtained results are shown in Figure 5 A and B (absence and presence of soot, respectively) in terms of concentration traces of the various evolved products (NO, NO_2, O_2, CO_2 and CO). In the case of the soot-free Ba/Al_2O_3 sample (Figure 5A), nitrates decompose above 350 °C (i.e. the adsorption temperature) with evolution mainly of NO_2. Evolution of O_2 is also observed while that of NO is very small. Worth to note that in spite of the long isothermal period at 500 °C, nitrate decomposition is not yet completed at the end

of the TPD run: in fact the NO_2 concentration shows a very long tail which extends for more than 4 h (not shown in the Figure). At the end of the run, only a portion of the stored nitrates have been decomposed.

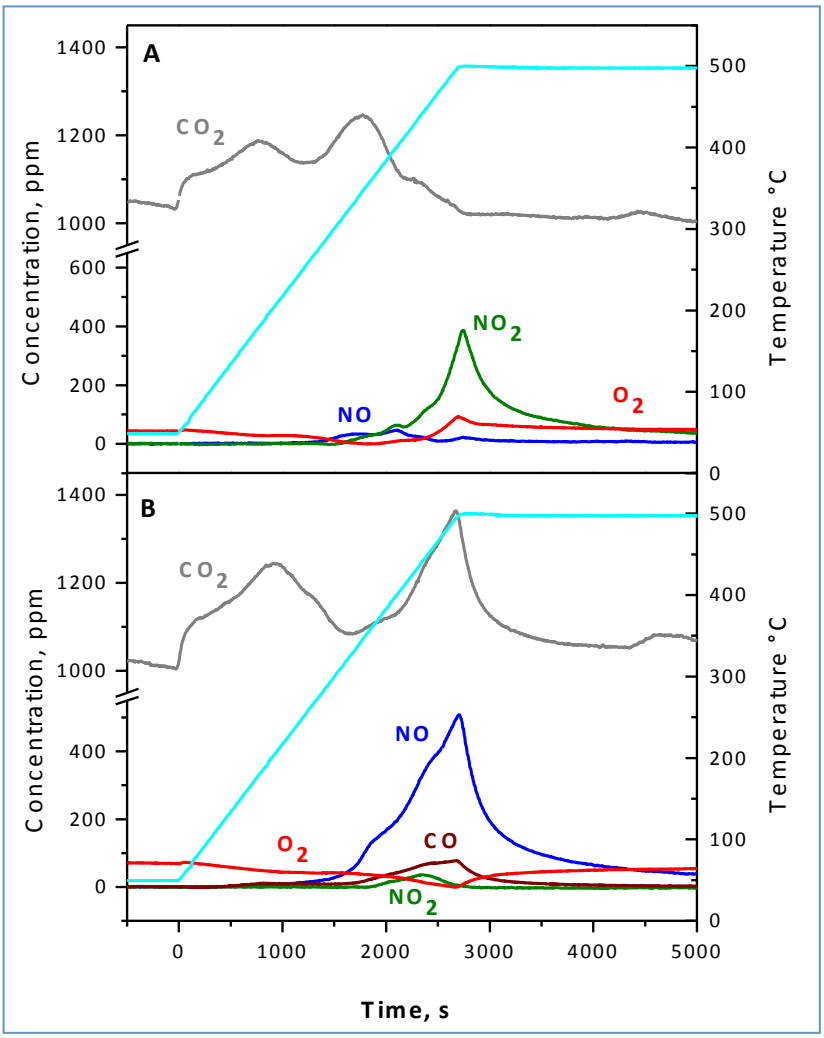

Fig. 5. TPD after NOx adsorption at 350 °C over Ba/Al_2O_3 catalyst in the absence (A) and in the presence of soot (B).

The TPD profile obtained in the presence of soot (Figure 5B) is very different: the decomposition onset of the stored NO_x is observed near 300°C, that is roughly 50 °C below that observed in the case of the soot-free sample, and is almost completed after the 4 h isothermal period at 500 °C. Also the distribution of the evolved products is different: in fact NO represents the major decomposition product and no significant amounts of NO_2 or O_2 are observed. Moreover, in correspondence with the NO evolution, a significant production of CO_2 is detected above the inlet value of 1000 ppm. Formation of significant amounts of CO (75 ppm) are also observed in this case, in line with other studies showing the formation of CO along with that of CO_2 during the non-catalytic soot oxidation by NO_2 [35].

These results indicate that the surface reaction between soot and the stored nitrates is not catalyzed by Pt: even in the absence of the noble metal, soot reacts with the NO_x ad-species which in fact decompose at lower temperatures if compared to the soot-free sample. This is in line with previous suggestions indicating that the soot particles may provide the driving force for nitrate mobility and reduction/decomposition.

Effect of the soot/nitrate contact **-** To further investigate the interaction between soot and nitrates, and in particular the effect of the soot/nitrate contact, TPD experiments were performed with samples with a loose and a full contact between soot and the nitrates. In the first case (loose contact) nitrates were deposited over alumina by impregnation with an aqueous solution of $Ba(NO_3)_2$ ($Ba(NO_3)_2/Al_2O_3$ sample) followed by drying at 80 °C and gently mixing with soot; in the other case (full contact) the soot was directly impregnated with $Ba(NO_3)_2$ ($Ba(NO_3)_2$/soot sample). The obtained results are shown in Figures 6 and 7, where the heating ramp was ended at 800 °C.

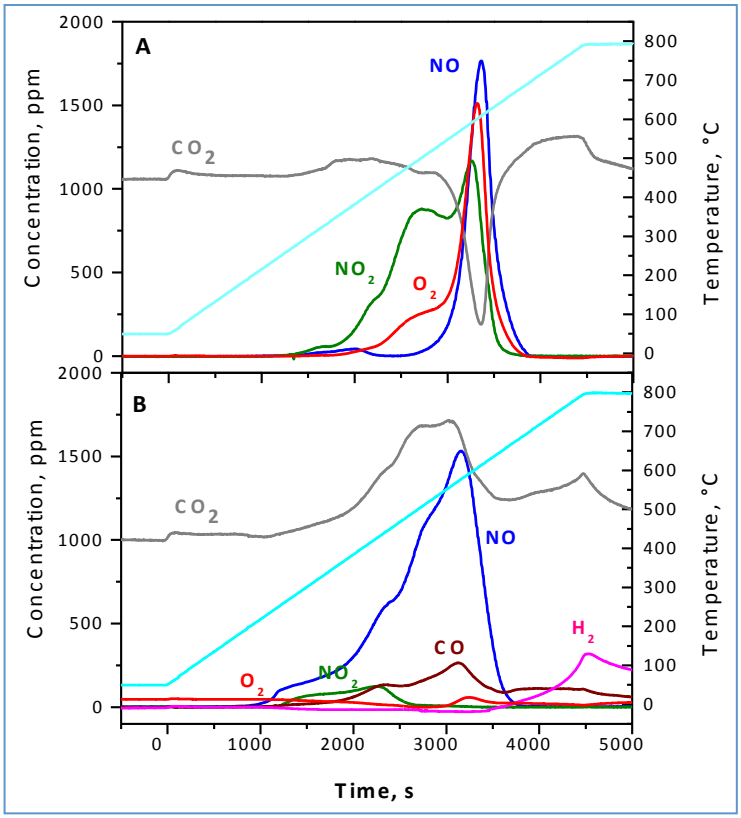

Fig. 6. TPD over Ba(NO3)2/Al2O3 catalyst in the absence (A) and in the presence of soot (B).

In the case of the loose contact system, a reference TPD run was also carried without mixing the $Ba(NO_3)_2/Al_2O_3$ sample with soot (Figure 6 A). In this case the decomposition of the Ba nitrate species is apparent above 300 °C with the initial evolution of NO_2 (and O_2), showing a maximum near 500 °C. Then a decomposition peak centered near 600 °C is observed, accompanied by the evolution of NO, O_2 and NO_2. In correspondence with the nitrate decomposition a decrease of the CO_2

concentration is also observed, from the inlet value (1000 ppm) to a minimum of 200 ppm, due to readsorption for carbonates formation onto the catalytic surface. Complete decomposition of the NO_x adsorbed species is achieved at temperatures slightly below 700 °C. This result is in line with the decomposition of nitrates formed upon NO_x adsorption (Figure 5 A); however in the case of Figure 5 A only the first NO_2 peak could be observed, since the heating ramp of the TPD run was limited at 500 °C.

A different picture is apparent in the presence of soot (Figure 6B): the temperature onset for nitrate decomposition is observed near 230 °C, i.e. more than 70 °C below that of the soot-free system. The evolution of mainly NO is observed in this case, with much lower amounts of NO_2 and O_2. Besides, in correspondence with the NO evolution, a significant CO_2 production is observed, along with CO (maximum 260 ppm). These results resemble those obtained in the case of the sample obtained by NO_x adsorption (Figure 5 B) and confirm the capability of nitrates to oxidize soot at temperature well below that of their decomposition (being reduced to NO).

Finally, worth to note that in the presence of soot (Figure 6B) the production of 300 ppm of H_2 is also evident at temperature above 700 °C, accompanied by the evolution of CO. This is due to the occurrence of the carbon gasification reaction (11):

$$C + H_2O \rightarrow CO + H_2 \qquad (11)$$

due to the presence of water (1 % v/v) in the feed stream. CO_2 formation is also observed likely due to the occurence of the water gas shift reaction (12):

$$CO + H_2O \rightarrow CO_2 + H_2 \qquad (12)$$

The carbon gasification reaction is catalyzed by Ba, in line with the well known effect of alkaline/ alkaline-earth oxides on this reaction [42,43]. In fact TPD experiments carried out over bare soot (here not shown) indicate that the carbon gasification reaction (11) takes place appreciably only at temperatures above 700 °C with very small production of CO and H_2.

The results of the TPD experiment carried out over the “full contact” sample is shown in Figure 7. When $Ba(NO_3)_2$ is directly deposited onto soot (i.e., when an intimate contact is provided between nitrates and the soot particle) significant changes in the TPD profile are observed with respect to the loose contact sample (compare Figure 7 and 6B). In fact in this case the temperature threshold for the nitrate decomposition significantly decreases with respect to that of the corresponding loose contact system (Figure 6B), being NO evolution observed at temperatures as low as 150 °C. Moreover complete nitrate decomposition is obtained near 550 °C (vs. 700 °C of $Ba(NO_3)_2/Al_2O_3$-soot system). The production of CO_2 in correspondence with NO evolution points out also in this case the soot oxidation by the nitrates. Finally also in this case at temperature above 700 °C the simultaneous

production of H_2, CO and CO_2 is observed due to the occurrence of reaction (11) and (12). Notably in this case a much higher soot gasification rate is measured: as matter of fact the maximum production of 3000 and 600 ppm is measured for H_2 and CO, respectively. The high H_2 and CO production is due to the catalytic effect of Ba (in close-contact with the soot) on the carbon gasification reaction.

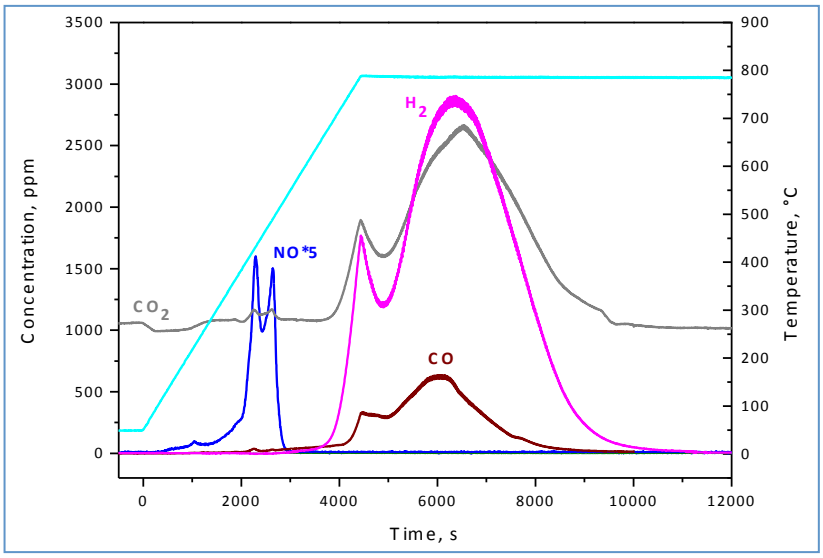

Fig. 7. TPD over $Ba(NO_3)_2$/soot "full contact" system.

Effect of the presence of oxygen **–** Finally, the effect of the presence of oxygen on the nitrate-soot interaction has also been addressed. For this purpose TPO runs have been performed with the $Ba(NO_3)_2/Al_2O_3$ sample in the absence and in the presence of soot, and results are shown in Figures 8 A and 8 B, respectively. In the case of the soot-free sample (Figure 8 A), the results closely resemble those obtained during the TPD experiments (Figure 6 A), with nitrate decomposition apparent above 300 °C with the evolution of NO_2, NO and O_2, showing maxima near 500 °C and 600 °C, and the uptake of CO_2. These results show that the decomposition of the nitrates is not significantly affected by the presence of oxygen in the feed stream.

In the presence of soot (Figure 8 B), the temperature onset for nitrate decomposition is observed well below that of the soot-free system, like during the TPD experiment. Accordingly the soot-nitrate interaction is not significantly affected by the presence of oxygen. The evolution of NO is observed in this case, with much lower amounts of NO_2. Formation of CO_2 (and of CO as well) is also detected above 300 °C, with a maximum near 700 °C and a shoulder at 550 °C. The shoulder of the CO_x concentration at 550 °C is associated with the soot oxidation by nitrates, whereas the maximum at 700 °C is due to soot oxidation by O_2 as confirmed by blank TPO experiments carried out in the absence of the catalyst (here not reported). Worth to note that a shoulder is observed at 550 °C in the O_2 concentration trace, corresponding to the maximum in the NO concentration and to the

shoulder in the CO_2 concentration traces. This suggests the participation of O_2 also during the soot oxidation by nitrates, in line with literature reports showing the participation of O_2 during the soot oxidation by NO_x [44].

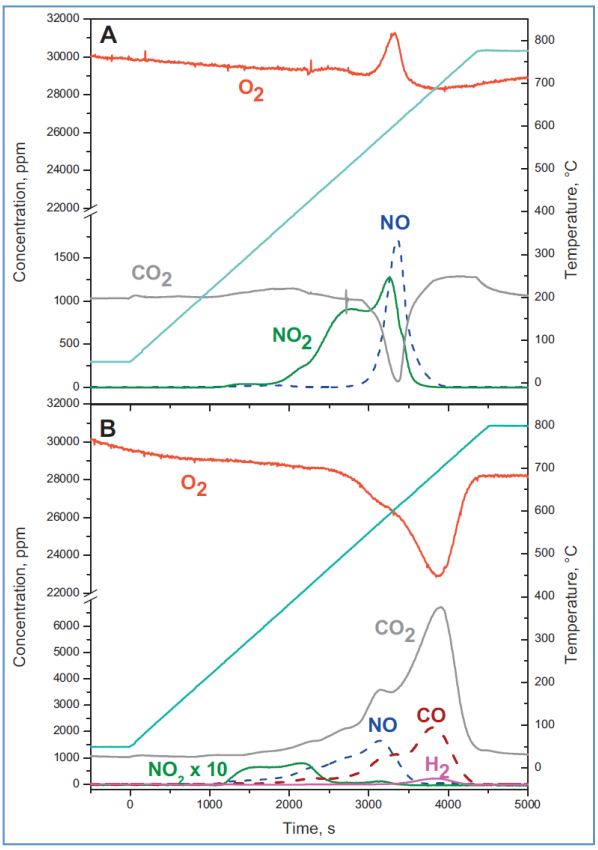

Fig. 8. TPO over Ba(NO3)2/Al2O3 catalysts in the absence (A) and in the presence of soot (B).

4. Conclusions

In the present study the interaction of soot with nitrates stored on a model PtBa/Al_2O_3 LNT catalyst sample has been investigated under realistic conditions, i.e. upon cycling under lean/rich conditions and in the presence of water and CO_2 in the feed stream. The results pointed out that the presence of soot decreases the NO_x storage capacity of the catalyst during the lean phase. The inhibiting effect of soot on the NO_x storage capacity increases with the soot amount, up to 11 % w/w (the maximum investigated soot loading), and is observed at different temperatures in the range 200-350 °C. However, the presence of soot does not affect significantly the catalyst behavior during the rich phase, i.e. during the regeneration of the stored nitrates.

Simultaneously with the NO_x storage, at temperatures above 300 °C soot is oxidized to CO_2 during the lean phase. Soot oxidation occurs thorough the participation of NO_2 formed by NO oxidation on Pt sites; in fact the NO_2 concentration measured at the reactor outlet is significantly lower in the presence of soot than in its absence. However, in parallel with this NO_2-soot oxidation pathway, the

participation of the stored nitrates in the soot oxidation is also likely. This has been shown by TPD/TPO experiments carried out over both the model PtBa/Al_2O_3 and Ba/Al_2O_3 samples in which the reactivity / thermal decomposition of nitrates has been investigated in the presence and in the absence of soot. Clear indication on the occurrence of a surface reaction involving soot and the stored nitrates has been pointed out, leading to soot oxidation (and nitrate reduction). In fact the stored nitrates are able to oxidize soot at temperatures well below those corresponding to their decomposition in the absence of soot. This reaction possibly involves the surface mobility of the stored nitrates, soot particles being the driving force for the process and acting as reduced centers. This process does not require the presence of the noble metal (Pt) in that it occurs in the case of the Ba/Al_2O_3 catalyst sample as well; as expected, it is favored by the contact between the nitrates and soot. In fact when nitrates are stored onto the soot, the nitrate/soot reaction is monitored at lower temperatures.

Acknowledgements

The financial support of MUR – PRIN project 2007HHCZP4 is acknowledged.

References

[1] T. Johnson, Platinum Metals Rev. 52 (2008) 23.

[2] B.A.A.L. van Setten, M. Makee, J.A. Moulijn, Catal. Rev. 43 (4) (2001) 489.

[3] A. Güthenke, D. Chatterjee, M. Weibel, B. Krutzsch, P. Kocˇí, M. Marek, I. Nova, E. Tronconi, Avd. Chem. Eng. 33 (2008) 103.

[4] P. Forzatti, Appl. Catal. A: Gen. 222 (2001) 221.

[5] W.S. Epling, L.E. Campbell, A. Yezerets, N.W. Currier, J.E. Parks, Catal. Rev. Sci. Eng. 46 (2004) 163.

[6] S. Matsumoto, Catal. Today 90 (2004) 183.

[7] S. Roy, A. Baiker, Chem. Rev. 109 (2009) 4054.

[8] L. Lietti, G. Ramis, F. Berti, G. Toledo, R. Robba, G. Busca, P. Forzatti, Catal. Today 42 (1998) 101.

[9] L. Xu, R. McCabe, W. Ruona, G. Cavataio, SAE Technical Paper, 2009-01-0285.

[10] A. Lindholm, H. Sjövall, L. Olsson, Appl. Catal. B: Environ. 98 (2010) 112.

[11] P. Forzatti, L. Lietti, Catal. Today 155 (2010) 131.

[12] M. Weibel, N. Waldbüßer, R. Wunsch, D. Chatterjee, B. Bandl-Konrad, B. Krutzsch, Top. Catal. 52 (2009) 1702.

[13] E.C. Corbos, M. Haneda, X. Courtois, P. Marecot, D. Duprez, H. Hamada, Catal.Commun. 10 (2008) 137.

[14] E.C. Corbos, M. Haneda, X. Courtois, P. Marecot, D. Duprez, H. Hamada, Appl. Catal. A: General 365 (2009) 187.

[15] K. Nakatani, S. Hirota, S. Takeshima, K. Itoh, T. Tanaka, SAE Paper SP-1674 2002-01-0957.

[16] J. Suzuki, S. Matsumoto, Top. Catal. 28 (2004) 171.

[17] J.A. Sullivan, O. Keane, A. Cassidy, Appl. Catal. B: Environ. 75 (2007) 102 .

[18] A.L. Kustov, M. Makkee, Appl. Catal. B: Environ. 88 (2009) 263.

[19] C.-N. Millet, R. Chédotal, P. Da Costa, Appl. Catal. B: Environ. 90 (2009) 339.

[20] H. Lin , Y. Li, W. Shangguan, Z. Huang, Combustion and Flame, 156 (2009) 2063.

[21] L. Castoldi, R. Matarrese, L. Lietti, P. Forzatti, Appl. Catal. B: Environ. 64 (2006) 25.

[22] R. Matarrese, L. Castoldi, L. Lietti, P. Forzatti, Top. Catal. 42–43 (2007) 293.

[23] R. Matarrese, L. Castoldi, L. Lietti, P. Forzatti, Top. Catal. 52 (2009) 2041.

[24] R. Matarrese, L. Castoldi, L. Lietti, P. Forzatti, Catal. Today 136 (2008)11.

[25] L. Castoldi, N. Artioli, R. Matarrese, L. Lietti, P. Forzatti, Cat Today 157 (2010) 384.

[26] N. Artioli, R. Matarrese, L. Castoldi, , L. Lietti, P. Forzatti, Cat Today 169 (2011) 36.

[27] I.S. Pieta, M. García-Diéguez, C. Herrera, M.A. Larrubia, L.J. Alemany, J. Catal. 270 (2010) 256.

[28] A.L. Kustov, M. Makkee, Appl. Catal. B: Environ. 88 (2009) 263.

[29] B.S. Sànchez, C.A. Querini, E.E. Mirò, Appl. Catal. A: Gen. 366 (2009) 166.

[30] B.S. Sànchez, C.A. Querini, E.E. Mirò, Appl. Catal. A: Gen. 392 (2011) 158.

[31] N. Miyoshi, T. Tanizawa, K. Kasahara, S. Tateishi, European Patent Application 0 669 157 A1, 1995.

[32] A. Setiabudi, M. Makee, J.A. Moulijn, Appl. Catal. B: Environ. 50 (2004) 185.

[33] L. Castoldi, R. Matarrese, L. Lietti, P. Forzatti, Appl. Catal. B: Environ. 90 (2009) 278.

[34] F. Prinetto, G. Ghiotti, I. Nova, L. Castoldi, L. Lietti, E. Tronconi, P. Forzatti, Phys. Chem. Chem. Phys.5 (2003) 4428.

[35] B.R. Stanmore, V. Tschamber, J.-F. Brilhac, Fuel 87 (2008) 131.

[36] L. Lietti, I. Nova, P. Forzatti, J. Catal. 257 (2008) 270.

[37] I. Nova, L. Lietti, P. Forzatti, Catal. Today 136 (2008) 128.

[38] P. Forzatti, L. Lietti, I. Nova, En. Environ. Sci. 1 (2008) 236.

[39] R.D. Clayton, M.P. Harold, V. Balakotaiah, C.Z. Wan, Appl. Catal. B: Environ. 90 (2009) 662.

[40] D. Bhatia, M.P. Harold, V. Balakotaiah, Catal. Today 151 (2010) 314.

[41] I. Nova, L. Castoldi, L. Lietti, E. Tronconi, P. Forzatti, SAE Technical papers, 2006-01-1368 (2006).

[42] D.W. MacKee, Fuel 62 (1983) 170.

[43] D.W. MccKee, C.L. Spiro, P.G. Kosky, E.J. Lamby, Fuel 64 (1985) 805.

[44] F. Jacquot, V. Logie, J.F. Brilhac, P. Gilot, Carbon 40 (2002) 335.

Paper IV

Diesel soot and NO_x abatement on Pt-K/Al_2O_3 LNT catalyst: influence of temperature and ageing

R. Matarrese, N. Artioli, L. Castoldi, L. Lietti,E. Finocchio, P. Forzatti

In preparation

Diesel soot and NOx abatement on Pt-K/Al_2O_3 LNT catalyst: influence of temperature and ageing

Abstract

Soot particles and nitrogen oxides are the main pollutants emitted by diesel engines. The Pt-K/Al_2O_3 catalyst is active for soot combustion and it is also able to works as lean NO_x trap. In this work, the effect of the reaction temperature on the catalytic activity is addressed. Both, the soot combustion and the NO_x storage are studied and a comparison with another LNT system Pt-Ba/Al_2O_3 is attempted.

Keywords

Soot oxidation, DPNR catalysts, simultaneous NO_x and soot removal, Diesel Particulate NO_x Reduction, LNT catalysts

1. Introduction

The main pollutants emitted by diesel engine exhausts are nitrogen oxides and soot particles. For this reason, the simultaneous abatement of NO_x and particulates from diesel exhaust gas represents an outstanding issue. The current three-way technology used near stoichiometric conditions is unable to meet upcoming regulations in Europe, United States, and Japan. The existing technical solutions involving an exhaust gas recirculation to get an optimal NO_x/particulates compromise by controlling the recirculated gas rate or modifying the distribution channel will likely be unable to fulfill the next Euro 6 standard regulation. The implementation of an optimal strategy is not an easy task because a reduction of NO_x induces an increase in particulate emission and reversibly subsequent reduction of particulate matter will induce an increase in NO_x emission. Consequently such a situation implies to reconsider the actual end-of-pipe technologies commercially available combining diesel particulate filter (DPF) and DeNO_x catalysts [1].

Commercial NO_x abatement technologies are actually available. They are essentially developed for heavy-duty vehicles such as the urea selective catalytic reduction (SCR). For the light vehicles a competition between SCR and NO_x storage and reduction after-treatment systems exist. In this complex technological context, the development of integrated De-NO_x and De-soot after-treatment technologies have also been proposed. One example is the Diesel Clean Advanced Technology (D-CAT) emission control system recently proposed by the Toyota group. Its Avensis model is equipped with the D-CAT package which includes the DPNR (Diesel PM and NO_x Reduction) system, a combination of a diesel particulate filter with a NO_x adsorber-catalyst [2].The DPNR converter features a newly developed, highly porous ceramic filter coated with a catalyst exclusively developed by Toyota for its NO_x storage reduction catalytic converter (NSR catalysts), initially designed for use with Toyota's lean-burn (high-oxygen) gasoline engines [3]. The NSR catalysts are generally composed of precious and base metal supported catalysts such as Pt-Rh/Ba-Al_2O_3 and Pt-Rh/K-Al_2O_3 [4]. During longer lean period NO in the exhaust gas is oxidized to NO_2 over Pt and NO_2 is stored as nitrates over Ba and K. Under rich conditions the stored nitrates are released as NO_x, which is further reduced to N_2 by CO, H_2 and HC over Pt/Rh. Various surface compounds such as nitrates and active oxygen generated during storage and reduction steps are proposed as active soot oxidation species and, thereby, decreasing the oxidation temperature. NO_2 produced over noble metals of NSR catalysts can be trapped as nitrates and can also react with soot generating NO again [5]. Under lean conditions NSR system can be expected to function as catalyzed soot filter (CSF). It is also proposed that under rich conditions active oxygen generated on the catalyst can oxidize the trapped soot. DPNR or NSR catalysts in this respect will have obvious advantages as it can reduce emission of both the pollutants and acts as '4-way' catalyst.

Only a few studies over '4-way' catalytic materials that can store NO_x, such as CeO_2, Ba and K-containing catalysts, for soot oxidation are reported [5,6]. In our previous works [7,8], it has been shown that soot

oxidation occurs during the lean phase only, while NO is being oxidized to NO_2 and nitrites/nitrates are being stored on the catalyst surface. NO_2 is an efficient and well recognized oxidizing agent for soot, but surface nitrates may have a role as well according to that proposed by Makkee et al. [9]. In particular, in [10] the reactivity of model Pt-Ba/Al_2O_3 and Pt-K/Al_2O_3 catalysts in the simultaneous removal of NO_x and soot has been investigated under a variety of experimental conditions (NO concentration, temperature, and particulate loading).

In this paper similar experiments have been performed over Pt-K/Al_2O_3 catalyst under more realistic conditions (i.e. in the presence of CO_2 and H_2O) in the range 250-350°C, both in the absence and in the presence of soot, and a comparison with Pt-Ba/Al_2O_3 catalyst is presented.

It is well known that the high mobility of some K compounds improves the effective contact with soot and, consequently, K-promoted catalysts have good activity in the soot combustion. However, the high mobility causes K to present a technological problem associated with its interaction with the monolith support, and looses due to volatilization and/or stripping by condensed water. For this reason, in this paper attention has been paid to how the Pt-K/Al_2O_3 catalyst modify its catalytic activity during lean-rich cycles, studying the effect of soot on the NO_x storage activity and in particular on the stability of the Pt-K/Al_2O_3 catalyst. ISC experiments and FT-IR analysis have been used in this case has complementary techniques.

2. Experimental

2.1. Catalysts preparation and characterization

A homemade Pt-K/Al_2O_3 (1/5.4/100 w/w/w) catalyst has been prepared by incipient wetness impregnation of a commercial alumina sample (Versal 250 from UOP) with aqueous solutions of dinitro-diammine platinum (Strem Chemicals, 5% Pt in ammonium hydroxide) and subsequently with a solution of potassium acetate (Aldrich, 99%). The powder has been dried at 80 °C and calcined in air at 500 °C for 5 h after each impregnation step. The impregnation order (first Pt and then K) has been selected in order to ensure a good dispersion and stability of the noble metal and of the alkaline component on the alumina support, in line with recipes of Toyota patents [3]. This sample has molar amount of K comparable to that contained in the Pt-Ba/Al_2O_3 (1/20/100 w/w/w) model catalyst previously used for similar studies (0.146 mol K or Ba/100 g of Al_2O_3) and reported here for comparisons [10]. The catalyst was characterized by XRD analysis (Brüker D8 Advanced Instrument equipped with graphite monochromator on the diffracted beam), surface area and pore size distribution by N_2 adsorption-desorption at 77K (Micromeritics TriStar 3000 instrument) and Pt dispersion by hydrogen pulse chemisorption at 0◦C (TPD/R/O 1100 Thermo Fischer Instrument). The Pt-K/Al_2O_3 sample presents a surface area near 167m^2/g_{cat} and pore volume of 0.90 cm^3/g_{cat}, while the Pt dispersion is close to 30%. Printex-U (Degussa) was used as model soot [9]. Catalyst-soot mixtures were

prepared by gently mixing in a vial the catalyst powder with soot (9:1 catalyst/soot ratio), thus realizing a loose contact.

Further details of catalyst preparation and characterization are reported elsewhere [11,12].

2.2. Catalytic tests

All reactivity tests were performed in a flow-reactor apparatus consisting of a quartz tube reactor (7mm i.d.) connected to a mass spectrometer (Omnistar 200, Pfeiffer Vacuum), a micro-GC (Agilent 3000A) and an UV analyzer (Limas 11HW, ABB) for the on-line analysis of the outlet gases (NO, NO_2, N_2, O_2, CO, CO_2, N_2O and NH_3). 66 mg of the soot-catalyst mixture (or 60 mg of bare catalyst) was used in each run. Prior catalytic activity runs, the catalyst sample has been conditioned by performing few storage/regeneration cycles. For this purpose, Isothermal Step Concentration (ISC) experiments have been performed at 350°C by imposing a rectangular step feed of NO (1000 ppm) + 3% v/v O_2 in flowing He + 1% H_2O + 0.1% CO_2 (lean phase) until catalyst saturation. Then the NO and O_2 concentrations have been stepwise decreased to zero, and a He purge at the same temperature (350°C) has been performed. This leads to the desorption of weakly adsorbed NO_x species. After the He purge, catalyst regeneration (rich phase) has been carried out with H_2 (3500 ppm) in flowing He + 1% H_2O + 0.1% CO_2. Conditioning lasted until a reproducible behavior was obtained; this typically required 3-4 adsorption/reduction cycles.

After catalyst conditioning at 350°C, the catalytic activity of Pt-K/Al_2O_3 has been tested with typical ISC run in the range 250-350°C, both in the absence and in the presence of soot. A comparison with Pt-Ba/Al_2O_3 is addressed at 300°C.

Finally, the effect of soot on the stability of the Pt-K/Al_2O_3 catalyst has been studied. The fresh catalyst has been mixed with soot (9:1 w/w ratio) and ISC experiment has been performed at 350°C. During this first run (Run 1 in the Figures), soot has been progressively consumed. After the complete consumption of soot, the clean catalyst has been mixed again with soot (in the same ratio) (Run 2) and further lean-rich cycle at 350°C have been carried out until the complete oxidation of particulate. The soot mixing and the catalyst cycling have been replicated another time (Run 3).

3.Results and discussion

3.1. Effect of temperature on the NO_x storage-reduction

The storage/reduction of NO_x activity over Pt–K/Al_2O_3 catalyst in the absence of soot has been investigated in the 250-350°C temperature range. The NO, NO_2, NO_x and CO_2 concentration profiles measured during the lean phase when 1000 ppm NO are fed to the reactor in the presence of O_2, H_2O and CO_2 are shown in Figure 1.

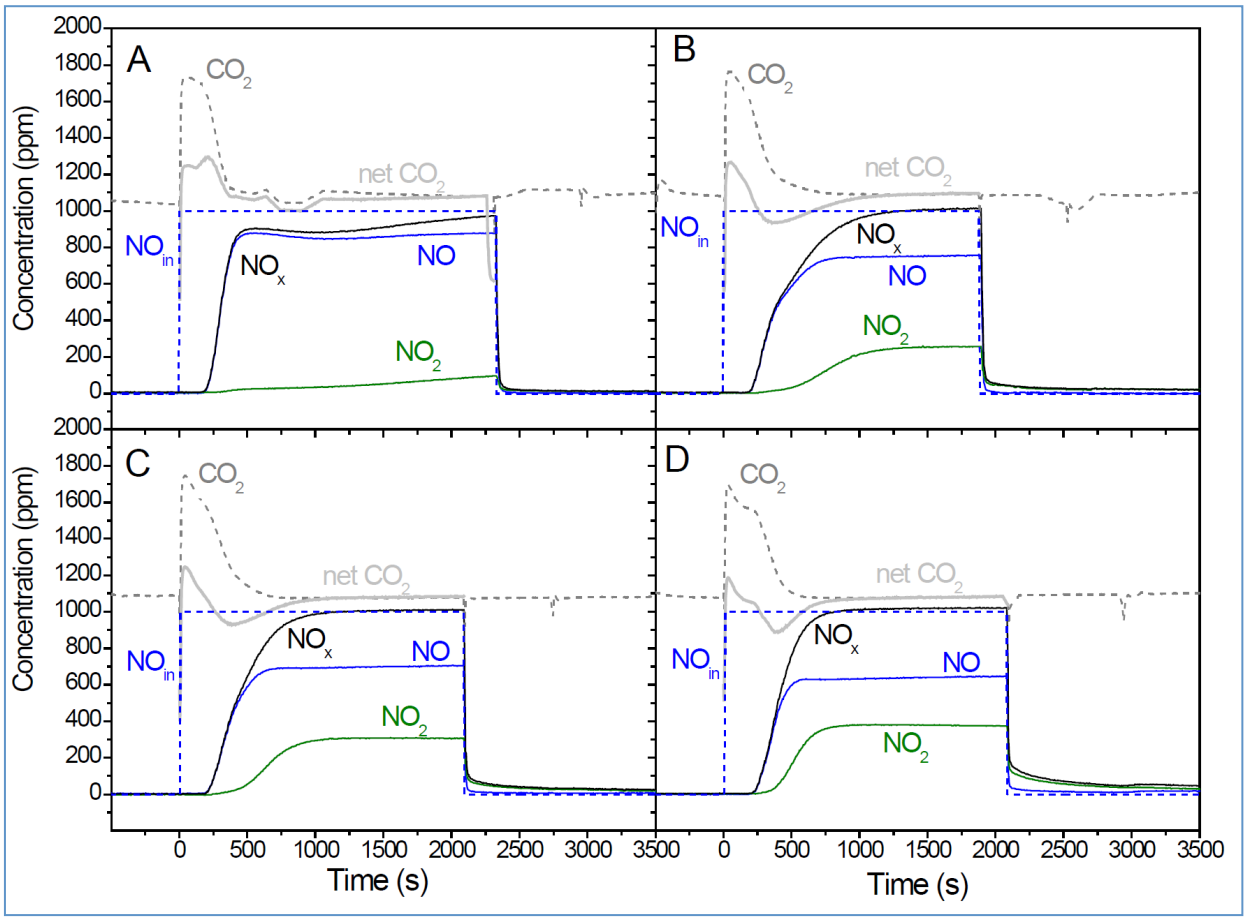

Fig. 1 - Adsorption phase over Pt-K/Al2O3 catalyst in the absence of soot at different temperatures (A 250°C, B 300°C, C 320°C, D 350°C) with 1000 ppm NO + O2 (3% v/v) in He + H2O (1% v/v) + CO2 (0.1% v/v)

At the highest investigated temperature (350 °C, Fig. 1D), upon NO admission to the reactor (t = 0 s) a delay near 200s is observed in the NO detection at the reactor outlet. Then, the NO concentration increases with time and reaches the steady state value of 645ppm. NO_2 breakthrough is observed with a delay of 50s respect to NO and increases until its asymptotic level of 375ppm. As well known, NO_2 production is related to the NO oxidation on Pt sites (reaction 1):

$$NO + 1/2\ O_2 \rightarrow NO_2 \qquad (1)$$

The amount of NO_x stored at this temperature up to the stationary level is near 0.56 mmol/g_{cat}, as apparent from Fig. 2A which shows the amounts of stored NO_x as a function of time-on-stream. When the NO inlet concentration is switched off (2000 s), a tail is observed in the NO_x concentration profile, due to the desorption of weakly adsorbed NO_x species [13]. The net amount of stored NO_x has been calculated by difference of the NO_x adsorbed during NO feeding and the NO_x desorbed and it is close to 0.42 mmol/g_{cat}, that corresponds to a decrement of roughly 25% respect to the storage capacity (see Table 1).

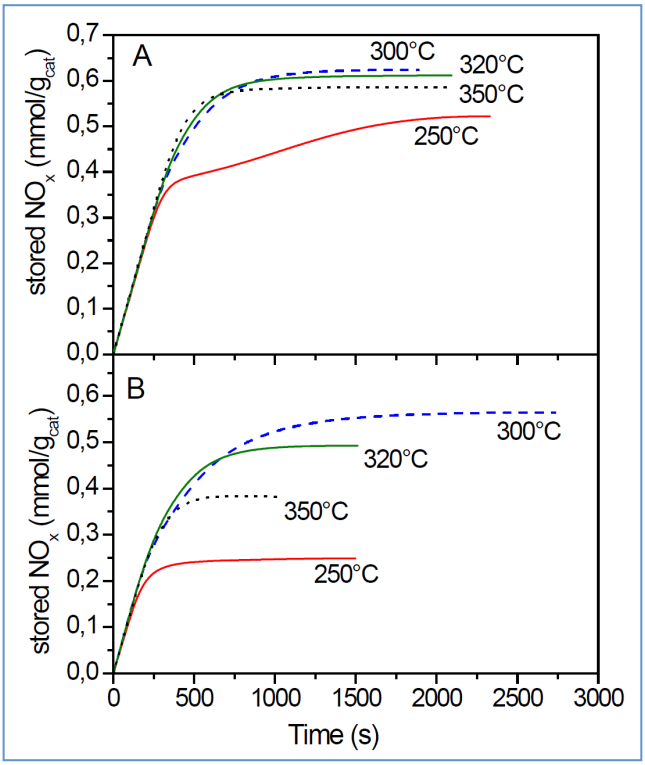

Fig. 2 – Integral curves of stored NOx versus time over Pt-K/Al_2O_3 catalyst in the absence of soot (A) and Pt-K/Al_2O_3 / soot mixture (B) at different temperatures

Upon NO admission, an increase in the CO_2 concentration is also observed. A peak is initially detected in correspondence to NO_x breakthrough; then, the CO_2 concentration gradually decreases to its background level until NO_x reach their stationary level. The increase in the CO_2 outlet concentration is due to the decomposition of surface carbonates upon NO_x uptake according to the stoichiometry of the following reaction:

$$K_2CO_3 + 2\,NO + 3/2\,O_2 \rightarrow 2\,KNO_3 + CO_2 \qquad (2)$$

It is possible calculate the amount of CO_2 evolved due to carbonate decomposition considering the stoichiometry of reaction (2) and the amount of stored NO_x. By subtracting from the CO_2 concentration trace this estimated CO_2 amount, a net CO_2 concentration trace is obtained [14]. In Fig. 1D this curve closely resembles the inlet CO_2 concentration value (1000 ppm), indicating that the evolution of CO_2 is uniquely related to the formation of nitrates species at the expense of carbonates, according to the stoichiometry of reaction (2). After NO shutoff, a small CO_2 uptake is observed, due to the occurrence of the reverse of reaction (2).

ISC experiments have been performed in similar condition varying the reaction temperature in the range 250-350°C and the results are reported in Fig. 1A-C. As clearly appear from the Figures, the NO_x storage behavior of the catalyst is affected by the temperature. In fact, the NO_x breakthrough increases from 90 s at 250°C (Fig. 1A) to 180 s at 300°C (Fig. 1B) and 200 s at 320°C (Fig. 1C). Besides the amounts of NO_x stored

up to steady state increase with temperature, from 0.52 mmol/g_{cat} at 250°C to 0.62 mmol/g_{cat} at 300°C (Fig. 2A and Table 1); above this temperature the amounts of stored NO_x slightly decrease.

Finally, the NO_2 concentration measured at the reactor outlet at the end of the NO_x dose (i.e. at steady-state) increases with temperature. In fact under our experimental conditions NO_2 formation is far from chemical equilibrium and the observed increase with temperature of the NO_2 concentration is hence expected being the reaction kinetically controlled. Accordingly, the NO/NO_2 molar ratio calculated at the end of the storage phase decreases with temperature from 9.8 at 250°C to 1.72 at 350°C.

Temperature also affects the rate of NO_x adsorption, as expected. As shown by the slope of the adsorption curves in Fig. 2A, in the initial part the curves are almost superimposed since an almost complete NO uptake is initially observed at all temperatures (i.e. NO_x uptake is initially limited by the NO feed). After 200s the adsorption curves slightly diverge and the steady-state loadings of the stored NO_x are reached earlier upon increasing the temperature. A similar effect has been observed in the case of Pt-Ba/Al_2O_3 catalysts as well [14], since also for this catalyst the rate of adsorption increases with temperature. A direct comparison between the amounts of NO_x stored at steady-state on the Pt-K/Al_2O_3 and Pt-Ba/Al_2O_3 catalyst samples is shown in Fig. 3 .

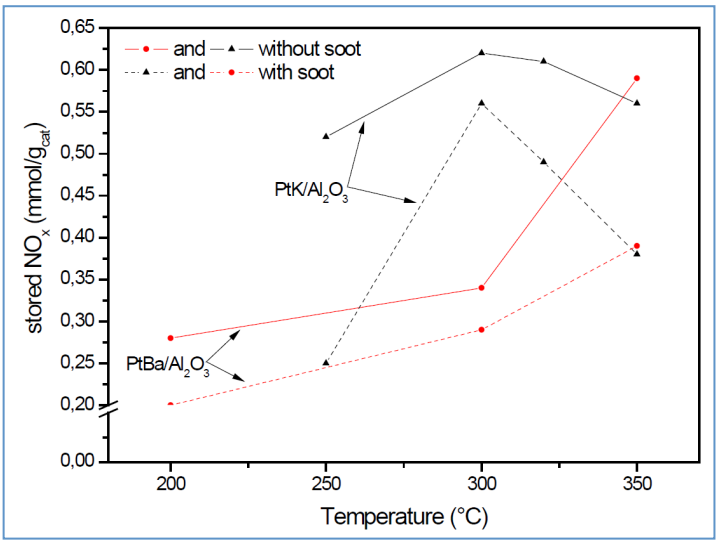

Fig. 3 – Amounts of stored NOx versus time over Pt-K/Al_2O_3 and Pt-Ba/Al_2O_3 catalysts (A) in the absence of soot and (B) in the presence of soot

It appears that the amounts of NO_x stored on Pt-K/Al_2O_3 are higher than those on Ba-based catalyst, although at 350°C the storage capacity of the two catalysts is very similar. Finally, the amounts of NO_x desorbed upon NO shutoff are higher over Pt-K/Al_2O_3 than over Pt-Ba/Al_2O_3 (see Table 1).

Table 1 resumes the quantitative analysis discussed above. In the Table are also reported the amounts of NO_x desorbed in correspondence of NO shutoff. As may be seen, this contribute is more significant at

higher temperature and at 350°C corresponds to the 25% of the total amount of NO_x stored during NO pulse.

Pt-K/Al_2O_3 catalysts	Without soot			With soot		
	Stored NOx up to steady state	Desorbed NOx upon NO shutoff	Desorbed NOx/Stored NOx	Stored NOx up to steady state	Desorbed NOx upon NO shutoff	Desorbed NOx/Stored NOx
	mmol/g_{cat}	mmol/g_{cat}	%	mmol/g_{cat}	mmol/g_{cat}	%
250°C	0.52	0.05	10	0.24	0.03	13.5
300°C	0.62	0.05	8	0.55	0.15	27
320°C	0.61	0.12	20	0.46	0.18	40
350°C	0.56	0.14	25	0.38	0.20	53

Pt-Ba/Al_2O_3 catalysts	Without soot			With soot		
	Stored NOx up to steady state	Desorbed NOx upon NO shutoff	Desorbed NOx/Stored NOx	Stored NOx up to steady state	Desorbed NOx upon NO shutoff	Desorbed NOx/Stored NOx
	mmol/g_{cat}	mmol/g_{cat}	%	mmol/g_{cat}	mmol/g_{cat}	%
200°C	0.28	0.09	32	0.20	0.09	44
300°C	0.34	0.02	7	0.29	0.06	19
350°C	0.59	0.06	10	0.39	0.1	27

Table 1 – Stored NOx up to steady state, desorbed NOx and percentage of desorbed NOx/stored NOx ratio at different temperatures, in the absence and in the presence of soot over Pt-K/Al_2O_3 and Pt-Ba/Al_2O_3 catalysts (NO 1000 ppm, O_2 3% v/v, H_2O 1% v/v, CO_2 0.1% v/v).

The NO_x stored at different temperatures are then reduced under isothermal conditions by admitting H_2 (3500 ppm) in He + H_2O (1% v/v) + CO_2 (0.1% v/v) and the results are shown in Fig. 4.

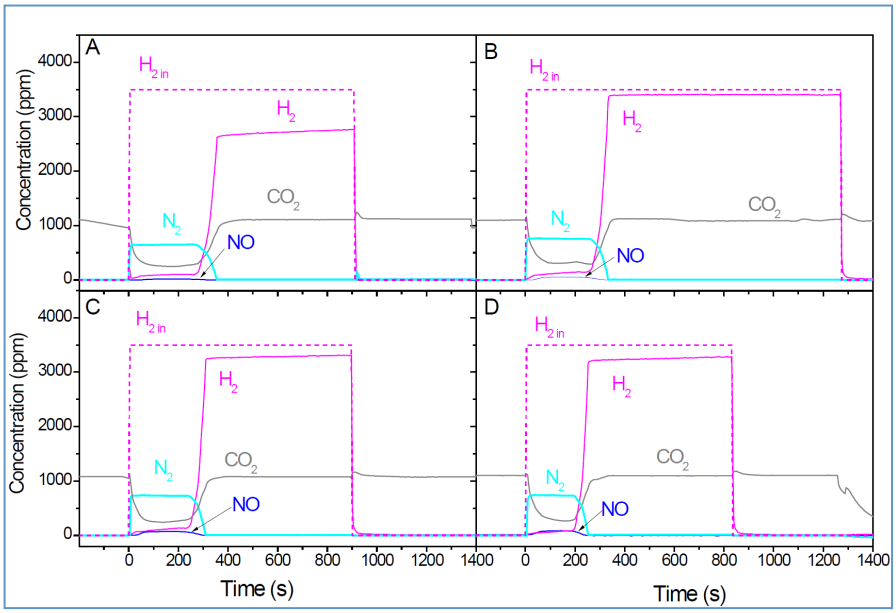

Fig. 4 - Reduction phase over Pt-K/Al2O3 catalyst in the absence of soot at different temperatures (A 250°C, B 300°C, C 320°C, D 350°C) with 3500 ppm H2 in He + H2O (1% v/v) + CO2 (0.1% v/v)

At 350°C (Fig. 4D), upon the addition of H_2 (at t= 0 s) N_2 is immediately observed at the reactor outlet along with a CO_2 consumption. This uptake of CO_2 is in line with the occurrence of reaction (3) which consider the

re-adsorption of CO_2 onto the K sites once NO_x has been reduced:

$$2\ KNO_3 + 5\ H_2 + CO_2 \rightarrow K_2CO_3 + N_2 + 5\ H_2O \quad (3)$$

The H_2 consumption is initially nearly complete and after a delay near 200 s its concentration increases with time until the initial value of 3500 ppm. Furthermore, no production of ammonia or other byproducts like N_2O is observed. Only a small amount of NO is detected along with nitrogen and this leads to a N_2 selectivity of 95%. At the end of the reduction phase (t = 300 s) the nitrates are all reduced and the catalytic surface is fully regenerated, as confirmed by N-balance.

The reduction pathway over Pt-K/Al_2O_3 catalyst has been recently studied by some of us [13] and carefully compared with that already proposed in the case of Pt-Ba/Al_2O_3 catalyst [15]. Both studies have pointed out that under nearly isothermal conditions N_2 formation occurs via an in series two-steps Pt-catalyzed molecular process involving the formation of ammonia as an intermediate. The first step of the series is ammonia formation through the reaction of H_2 with stored nitrates; ammonia then reacts with the nitrates left on the catalyst surface leading to the formation of nitrogen. The higher N_2 selectivity observed in the case of the Pt-K/Al_2O_3 catalyst is due to the fact that the onset for the H_2 + nitrate reaction leading to ammonia occurs at temperatures very close to the threshold for the NH_3 + nitrate reaction leading to N_2. Accordingly, ammonia, once formed, readily reacts with surface nitrates to give N_2, and this drives the selectivity of the reduction process to N_2 [13].

Similar results have been obtained (in the absence of soot) at the other temperatures, i.e. 250, 300, 320°C (Fig. 2A-C): the main reduction product is nitrogen and only small amounts of NO are detected as byproduct. However, upon increasing the temperature from 250 to 300°C it is observed that the amounts of the evolved reduction products increase due to the larger amounts of stored NO_x with temperature in the adsorption phase (see also Fig. 1).

The overall nitrogen selectivity is in all cases higher than 95% and slightly increases with temperature (in the range 250-300°C). At all the investigated temperatures, the catalyst is fully regenerated at the end of the reduction phase, as pointed out from the N-balance.

3.2. NO_x storage-reduction in the presence of soot

The results obtained when the same experiments have been carried out in the presence of soot in the 250-350°C temperature range are shown in Fig. 5 A-D, respectively, in terms of NO, NO_2, NO_x and CO_2 concentration profiles measured during the lean phase when 1000 ppm NO (+O_2 + H_2O + CO_2) are feed to the reactor.

Inspection of Fig. 5D, referring to 350°C, shows that in the presence of soot the NO_x outlet concentration shows a dead time lower than in the absence of soot (90 s vs 210 s); then, its curve increases approaching

the asymptotic values corresponding to 880 ppm. The NO_2 concentration measured at steady state is roughly 100 ppm.

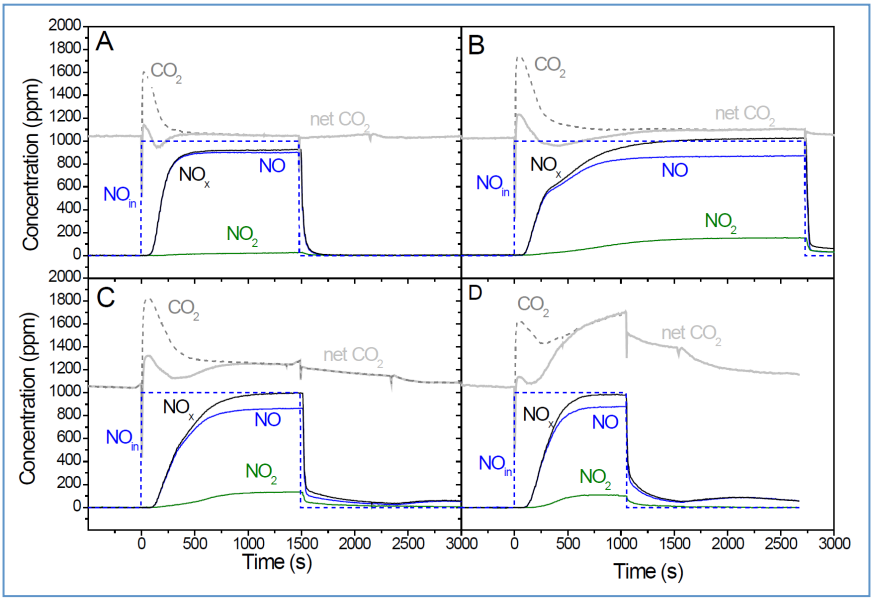

Fig. 5 - Adsorption phase over Pt-K/Al_2O_3 catalyst in the presence of soot at different temperatures (A 250°C, B 300°C, C 320°C, D 350°C) with 1000 ppm NO + O_2 (3% v/v) in He + H_2O (1% v/v) + CO_2 (0.1% v/v)

The amounts of NO_x stored at steady-state in the presence of soot are near 0.38 mmol/g_{cat}, i.e. much lower if compared to those measured in the absence of soot (0.58mmol/g_{cat}). Similar results have been obtained at the other investigated temperatures, as apparent upon comparison of the data shown in Fig. 2A and 2B (and Table 1).

The effect of soot on the storage capacity of LNT catalyst has also been investigated on Ba-based systems [14,16], and similar results have been obtained. In fact also in the case of Ba-based catalysts, the data clearly indicated that soot reduced the NO_x storage capacity of the catalyst, in line with the results of Sullivan et al. [17] and of Pieta et al. [18]. The decrease in the NO_x storage capacity of the catalyst at steady state is primarily related to the decrease in the NO_2 concentration. In fact the NO_2 concentration at the reactor outlet in the presence of soot is significantly lower than that observed in the absence of soot (compare with Fig. 5D vs 1D); this could be explained with a participation of NO_2 in the combustion of soot according to the following reaction:

$$2\ NO_2 + C \rightarrow CO_2 + 2\ NO \qquad (4)$$

Accordingly, in the presence of soot the NO/NO_2 molar ratio is higher than on the soot - free catalyst (near 8.8 vs 1.72).

The low NO_2 concentration explicates also the lower storage capacity of the catalyst - soot mixture. In fact, also over Pt-K/Al_2O_3 catalyst, like over Ba-based LNT system, operates the “nitrate” pathway for the storage of NO_x [13] which involves a direct adsorption of NO_2 over K sites in the form of nitrates via a disproportion

reaction. Accordingly, K and soot compete for reaction with NO_2 leading to the observed decrease in the NO_x storage properties.

The presence of soot also influences the stability of the adsorbed NO_x species. As shown in Fig. 5D, upon NO shutoff at the end of the adsorption phase (He purge) a tail is observed in the NO_x concentration indicating the desorption/decomposition of the NO_x previously stored; a significant effect is detected in correspondence of the O_2 shutoff as well. These effects decrease the amounts of NO_x which have been stored up to steady-state from 0.38 mmol/g_{cat} to 0.18 mmol/g_{cat}, i.e. the amounts of stored NO_x decrease roughly by 50% during the purge. Inspection of Table 1 shows that in the absence of soot the amount of NO_x desorbed is lower (25%) and no significant contribution of desorption in correspondence of O_2 shutoff is detected.

This destabilizing effect of soot on the stored NO_x was already observed in the case of Pt-Ba/Al_2O_3 catalyst [14]. In fact, in the absence of soot near 10% of the initially stored NO_x are decomposed after the NO shut off at 350°C, whereas in the presence of soot, the relative amounts of NO_x desorbed at the same temperature are 2-3 times higher than in its absence, being near 27% of those initially adsorbed (see Table 1).

During NO_x storage in the presence of soot, the evolution of CO_2 is also observed (Fig. 5D). The CO_2 curve shows a very complex trend. In correspondence of NO feeding, the CO_2 increases from the inlet value up to 1700 ppm at the end of NO pulse. Then its concentration slowly decreases and tends to reach the inlet value (1000 ppm) after O_2 shutoff.

The CO_2 production is due to two contributions: i) the decomposition of surface carbonates on the catalytic surface upon nitrates formation (reaction (3)); ii) soot combustion according to the reaction (4) previously reported. Note that reaction (4) is a global reaction; two steps could be considered:

$$NO_2 + C \rightarrow CO + NO \qquad (5)$$

$$CO + ½\ O_2 \rightarrow CO_2 \qquad (6)$$

During our experiments CO formation is not observed, likely because CO is oxidized to CO_2 by O_2 at Pt sites, as reported elsewhere [14].

In order to determine the amounts of CO_2 produced upon soot oxidation, the net CO_2 production has been calculated as previously indicated, and the results are shown in Fig. 5D. In the presence of soot a net CO_2 production is observed, not only in the presence of NO but also after NO shutoff, i.e. in the presence of O_2 only. Since the soot combustion in Fig. 5 D is apparent only after NO addition to the reactor (i.e. in the presence of O_2 only no CO_2 production is observed), it could be speculated that O_2 does not act as direct oxidizing agent of soot at these temperatures. Notably, the tail in NO_x concentration suggests that adsorbed NO_x species are involved in the combustion of soot as also suggested in previous papers [14] and

according to reaction (7):

$$C + 2\ NO_3^- \rightarrow CO_3^{2-} + 2\ NO + ½\ O_2 \quad (7)$$

At 350°C roughly 50% of the total amount of CO_2 produced after NO and O_2 shutoff is due to the nitrates oxidation. ISC experiments in the presence of soot have been performed in similar condition varying the reaction temperature in the range 250-350°C and the results are reported in Fig. 5A-D. In analogy to that observed in the case of soot-free catalyst, in all cases NO_x breakthrough increases with temperature but it is always lower than in the absence of soot (50s at 250°C, 75s at 300°C, 120s at 320°C) and also the amounts of NO_x stored up to steady-state increase with temperature until 300°C, as appears from Fig. 2B and Table 1. At temperature higher than 300°C the amounts of stored NO_x decreases. The data clearly show a more pronounced trend to a maximum in the amounts of stored NO_x and indicate that the amounts of NO_x stored in the presence of soot are always lower than those measured in its absence.

The temperature affects also the rate of NO_x adsorption, as already observed in the absence of soot. Indeed, in Fig. 2B the slope of stored NO_x curves is equal up to 130 s, then the curves diverge. As observed in the absence of soot, the stored NO_x curves increase with a slope that, at fixed amounts of adsorbed NO_x, increases with temperature with a maximum at 300°C. In the presence of soot this effect of temperature is much more pronounced.

The amounts of desorbed NO_x after NO shutoff increase with temperature and are always higher than in the absence of soot. It is noted that in the presence of soot near 27% (vs. 8%) and 40% (vs. 20%) of the initially stored NO_x are decomposed after the NO shutoff at 300°C and 320°C, respectively. This confirm the destabilizing effect of soot on the stored species, that is more evident at high temperature.

Also the amounts of NO_2 increases with temperature, but its concentration at steady state is always lower than in the absence of soot (155 ppm vs. 256 ppm at 300°C and 134 ppm vs. 305 ppm at 320°C). Accordingly, higher NO/NO_2 ratios are measured (5.6 vs. 2.9 at 300°C, 6.4 vs. 2.3 at 320°C). This trend is related to the participation of NO_2 in soot oxidation that became significant at temperature higher than 300°C. In fact, at each temperature a CO_2 evolution is always observed (see Fig. 5A-C) during the NO adsorption (occurrence of reaction (3)) but only above 300°C the trace of net CO_2 reveals a contribute to soot oxidation (reaction (4)). Note that by increasing the temperature the contribute of adsorbed NO_x species to the soot combustion increases as well. After NO and O_2 shutoff, the occurrence of reaction (7) represents the 20% and 30% of the total amount of CO_2 produced.

The data herein presented well parallel those obtained over Pt-Ba/Al_2O_3 [14] where a detrimental effect of soot on the NO_x storage capacity has been observed to increase with temperature in the range 250-350°C. As reported in Fig. 3 and Table 1 the performances of Pt-K/Al_2O_3 keep higher than that of Ba-based catalyst also in the presence of soot. Finally, inspection of Table 1 shows that at temperature higher than 300°C a

larger amounts of NO_x are desorbed from Pt-K/Al_2O_3 than from Pt-Ba/Al_2O_3. This is accompanied by an increased production of CO_2 after NO shutoff, indicating a greater contribution of reaction (7) to soot combustion.

Fig. 6A-D show data collected during the rich phase of cycling in the presence of soot in the range 250-350°C. The products evolution is similar to that previously described for the regeneration phase in the absence of soot (Fig. 2), being nitrogen the main reduction product; negligible amounts of NO are detected only at high temperature (i.e. 350°C). A comparison with the results obtained in the absence of soot indicates that the presence of soot does not influence significantly the reduction of the stored NO_x at any temperature.

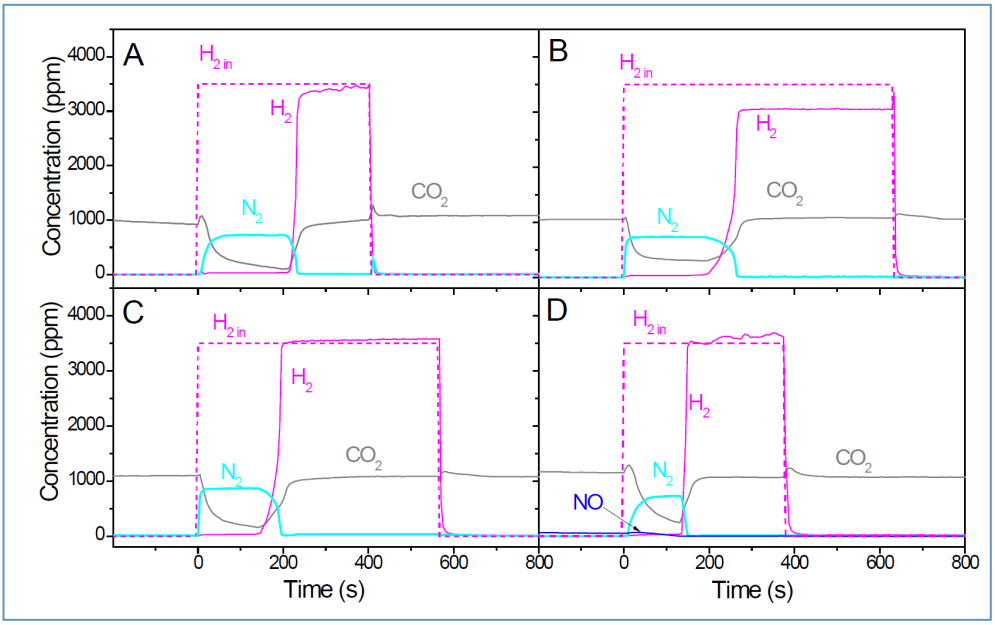

Fig. 6 - Reduction phase over Pt-K/Al_2O_3 catalyst in the presence of soot at different temperatures (A 250°C, B 300°C, C 320°C, D 350°C) with 3500 ppm H_2 in He + H_2O (1% v/v) + CO_2 (0.1% v/v)

3.3 effect of soot loading and stability of the Pt-K/Al_2O_3 catalyst

The results herein presented point out that the presence of soot affects the catalytic performance of the Pt-K/Al_2O_3 catalyst by lowering not only the amount but also the stability of the NO_x adsorbed species. In order to investigate more in details the effect of the soot loading on the catalyst behaviour, and the stability of the Pt-K/Al_2O_3 upon repeated soot oxidation cycles, several lean-rich cycles have been carried out over the same sample. For this purpose a sequence of NO_x adsorption and reduction cycles (6-7 cycles) has been performed in the presence of soot over a fresh Pt-K/Al_2O_3 at 350°C until the complete consumption of soot (run 1); after that, the clean catalyst has been mixed again with soot and has been again cycled under the same experimental conditions until complete soot oxidation (Run 2). This procedure has been repeated three times.

The amounts of NO_x stored at steady-state during the various lean-rich cycles are shown in Figure 7 as function of the residual soot. During the first run (black squares) with the full soot loading (near 11 % w/w) roughly 0,31 mmol/g_{cat} of NO_x could be loaded on the catalyst. The amounts of NO_x stored on the catalyst increase upon decreasing the soot loading; roughly 0.46 mmol/g_{cat} of NO_x could be stored at the end of Run 1, on the soot-free sample (point 3 in Fig. 7).

After that, the clean catalyst has been mixed again with soot and has been again cycled in the same conditions (Run 2, points 4-5 in Fig. 7) until the complete oxidation of particulate. Finally the procedure has been repeated for the third time (Run 3, points 6-7 in Fig. 7).

The clean catalyst has been mixed again with soot (point 4 in Fig. 7) and Run 2 has been performed; at the end of this run the the storage capacity is further decreased. A new mixing and a new run (Run 3) show that the clean catalyst (point 7 in Fig. 7) has lost its storage capacity, which is about half of that of the fresh catalyst.

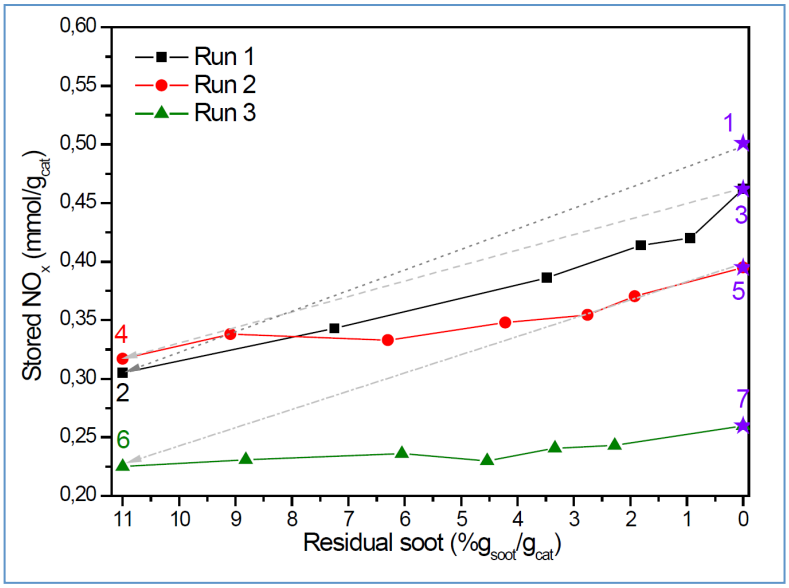

Fig. 7 – Stored NOx as function of residual soot in subsequent lean-rich cycles over Pt-K/Al_2O_3 catalyst during three different runs

The data point out that ageing the LNT Pt-K/Al_2O_3 catalyst by repeated soot oxidation cycles, the NO_x storage capacity decreases; indeed, the amount of NO_x stored on aged Pt-K/Al_2O_3 catalyst (i.e. clean catalyst) is lower than that on the fresh catalyst. This is in line with the results obtained by Krishna et al. [5].

The soot oxidation activity of Pt-K/Al_2O_3 catalyst has also been evaluated calculating the soot conversion in the lean phase of such Run (Fig. 8). Comparing the amount of soot oxidized in the tree different runs after the same number of lean phase, it clearly appears that second and the third cycle are almost identical and lower that the first one. On the other hand, the NO/NO_2 molar ratio (Fig. 9) strictly depends on the soot present; the amount of soot decreases the ratio decreases since NO_2 is not involved in the soot

combustion. Notably, the same NO/NO_2 molar ratio is calculated on the fresh and aged catalyst, indicating the ageing process does not involve Pt sites.

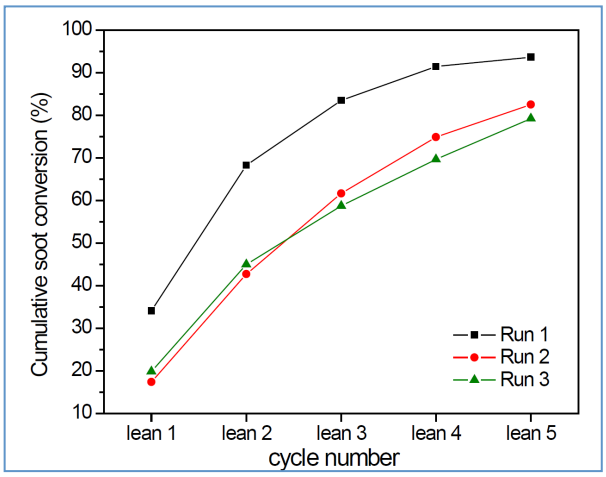

Fig. 8 - Cumulative conversion of soot (%) in subsequent lean phases (1000 ppm NO + O2 (3% v/v) in He + H2O (1% v/v) + CO2 (0.1% v/v) at 350°C) during three different runs

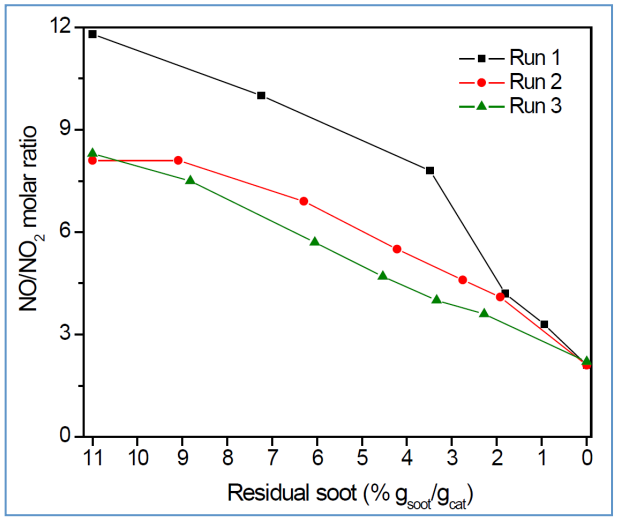

Fig. 9 - NO/NO2 molar ratio as function of residual soot over Pt-K/Al2O3 catalyst at NO shutoff

The observed decrease in soot oxidation activity over aged K-containing catalyst can be attributed to the volatile nature of K-active species, like nitrates (melting point 334°C) [5,[19],[20]]. The mobility of such compounds is expected to be high, leading to good contact with soot and bringing an additional activity. The degradation of catalyst should be due to the sublimation of K during soot combustion [[21]]. The loss of K have as consequence a lower amount of storage sites; accordingly, the storage capacity of system decreases and a lower amount of K-nitrates are available to oxidize soot. This also in line with that reported by Wu et al. [[22]].

On the other hand, after the first run the catalyst seems to stabilized its oxidation activity. Also Gross has observed a similar behaviour [23] studying the catalyst stability. Based on the results collected the Authors conclude that during the ageing the catalyst reaches a steady-state concerning the most relevant species, for example, carbonates or carbonate-type compounds produced via chemisorbed CO_2. These compounds could be formed and decomposed in a range of intermediate temperatures, such as the soot oxidation temperatures. This is a key point, since if these compounds do not decompose, the catalytic surface would be enriched in carbonates composition and a deactivation could be observed.

Bibliography

[1] P. Granger, V.I. Parvulescu, Chem. Rev. 111 (2011) 3155–3207

[2] M. Hiroki, S. Tatsumasa, Y. Shunsuke, T. Masato, O. Hisashi, O. Seiji, Toyota Tech Rev 52 (2002) 66-71

[3] Toyota Patent, European Patent Application No 01107629.6 (2001)

[4] J. Suzuki, S. Matsumoto, Top. Catal., 28 (2004) 171

[5] K. Krishna, M. Makkee, Catal. Today, 114 (2006) 48–56

[6] V.G. Milt, C.A. Querini, E.E. Miro, M.A. Ulla, J. Catal., 220 (2003) 424

[7] L. Castoldi. R. Matarrese, L. Lietti, P. Forzatti, Appl. Catal. B: Environ. 64 (2006) 25

[8] R. Matarrese, L. Castoldi, L. Lietti, P. Forzatti, Top. Cat. 42-43 (2007) 293

[9] A.L. Kustov, M. Makkee, Appl Catal B: Environ 88 (2009) 263-271

[10] R. Matarrese, L. Castoldi, L. Lietti, P. Forzatti, Top. Catal. 52 (2009) 2041-2046

[11] R. Matarrese, L. Castoldi, L. Lietti, P. Forzatti, Top. Catal.42-43 (2007) 293

[12] L. Castoldi, N. Artioli, R. Matarrese, L. Lietti, P. Forzatti, Catal. Today 157 (2010) 384–389

[13] L. Castoldi, L. Lietti, P. Forzatti, S. Morandi, G. Ghiotti, F. Vindigni, J. Catal. 276 (2010) 335–350

[14] N. Artioli, R. Matarrese, L. Castoldi, L. Lietti, P. Forzatti, Catal. Today 169 (2011) 36-44

[15] L. Lietti, I. Nova, P. Forzatti, J. Catal. 257 (2008) 270

[16] L. Castoldi, N. Artioli, R. Matarrese, L. Lietti, P. Forzatti, Catal. Today 157 (2010) 384

[17] J.A. Sullivan, O. Keane, A. Cassidy, Appl. Catal. B: Environ. 75 (2007) 102

[18] I.S. Pieta, M. García-Diéguez, C. Herrera, M.A. Larrubia, L.J. Alemany, J. Catal. 270 (2010) 256

[19] Z. Zhang, Z. Mou, P. Yu, Y. Zhang, X. Ni, Catal. Comm. 8 (2007) 1621–1624

[20] L. Castoldi, R. Matarrese, L. Lietti, P. Forzatti, Appl. Catal. B: Environ. 90 (2009) 278–285

[21] H. An, P.J. McGinn, Appl. Catal. B: Environ. 62 (2006) 46-56

[22] X. Wu, D. Liu, K. Li, J. Li, D. Weng, Catal. Comm. 8 (2007) 1274–1278

[23] M.S. Gross, M.A. Ulla, C.A. Querini , Appl. Catal. A: General 360 (2009) 81-88

Paper V

The NO_x reduction by CO on Pt-K/Al_2O_3 Lean NOx Trap Catalyst

Lidia Castoldi, Luca Lietti, Rossella Bonzi, Nancy Artioli, Pio Forzatti, Sara Morandi, Giovanna Ghiotti

The Journal of Physical Chemistry C, Vol. 115, No. 4, 2011

ABSTRACT

The reduction by CO under dry condition of NO_x species stored at 350 °C onto a Pt-K/Al_2O_3 Lean NO_x Trap catalyst is investigated by means of transient response methods (CO-TPSR and CO-ISC experiments) and complementary FT-IR spectroscopy. The results show that the pathway for the reduction of stored NO_x by CO under dry and near isothermal conditions is the same proposed by some of us in a previous work for Pt-Ba/Al_2O_3 catalyst. In particular: i) the reduction of stored NO_x by CO occurs according to a Pt catalyzed surface pathway that does not involve as a first step the release of NO_x in the gas phase, is effective already at low temperature and leads to nitrogen; ii) the reaction scheme implies the formation of surface isocyanate species followed by the reaction of these species with residual NO_x to give nitrogen; iii) the reaction of NCO species with nitrates to give nitrogen is slightly slower than the reduction of nitrates to give NCO species; but on Pt-K/Al_2O_3 catalyst this last step is faster than on Pt-Ba/Al_2O_3 system. As a consequence, the amount of isocyanates species present on the surface at the end of the reduction is lower for Pt-K/Al_2O_3 then Pt-Ba/Al_2O_3 catalyst.

Keywords: Lean NO_x Trap - Pt-K/Al_2O_3 - Reduction by CO - Transient Response Methods – FTIR – Nitrates – Nitrites – Isocyanates - Reaction Pathway

INTRODUCTION

Commercial vehicles and diesel passenger cars will be subjected in a near future to very stringent emission regulations regarding nitrogen oxides (NO_x). In fact EU emission standards coming in force in 2014 (Euro 6) impose strict emissions limits on these pollutants, in addition to hydrocarbon, carbon monoxide and particulate matter (soot): accordingly improved and viable solutions for NO_x reduction under lean conditions are required.

Different strategies have been proposed to handle the strict NO_x limits in lean-burn automotive emissions. One such strategy is the NO_x Storage-Reduction (NSR) system, or Lean NO_x traps (LNTs) [1,2,3]. This technique is based on the use of a catalyst containing precious metals such as Pt, Pd and Rh for the reduction and oxidation reactions, and alkali or alkaline-earth metal components such as Ba or K that store NO_x as nitrite and nitrate species [4,5]. Overall, NO_x are reduced to N_2 over NSR catalyst by alternating lean and rich periods, i.e. a lean period of 30-90 s during which the NO_x emitted in the exhaust gases are stored on the catalyst surface, and a short 3-5 s rich period during which the stored NO_x are reduced to N_2 by H_2, CO and unburned hydrocarbons.

Several studies deal with the reactivity and characteristics of Ba containing catalysts (see for example Refs. [6,7,8,9]), but reports on the specific behaviour of K-based catalysts are scarce in the literature, particularly on the reduction step. In this respect, the reactivity of different reducing agents (e.g. H_2, CO, C_3H_6 and C_3H_8) has been investigated in the case of Ba-containing catalysts; these studies indicate that hydrogen is the most effective reductant for lean NO_x traps [10,11,12,13,14].

In recent papers of various research groups, including ours, mechanistic aspects of the reduction of NO_x stored over Ba-based NSR catalytic systems have been reported when H_2 is used as a reductant [15,16,17]. It has been shown that the reduction by H_2 under near isothermal conditions of NO_x stored onto Pt-Ba/Al_2O_3 (and onto Pt-K/Al_2O_3 as well) is not initiated by the thermal decomposition of nitrates/nitrites ad-species with release of NO_x in the gas phase, but involves a Pt catalyzed surface pathway which is active at low temperature and leads to nitrogen [18,19]. It has also been proposed that under near isothermal conditions N_2 is formed exclusively via a consecutive reaction scheme which involves the fast reaction of H_2 with stored NO_x to give ammonia followed by the slower reaction of ammonia with residual stored NO_x to give N_2 [15,16,17,20]. However, it has been also pointed out that the reaction of ammonia with residual stored NO_x to give N_2 is slower over Pt-Ba/Al_2O_3 than over Pt-K/Al_2O_3.

In general, the reduction by CO of NO_x stored on LNT catalysts has attracted lower interest. In a very recent paper, some of us have performed a systematic and quantitative study of the reduction by CO under dry conditions of NO_x stored onto a Pt-Ba/Al_2O_3 LNT catalyst in order to clarify the reaction pathway and the mechanism of the reaction [21]. By using transient reactivity methods and complementary FT-IR spectroscopy, it was shown that also in the case of CO and under nearly isothermal conditions the

reduction of nitrates stored onto Pt-Ba/Al_2O_3 occurs through a Pt-catalyzed surface pathway. A mechanism was proposed for the reduction of surface nitrates by CO under dry conditions which proceeds through a stepwise reduction of nitrates with formation of nitrites and then of surface isocyanate/cyanate species followed by the reaction of these species with residual nitrites to give nitrogen. This last reaction is slower than the reduction of nitrates to give nitrites and then NCO species. Dedicated experiments have also shown that NCO species can be re-oxidized to surface nitrites at first and then to surface nitrates upon contact with oxygen at increasing temperature. This explains the formation of nitrogen observed during the reduction of stored NO_x by CO, and during the oxidation of surface NCO species upon oxygen addition and upon admission of NO in the presence of excess O_2.

The work here presented focuses on the study of the reduction steps when K replaces Ba as the storage component and CO is used as a reductant. For this purpose, the reduction with CO under dry conditions of NO_x stored onto a model Pt-K/Al_2O_3 catalyst has been analyzed. For this purpose NO_x have been adsorbed on the catalyst surface starting from NO/O_2; then the reactivity of the stored NO_x with CO has been investigated by means of Temperature Programmed Surface Reaction experiments (TPSR). Isothermal Step Concentration experiments (ISC) have also been performed in which the storage and the reduction phases have been carried out under nearly isothermal conditions, i.e. in the absence of significant temperature effects during cycling. These conditions have been accomplished by using low CO concentration and by separating the lean and the rich phases by an inert purge in between. Accordingly a more precise rationalization of the catalytic behaviour and a better understanding of the chemical uncontrolled thermal effects.

In parallel with reactivity experiments, FT-IR spectroscopy has been employed as complementary technique to obtain information about the nature, reactivity and evolution of surface species. The results collected over the Pt-K/Al_2O_3 catalyst sample in this study have been compared with those collected in the case of a Pt-Ba/Al_2O_3 catalyst [21] in order to highlight possible similarities and differences.

EXPERIMENTAL

1. Materials

K/Al_2O_3 and Pt-K/Al_2O_3 catalysts were prepared by the incipient wetness impregnation method, using aqueous solutions of CH_3COOK (Sigma Aldrich, 99%) and $Pt(NH_3)_2(NO_2)_2$ (Strem Chemicals, 5% Pt in ammonium hydroxide) to impregnate the γ-alumina support calcined at 700°C (Versal 250 from UOP, surface area of 207 m^2/g and pore volume of 0.96 cm^3/g). In the case of the Pt-K/Al_2O_3 catalyst the impregnation was carried out in sequential manner: the alumina support was first impregnated with the Pt dinitrodiammine solution, and then with the K acetate solution. After each impregnation step the catalysts

were dried at 80°C overnight and then calcined at 500°C for 5 h. The final loading was 5.4/100 w/w for the K/Al_2O_3 catalyst and 1/5.4/100 w/w for the Pt-K/Al_2O_3 catalyst. The following surface areas and pore volumes were measured by N_2 adsorption-desorption at 77K: 179 m^2/g and 0.84 cm^3/g for the K/Al_2O_3 sample; 176 m^2/g and 0.9 cm^3/g for the Pt-K/Al_2O_3 sample. The Pt dispersion, as determined by H_2 chemisorption at 0°C, was ~ 65 %. Mean Pt particle size measured by HRTEM was 1.5 nm [22], in good agreement with the mean Pt particle sizes (d_{Pt}) calculated from the empirical relationship often used for monometallic catalysts, $d_{Pt}(nm) = 1.1/(H/Pt)$, where H/Pt is the Pt dispersion measured from H_2 chemisorption.

2. Reactivity tests

The reactivity tests were performed over the Pt-K/Al_2O_3 and the K/Al_2O_3 samples previously conditioned. In the case of the Pt-K/Al_2O_3 catalyst, conditioning involved few adsorption/reduction cycles with NO/O_2 (1000 ppm NO and 3% v/v O_2 in He) and H_2 (2000 ppm in He) at 350 °C, respectively, with an inert purge (He) between the two phases. Conditioning was done until a reproducible behavior was obtained, and this typically required 2 or 3 lean-rich cycles [19,20]. For the K/Al_2O_3 binary catalyst, which does not adsorb significant amounts of NO in line with previous observations for the homologous Ba/Al_2O_3 [9] and does not react with H_2, the adsorption was carried out with NO_2 (1000 ppm in He), and the adsorbed NO_x were removed by heating at 400°C. Like Pt-K/Al_2O_3, also in the case of K/Al_2O_3 NO_x are stored on the catalyst surface in the form of nitrates [20,22].

Temperature Programmed Surface Reaction experiments (TPSR) were carried out in the presence of CO as reducing agent to analyze the reactivity of adsorbed nitrates. For this purpose NO_x were stored at 350°C with NO/O_2 mixtures (1000 ppm NO, 3% v/v O_2 in He). For the K/Al_2O_3 catalyst the adsorption was carried out with NO_2 (1000 ppm in He). The NO + O_2 (or NO_2) flow was maintained up to adsorption equilibrium; then the inlet NO + O_2 (or NO_2) concentration was decreased to zero. After storage, the samples were kept under inert He flow at the same temperature to provoke the desorption of weakly adsorbed species (He purge). Afterwards, the samples were cooled down to RT under flowing He and the CO-TPSR experiment was started by heating the catalyst at 10°C/min up to 400°C in He + 6500 ppm CO.

The storage/reduction of NO_x over Pt-K/Al_2O_3 was also investigated at constant temperature by imposing stepwise changes in the inlet concentration of the reagents (Isothermal Step Concentration experiments, ISC), according to the following sequence. After catalyst conditioning (see above), the storage of NO_x (Lean phase) was accomplished at 300°C by admitting NO (1000 ppm) in He+ 3 % v/v O_2. After storage, the NO + O_2 concentration was decreased to zero, while maintaining the catalyst at the same temperature (He purge). The reduction of the stored NO_x was then carried out by imposing a stepwise change in the CO

inlet concentration (0 → 2000 ppm→ 0) in flowing He (Rich phase). Three or four cycles have been carried out until a reproducible catalytic behaviour was attained.

All reactivity tests were performed in a flow-reactor apparatus consisting of a quartz tube reactor (7 mm i.d.) directly connected to a mass spectrometer (Omnistar 200, Pfeiffer Vacuum) and to a micro GC (Agilent 3000A) for the on-line analysis of the outlet gases (N_2, O_2, CO, CO_2, N_2O). The outlet NO, NO_2, NH_3 concentrations were also detected by a UV analyzer (Limas 11HW, ABB).

60 mg of catalyst with small particle diameter (100-120 μm) and a total flow rate of 100 cc/min (at 1 atm and 0°C) were used in each run in order to minimize intra- and inter-particle diffusion limitations. The flow rates of the gases were measured and controlled by mass-flow controllers (Brooks 5850 TR), and the gases were mixed before entering the reactor. The reactor was inserted into an electric furnace driven by a PID temperature controller/programmer. A K-type thermocouple (outer diameter 0.5 mm) directly immersed in the catalyst bed was used to measure and control the catalyst temperature.

Further details about the experimental apparatus and procedures can be found elsewhere [8,9,15,20,21].

3. FT-IR study

Absorption/transmission IR spectra were run on a Perkin-Elmer FT-IR System 2000 spectrophotometer equipped with a Hg-Cd-Te cryo-detector, working in the range of wavenumbers 7200-580 cm^{-1} at a resolution of 2 cm^{-1}. For IR analysis powder samples were compressed in self-supporting discs (10 mg cm^{-2}) and placed in a commercial heated stainless steel cell (Aabspec) allowing thermal treatments *in situ* under vacuum or controlled atmosphere and the simultaneous registration of spectra at temperatures up to 600°C.

Before the NO_x storage, the samples were conditioned by *i)* outgassing at 500°C for 30 min, *ii)* one or two cycles consisting of NO_2 adsorption at 350°C and reduction with H_2 at 350°C (for Pt-K/Al_2O_3 catalyst) or out-gassing at 500°C (for K/Al_2O_3 sample), necessary to eliminate the carbonates present on calcined powder [22], *iii)* oxidation at 500°C for 30 min and cooling in oxygen down to the temperature requested.

NO_x storage was carried out at 350°C by admitting, on the Pt-K/Al_2O_3 disc, freshly prepared NO/O_2 mixtures (p_{NO} = 5 mbar, p_{O2} = 20 mbar) or, on the K-Al_2O_3 disc, NO_2 (p_{NO2} = 5 mbar) up to catalysts saturation (ca. 20 min), and outgassing at the same temperature. The spectra of the stored NO_x were collected at 350°C or after cooling down the discs at the chosen temperature. The reduction was accomplished in CO (P_{CO} = 10 mbar) and was performed both in isothermal conditions and at increasing temperature. The reduction in isothermal conditions was accomplished at 280°C and 350°C: at each temperature the spectra were run at increasing exposure times. For the reduction experiments at increasing temperature, the samples were cooled down at 100°C under vacuum, then heated in CO in the range 100-400°C. NO (Praxair, purity ≥ 99.0 %) was freshly distilled before use. Conversely, NO_2 (Praxair, purity ≥ 99.5 %), O_2 (Praxair, purity ≥ 99.999 %) and CO (Praxair, purity ≥ 99.9 %) were directly used.

RESULTS AND DISCUSSION

1) K/Al_2O_3 sample.

CO-TPSR experiments and FT-IR study **-** The reactivity of CO towards NO_x species stored at 350°C onto K/Al_2O_3 was investigated by performing a CO-TPSR experiment and the results are presented in Figure 1A.

CO is consumed above ~ 330°C while CO_2 and NO are simultaneously formed, along with trace amounts of N_2. The concentrations of the products increase up to 400°C, and then slowly decrease to 0 ppm while the system is hold at this temperature (400°C); in the meantime the concentration of CO slowly approaches the inlet value.

It is worth noticing that CO reacts with stored NO_x at temperatures (330°C) near to the onset temperature for nitrates thermal decomposition (~ 340°C), as appears from the He-TPD experiment reported in the insert of Figure 1A. In this experiment the thermal decomposition of nitrates species present on the catalyst surfaces results in the initial evolution of NO_2, followed by O_2 and NO. The process is not complete at temperatures as high as 500°C; the catalyst was then kept at 500°C until desorption of NO_x was complete. The comparison between He-TPD and CO-TPSR experiments points out that the presence of CO in the feed does not affect appreciably the temperature threshold of nitrate thermal decomposition. In contrast, decomposition under a reducing atmosphere leads to a different product distribution, with the lack of any significant NO_2 evolution, and a corresponding increase in NO concentration. Besides, also oxygen evolution was not observed, whereas the formation of nitrogen was seen together with that of CO_2. These results well parallel those obtained in the case of Ba/Al_2O_3 catalyst [18,21].

The reduction of the NO_x stored onto K/Al_2O_3 catalyst at 350°C with CO has also been investigated by *in situ* FT-IR spectroscopy and the spectra obtained at increasing exposure times are reported in Figure 1B. In particular curve a is the spectrum of NO_x species previously stored at 350°C, i.e. ionic nitrates (related bands at 1375 and 1033 cm^{-1}, assigned to $\nu(NO_3)_{asym}$ and $\nu(NO_3)_{sym}$ modes, respectively) and bidentate nitrates (related bands at 1550, 1306 and 1006 cm^{-1}, assigned to ν(N=O), $\nu(NO_2)_{asym}$ and $\nu(NO_2)_{sym}$ modes, respectively) [20,22]; curves b and c correspond to the spectra recorded during the interaction with CO at increasing exposure times at 350°C. The extent of nitrates reduction is nihil after 20 min of exposure (not reported). After 40 min of exposure (curve b) small amounts of ionic nitrates are consumed and it needs 3 hs of exposure (curve c) to further reduce the ionic nitrates and to reveal minor amounts of reaction products (carbonate species, shoulder at 1620 cm^{-1}, corresponding to ν(C=O) mode, [22]) along with minor amounts of isocyanate species (weak band at 2235 cm^{-1}) [23].

In line with CO-TPSR experiment reported in Figure 1A, FT-IR data show that the reduction by CO of

nitrates stored onto K/Al_2O_3 sample is extremely slow at 350°C and only occurs to a rather limited extent.

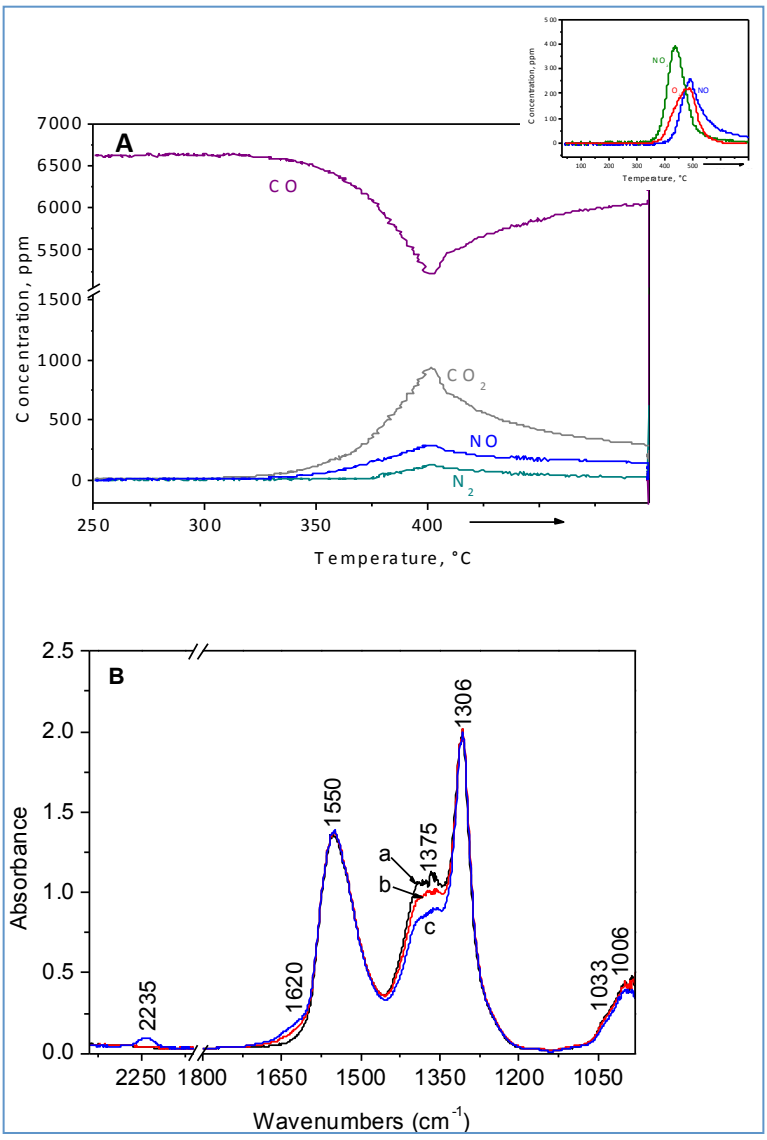

Figure 1 - A) CO-TPSR (6500 ppm CO in He) after NO_2 adsorption at 350°C over the K/Al_2O_3 catalyst. The results of the TPD run in He after NO_2 adsorption at 350°C over the same catalyst is shown in the insert. B) FT-IR spectra of NO_x reduction at 350°C in CO (10 mbar) at increasing exposure time over the K/Al_2O_3 catalyst. Curve a, spectrum of NO_x stored at 350 °C by NO_2 adsorption; curves b and c, spectra after reduction for 40 min and 3h, respectively.

2) Pt-K/Al_2O_3 catalyst

CO-TPSR experiment and FT-IR study - The reactivity of CO towards NO_x species previously stored at 350°C over the Pt-K/Al_2O_3 sample was investigated by performing a CO-TPSR experiment (CO inlet 6500 ppm) and the results are presented in Figure 2A.

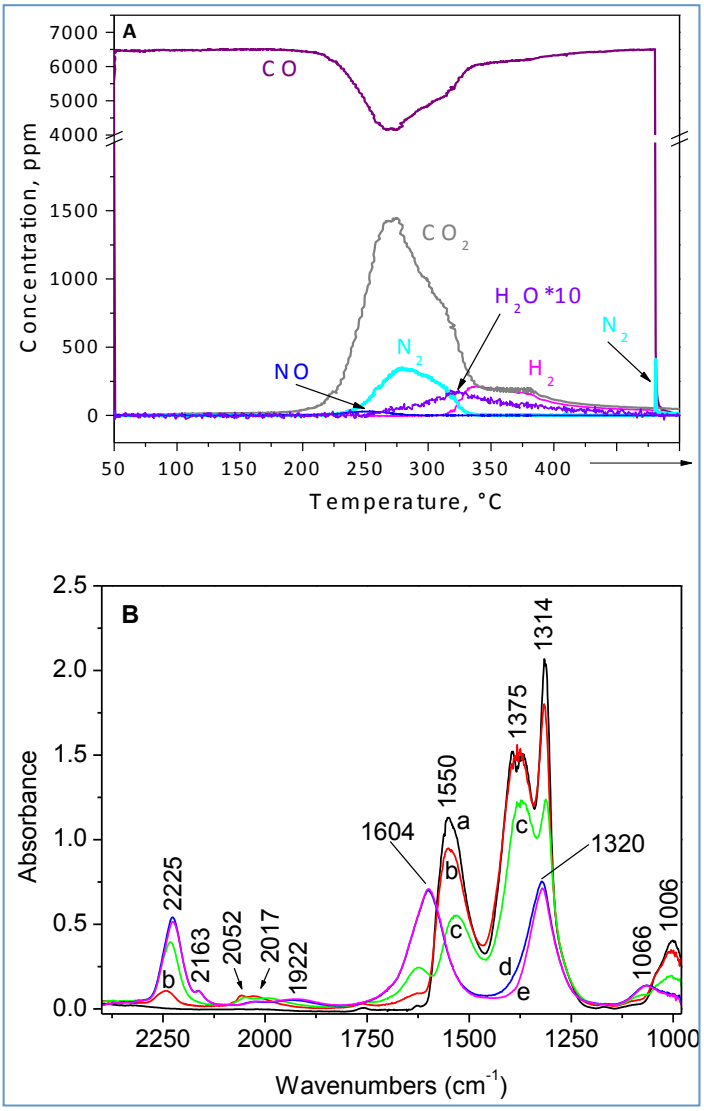

Figure 2 - CO-TPSR (6500 ppm CO in He) after NO/O_2 adsorption at 350°C over the Pt-K/Al_2O_3 catalyst. The results of the TPD run in He after NO/O_2 adsorption at 350°C over the same catalyst is shown in the insert. B) FT-IR spectra of NO_x reduction in CO (10 mbar) at increasing temperature over the Pt-K/Al_2O_3 catalyst. Curve a, spectrum of NO_x stored at 350°C by NO/O_2 adsorption; curves b-e, spectra after reduction at 250, 300, 350 and 400°C, respectively.

CO consumption starts near 210°C: the CO trace shows a minimum of ~ 4150 ppm at 270°C and then slowly increases approaching at 340°C an asymptotic value which is slightly below the inlet concentration. A shoulder in the CO consumption peak is observed near 315°C. The formation of CO_2 is detected simultaneously with the consumption of CO, showing a maximum of ~ 1420 ppm in the temperature range where the CO trace shows its minimum. At the same time nitrogen is formed at slightly higher temperature, starting from 230°C; its concentration gradually increases up to 340 ppm at 280°C, then slowly decreases. A shoulder in N_2 and CO_2 traces is observed corresponding to the shoulder of CO peak at 315°C. Finally, very small amounts of NO are also detected near 235°C.

From ~ 330°C, when the nitrogen concentration is close to zero, hydrogen is detected in the gaseous products together with CO_2.

The production of H_2 and CO_2 at high temperature, jointly with a constant consumption of CO, suggests

the occurrence of the Water Gas Shift (WGS) reaction:

$$CO + H_2O \rightarrow H_2 + CO_2 \quad (1)$$

Indeed, inspection of Figure 2A shows the presence of small amounts of water starting from 250°C; according to that observed during the He-TPD (not reported), the water concentration trace increases with temperature, suggesting that it is likely related to a desorption from the catalyst surface. The desorption of H_2O could be likely associated to the presence of trace amounts of water in the feed that causes the surface catalyst rehydration at the low temperatures (RT-200 °C) and is released at the high temperature (250-350°C). It is worth to note that the occurrence of the WGS reaction occurs over the Pt-K/Al_2O_3 sample starting from 180°C in the absence of stored nitrates (data not reported), but is observed at higher temperature (330°C) when the stored nitrates are almost completely depleted. A similar behavior has been observed over the Pt-Ba/Al_2O_3 sample [21]; in addition it has also been shown in the past that the catalyst promotes the Reverse Water Gas Shift (RWGS) reaction as well and also in this case the reaction was seen to take place after stored NO_x groups have been depleted [8].

It is cloncluded that over Pt-K/Al_2O_3 the consumption of CO occurs at temperatures well below that of NO_x thermal desorption over the same catalyst. In fact in the absence of CO nitrates stored at 350°C decompose only starting from the temperature of adsorption, as pointed out by dedicated He-TPD experiments where the stability of nitrates stored at 350°C over the Pt-K/Al_2O_3 sample has been investigated (data not reported). Moreover, a comparison with the results of CO-TPSR experiments carried out over the Pt-free sample (Figure 1) pointed out that the reduction of the stored nitrates is catalyzed by Pt, since over K/Al_2O_3 the reduction is only observed starting from the temperature of the thermal decomposition of stored NO_x. This clearly indicates that over Pt-K/Al_2O_3 a Pt-catalysed surface route is responsible for the reduction of the stored nitrates, similarly to the case of Pt-Ba/Al_2O_3 [15,21].

Notably, the CO trace is complex, with a first peak at about 270°C and a shoulder near 315°C. This may suggest the involvement of stored NO_x species with different reactivity. These features have been observed also when H_2 is used as a reductant instead of CO [19,20]: also in that case two major H_2 consumption peaks were apparent in the TPSR experiments, associated with the formation of different products, i.e. N_2 in the first peak and NH_3 in the shoulder at higher temperature. As will be discussed later on, FT-IR measurements pointed out that this is possibly related to the presence of NO_x adsorbed species having different reactivity, i.e. ionic and bidentate nitrates.

The moles of CO consumed and of the different products formed during CO-TPSR were calculated from Figure 2A and are reported in Table 1 for different temperature ranges. 1.90 10^{-4} moles/g_{cat} of N_2 and 0.12 10^{-4} moles/g_{cat} of NO are released in the gas phase during the whole TPSR run. Since 4.33 10^{-4} moles/g_{cat} of NO_x species have been previously stored onto the catalyst, ~ 90 % of the stored nitrates are reduced to gaseous N-containing products. Accordingly small amounts of N-containing species could be present at the

catalyst surface at the end of the CO-TPSR experiment. In fact, as it will be shown in the following, FT-IR spectra show that NCO species still remain onto the catalyst surface at the end of the reduction phase.

	Temperature range	
reagent and product species (moles/g_{cat})	RT – 250°C	RT - 330 °C
CO consumed	$2.91\ 10^{-4}$	$14.7\ 10^{-4}$
CO_2 formed	$1.49\ 10^{-4}$	$9.05\ 10^{-4}$
N_2 formed	$0.08\ 10^{-4}$	$1.90\ 10^{-4}$
NO formed	-	$0.12\ 10^{-4}$
H_2 formed	-	$1.63\ 10^{-4}$
NH_3 formed	-	-

Table 1. Moles/g_{cat} of CO consumed and of products formed during CO-TPSR over Pt-K/Al_2O_3 (NO_x stored at 350°C in NO/O_2 are $4.33\ 10^{-4}$ moles/g_{cat})

The features herein discussed suggest that the reduction of stored NO_x species primarily occurs according to the reactions:

$$2\ KNO_3 + 5\ CO \rightarrow K_2CO_3 + N_2 + 4\ CO_2 \qquad (2)$$

$$2\ KNO_3 + 8\ CO \rightarrow 2\ KNCO + 6\ CO_2 \qquad (3)$$

Close inspection of Figure 2A shows that in the low-T region (below 250°C) the consumption of CO is accompanied by the evolution of CO_2 and of a very small quantity of N-containing species ($0.08\ 10^{-4}$ moles/g_{cat} of N_2; Table 1). This points out that the initial step in the reduction of stored nitrates is described by reaction (3), as also confirmed by FT-IR study (see infra).

A similar TPSR experiment performed over Pt-Ba/Al_2O_3 catalyst demonstrated that at the end of the CO-TPSR experiment only ~ 43 % of the stored nitrates were reduced to gaseous N-containing products and consequently N-containing species were still present at the catalyst surface [21]. Also in that case in the low temperature region (below 250°C) the CO consumption is higher than that expected from N_2 and CO_2 production and the formation of isocyanates species has been pointed out by FT-IR experiments, according to the stoichiometry of the following reaction:

$$Ba(NO_3)_2 + 8\ CO \rightarrow Ba(NCO)_2 + 6\ CO_2 \qquad (4)$$

As shown in the following, FT-IR measurement reveals that the formation of isocyanates ad-species is effective in the case of Pt-K/Al_2O_3 catalyst as well. However, as opposite to the homologous Pt-Ba/Al_2O_3 catalyst [21], over Pt-K/Al_2O_3 the amounts of NCO species left onto the catalyst surface at the end of the reduction are small, in line with the observation that ~ 90 % of the stored nitrates are reduced to gaseous N-containing products (see above).

The reduction by CO of NO_x species previously stored at 350°C onto the Pt-K/Al_2O_3 catalyst investigated by means of in situ FT-IR spectroscopy is reported in Figure 2B. In this Figure curve a is the spectrum of NO_x species stored at 350°C and cooled down to 100°C, and curves b-e correspond to the spectra recorded during interaction with CO at increasing temperature up to 400°C. The stored nitrates are not perturbed in the range 100-200°C (not reported), at 250°C the bidentate nitrates become to be reduced (curve b, bands at 1550, 1314, 1006 cm^{-1}) and completely removed at 350°C (curve d). Starting from 300°C (curve c) also the ionic nitrates (band at 1375, 1033 cm^{-1}) start to be reduced and their reduction is complete at 400°C. It is worth noting that ionic nitrates are more resistant to the reduction with respect to the bidentate ones, but ionic nitrates start to react before the complete removing of bidentate species: this justifies the presence of the two contributions of CO consumption in TPSR measurement (Figure 2A), with a minimum near 270°C and a shoulder at 315°C.

Simultaneously to the nitrate reduction, increasing amounts of NCO surface species (band at 2225 cm^{-1} and a very weak one at 2163 cm^{-1}) and of surface carbonates (bands at 1604, 1320 and 1066 cm^{-1}, corresponding to ν(C=O), $\nu(CO_2)_{asym}$ and $\nu(CO_2)_{sym}$ modes, respectively [22]) are also revealed. Actually, up to 350°C the $\nu(CO_2)_{asym}$ mode of carbonates is superimposed with some of nitrate modes. The NCO species responsible for the band at 2163 cm^{-1} appear only by reduction at 350°C. The two bands at 2225 and 2163 cm^{-1} are in the same positions of the bands related to isocyanate species formed in a similar experiment accomplished (i.e. reduction with CO of stored NO_x) on a Pt-Ba/Al_2O_3 catalyst [21]. In the literature, these bands have been assigned to isocyanate species coordinated to Al^{3+} in tetrahedral coordination and on the Ba phase, respectively [24,25,26]. However, our results obtained from experiments performed with assignment purposes do not match with literature. We found that both the bands are related to different isocyanate species on the Ba-phase [21,27,28]. For the same reasons, and on the basis of dedicated experiments (not reported because out of the aim this work), we assign both the bands found on Pt-K/Al_2O_3 catalyst to different NCO species on the K-phase.

In line with TPSR data, FT-IR experiments confirm that nitrates stored onto Pt-K/Al_2O_3 catalyst are reduced by CO at temperatures lower than that corresponding to their thermal decomposition. However, FT-IR measurements reveal a beginning of the reduction at temperatures slightly higher (250°C) than that found in the TPSR experiment (210°C). This can be related to the different operating conditions: vacuum pretreatment and static conditions for FT-IR measurements and flow conditions for TPSR ones. Moreover, FT-IR experiments confirm that onto Pt-K/Al_2O_3 catalyst a certain amount of nitrogen is still present on the surface as isocyanate species after reduction of stored nitrates with CO up to 400°C. As already mentioned, the formation of strongly adsorbed NCO species justifies the absence of N_2 evolution at the beginning of the TPSR experiment, while CO is being consumed. NCO species might be involved in N_2 formation, as

pointed out by the observation that a close inspection of the bands in Figure 2B shows that increasing the temperature, keeping constant the erosion rate of nitrate bands, the growing rate of NCO absorption at 2225 cm^{-1} decreases. This point will be further addressed below.

Isocyanate species formed on Pt-K/Al_2O_3 catalyst at the end of the reduction (see Figure 2B, curve e) are in very low amounts if compared with those formed in similar conditions by reduction with CO of NO_x stored on the Pt-Ba/Al_2O_3 [21]. This statement needs some considerations. The more correct mode to support the statement should be an evaluation of the ratio between the integrated intensities of absorption bands related to NCO at the end of the reduction and of nitrate absorption bands before the reduction. In this way should be possible to evaluate the ratio between the total amount of nitrogen stored as nitrates and of nitrogen that remains at the surface after the reduction step on the two catalysts. However, while on Pt-Ba catalyst practically only ionic nitrates are presents, on Pt-K catalyst both ionic (with different spectroscopic features with respect to Pt-Ba system) and bidentate nitrates are present. The different distribution of nitrate types with different absorption coefficients on the two systems makes this kind of evaluation not feasible.

Conversely, having the NCO species the same spectroscopic features on Pt-K/Al_2O_3 and Pt-Ba/Al_2O_3 systems, it is reasonable to assume that they have the same absorption coefficients. Moreover, we have to take into account that: i) the molar amounts of K and Ba per gram of catalyst are similar on both the systems; ii) the dispersion of the basic phase is high on both the catalyst [22,29]; iii) we used discs with comparable weights; iv) the ratio between the specific surface areas of Pt-K/Al_2O_3 (176 m^2/g) and Pt-Ba/Al_2O_3 (137 m^2/g) is 1.3; v) the amounts of NO_x stored at 350°C on the two systems are comparable (4.33 10^{-4} mol/$g_{cat.}$ for Pt-K/Al_2O_3 and 5.8 10^{-4} mol/$g_{cat.}$ for Pt-Ba/Al_2O_3) [20,21]. On the basis of these considerations, it is possible to directly compare the integrated intensities (normalized to the surface areas of the catalysts) of the isocyanate species formed in similar experiments to make an evaluation of the difference in the amounts of isocyanates formed on the two systems. These calculations suggest that the amount of isocyanates formed on Pt-K catalyst is roughly 5 times lower than that formed on Pt-Ba catalyst.

Another possibility is considering the ratio between the integrated intensities of the bands related to isocyanate species and to the carbonate species formed at the end of the reduction. In this case, no assumptions about surface areas, discs weights, amount and dispersion of the storage phase are necessary. However, it is necessary to assume: i) the same absorption coefficients for the carbonates on the surface of Pt-K and Pt-Ba systems. This is reasonable, since they show same spectroscopic features for the two catalysts; ii) a similar equilibrium between CO_2 in the gas phase and CO_2 adsorbed as carbonates on the surface of Pt-K/Al_2O_3 and Pt-Ba/Al_2O_3. Another crucial assumption is that the carbonate amounts for gram of catalyst should be the same, even if carbon consumed from CO to form NCO species is surely higher for

Pt-Ba than for Pt-K catalyst. However, the reaction pathway proposed (see infra) show the formation of an high CO_2 excess with respect to isocyanates, ensuring a negligible error in the evaluation here proposed. On the basis of these considerations, the ratio between the amounts of NCO (in the range 2330-2080 cm^{-1}) and CO_3^{2-} species (in the range 1800-1160 cm^{-1}) formed at the end of the nitrate reduction at increasing temperature is 0.27 for Pt-K/Al_2O_3 and 1.4 for Pt-Ba/Al_2O_3. This calculation suggest that, assuming constant the amount of carbonates formed on the two catalysts, the quantity of isocyanates on Pt-K system is roughly 5 times lower than that on Pt-Ba one, perfectly in line with the previous evaluation.

The calculated values are in agreement with data obtained from TPSR experiments over both Pt-K/Al_2O_3 and Pt-Ba/Al_2O_3 catalysts. In fact for Pt-Ba/Al_2O_3 catalyst [21] 43% of the stored nitrates are reduced to gaseous N-containing products and consequently 57% of nitrogen remains on the surface as isocyanates, whereas for Pt-K/Al_2O_3 90% of the stored nitrates are reduced to gaseous N-containing products and consequently only 10% of nitrogen remains on the surface as isocyanates. This means that the quantity of isocyanates present on Pt-K system is roughly 5-6 times lower than that on the Pt-Ba one.

Finally, it is also worth noticing that, after CO interaction at 250°C up to 300°C FT-IR spectra showed two weak bands at 2052 and 2017 cm^{-1} (Figure 2B) related to the stretching modes of linear carbonyls adsorbed on reduced Pt sites [22], indicating that the platinum is already reduced by CO at 280°C. Actually, these bands start to decrease at 350°C for carbonyl desorption with a contemporary shift to lower frequencies, as expected on decreasing the CO coverage.

CO-ISC experiment and FT-IR study **-** The reactivity towards CO of NO_x stored at 300°C over the Pt-K/Al_2O_3 sample was investigated by performing isothermal reactivity experiments.
The results of a CO-ISC experiment run at 300°C reported and discussed in the following are collected over a sample that showed reproducible cyclic behavior, i.e. after performing few lean rich cycles (i.e. NO_x storage and reduction by CO with an inert purge in between).

Figure 3 shows the results of a lean-rich cycle at 300°C (storage and reduction) over the Pt-K/Al_2O_3 catalyst performed by admitting 1000 ppm of NO in the presence of O_2 (3% v/v in He), followed by reduction of the stored NO_x by admission of 2000 ppm of CO (in He). An helium purge was fed between the lean and rich phases.

As shown in Figure, the admission of 3% v/v O_2 (Figure 3, t = - 1000 sec) causes the evolution of small amount of N_2, produced by the oxidation of surface N-containing species that remain adsorbed at the catalyst surface after the previous reduction with CO. Then, upon the NO step addition (at t = 0 s) NO and NO_2 show a dead time of about 30 and 100 s respectively; their concentration rapidly increases with time approaching the asymptotic concentrations corresponding to the NO_x feed concentration

($NO + NO_2$) after about 2000 s. Accordingly, significant amounts of NO_x were stored ($5.41\ 10^{-4}$ moles/g_{cat}). Formation of NO_2 in the gas phase indicates that Pt is active in the NO oxidation reaction; as indicated in a dedicated FT-IR analysis, nitrates are the major adsorbed species present after adsorption in NO/O_2 at 300°C [19,20].

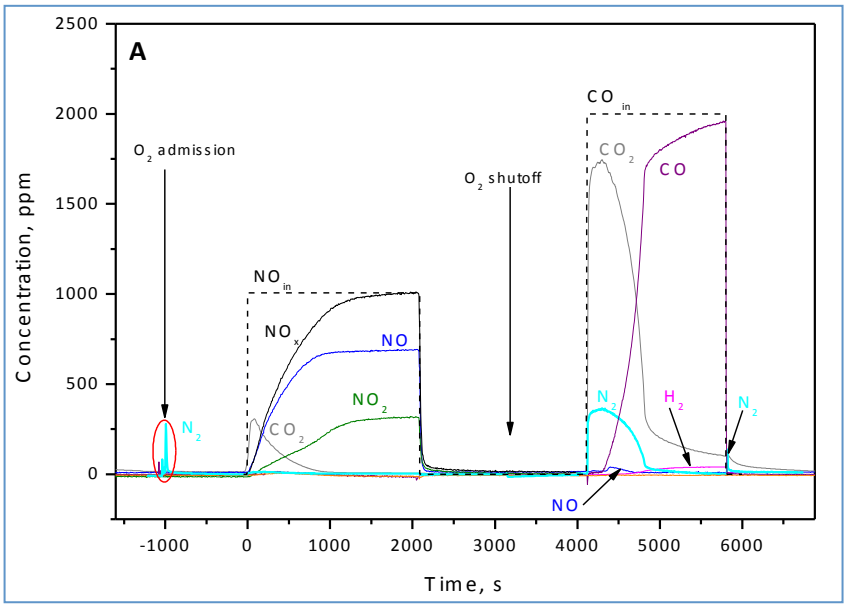

Figure 3 - ISC experiments at 300°C over the Pt-K/Al_2O_3 catalyst (storage phase: NO 1000 ppm + O_2 3 % v/v in He; reduction phase: CO 2000 ppm in He).

Upon admission of CO (t = 4114 s), ~ 360 ppm of N_2 and ~ 1730 ppm of CO_2 are immediately produced, together with negligible amounts of NO (30 ppm). CO is completely consumed for about 200 s; afterwards CO is detected at the reactor outlet: its concentration increases and approaches the inlet value within ~ 1700 s after CO admission. After CO breakthrough the N_2 and CO_2 concentrations (and NO production) decrease. When the nitrogen concentration is close to zero (i.e., when stored NO_x are almost depleted) H_2 production is observed as in the case of the CO-TPSR experiment.

Worth to note that a very small increase in the catalyst temperature (≤ 2°C) is measured upon CO admission, so that the reduction is performed under nearly isothermal conditions.

When the CO feed is stopped (after 1700 s from the CO admission), a small amount of nitrogen is produced, along with CO_2 (see Table 2).

The moles of CO consumed and of the different products formed during CO-ISC experiment over Pt-K/Al_2O_3 were calculated from Figure 3 and reported in Table 2. From the amounts of CO consumed and of evolved N_2 and CO_2 it appears that the reduction of the stored NO_x roughly obeys the stoichiometry of reaction (2):

$$2\ KNO_3 + 5\ CO \rightarrow N_2 + K_2CO_3 + 4\ CO_2 \qquad (2)$$

reagent and product species (moles/g_{cat})	O_2 admission (t = -1000 s)	CO admission (t = 4114 - 5770 s)	CO shutoff (t = 5770 - 6600 s)
CO consumed	-	$16.2\ 10^{-4}$	-
CO_2 formed	-	$13.9\ 10^{-4}$	$0.334\ 10^{-4}$
N_2 formed	$0.035\ 10^{-4}$	$2.61\ 10^{-4}$	$0.024\ 10^{-4}$
NO formed	-	$0.09\ 10^{-4}$	-
NH_3 formed	-	-	-

Table 2. Moles/g_{cat} of CO consumed and of different products formed during CO-ISC carried out at 300 °C over Pt-K/Al_2O_3 (NO_x stored at 300°C in NO/O_2 are $5.41\ 10^{-4}$ moles/g_{cat})

Besides, the N-balance is almost satisfied, thus suggesting that almost all the stored NO_x have been removed by CO. As a matter of fact, FT-IR results pointed out that only small amount of N-containing species remains onto the catalyst surface after reduction with CO (see below), but this is within the experimental error of our experiments.

The interaction of CO with the NO_x species stored on Pt-K/Al_2O_3 catalyst in isothermal condition followed by FT-IR spectroscopy and obtained at 280°C and 350°C is presented in Figure 4 A and 4B, respectively. In Figure 4A curve a is the spectrum of NO_x species previously stored at 350°C, whereas curves b-i correspond to the spectra recorded during interaction with CO at increasing exposure times at 280°C. As expected on the basis of the results obtained at increasing temperature, the reduction of bidentate nitrates starts before (after 30 seconds, Fig. 4A, curve b, bands at 1550, 1314, 1006 cm^{-1}) than the reduction of ionic ones (after 1 min., Fig. 4A, curve c, band at 1375, 1033 cm^{-1}). At 280°C the reaction evolves slowly and it is not completed even after 2 hours (Fig. 4A, curve i). This can be evinced by the linear intensity of the carbonate band at 1320 cm^{-1} formed during the reduction: it should be almost the same of that of the band at 1604 cm^{-1} (as evidenced in the experiment at increasing temperature, Fig. 2B), but this is not the case, revealing the contribution of residual ionic nitrates under the band at 1320 cm^{-1}. NCO species formed are practically only those responsible of the absorption at 2225 cm^{-1}. Furthermore, also in this kind of FT-IR experiments it is possible to observe the presence of bands in the region 2090-1880 cm^{-1} related to the presence of carbonyls onto reduced Pt sites.

In Figure 4B curve a is the spectrum of NO_x species previously stored at 350°C, while curves b-f correspond to the spectra recorded during CO interaction at increasing exposure times at 350°C. The reduction of nitrates is very fast since the band intensities of both bidentate and ionic nitrate are reduced markedly after 30 s of CO contact, even more after 1 min. of contact (Fig. 4B, curve c). Their consumption is complete after 4 min. (Fig. 4B, curve f), even if already at 2 min. of contact their amounts are really low, being revealed by a very weak shoulder on the high wavenumber side of the carbonate band at 1320 cm^{-1}.

Simultaneously to the nitrate reduction, the carbonate species appear, due to the adsorption of CO_2 produced during the reduction, along with NCO species (bands at 2225, 2163 cm^{-1}).

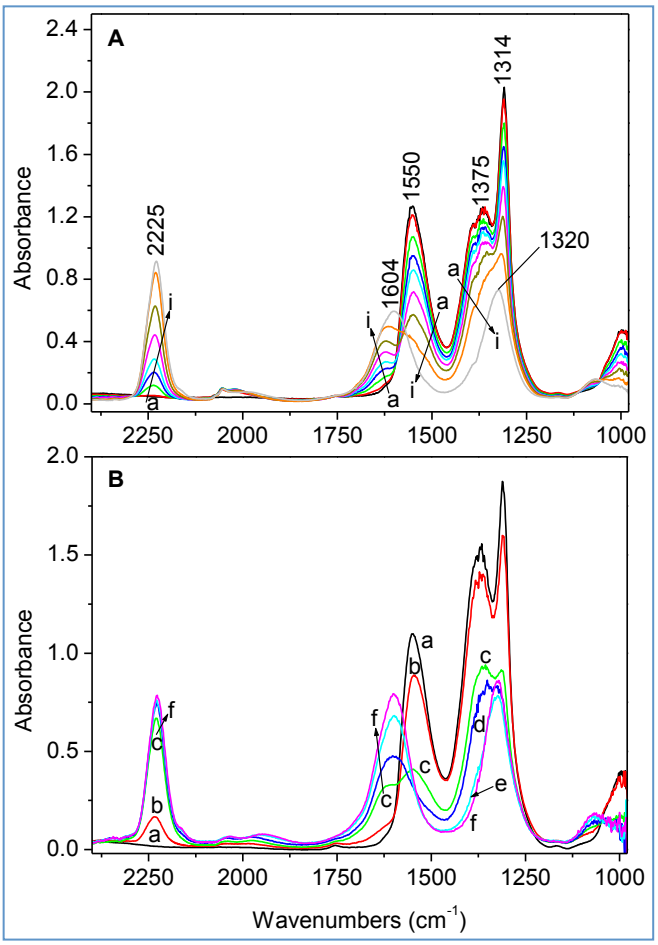

Figure 4 - A) FT-IR spectra of NO_x reduction in CO (10 mbar) at 280°C at increasing exposure time over the Pt-K/Al_2O_3 catalyst. Curve a, spectrum of NO_x stored at 350 °C by NO/O_2 adsorption; curves b-i, spectra after reduction at 280°C for 30 sec, 1 min, 2 min, 4 min, 8 min, 15 min, 30 min and 2h, respectively. B) FT-IR spectra of NO_x reduction in CO (10 mbar) at 350°C at increasing exposure time over the Pt-K/Al_2O_3 catalyst. Curve a, spectrum of NO_x stored at 350 °C by NO/O_2 adsorption; curves b-f, spectra after reduction for 15 sec, 30 sec, 1 min, 2 min and 4 min, respectively.

As observed for FT-IR experiment at increasing temperature, also isothermal measurements confirm that onto Pt-K/Al_2O_3 catalyst after NO_x reduction in CO, only small amounts of nitrogen are still present on the surface as isocyanate species. Indeed, isocyanate species formed on Pt-K/Al_2O_3 catalyst at 350°C (at 280°C the reduction is not complete) are in very low amounts if compared with those formed in the same condition by reduction with CO of NO_x stored on the Pt-Ba/Al_2O_3 catalyst [21]. As already performed for experiments at increasing temperature, it is possible to coarsely evaluate the integrated intensities of absorption bands related to NCO, or the ratio between the integrated intensities of NCO band (in the range 2330-2080 cm^{-1}) and of CO_3^{2-} absorptions (in the range 1800-1160 cm^{-1}), taking into account the same assumptions already mentioned. Whatever of the two methods of calculation is employed, the result is that the quantity of isocyanates on Pt-K system is roughly 4 times lower than that on Pt-Ba/Al_2O_3 catalyst. CO-ISC data performed on Pt-Ba/Al_2O_3 catalyst [21] showed that 58% of the stored nitrates is reduced to

gaseous N-containing products and consequently 42% of nitrogen remains on the surface as isocyanates. On this basis, we can estimate that about 10% of nitrogen, stored in form of nitrates, remains on the surface as NCO species for Pt-K/Al_2O_3.

At the end of the FT-IR reduction experiment at 350°C, the thermal stability of NCO species was also investigated by FT-IR analysis, and results are shown in Figure 5A. The prolonged outgassing at 350°C and 400°C (Figure 5A) indicates that NCO species are very stable at these temperatures; notably, on the basis of the integrated intensity of the band at 2225 cm^{-1}, 57% of the NCO species is still present after 2h of outgassing at 350°C (Fig. 5A, curve d) and 39% after 1h of outgassing at 400°C (curve e). It is also possible to evaluate the carbonate thermal stability (bands at 1600, 1320, 1064 cm^{-1}), which results lower than that of isocyanates: 31% of carbonates remains on the surface after 2h of outgassing at 350°C (Fig. 5A, curve d) and 24% after 1h of outgassing at 400°C (curve e).

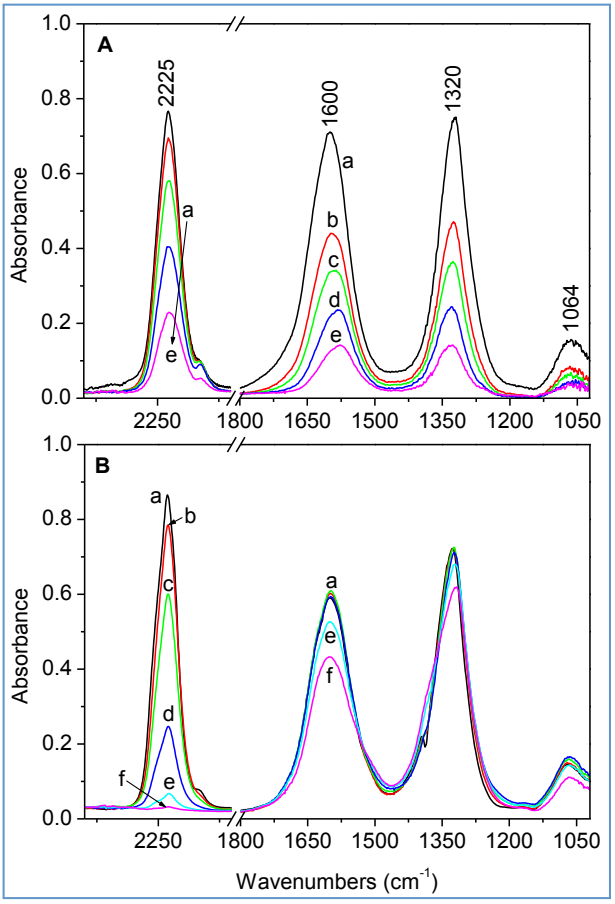

Figure 5 - A) FT-IR investigation of the thermal stability of NCO species under evacuation at 350°C and 400°C. Curve a, spectrum of NCO species formed in CO at 350°C; curves b-d, spectra after evacuation at 350°C for 10 min, 30 min and 2h, respectively; curve e, spectrum after evacuation at 400°C for 1h. B) FT-IR investigation on the reactivity of NCO species toward oxygen. Curve a, spectrum of NCO species formed at 350°C and cooled down to RT; curves b-f, spectra during treatment in O_2 (10 mbar) at 240, 280, 320, 360 and 400°C, respectively (heating at 10°C/min, spectrum recording each 2 min).

Oxidation measurements of NCO species were also performed after NO_x reduction in CO at 280°C (Figure 5B): after reduction, the sample was outgassed at 350°C and then cooled down at 100°C (Fig. 5B, curve a). Then oxygen was admitted at 100°C: the sample was heated in O_2 at 10°C/min and the spectra were run at intervals of 2 min up to 400°C. The isocyanates are not perturbed in the range 100-240°C (not reported). Their erosion starts at 240°C (curve b) and it is complete only at 400°C (curve f). This justifies N_2 evolution in the ISC experiment, when oxygen is admitted after a reduction step in CO.

Mechanistic aspects - The results collected during CO-TPSR over K/Al_2O_3 (Figure 1A) and over Pt-K/Al_2O_3 (Figure 2A) highlight that in the presence of Pt the reduction of nitrate species by CO is faster considering that the onset temperature of the reaction is lower (~ 210°C vs 340°C), and the conversion of CO is higher. Besides, it appears that the reduction does not require as first step the thermal release of NO_x in the gas phase since the reaction is seen at temperatures well below that of the thermal decomposition of adsorbed NO_x (340°C).

The results collected during CO-ISC experiment over Pt-K/Al_2O_3 (Figure 3) are in line with the results of CO-TPSR experiments and further indicate that the reduction at 300°C by CO of NO_x stored onto the Pt-K/Al_2O_3 catalyst is very fast and controlled by the concentration of CO. It is possible to conclude that the reduction by CO under nearly isothermal conditions of nitrates stored onto Pt-K/Al_2O_3 catalyst at high temperature (i.e. 300°C) occurs according to a Pt catalyzed surface pathway. As it is apparent from Figure 3, this catalytic route of nitrates reduction by CO leads mainly to nitrogen and CO_2 in the gas phase.

It is worth noticing that a low temperature Pt-catalyzed surface pathway has already been demonstrated for the reduction by H_2 of NO_x stored over the same catalyst used in this study [20], leading mostly to nitrogen; hydrogen is more effective than CO since the onset temperature of the reduction is lower (120°C vs. 210°C). The same conclusions apply to a Pt-Ba/Al_2O_3 catalyst used in previous works [15,21] and this suggests that the reduction of stored NO_x with H_2 and with CO over LNT catalysts might present analogies that are worth to be investigated.

The results of CO-TPSR and CO-ISC experiments over Pt-K/Al_2O_3 (Figure 2A and 3) and of the complementary FT-IR study (Figure 2B and 4) indicate that the reduction by CO of nitrates stored onto the Pt-K/Al_2O_3 catalyst occurs under dry conditions according to the stoichiometry of the following overall reactions:

$$2\ KNO_3 + 5\ CO \rightarrow K_2CO_3 + N_2 + 4\ CO_2 \qquad (2)$$

$$2\ KNO_3 + 8\ CO \rightarrow 2\ KNCO + 6\ CO_2 \qquad (3)$$

Reactions (2) and (3) account for the consumption of CO and of nitrates, and for the formation of CO_2. In particular, reaction (3) accounts for the consumption of nitrates with formation of isocyanates (revealed by

FT-IR) and CO_2; reaction (2) accounts for the formation of N_2, CO_2 and carbonates at the catalyst surface, as revealed by FT-IR. The formation of isocyanates and carbonates at the surface explains the fact that the N balance and the C balance in the gas phase do not close at the end of CO-TPSR experiment. In particular, reaction (2) does not occur in the low temperature range (210-250°C) where N_2 is not detected.

FT-IR spectra reveal also that bidentate nitrates stored onto the catalytic surface are reduced at first and ionic ones start to be reduced later on, resulting more resistant to the CO reduction. Similar results have been obtained when H_2 was used as a reductant instead of CO [19,20]; also in that case, FT-IR measurements put in evidence a different reactivity between ionic and bidentate nitrates towards H_2. These features well agree with TPSR data where two contribution of reductant (H_2 and/or CO) consumption are apparent.

The data herein discussed are consistent with the reaction pathway already proposed for N_2 formation in the case of Pt-Ba/Al_2O_3 [21,28]. In that case ISC, TPSR and FT-IR results have demonstrated that large amounts of NCO species are left at the catalyst surface after reduction of CO under dry conditions; these species can be oxidized to give N_2 during the subsequent lean phase either by oxygen or by NO+O_2, NO_2, surface nitrites and/or surface nitrates. N_2 is formed primarily according to an in series two steps process where NCO species are formed first and then are converted to nitrogen upon reaction with NO_x stored species. In analogy with the reaction pathway for the reduction by CO of nitrates stored over Pt-Ba/Al_2O_3 under dry conditions, the reduction by CO of nitrates stored onto the Pt-K/Al_2O_3 catalyst occurs according to the stoichiometry of the following overall reactions:

$$2\ KNO_3 + 8\ CO \rightarrow 2\ KNCO + 6\ CO_2 \qquad (3)$$

$$6\ KNO_3 + 10\ KNCO \rightarrow 8\ N_2 + 8\ K_2CO_3 + 2\ CO_2 \qquad (5)$$

Hence NCO species are considered intermediates in the formation of N_2, whose formation occurs exclusively according to the stoichiometry of the reactions (3) + (5) (the sum giving the overall reaction (2)).

Besides, analogies could be found for both the catalytic systems also with the reduction of stored nitrates by H_2, where an in series 2-steps molecular pathway has been proposed for N_2 formation involving at first the formation of ammonia upon reaction of nitrates with H_2, followed by the reaction of the so-formed ammonia with the residual stored nitrates leading to the formation of N_2 [15,16,19,20]. The following overall reactions are involved:

$$2\ KNO_3 + 8\ H_2 \rightarrow 2\ NH_3 + KOH + 4\ H_2O \qquad (6)$$

$$6\ KNO_3 + 10\ NH_3 \rightarrow 8\ N_2 + 6\ KOH + 12\ H_2O \qquad (7)$$

In the case of reduction by CO, NCO ad-species play as intermediate in the reduction instead of NH_3.

The reduction by CO of NO_x stored over Ba- and K-containing catalyst shows slightly distinct features. Over Pt-Ba/Al_2O_3 only ionic nitrates were observed, giving during the CO reduction two FT-IR bands at 2222 and 2164 cm^{-1} related to NCO species, whereas both bidentate and ionic nitrates are present on Pt-K/Al_2O_3 and mainly the band at 2225 cm^{-1} is detected.

The CO-TPSR experiment over Pt-Ba/Al_2O_3 has shown [21,28] that the reaction of surface nitrates to give nitrogen (analogous of reaction (2)) is slower than that responsible for the initial reduction of nitrates to give NCO species (analogous of reaction (3)). The formation of nitrogen in this case via the reduction of nitrates by CO is explained as the sum of the reduction of nitrates by CO to give surface NCO species (analogous of reaction (3)) and the subsequent oxidation of these species by surface nitrates to give nitrogen (analogous of reaction (5)).

Also in the case of Pt-K/Al_2O_3 the reaction of surface nitrates to give nitrogen seems to be slower than that responsible for NCO species formation. In fact, the formation of nitrogen is observed only above 250°C while evidence for the formation of N-containing species from 210°C is provided by the consumption of CO and by the simultaneous evolution in the gas phase of CO_2 with no N-containing species. Accordingly, FT-IR measurement shows that isocyanates are formed and their storage on the surface is higher in the low temperature range. However, in this case the reaction between surface nitrates and surface NCO species to give nitrogen is faster and more efficient than over Ba-containing system. Accordingly, at the end of the CO-ISC experiments both the C and N balances close in the case of K-containing catalyst (300°C) but not over Pt-Ba/Al_2O_3 (350°C).

The reason for the higher NO_x reduction efficiency to N_2 pointed out by the Pt-K/Al_2O_3 catalyst may be related to the higher mobility of the adsorbed surface species. It has been speculated that the reduction of the stored NO_x implies the surface mobility of these species towards Pt, where they are reduced by the reductant [21]. In the case of CO as reductant, isocyanate species are formed as intermediates. In the suggested pathway of the reduction of stored NO_x by CO, the rate determining step is the slow reaction between nitrates and isocyanates (reaction (5)) which involves two surface species; hence the surface mobility of the species is expected to play a major role on the reaction. It is known that K-nitrates have a melting point lower than of Ba-nitrates (334°C vs. 592°C). Along this line, K-nitrates might have a higher surface mobility that facilitate their spillover from the K component onto the Pt particles and as consequence their reaction with K-NCO species. As result, the CO reduction is more efficient over Pt-K/Al_2O_3 catalyst than over Pt-Ba/Al_2O_3 catalyst.

CONCLUSIONS

In this paper the reactivity of NO_x stored at 350°C onto Pt-K/Al_2O_3 LNT catalyst in the reduction by CO under dry conditions was investigated by means of transient experiments (CO-TPSR and isothermal CO-ISC) and complementary FTIR study.

It was shown that the reduction by CO of nitrates stored onto Pt-K/Al_2O_3 at high temperature under nearly isothermal conditions occurs through a Pt catalyzed surface pathway, which does not involve the thermal decomposition of stored NO_x with release of NO_x in the gas phase and leads mainly to

nitrogen and CO_2. The reaction scheme already proposed in the case of Pt-Ba/Al_2O_3 catalyst operates also in the case of Pt-K/Al_2O_3 system and implies the formation of surface isocyanate species at first and in the second step the reaction of these superficial species with residual nitrates to give nitrogen. Over Pt-K/Al_2O_3 system this last surface reaction is more efficient than over the Ba-containing catalyst, so at the end of the reduction the amount of isocyanates species present on the surface is lower for Pt-K/Al_2O_3 then Pt-Ba/Al_2O_3 catalyst. A different mobility of the surface species involved in these reactions is invoked, having K-containing species higher mobility than Ba ones.

References

[1] Takahashi, N.; Shinjoh, H.; Iijima, T.; Suzuki, T.; Yamazaki, K.; Yokota, K.; Suzuki, H.; Miyoshi, N.; Matsumoto, S.; Tanizawa, T.; Tanaka, T.; Tateishi, S.; Kasahara, K.; *Catal. Today* **1996**, *27,* 63-69

[2] Epling, W.S.; Campbell, L.E.; Yezerets, A.; Currier, N.W.; Parks, J.E. *Catal. Rev. – Sci. Eng.* **2004**, *46,* 163-245

[3] Shinojh, H.; Takahashi, N.; Yokota, K.; Sugiura, M. *Appl. Catal. B: Environ.* **1998**, *15,* 189-201

[4] Takeuchi, M.; Matsumoto, S.I. *Top. Catal.* **2004**, *28,* 151-156

[5] Konsolakis, M.; Yentekakis, I.V. *Appl. Catal. B: Environ.* **2001**, *29,* 103-113

[6] Mahzoul, H.; Brilhac, J.F.; Gilot, P. *Appl. Catal. B: Environ.* **1999**, *20,* 47-55

[7] Prinetto, F.; Ghiotti, G.; Nova, I.; Lietti, L.; Tronconi, E.; Forzatti, P. *J. Phys. Chem. B* **2001**, *105,* 12732-12745

[8] Lietti, L.; Forzatti, P.; Nova, I.; Tronconi, E. *J. Catal.* **2001**, *204,* 175-191

[9] Nova, I.; Castoldi, L.; Prinetto, F.; Ghiotti, G.; Lietti, L.; Tronconi, E.; Forzatti, P. *J. Catal.* **2004**, *222,* 377-388

[10] Poulston, S.; Rajaram, R. *Catal. Today* **2003**, *81,* 603-610

[11] Liu, Z.; Anderson, A. *J. Catal.* **2004**, *228,* 243-253

[12] Jozsa, P.; Jobson, E.; Larsson, M. *Top. Catal.* **2004**, *30,* 177-180

[13] James, D.; Fourre, E.; Ishii, M. *Appl. Catal. B: Environ.* **2003**, *45,* 147-159

[14] Abdulhamid, H.; Fridell, E.; Skoglundh, M. *Top. Catal.* **2004**, *30,* 161-168

[15] Lietti, L.; Nova, I.; Forzatti, P. *J. Catal.* **2008**, *257,* 270-282

[16] Nova, I.; Lietti, L.; Forzatti, P. *Catal. Today* **2008**, *136,* 128-135

[17] Forzatti, P.; Lietti, L.; Nova, I. *Energ. Env. Sc,* **2008**, *1,* 236-247

[18] Nova, I.; Lietti, L.; Castoldi, L.; Tronconi, E.; Forzatti, P. *J. Catal.* **2006**, *239,* 244-254

[19] Castoldi, L.; Lietti, L.; Nova, I.; Matarrese, R.; Forzatti, P.; Vindigni, F.; Morandi, S.; Prinetto, F.; Ghiotti, G. *Chem. Eng. J.* **2010**, *161,* 416-423

[20] Castoldi, L.; Lietti, L.; Forzatti, P.; Morandi, S.; Ghiotti, G.; Vindigni, F. *The NO_x storage-reduction on Pt-K/Al_2O_3 Lean NO_x Trap Catalyst, submitted to J. Catal.*

[21] Forzatti, P.; Lietti, L.; Nova, I.; Morandi, S.; Prinetto, F.; Ghiotti, G. *Reaction pathway of the reduction by CO under dry conditions of NOx species stored onto Pt-Ba/Al_2O_3 Lean NO_x Trap catalysts*, *J. Catal. in press* **2010** , doi:10.1016/j.jcat.2010.06.014

[22] Prinetto, F.; Manzoli, M.; Morandi, S.; Frola, F.; Ghiotti, G.; Castoldi, L.; Lietti, L.; Forzatti P. *J. Phys. Chem. C* **2010** *114,* 1127-1138

[23] Socrates, G. *Infrared Characteristic Group Frequencies*: John Wiley & Sons: Great Britain, 1980

[24] Szailer, T.; Kwak, J.H.; Kim, D.H.; Hanson, J.C.; Peden, C.H.F.; Szanyi, J. *J. Catal.* **2006**, *239*, 51-64

[25] Bion, N.; Saussey, J.; Haneda, M.; Daturi, M. *J. Catal.* **2003**, *217,* 47-58

[26] Bion, N.; Saussey, J.; Hedouin, C.; Seguelong, T.; Daturi, M. *Phys. Chem. Chem. Phys.* **2001**, *3,* 4811-4816

[27] Frola, F. *Ph. D. Thesis, University of Turin*, 2007

[28] Nova, I.; Lietti, L.; Forzatti, P.; Frola, F.; Prinetto, F.; Ghiotti, G. *Top. Catal.* **2009**, *52,* 1757-1761

[29] Frola, F.; Manzoli, M.; Prinetto, F.; Ghiotti, G.; Castoldi, L.; Lietti, L. *J. Phys. Chem. C* **2008,** *112,* 12869-12878

Paper VI

FT-IR study of the surface redox states on platinum-potassium-alumina catalysts

Tania Montanaria, Roberto Matarrese, Nancy Artioli, Guido Busca
Applied Catalysis B: Environmental 105 (2011) 15–23

Abstract

Pt-K/Al2O3 (Pt 1%; K 5.4% wt/wt) catalyst active for the simultaneous Diesel particulate oxidation and NOx reduction have been characterized in comparison with 1% Pt/Al_2O_3 catalyst. IR spectra of adsorbed CO at −140 °C and at room temperature allowed the detection of oxidized Pt centers and of their very strong oxidizing ability. TPD and IR spectra of adsorbed CO_2 allowed to characterize the basicity of the samples.

The data indicate that Pt centers lie in close proximity of potassium oxide species generating basicity.

1. Introduction

Platinum/alumina based catalysts are largely used in industry for several reactions, such as hydrogenations and dehydrogenations. As examples, Pt/Al_2O_3 is used in the BenSat process to hydrogenate benzene to cyclohexane in gasoline fractions [1], in the Oleflex light paraffin dehydrogenation technology and in the Pacol long linear paraffin dehydrogenation technology, all from UOP [2]. Such catalysts may also contain alkalis and additional activator metals, such as Sn [3]. Pt/Al_2O_3 based catalysts are also applied to reactions where water acts as a reactant, like for water gas shift reaction for fuel cell applications [4], and act as of promising catalysts for dry reforming of methane [5].

Platinum/alumina represents also an important system for catalytic oxidation, like the SELECTOXOTM process for the preferential oxidation of CO in the presence of hydrogen (PROX) [6]. For this reaction K is reported to act as a promoter of Pt/Al_2O_3 [7]. Pt/Al_2O_3 based catalysts containing also base metals are patented for ammonia selective oxidation (SCO) to N_2 [8], and are used as VOC catalytic oxidation catalysts [9]. For this reaction potassium may act as a promoter as well [10].

Generally speaking, alkali ions are frequently added as dopants at the surface of metal catalysts to introduce basicity or to reduce acidity, and in catalysis "assisted by basicity" [11]. Potassium is frequently preferred to sodium possibly because of its larger ionic size that limits reactivity towards supports and the formation of bulk salts, as well as results in higher basicity.

Pt-K/Al_2O_3 sorbents-catalysts, typically containing ~1 and 8%wt/wt of Pt and K have also been proposed for the "NOx storage reduction" (NSR) reaction, a recent technology developed by Toyota in the early nineties [12,13] to reduce the NOx content in the exhaust gases of lean-burn gasoline engines. A further evolution of this technology is the DPNR (Diesel particulate-NOx reduction) process, for the simultaneous NOx and soot removal [14,15]. This catalytic system works alternatively in oxidizing (lean burn) condition (where Pt is supposed to catalyze the oxidation of NO to NO_2, favouring NOx storage and soot combustion) and in reducing conditions (where Pt is supposed to catalyze the reduction of adsorbed NOx to N_2). Potassium acts as the sorbent for NOx storage [16].

While most characterization studies concern reduced noble metal catalysts, much less is known about Pt/Al_2O_3 in oxidized or unreduced state. According to some of us [17], the location of Pt species on the alumina surface is "selective", substituting or exchanging the OH sites located on tetrahedral Al species, giving rise to isolated oxidized Pt ions, while they only perturb the OHs located over octahedral Al species. Quite in contrast with this, Kwak et al. proposed that bulk-like PtO layers form at the surface of γ-Al_2O_3 by interacting with pentacoordinated Al^{3+} species [18].

The IR spectroscopy of low temperature adsorption of CO is today a very popular technique for the characterization of solid surfaces, both of metallic and of oxide nature [19,21]. This is because CO, if adsorbed at low temperature (350–423 °C), is a very good and gentle probe for surface hydroxy-groups, cationic and

metallic centers, with small or not surface perturbation nor reactivity. When dealing with noble-metal based oxidation catalysts, this technique allows the detection of oxidized ions, which is not always an easy matter [22,24].

In this paper we will summarize our data concerning IR spectroscopy of low temperature adsorption of CO on catalysts belonging to the Pt-K/Al_2O_3 system, with the aim to clarify the role of potassium in modifying the behavior of Pt/Al_2O_3 catalysts. This characterization study has been performed with and without previous reduction, just because Pt-K/Al_2O_3 catalysts work in oxidizing conditions when working as NOx traps as well as total oxidation catalysts, while they work in reducing conditions in the short step needed to reduce adsorbed NOx.

2. Experimental

Pt-K/Al_2O_3 catalyst (Pt: ~1 wt.%, K: 5.4 wt.%) was obtained by impregnation in two sequential steps of a commercial γ-Al_2O_3 carrier (Versal 250 from UOP, surface area of 200 m^2/g and pore volume near 1 cm^3/g), as follows: the γ-Al_2O_3 powder was at first impregnated with a solution of $Pt(NH_3)_2(NO_2)_2$ (Strem Chemicals, 5% Pt in ammonium hydroxide) with an appropriate concentration so as to yield 1 wt.% Pt metal loading. After drying in air for 12 h at 80 °C and calcination at 500 °C for 5 h, the sample was impregnated with CH_3COOK (Sigma Aldrich, 99%) solution so as to yield a K content equal to 5.4 wt.%. After that, the sample was dried for 12 h at 80 °C and then calcined at 500 °C for 5 h (sample denoted as prepared, a.p. in the following). For comparative purposes, two reference binary systems, Pt/Al_2O_3 (Pt: 1 wt.%) and K/Al_2O_3 (K: 5.4 wt.%), were also prepared using the same precursors and procedures. The Pt dispersion on samples activated by heating in vacuo and subsequently in dry oxygen at 1096 °C and finally reduced in H_2 at 896 °C was estimated by hydrogen chemisorption to be 64.8% on Pt/Al_2O_3 and 71.7% on Pt-K/Al_2O_3.

IR skeletal studies have been performed using KBr pressed disks. For IR adsorption studies, pressed disks of the pure catalysts powders were activated “in situ” by using an infrared cell connected to a conventional gas manipulation/outgassing ramp. All catalysts were first submitted to a treatment in oxygen (200 Torr) at 350 °C, for 1 h, followed by evacuation at the same temperature before the adsorption experiments. In order to obtain the reduced catalysts, after the mentioned evacuation, they were put in contact with a H_2 pressure (~400 Torr) at 350 °C, two cycles for 30 min, and successively outgassed at the same temperature. CO adsorption was performed at −140 ◦C by the introduction of a known dose of the gas (1 Torr) inside the low temperature infrared cell containing the previously activated wafers. IR spectra were collected evacuating at increasing temperatures between −140 °C and room temperature (r.t.). Spectra have been recorded in the same temperature range by a Nicolet Nexus FT instrument.

The thermal stability of carbonate species formed on K/Al_2O_3 and Pt–K/Al_2O_3 was analyzed by thermal decomposition in inert flow (temperature programmed desorption, TPD) in a flow-reactor apparatus

consisting of a quartz tube reactor (7mmi.d.) connected to a mass spectrometer (Omnistar 200, Pfeiffer Vacuum) and to a microGC (Agilent 3000A) for the on-line analysis of the outlet gases. For this purpose after CO2 adsorption (3000ppmv/v in flowing helium) at 100 °C the sample was then heated (10 °C/min) in He up to 500 °C. 60mg of catalyst was used in each run, and the total gas flow was always set at 100cm^3/min (at 0 °C and 1 atm). Before catalytic tests, the samples have been heated at 500 °C in He to remove any adsorbed species on the catalytic surface.

3. Results and discussion

3.1. Surface hydroxyl groups

The spectra of the pure powder pressed disks of both K/Al_2O_3 and Pt-K/Al_2O_3 samples before any activation treatment are very similar (see Fig. 1 for Pt-K/Al_2O_3) and show the strong bands of carbonate and hydroxide species with additional features at 3443, 3411, 1550, 1406, 997cm^{-1}. The absence of evident scissoring mode of water suggests that this species is essentially an hydroxycarbonate species. A similar spectrum was found previously for a 12% wt/wt K_2CO_3-Al_2O_3 catalyst [25]. Outgassing at 350 °C of both K/Al_2O_3 and Pt-K/Al_2O_3 samples causes the almost complete disappearance of these bands, suggesting that such species are decomposed with release of CO_2 and water. Both samples show, after activation at 350 °C, only weak bands in the region 1700–1200cm^{-1} (see Fig. 1 for Pt-K/Al_2O_3), due to surface impurities (carbonates and/or carboxylates).

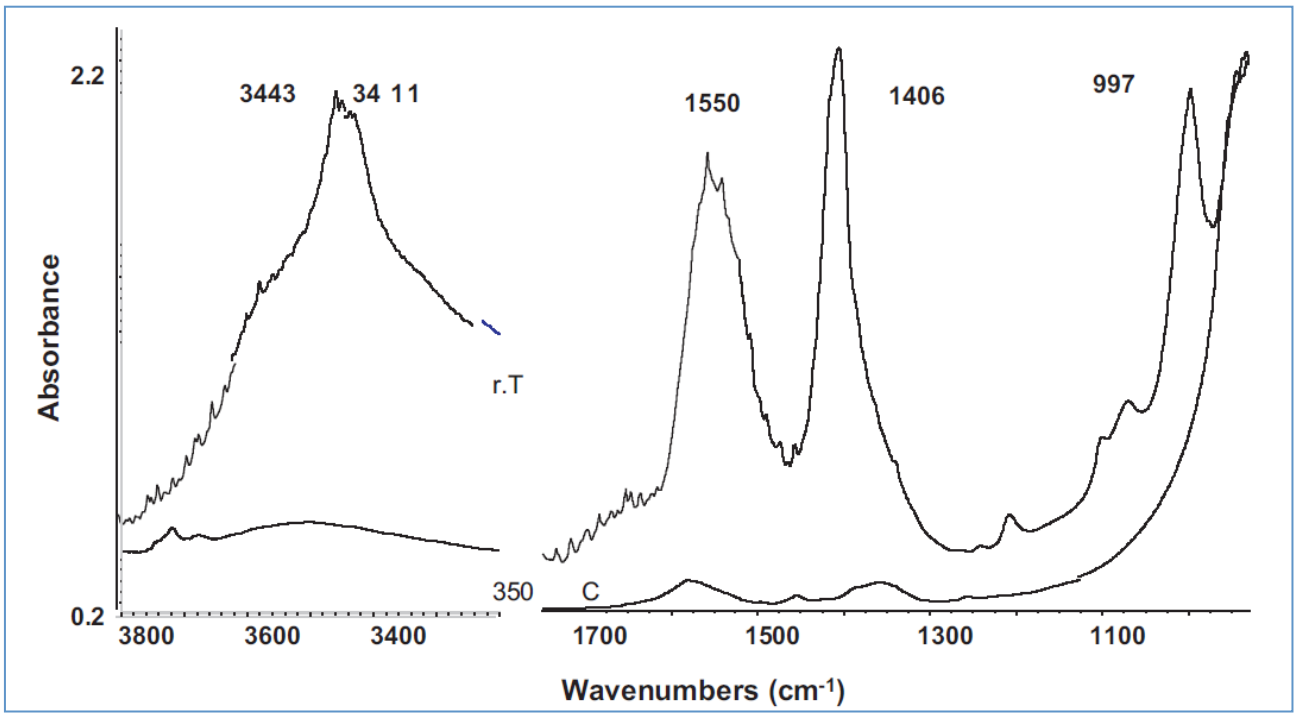

Fig. 1. FT-IR spectra of pure powder pressed disk of the Pt-K/Al_2O_3 sample after brief outgassing at r.t. and after activation at 350 ◦C.

As expected, all samples show bands in the region 3800–3400cm^{-1} (Fig. 2), due to OH stretchings of surface hydroxy groups. In the case of alumina support we find maxima at 3726, 3675 and 3575cm^{-1}, with additional shoulders at 3765cm^{-1} and near 3500cm^{-1}. This spectrum is quite typical for γ-Al_2O_3 samples outgassed at medium temperature. Our previous studies [26] suggested that the higher frequency component at 3765cm^{-1} is due to terminal hydroxy-groups bonded to Al ions in a tetrahedral-like environment, the splitting being associated to vacancies with respect to the spinel-type composition. The band at 3725cm^{-1}, instead, is present also at the surface of α-Al_2O_3 and of stoichiometric spinels, and is consequently likely due to terminal OHs on Al ions in octahedral-like environment. The additional components at 3675 and 3575cm^{-1} are assigned to bridging and triply bridging OHs, respectively.

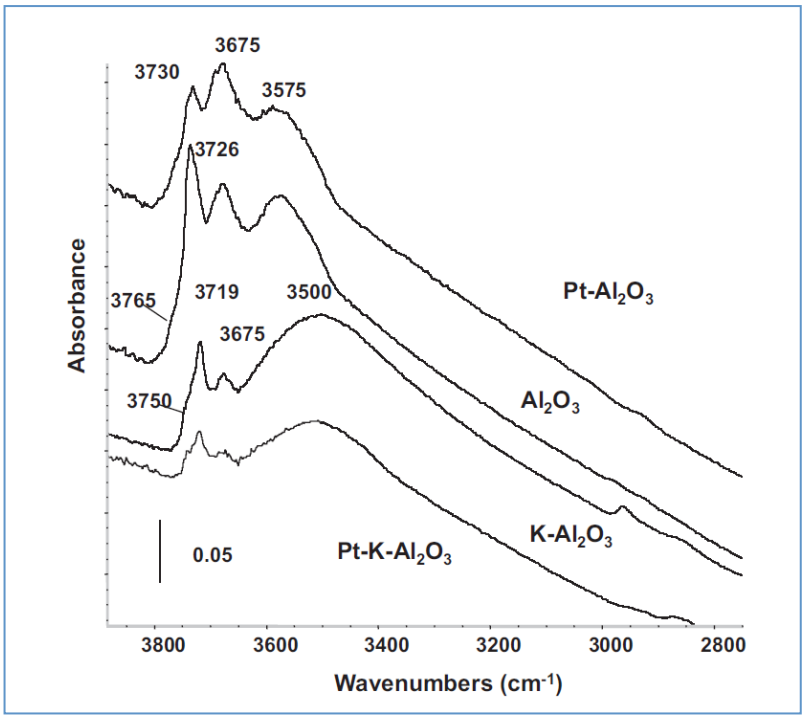

Fig. 2. FT-IR spectra of pure powder pressed disks of the catalysts after activation at 350 ◦C (OH stretching region).

The Pt/Al2O3 sample shows, in these conditions, a quite similar spectrum with respect to the support, but the intense band at 3725cm^{-1} on alumina is shifted a bit upwards and significantly weakened in intensity. A similar result was observed previously with respect to another Pt/Al_2O_3 catalyst [17]. The K/Al_2O_3 sample shows the lower frequency feature broadened and shifted to near 3500cm^{-1}, while all higher frequency features are definitely weaker than on the support. This is likely due to partial K^+ for H^+ cationic exchange. Here we find very sharp a band at 3719cm^{-1} with a shoulder at 3750cm^{-1}. The position of this band is similar to that reported previously for different K-Al_2O_3 samples (3715cm^{-1} [27]) and for a 12% wt/wt K_2CO_3-Al_2O_3 catalyst (3710cm^{-1} [25]). On titania, K doping causes the formation of a band at 3720–3712cm^{-1} [28]. The spectrum of the Pt-K/Al_2O_3 sample is very similar to that of K/Al_2O_3.

3.2. IR study of the adsorption of carbon monoxide

In Fig. 3 the spectra of carbon monoxide adsorbed on the support γ-Al_2O_3 (upper spectra, A–C) as well as on the K/Al_2O_3 (lower spectra, D–F) are reported and compared. In the left parts of the figure the spectra are recorded during adsorption after admission of CO into the cell, in the right section the spectra recorded during outgassing upon warming. At the highest coverages the main maximum on alumina is at 2153cm^{-1}. Looking at the OH stretching region (see the insert C in Fig. 3) it is evident that this band is associated to the H-bonding of CO with surface hydroxygroups. Upon this interaction, the band at 3725cm^{-1} is involved partially, being shifted in part to near 3600cm^{-1}. The component at 3675cm^{-1} seems almost not involved, being still evident. The shift of the OH stretching band is, consequently, in the range $\Delta\nu$OH ~125cm^{-1}, which allows to denote the alumina's OH as medium strength Brønsted acid sites. Thus the band at 2153cm^{-1} is attributed to CO H-bonded on the terminal hydroxy groups of alumina on Al ions in octahedral-like environment. In agreement with this assignment, this band disappears fast upon outgassing at low temperature.

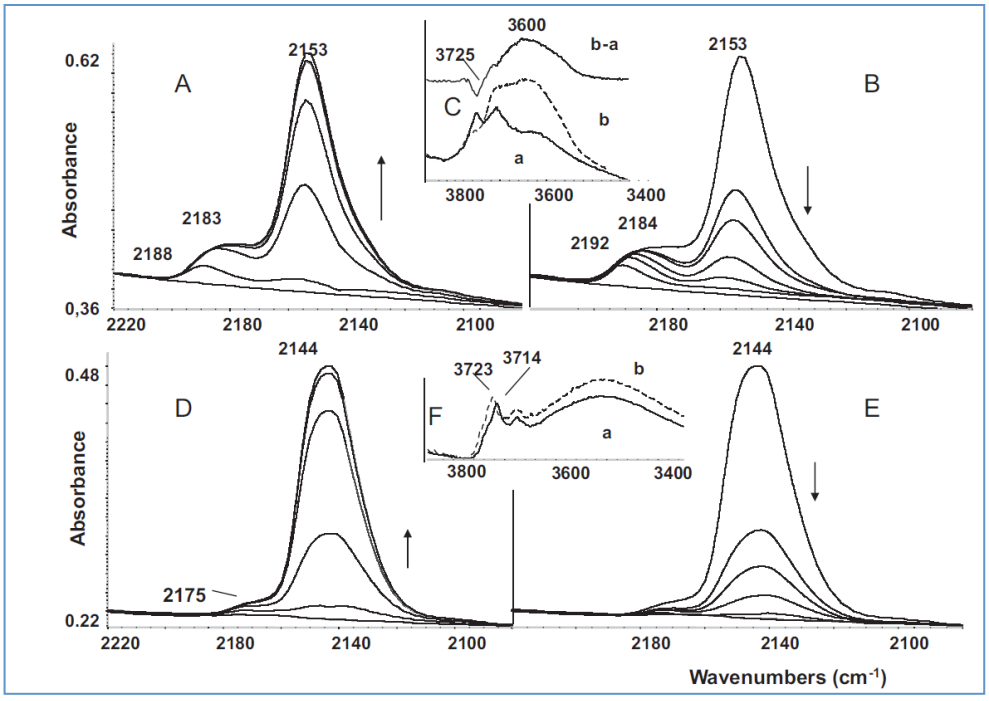

Fig. 3. FT-IR spectra of Al_2O_3 (A–C) and of K/Al_2O_3 (D–F) at −140 °C after admission of CO gas into the cell until saturation (A and D) and upon outgassing at increasing temperatures from −140 to −90 °C (B and E). In the inserts C and E: OH stretching region of the samples at −140 °C before (a) and after (b) saturation with CO, and the corresponding difference (after saturation−before saturation).

A weaker feature, more resistant to outgassing, is observed at higher frequencies, shifting from near 2180cm^{-1} to 2192cm^{-1} upon outgassing. It does not correspond to any perturbation of the νOH bands. It is assigned to CO species interacting with Lewis acidic Al^{3+} cations. The shift with respect to νCO of gas or liquid CO is relatively weak, and this shows that after outgassing at 350 ◦C the strongest Lewis sites of alumina are still not produced, being the surface still in a highly hydroxylated state.

In the low section of Fig. 3 the spectra of carbon monoxide adsorbed on sample K/Al_2O_3 are reported. At the highest coverages the main maximum is at 2144cm^{-1}, i.e. definitely lower than in the case of pure alumina. The height of the band is similar in the two cases. However, the shape of the band is different, being definitely broader for K/Al_2O_3. A deconvolution of this spectrum is shown in Fig. 4, where it is superimposed to the band observed on alumina. At least two components are evident in the deconvolution of the spectrum observed on K/Al_2O_3, located at 2149cm^{-1}, less intense, and at 2139cm−1, more intense. Looking at the OH stretching region (compare inserts C and d in Fig. 3) we note here that the spectrum is, in this region, less perturbed. The sharp band at 3714cm^{-1} is shifted up to 3723cm^{-1}, certainly due to a secondary interaction. No H-bonding with CO is found in this case. Our data support the assignment of this band to CO adsorbed on two different families of K^+ ions. In fact, the position of this band is at slightly lower frequency than that found on K-zeolites (2170–2150cm^{-1} [29]) where K ions are bonded to a less basic structure. Low temperature CO adsorption on $K_2O–TiO_2$ was reported previously to produce a band at 2148cm^{-1} [28]. At least two different families of potassium ions are formed, differing in their Lewis acidity.

The data reported here show that, over this heavily K-doped alumina, the surface hydroxy groups have totally lost their Brønsted acidity and K^+ ions display very weak Lewis acidity, although they appear to be well exposed at the surface. The weaker feature, more resistant to outgassing, found near 2175cm^{-1}, is assigned to CO species interacting with residual Lewis acidic Al^{3+} cations. The position of this band, shifted downwards with respect to pure alumina, and the intensity, definitely weaker than on pure alumina (compare Fig. 3, A and B, with Fig. 3, C and D, and see Fig. 4), show that potassium species cover the surface, mainly interacting with the strongest Lewis sites.

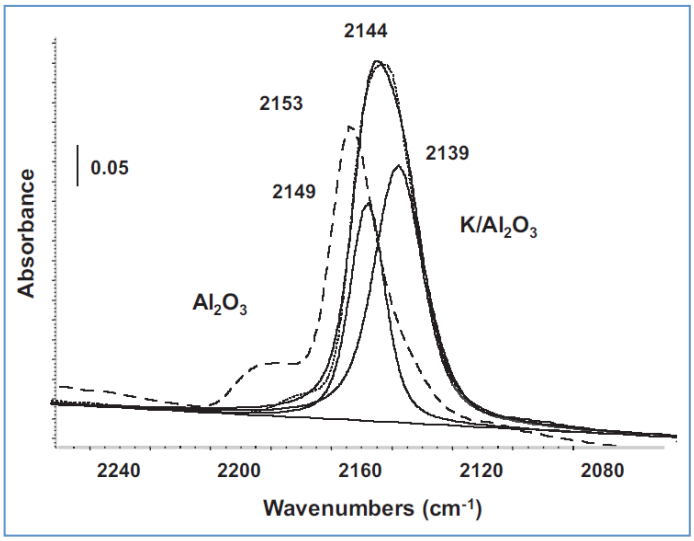

Fig. 4. FT-IR spectra of CO adsorbed (at saturation at −140 °C) on Al_2O_3 (dashed line), K/Al_2O_3 (pointed line), and the deconvolution of the spectrum recorded on K/Al_2O_3 (light full lines peak deconvolution; heavy full line sum).

Thus only part of weaker Lewis sites of alumina are residual, in small amounts. This result is quite similar to that reported previously for K-doped alumina using pyridine and nitrile as the probes [27].

In Fig. 5 the spectra of carbon monoxide adsorbed on the Pt/Al_2O_3 catalyst are reported. In the upper part of the figure (A) the spectra are recorded during adsorption after admission of CO into the cell, in the lower section (B) the spectra recorded during outgassing upon warming. At the highest coverages the main maximum is at 2158cm^{-1}, i.e. 5 cm^{-1} higher than on pure alumina. Looking at the OH stretching region (see the insert C in Fig. 5) it is evident that this band is associated to the H-bonding of CO with surface hydroxy-groups. Upon this interaction, the band at 3735cm^{-1} is involved partially, being shifted in part to near 3600cm^{-1}. Actually, we find two unresolved components at 3610 and 3540cm^{-1}.

The component at 3675cm^{-1} seems again almost not involved, being still evident. The shift of the OH stretching band is, consequently, in the range $\Delta\nu$OH ~125–200cm^{-1}. In any case it seems that the Brønsted strength of alumina's OH is not much perturbed by addition of Pt, being perhaps a little strengthened, in agreement also to the slight shift up of the corresponding *ν*CO.

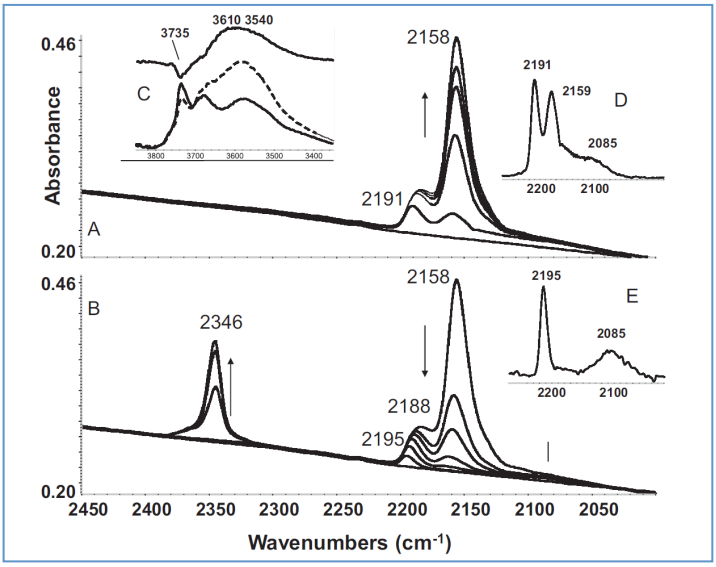

Fig. 5. FT-IR spectra of unreduced Pt/Al_2O_3 at−140 °C after admission of CO gas into the cell until saturation (A) and upon outgassing at increasing temperatures from −140 to −90 °C (B). In the inserts: (C) OH stretching region of unreduced Pt/Al_2O_3 at −140 °C before and after saturation with CO, and the corresponding difference (after saturation−before saturation); (D) the spectrum of CO adsorbed just after admission (lowest coverage); (E) the spectrum of residual CO adsorbed after outgassing at −90 °C.

On the other hand, a weak tail at lower frequency is observed on the spectrum recorded during adsorption, which is more clearly evident upon desorption as a single band centred at 2085cm^{-1}. This absorption is typical for terminal carbonyls on Pt◦ particles whose average size is of the order of few nanometers [30].Uponoutgassing and warming, a band also grows at 2346cm^{-1}, due to OCO asymmetric stretching of adsorbed CO_2. This reactivity is not found on pure alumina. This shows that unreduced Pt centers exist and are able to oxidize CO to CO_2. Quite obviously, the second oxygen atom comes from the oxide species balancing Pt cations.

Also on Pt/Al_2O_3 a band more resistant to outgassing is observed at higher frequencies, shifting from near 2188cm^{-1} to 2195cm^{-1} upon outgassing. This absorption is in the region of bands typically assigned to CO species interacting with Lewis acidic Al^{3+} cations.

The same experiment has been performed with pre-reduced Pt/Al_2O_3, as shown in Fig. 6. In this case the main band is in the same position than on pure alumina (2153cm^{-1}). The formation of CO_2 is much lower, confirming that our mild reduction pre-treatment reduced a large part of cationic Pt. The carbonyls on zerovalent Pt are evident but the maximum is at a definitely higher frequency (2098cm^{-1}), suggesting that larger metal particles are formed by reduction. However, the band is large with components at lower frequency suggesting a large distribution of particle size. On the other hand, in agreement with the well-known preference of CO adsorbed over metallic Pt for on-top position, due to electronic factors [31], we do not find evidence of bands of bridging species, in fact usually not observed or extremely small in low loading Pt- Al_2O_3 [30,32].

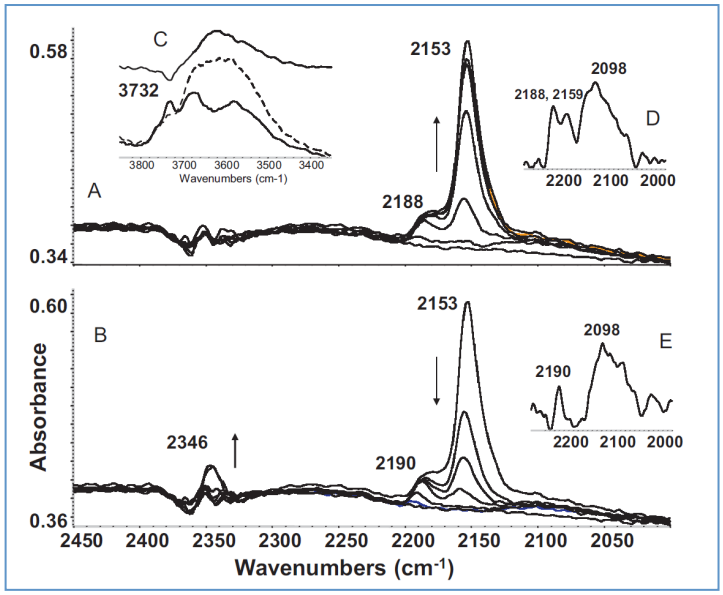

Fig. 6. FT-IR spectra of prereduced Pt/Al_2O_3 at −140 °C after admission of CO gas into the cell until saturation (A) and upon outgassing at increasing temperatures from −140 to −90 °C (B). In the inserts: (C) OH stretching region of prereduced Pt/Al_2O_3 at −140 °C before and after saturation with CO, and the corresponding difference (after saturation−before saturation); (D) the spectrum of CO adsorbed just after admission (lowest coverage); (E) the spectrum of residual CO adsorbed after outgassing at −90 °C.

In Fig. 7 the spectra of CO adsorbed on Al_2O_3, unreduced Pt/Al_2O_3 and reduced Pt/Al_2O_3 and their deconvolutions are reported. The deconvolution of the spectrum of CO adsorbed on alumina allows to only separate the component due to CO interacting with Al^{3+}, found at 2183cm^{-1}, from that due to CO H-bonded on OHs, found at 2152cm^{-1}. In the case of the spectrum of CO adsorbed on unreduced Pt/Al_2O_3 the higher frequency band increases in intensity and shifts up to 2186cm^{-1}, the most intense band shifts up a little bit to 2155cm^{-1} while a new absorption appears clearly centered at 2135cm^{-1}. In the case of reduced Pt/Al_2O_3

the higher frequency band shifts back down to 2183cm^{-1} and decreases in intensity, the most intense band shifts also back to 2153cm^{-1}, while the new absorption increases in intensity and shifts up to 2139cm^{-1}.

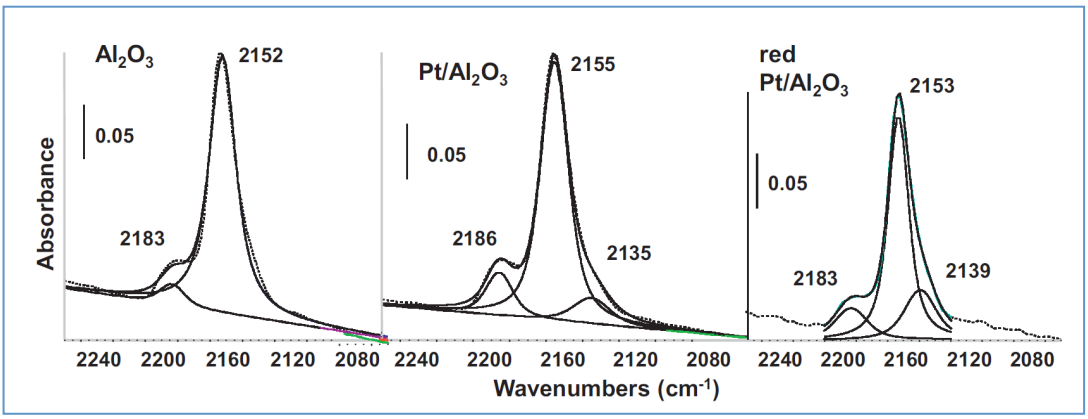

Fig. 7. FT-IR spectra of CO adsorbed on Al_2O_3, on unreduced and prereduced Pt/Al_2O_3 at −140 °C at saturation (pointed lines), and deconvolution of the spectra.

These data suggest that highly oxidized and oxidizing Pt ions contribute to the band at 2186cm^{-1}, and are reduced in the reduced sample. We assign the band at 2186cm^{-1} predominantly to Pt^{n+}–CO (with n = 4 or 2). The band at 2135–2139cm^{-1} should be assigned to another form of Pt^{n+}–CO, less oxidized and less oxidant, with n = 2 or 1. The amount of the latter species should increase by reduction of the former one. These assignments are consistent with data arising from different authors (reviewed in Ref. [20]) as well as with a previous study from one of our laboratories [17].

In Figs. 8 and 9 the spectra of carbon monoxide adsorbed on the Pt-K/Al_2O_3 catalyst unreduced and reduced, respectively, are reported. At the highest coverage the spectrum is dominated by the band assigned to carbonyl species on K^+ centers. In this case, as for the experiment done with K/Al_2O_3, this band is evidently split into two partially resolved components, as shown by the deconvolutions reported in Fig. 4, located at 2149–2150 and near 2139–2140cm^{-1}. It seems that the intensity of the higher frequency components increases for the unreduced Pt-K/Al_2O_3 sample with respect to K/Al_2O_3, but decreases back for reduced Pt-K/Al_2O_3. Maybe carbonyls of cationic Pt may contribute to the higher frequency component here. In any case the quality of the two K^+ sites is fully unchanged as an effect of the presence of small amounts of platinum. Also in these cases, like for K/Al_2O_3, the adsorption of CO does not result in any direct interaction with surface OHs. In fact the only perturbation of the OH stretching band consists in a very slight shift up of the band observed at 3719cm^{-1}. This confirms that, at these high K loading levels, surface OHs exist but do not show any Brønsted acidity.

The presence of reduced zerovalent Pt centers is evident on the unreduced Pt-K/Al_2O_3 sample, due to the presence of a broad band of carbonyl species at 2075–2065cm^{-1}. The lower frequency observed for these Pt^0 carbonyls with respect to those observed on Pt/Al_2O_3 is likely due to the effect of the increased basicity of the neighbouring [33]. On the other hand, reductions seem to give rise to better defined Pt particles, where CO adsorbs on-top producing a sharp maximum at 2072cm^{-1} with a tail at lower frequencies.

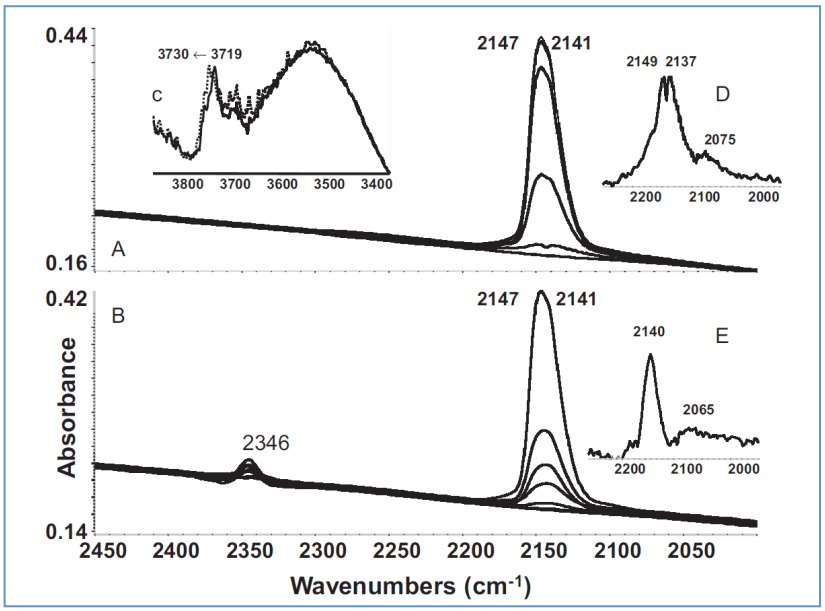

Fig. 8. FT-IR spectra of unreduced Pt-K/Al_2O_3 at −140 °C after admission of CO gas into the cell until saturation (A) and upon outgassing at increasing temperatures from −140 to −90 °C (B). In the inserts: (C) OH stretching region of unreduced Pt-K/Al_2O_3 at −140 °C before and after saturation with CO, and the corresponding difference (after saturation−before saturation); (D) the spectrum of CO adsorbed just after admission (lowest coverage); (E) the spectrum of residual CO adsorbed after outgassing at −90 °C.

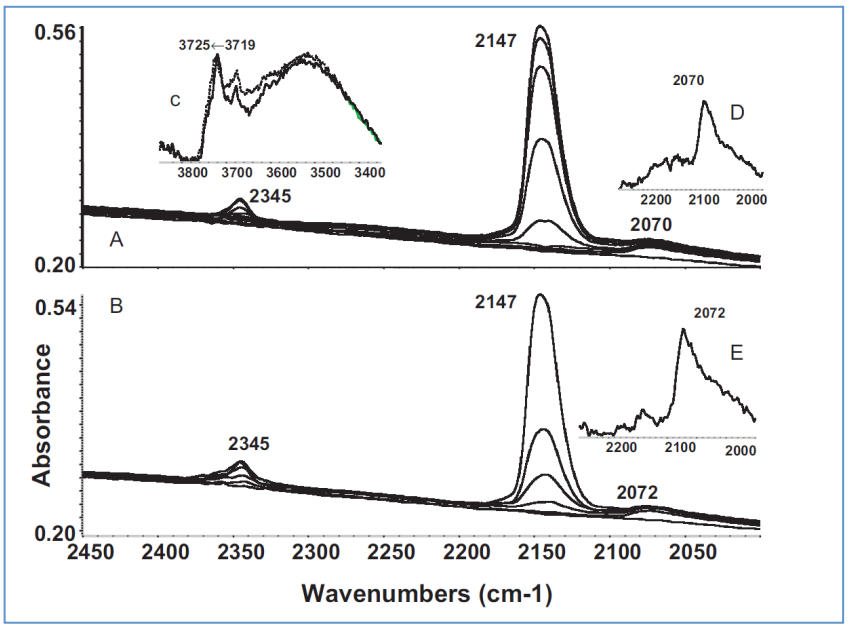

Fig. 9. FT-IR spectra of prereduced Pt-K/Al_2O_3 at −140 °C after admission of CO gas into the cell until saturation (A) and upon outgassing at increasing temperatures from −140 to −90 °C (B). In the inserts: (C) OH stretching region of prereduced Pt-K/Al2O3 at −140 °C before and after saturation with CO, and the corresponding difference (after saturation−before saturation); (D) the spectrum of CO adsorbed just after admission (lowest coverage); (E) the spectrum of residual CO adsorbed after outgassing at −90 °C.

In this experiment the oxidation of CO to CO_2 is more limited than on the K-free catalyst, but is not much affected by pre-reduction, suggesting that Pt is more reduced already in the unreduced sample. This may be associated to a higher reactivity of Pt cations as an effect of the presence of potassium, that

consequently reduces by decomposition already during outgassing at 350 °C. To reveal whether CO adsorption is able to detect unreduced Pt centers on Pt-K/Al_2O_3 sample, we analyzed the subtraction spectra of CO adsorbed on reduced and unreduced sample (Fig. 10) after outgassing at −130 °C. While the absorption of CO on metallic Pt is well evident only on the reduced sample, as expected indeed, and appears as a negative peak in the subtraction, in the higher frequency region a small peak at 2150cm^{-1} is evident as a positive peak, together with an even smaller feature near 2120cm^{-1}. It is possible that these very weak bands arise from Pt^{n+}–CO species over the unreduced sample, although a small perturbation of the K^+–CO band could also be responsible for them.

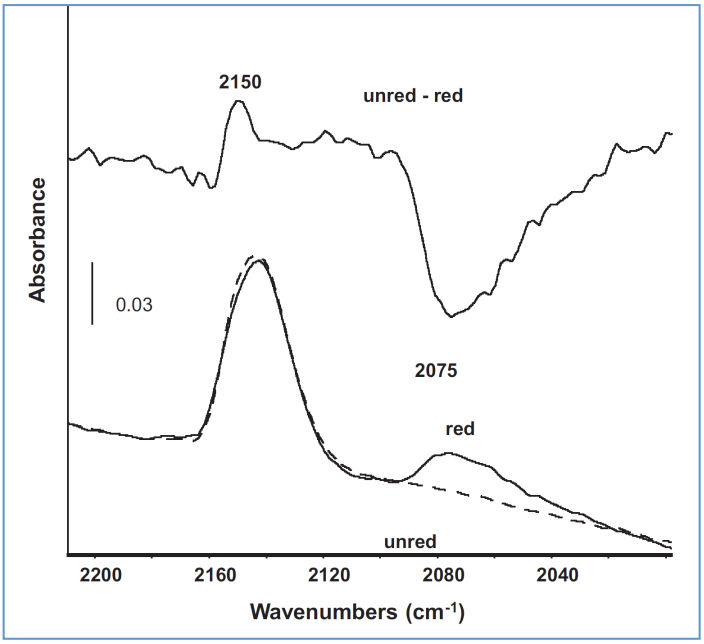

Fig. 10. FT-IR spectra of CO adsorbed on unreduced and pre-reduced Pt-K/Al_2O_3 at −140 °C at saturation, and subtraction of the spectra.

The spectra we report in Fig. 9 are well different with respect to those reported in the literature for CO adsorption on similar catalysts [34,36], which have, however, been recorded at r.t. To compare better with spectra reported in the literature, we also performed experiments of CO adsorption at room temperature. The spectrum obtained on reduced Pt-K/Al_2O_3 sample, after room temperature adsorption of CO and short room temperature outgassing is reported in Fig. 11a. The band due to CO interacting with K^+ ions as well as with Al^{3+} and Pt^{n+} ions (i.e. at νCO> 2100cm^{-1}) cannot be observed at r.t., as indeed expected to the weakness of these interactions which are only detectable at low temperature. However, a stronger band is observed in the field of terminal carbonyls on platinum, centred at 2056cm^{-1}, with a prominent shoulder centred at 2008cm^{-1}, while an additional band is found at 1800cm^{-1}, in the typical region of bridging carbonyls. Additionally, also very strong bands are observed at 1580 and 1332cm^{-1}, that should be assigned to carbonate ions, which are observed much weaker at low temperature, in parallel to the formation of CO_2. The spectrum we observe in these conditions is similar to those reported by other authors at room or

higher temperatures, on similar catalysts. Derrouiche et al. [34] with a 2.9% Pt-10%K-Al_2O_3 catalyst observe at room and higher temperatures bands at 2050, 1950 and 1763cm^{-1}, assigned to linear and bridging CO on Pt◦, and species adsorbed on a Pt-K site, respectively. Prinetto et al. [35,36] at room temperature find a similar spectrum, with a band in the region 2045–2015cm^{-1} assigned to on-top carbonyls on Pt°, a band at 1945–1955cm^{-1}, of uncertain assignment, and a third band at 1735–1690cm^{-1}, assigned to bridging carbonyls. In fact the experiments of CO adsorption at room or higher temperatures are affected by the reactivity of CO itself, that produces also relevant amounts of carbonate species and CO_2, and perhaps undetectable carbide species, that likely modify the state of the surface and may be also responsible for the band in the 1800–1700cm^{-1} region [37] previously assigned to bridging CO. Other works report that bridging carbonyls on Pt absorb in the 1950–1850cm^{-1} range on both low index faces [38] and on stepped surfaces [39]. In an early work [25] it has been reported that CO adsorption on 12% wt/wt K_2CO_3-Al_2O_3 catalyst does not give rise to any carbonyl formation but produces (in the absence of oxidizing agents) further carbonates, like observed here for Pt-K/Al_2O_3, confirming some kind of Boudouard-like reactivity.

Interestingly, upon outgassing at 100 ◦C (Fig. 11b) the bands of carbonate species even grow, likely due to the further oxidation of CO by unreduced Pt centers. The spectra of carbonate species are in similar (although not identical) positions as those observed upon adsorption of carbon dioxide over the same reduced surface (Fig. 11c).

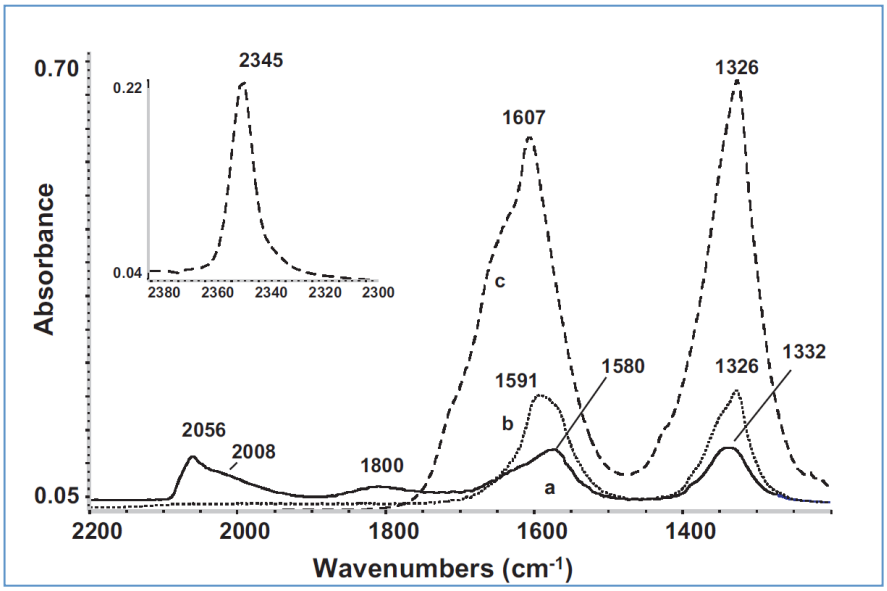

Fig. 11. FT-IR spectra of CO adsorbed on prereduced Pt-K/Al_2O_3 at r.t. (a) and after outgassing at 100 °C (b), and spectrum of CO_2 adsorbed on prereduced Pt-K/Al_2O_3 at r.t. (c).

Low temperature adsorption experiments allow the observation of weakly acidic but very active sites like K^+, not observed in room or higher temperature experiments, but also to avoid excessive reactivity of CO, finally giving a more precise picture of the state of the surface. However, room temperature experiments may perhaps provide evidence for some kind of “activated” adsorption phenomena, allowing several kinds

of different adsorption modes needing some energy to be allowed. The spectra observed after adsorption of CO on the Pt-K/Al_2O_3 catalyst, in analogy with those reported recently for Pt-Na/TiO_2 catalysts [40], show the shiftdown of the absorption due to terminal carbonyls and the increased formation of bridging species caused by the addition of potassium. This could be interpreted as a further evidence of the increased electrondonating character of Pt metal centers when potassium is copresent. However, the difference among the spectra recorded at low and room temperature is indicative of more complex interactions occurring at room temperature that need some activation energy to be established. We suggest the occurrence, only upon adsorption at sufficiently high temperatures (room and higher), of complex interactions similar to those occurring on some deeply cation exchanged alkali zeolites such as Na^-, K^- and Cs-ferrierite [41]. In this case, in addition of the normal C-bonding of CO to metal centers, additional interaction occurs either through the oxygen lone pairs or through the π-type orbitals, leading to a lowering of CO stretching frequency. We tentatively suggest that some kind of additional interaction of Pd°-carbonyls with K^+ cations may be established on Pt-K/Al_2O_3 catalyst only at room or higher temperatures.

3.3. IR spectra of adsorption of CO2 adsorption and CO/CO_2 coadsorption

In Fig. 12 the IR spectra obtained after CO_2 adsorption on Al_2O_3, on K/Al_2O_3 and on unreduced and reduced Pt-K/Al_2O_3 are compared.

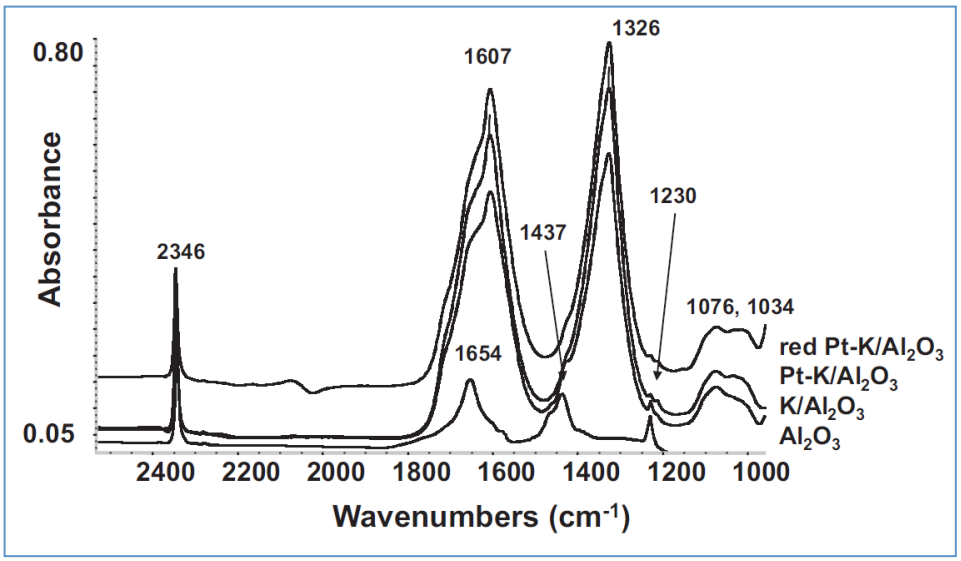

Fig. 12. FT-IR spectra of CO_2 adsorbed on Al_2O_3, K/Al_2O_3 and unreduced and prereduced Pt-K/Al_2O_3 at r.t. at saturation.

The spectra obtained on K/Al_2O_3 and both reduced and unreduced Pt-K/Al_2O_3 are almost identical, being dominated by features typical of bridging or bidentate carbonates (main features at 1607, 1326 and 1076cm^{-1} [42], in contrast to the bands at 3618 (not shown), 1654, 1437 and 1230cm^{-1}), due to surface bicarbonate species. These data confirm the significant basicity (or acidobasicity) induced by potassium that totally transforms at these loading levels the acidobasicity of alumina. This is also evident from the CO_2-TPD curves shown in Fig. 13. While CO_2 desorption from Pt/Al_2O_3 is complete already at 200°C, to have

an almost complete desorption from Pt-K/Al_2O_3 350°C are needed with a small desorption of CO_2 also at 500 °C. Also the amount of CO_2 desorbed from Pt-K/Al_2O_3 is more than 5 times that desorbed from Pt/Al_2O_3.

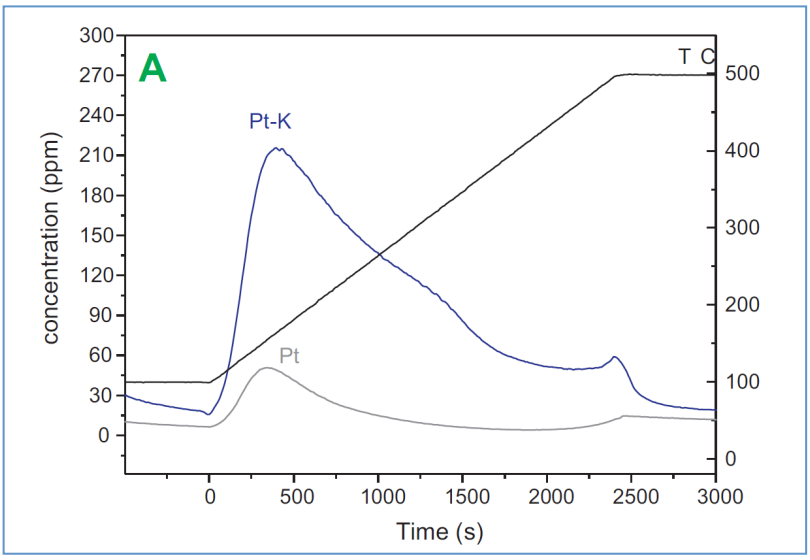

Fig. 13. TPD curves of CO_2 from Pt/Al_2O_3 and Pt-K/Al_2O_3.

To have a further indication on the role of K-Pt interactions, we performed an experiment of sequential adsorption of CO_2 and CO over the reduced Pt-K/Al_2O_3 catalyst. In Fig. 14a, the spectrum of the reduced Pt-K/Al_2O_3 is reported. We note that the sample shows two very weak absorptions at 1562 and 1355cm^{-1} which can be assigned to carboxylate/carbonate impurities arising from chemicals used in the preparation (e.g. acetate ions used in potassium impregnation). Additionally the spectrum shows a residual weak band at 2048cm^{-1} (Fig. 14a), which may be attributed to CO stretching of Pt carbonyl species, that probably also origin from the conversion of chemicals used in the preparation. The frequency observed is in the same range as that observed in the experiment of CO adsorption at r.t. in Fig. 11. Adsorption of carbon dioxide causes, as said, the formation of the bands of carbonates (main maxima at 1607 and 1326cm^{-1}) and linearly adsorbed CO_2 (2345cm^{-1}). Additionally, the shift up to 2082cm^{-1} of the band previously observed at 2048cm^{-1} is also evident (Fig. 14b). The band resists in this position also after outgassing at r.t. (Fig. 14c), that causes the disappearance of molecularly adsorbed CO_2 but leaves bridging carbonates on the surface. This indicates that Pt species responsible for the strongest adsorption of CO is sensitive to the presence of carbonate species, thus being very likely located near the basic sites where carbonates form. Further additional contact with CO produces a new maximum now at 2066cm^{-1}. As shown by the comparison reported in Fig. 15, the spectrum observed after CO adsorption on the “carbonate precovered” reduced surface is very similar (in the 2200–1800cm^{-1} region) to that observed after CO adsorption on the clean reduced surface, but definitely less intense. The main maximum is observed at 2066cm^{-1} (Fig. 15c), i.e. at an intermediate position between those observed on the reduced surface at room (2056cm^{-1}, Fig. 15b) and

at low temperature (2072cm^{-1}, Fig. 15a). These data indicate that Pt centers should lie in close proximity of potassium oxides generating basicity. In fact part of Pt sites seem to be "poisoned" by carbonate species formed on K oxide centers, while part of them are perturbed electronically by the presence of such species, thus showing higher CO stretching frequencies.

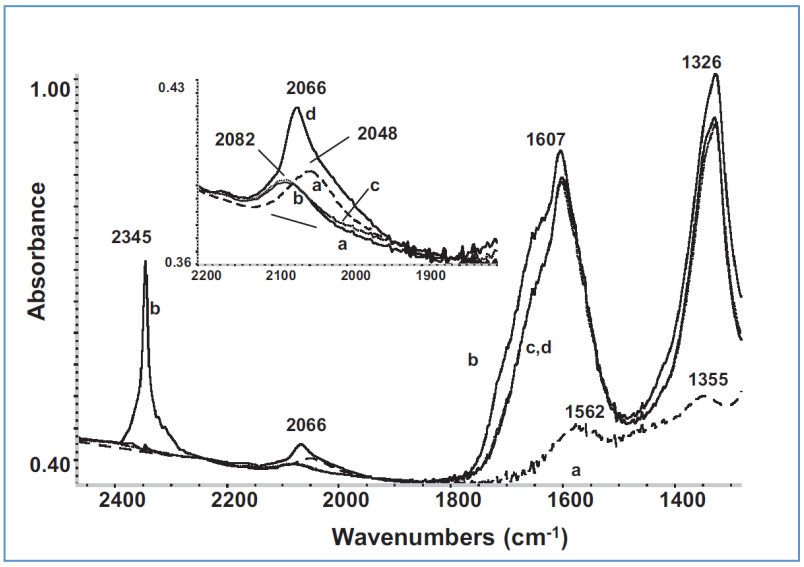

Fig. 14. FT-IR spectra of activated prereduced Pt-K/Al_2O_3 at room temperature (a), after adsorption of CO_2 (b), after outgassing at r.t. (c) and after successive adsorption of CO (d).

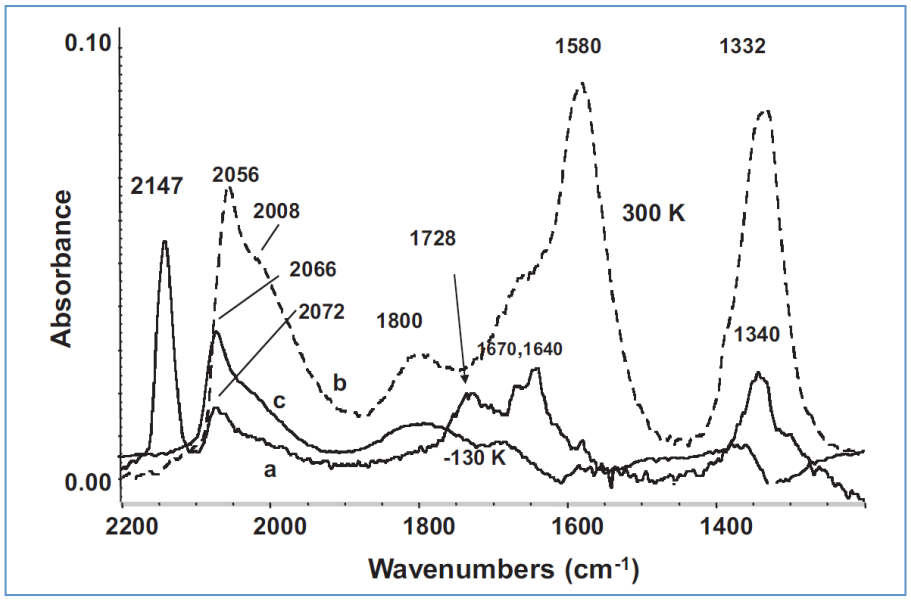

Fig. 15. Comparison of the FT-IR spectra of CO adsorbed on prereduced Pt-K/Al_2O_3 at −140°C (a) and at room temperature (b), and over CO_2-precovered prereduced Pt-K/Al_2O_3 at room temperature (c).

4. Conclusions

The data discussed above allow us to draw the following conclusions.

1. Platinum in small amounts on alumina does not affect the number and the strength of Lewis acid sites of hydroxylated alumina. This suggests that Pt atoms tend to locate over basic sites of alumina.
2. Unreduced Pt deposed on alumina upon outgassing at 350 °C gives rise to at least three different species: i) highly oxidizing Pt cations (Pt^{4+} or Pt^{2+}),whose carbonyls are found at 2186cm^{-1}; ii) less oxidizing Pt cations (Pt^{2+} or Pt^{+}) whose carbonyls are found at 2135–39cm^{-1}; iii) well dispersed reduced zerovalent Pt particles whose carbonyls are found at 2085cm^{-1}. Highly oxidizing Pt cations are so active to oxidize CO to CO_2 at 150 K.
3. Mild reduction in our condition reduced highly oxidizing Pt cations to the less active cationic species and perhaps to the zerovalent state. In any case, zerovalent Pt tends to coalesce to give rise to larger particles characterized by CO of carbonyl species at 2098cm^{-1}. No bridging carbonyl species are found in these conditions.
4. The presence of K in Pt-K/Al_2O_3 catalysts seems to increase the reducibility of Pt, whose highly oxidizing species are not observed after outgassing at 350 °C. Additionally, the basicity of K/Al_2O_3 increases the electron density on reduced Pt, as evidenced by the slightly lower CO stretching frequency of Pt carbonyls.
5. The comparison of the data obtained upon low temperature adsorption of CO with those obtained by adsorption at room temperature show that CO acts, at room temperature, not as a completely inert probe. In fact, the formation of carbonates without any oxidant (except Pt species, in case) and the relevant modification of the spectrum of adsorbed CO suggest some reactivity of CO at r.t. On the other hand, already at −100 °C CO reduces a small part of the surface Pt ions producing CO_2. This makes low-temperature CO adsorption experiments an informative tool for the surface characterization.
6. Pt species are located near the basic oxide species of the K/Al_2O_3 “support” and their behavior is influenced by the presence of adsorbed carbonate species.

Acknowledgement

The financial support of MUR – PRIN project 2007HHCZP4 is acknowledged.

References

[1] R.S. Haizmann, L.H. Rice, M.S. Turowicz, US patent 5453552 (1995) to UOP.

[2] M.M. Bhasin, J.H. McCain, B.V. Vora, T. Imai, P.R. Pujadó, Appl. Catal. A: Gen. 221 (2001) 397.

[3] D.R. Dyroff, U.S. Patent No. 6,700,028 B2, to Huntsmann Petrochem. Co. (2004).

[4] A.A. Phatak, N. Koryabkina, S. Rai, W. Ruettinger, R.J. Farrauto, G.E. Blau, W.N. Delgass, F.H. Ribeiro, Catal. Today 123 (2007) 224–234.

[5] M. Garcia-Diéguez, E. Finocchio, M.A. Larrubia, L.J. Alemany, G. Busca, J. Catal. 274 (2010) 11–20.

[6] Y. Choi, H.G. Stenger, J. Power Sources 129 (2004) 246–254.

[7] H. Tanaka, M. Kuriyama, Y. Ishida, S. Ito, K. Tomishige, K. Kunimori, Appl. Catal. A: Gen. 343 (2008) 117–124.

[8] P. Harrison Tran, J.M.H. Chen, G.D. Lapadula, T. Blute, US patent 7410626 B2 (2008) to BASF Catalysts LLC.

[9] P. Hurtado, S. Ordóˇnez, A. Vega, F. Diez, Chemosphere 55 (2004) 681–689.

[10] G. Avgouropoulos, E. Oikonomopoulos, D. Kanistras, T. Ioannides, Appl. Catal. B: Environ. 65 (2006) 62.

[11] G. Busca, Ind. Eng. Chem. Res. 48 (2009) 6486.

[12] W.S. Epling, L.E. Campbell, A. Yezerets, N.W. Currier, J.E. Parks II, Catal. Rev. 46 (2004) 163.

[13] N. Takahashi, H. Shinjoh, T. IIjima, T. Suzuki, K. Yamazaki, K. Yokota, H. Suzuki, N. Miyoshi, S. Matsumoto, T. Tanizawa, T. Tanaka, S. Tateishi, K. Kasahara, Catal. Today 27 (1996) 63.

[14] K. Nakatani, S. Hirota, S. Takeshima, K. Itoh, T. Tanaka, SAE Paper SP-1674 (2002) 2002-01-0957.

[15] I.S. Pieta, M. Garcia Diguez, C. Herrera, M.A. Larrubia, L.J. Alemany, J. Catal. 270 (2010) 256–267.

[16] M.R. Lee, E.R. Allen, J.T. Wolan, G.B. Hoflund, Ind. Eng. Chem. Res. 37 (1998) 3375.

[17] I. Malpartida, M.A. Larrubia Vargas, L.J. Alemany, E. Finocchio, G. Busca, Appl. Catal. B: Environ. 80 (2008) 214–225.

[18] J.H. Kwak, J. Hu, D. Mei, C.-W. Yi, D.H. Kim, C.H.F. Peden, L.F. Allard, J. Szanyi, Science 325 (2009) 1670–1673.

[19] H. Knözinger, S. Huber, J. Chem. Soc., Faraday Trans. 94 (1998) 2047.

[20] K.I. Hadjiivanov, G.N. Vayssilov, Adv. Catal. 47 (2002) 307.

[21] G. Busca, in: S.D. Jackson, J.S.J. Hargreaves (Eds.), Metal Oxide Catalysis, vol. 1, Wiley-VCH, 2008, p. 95.

[22] V. Sanchez-Escribano, L. Arrighi, P. Riani, R. Marazza, G. Busca, Langmuir 22 (2006) 9214.

[23] E. Finocchio, G. Busca, P. Forzatti, G. Groppi, A. Beretta, Langmuir 23 (2007) 10419.

[24] S. Specchia, E. Finocchio, G. Busca, P. Palmisano, V. Specchia, J. Catal. 263 (2009) 134.

[25] M. Kantschewa, E.V. Albano, G. Ertl, H. Knözinger, Appl. Catal. 8 (1983) 71.

[26] G. Busca, V. Lorenzelli, G. Ramis, R. Willey, Langmuir 9 (1993) 1492.

[27] P.O. Scokart, A. Amin, C. Defosse, P.G. Rouxhet, J. Phys. Chem. 85 (1981) 1406.

[28] G. Busca, G. Ramis, Appl. Surf. Sci. 27 (1986) 114–126.

[29] T. Montanari, I. Salla, G. Busca, Micropor. Mesopor. Mater. 109 (2008) 216–222.

[30] L.-C. De Ménorval, A. Chaqroune, B. Coq, F. Figueras, J. Chem. Soc., Faraday Trans. 93 (1997) 3715.

[31] C. Hippe, R. Lambert, G. Schultz-Ekloff, U. Schubert, Catal. Lett. 43 (1997) 195.

[32] J. Raskò, J. Catal. 217 (2003) 478.

[33] S. Albertazzi, G. Busca, E. Finocchio, R. Glöckler, A. Vaccari, J. Catal. 223 (2004) 372.

[34] S. Derrouiche, P. Gravejat, B. Bassou, D. Bianchi, Appl. Surf. Sci. 253 (2007) 5894.

[35] L. Castoldi, L. Lietti, I. Nova, R. Matarrese, P. Forzatti, F. Vindigni, S. Morandi, F. Prinetto, G. Ghiotti, Chem. Eng. J. 161 (2010) 416.

[36] F. Prinetto, M. Manzoli, S. Morandi, F. Frola, G. Ghiotti, L. Castoldi, L. Lietti, P. Forzatti, J. Phys. Chem. C 114 (2010) 1127.

[37] G. Ramis, G. Busca, V. Lorenzelli, Mater. Chem. Phys. 29 (1991) 425–435.

[38] D. Curulla, A. Clotet, J.M. Ricart, F. Illas, J. Phys. Chem. 103 (1999) 5246.

[39] J. Xu, J.T. Yates, Surf. Sci. 327 (1995) 193.

[40] P. Panagiotopoulou, D.I. Kondarides, J. Catal. 260 (2008) 141.

[41] I. Salla, T. Montanari, P. Salagre, Y. Cesteros, G. Busca, Phys. Chem. Chem. Phys. 7 (2005) 2526.

[42] G. Busca, V. Lorenzelli, Mater. Chem. 7 (1982) 89.

Paper VII

Pathways for N_2 and N_2O formation during the reduction of NOx over Pt-Ba/Al_2O_3 LNT catalysts investigated by labelling isotopic experiments

Luca Lietti, Nancy Artioli, Laura Righini, Lidia Castoldi, Pio Forzatti
Industrial & Engineering Chemistry Research • Just Accepted Manuscript • DOI: 10.1021/ie2021976 • Publication Date (Web): 25 Jan 2012

Pathways for N2 and N2O formation during the reduction of NOx over Pt-Ba/Al2O3 LNT catalysts investigated by labelling isotopic experiments

Abstract

Mechanistic aspects involved in the formation of N_2 and of N_2O during the reduction of gas-phase NO and of NO_x stored over a model $PtBa/Al_2O_3$ NSR catalyst are investigated using unlabelled ammonia and labelled NO. The reduction of the stored NO_x species (labeled nitrites and nitrates) with NH_3 leads to the selective formation of N_2 as major product and of small amounts of nitrous oxide. Based on the nitrogen isotopic distribution, it appears that N_2 formation occurs primarily through the statistical coupling of N-atoms formed by dissociation of NO_x- and NH_3-related surface intermediates, although an SCR-pathway (involving the coupling of NH_3- and NO-derived ad-species) is also likely to occur. It appears as well that the formation of nitrous oxide involves either the coupling of two adsorbed NO molecules or the recombination of an adsorbed NO molecule with an adsorbed NH_x fragment.

Keywords

Isotopic labelling experiments, $PtBa/Al_2O_3$ NSR catalysts, NOx Storage-reduction, reduction of nitrites, reduction of nitrates.

Introduction

Both diesel- and lean burn gasoline-powered vehicles are spreading in the transportation sector due to higher efficiency and lower fuel consumption if compared to the traditional stoichiometric engines [1,2,3]. The Three Way Catalytic (TWC) converters, currently used for stoichiometric gasoline engines, are not effective in the reduction of NO_x for lean burn engines, which operate in the presence of excess oxygen. Viable solutions for the control of NO_x are in these cases the urea-SCR technique and the NO_x Storage Reduction (NSR) or Lean NO_x Trap (LNT) system [4,5,6]. To date, the urea-SCR technology is preferred for heavy-duty vehicles and minivans, whereas LNTs are preferred for small engines [7]. Besides, hybrid LNT/SCR systems have also been proposed1 [,8].

In the NSR technology long lean phases - typically lasting 60–90 s , during which NO_x are stored on the catalyst - are alternated with short rich periods – in the order of few seconds - where the exhaust is deliberately made rich. The trapped NO_x are reduced to N_2 although other by-products may be released (NO, N_2O, NH_3). NSR catalysts are composed of a high surface area support material (often γ-alumina or stabilized alumina), precious metals (usually a combination of Pt and Rh) and basic components, such as Ba or K, which act as NO_x storage material [9,10].

Mechanistic aspects of the reduction of NO_x stored over NSR catalytic systems have been investigated by several groups [11,12,13,14,15]. It has been shown that the reduction of stored nitrates by hydrogen under nearly isothermal conditions (i.e. in the absence of significant thermal effects upon the lean/rich switch) does not involve the thermal decomposition of the adsorbed NO_x species as a preliminary step [11,16] , but instead occurs via a Pt-catalyzed route already active at low temperatures. Besides, it has been suggested that N_2 is formed through a two-steps in series molecular pathway involving the fast reaction of nitrates with hydrogen to give ammonia, followed by the slower reaction of the so-formed NH_3 with residual stored nitrates to give N_2 [13,14,17,18,21]. Due to the high reactivity of H_2 towards nitrates, and to the integral nature of the reactor, an hydrogen front develops in the reactor so that NH_3 reacts with nitrates stored downstream the H_2 front to give nitrogen. This has been clearly demonstrated by spaciMS measurements[19] showing the intra-catalyst spatiotemporal species distributions during regeneration with H_2 of a Pt-Ba/Al_2O_3 LNT trap. As also pointed out by a dedicated kinetic analysis[20], the development of an H_2 front travelling in the reactor, along with the occurrence of the above two-steps in series pathway, is able to account for the temporal sequence of products observed at the reactor exit during the regeneration of NSR catalysts[15,14,21].

Based on these findings, it appears that N_2 formation during the regeneration of NSR catalysts occurs via the reaction of ammonia with stored NO_x. Mechanistic aspects of this reaction are still largely unclear: this has motivated the present study where the possible routes leading to the formation of N_2 during the reaction of NH_3 with the stored NO_x have been investigated. For this purpose, isotopic labeling experiments have been carried out using unlabeled NH_3 and ^{15}NO as a source for the stored $^{15}NO_x$. Since nitrites and

nitrates can be formed on the catalyst surface upon NO adsorption in the presence of O_2 at low and high temperature respectively [25,26], the reactivity of these adsorbed species with gaseous NH_3 has been investigated. The reactivity of NH_3 and ^{15}NO in the gas phase has also been studied for comparison purposes. This allowed to better clarify mechanistic aspects involved in the formation of N_2 during regeneration of NSR catalysts, as detailed below.

Materials and Methods

Catalysts preparation and characterization – An homemade Pt-Ba/Al_2O_3 (1/20/100 w/w) catalyst has been used in this study. The catalytic system has been prepared by incipient wetness impregnation of a commercial alumina sample (Versal 250 from UOP) with aqueous solution of dinitro-diammine platinum (Strem Chemicals, 5% Pt in ammonium hydroxide) and subsequently with a solution of Ba acetate (Aldrich, 99%). The powder has been dried at 80°C and calcined in air at 500°C for 5h after each impregnation step[22]. The impregnation order (first Pt and then Ba) has been chosen in order to ensure a good dispersion and stability of the noble metal and of the alkaline component on the alumina support, in line with recipes of Toyota patents[23].

The specific surface area of the sample, determined by N_2 adsorption–desorption using a Micromeritics TriStar 3000 instrument, is 160 m^2g^{-1} (BET method). The Pt dispersion was also estimated by hydrogen chemisorption at 0°C (TPD/R/O 1100 Thermo Fischer Instrument); a value of 52% has been obtained.

Catalytic tests - Catalytic tests have been performed in a quartz tube micro-reactor (7 mm I.D.) loaded with 60 mg of catalyst powder (70-100 μm). A total flow of 100 cm^3/min (at 1 atm and 0°C) has been used in the experiments, resulting in a GHSV of 10^5 h^{-1} being the density of the catalyst bed very close to 1 g/cm^3. The reactor outlet was directly connected to a mass spectrometer (Thermostar 200, Pfeiffer), an UV-NO_x analyzer (LIMAS 11HW, ABB) and a micro-gas chromatograph (Agilent 3000A) for on-line analysis of the reaction products [16,22,24].

Prior to the catalytic activity runs, the catalyst sample has been conditioned by performing a few storage/regeneration cycles. For this purpose NO_x has been adsorbed at 350°C by imposing a rectangular step feed of NO (1000 ppm) in flowing He + 3% v/v O_2 until catalyst saturation. Then the NO and O_2 concentrations have been stepwise decreased to zero, followed by a He purge at the same temperature (350°C). This leads to the desorption of weakly adsorbed NO_x species. After the He purge, catalyst regeneration (rich phase) has been carried out with H_2 (2000 ppm in He). Conditioning lasted until a reproducible behavior was obtained; this typically required 3-4 adsorption/reduction cycles. The conditioning procedure terminated with a reducing step; accordingly before the subsequent experiments the catalyst surface was free of any adsorbed NO_x species.

After catalyst conditioning at 350°C, Temperature Programmed Reaction (TPR) of NH_3 + ^{15}NO, and Temperature Programmed Surface Reaction (TPSR) / Isothermal Step Concentration (ISC) experiments of nitrites and nitrates with ammonia have been performed. In a typical TPR experiment, the catalyst has been exposed under temperature programming from room temperature (r.t.) to 400°C (10°C/min) to a flow of 660 ppm of NH_3 and 1000 ppm ^{15}NO in He (i.e. according to the stoichiometry of the slow SCR reaction:

$$6\ NO + 4\ NH_3 \rightarrow 5\ N_2 + 6\ H_2O).$$

Before TPSR and ISC experiments, labelled nitrites and nitrates have been adsorbed on the catalyst surface. Based on previous NO_x adsorption studies under *in-situ* and *operando* conditions

nitrite and nitrate ad-species are formed on the catalyst surface upon NO/O_2 adsorption at low (150 °C) and high (350 °C) temperature, respectively [25,26,27]. Accordingly labelled nitrites and nitrates have been accumulated by contacting the catalyst with a flow of 1000 ppm ^{15}NO in He + 3% v/v O_2 at 150°C and 350°C, respectively.

In the case of TPSR experiments, after $^{15}NO_x$ adsorption followed by a He purge at the same temperature, the catalyst has been cooled down to r.t. under He flow. Then a rectangular step feed of NH_3 (1000 ppm in He) has been admitted to the reactor at r.t. and the catalyst temperature has been linearly increased to 400°C (heating rate 10 °C/min, hold 1 hour), while monitoring the concentration of the products exiting the reactor. This procedure leads to complete removal of the stored $^{15}NO_x$, as confirmed by nitrogen balance.

In the case of the Isothermal Step Concentration experiments (ISC), after $^{15}NO_x$ adsorption and He purge at 150°C or 350°C, the reduction of the stored $^{15}NO_x$ species has been carried out at the same temperature by imposing a rectangular step feed of NH_3 (1000 ppm in He).

At the end of the regeneration procedure, the catalyst was heated up to 350°C under He flow and eventually hydrogen was added to the reactor to complete the reduction of residual stored $^{15}NO_x$, if any. This procedure allowed the quantification of the residual $^{15}NO_x$ species left after reduction.

The following mass-to-charge ratios (m/e) have been used to follow the reaction products: H_2 (m/e = 2), N_2 (m/e = 28), ^{15}NN (m/e = 29), $^{15}N_2$ (m/e = 30), NO (m/e = 30), ^{15}NO (m/e = 31), N_2O (m/e = 44), ^{15}NNO (m/e = 45), $^{15}N_2O$ (m/e = 46), H_2O (m/e = 18), NH_3 (m/e = 15), NO_2 (m/e = 46), $^{15}NO_2$ (m/e = 47), and $^{15}NH_3$ (m/e = 16). Due to large overlapping of the cracking patterns of the reaction products, quantitative analysis has been accomplished by simultaneous mass spectrometry, gas-chromatography and UV-Vis analysis.

Calibration factors and cracking patterns of the unlabeled species have been experimentally determined from calibrated gas cylinders; those of several labeled species have been obtained from cylinders (^{15}NO) or by dedicated experiments (e.g. lean rich cycles with ^{15}NO leading to the formation of $^{15}NO_2$, $^{15}N_2$ and $^{15}NH_3$). This procedure revealed that the calibration factors of $^{15}N_2$ and N_2 were almost identical; accordingly that of ^{15}NN was assumed to be the same. Along similar lines the calibration factors of $^{15}N_2O$ and ^{15}NNO were assumed to be identical to that of N_2O. These results have also been confirmed by GC measurements.

The analytical set-up used in this work allowed to identify and quantify species which overlap each other. For example the $^{15}N_2$ concentration was obtained from the MS m/e = 30 signal after "cleaning" the NO and NH_3 contributions provided by simultaneous UV-Vis analysis; the $^{15}NH_3$ concentration has been estimated by subtracting from the total amount of ammonia (NH_3 +$^{15}NH_3$) obtained from the UV analyzer the concentration of $^{14}NH_3$ obtained from the MS signal at m/e = 15 (taking into account the overlapping of ^{15}N). Besides, GC analysis allowed the quantification of the overall nitrogen (N_2 + ^{15}NN + $^{15}N_2$) and nitrous oxide (N_2O + ^{15}NNO + $^{15}N_2O$) concentrations at different instants of the runs. These total concentration values were compared to those calculated by the sum of the different isotopic species ($^{15}N_2$+ N_2+^{15}NN and $^{15}N_2O$+N_2O+^{15}NNO) measured with the mass spectrometer to verify the accuracy of the analysis method.

N-balances, calculated from the amounts of NO_x adsorbed and those of N-containing products, are generally within an experimental error of 10%.

All the experiments carried out with ^{15}NO (TPSR and ISC) have been performed with ^{14}NO as well to check for differences in the reactivity of the labeled and unlabeled molecules: differences have always been found to be negligible.

Results

Adsorption of nitrites and nitrates. Based on previous NO_x adsorption studies accomplished under *in-situ* and *operando* conditions [25,26,27] nitrite and nitrate ad-species are formed on the Pt-Ba/Al_2O_3 catalyst surface upon NO/O_2 adsorption at low (150 °C) and high (350 °C) temperature, respectively. The results of $^{15}NO/O_2$ storage are shown in Figures 1A and 1B. In Figure 1A (T= 150°C) the ^{15}NO breakthrough is immediately observed upon admission (t= 0s), along with very small amounts of $^{15}NO_2$ which are seen after 500 s. After steady-state conditions are attained, the ^{15}NO inlet concentration is switched to zero; a tail is observed in the NO_x outlet concentration (with a small "puff" in the NO_2 concentration) due to the desorption of weakly adsorbed species. At the end of the adsorption process (2750 s), nearly 0.26 mmol/g_{cat} of $^{15}NO_x$ have been stored on the catalyst surface.

In Figure 1B (T= 350°C) the ^{15}NO breakthrough is observed at 200 s, and the evolution of significant amounts of $^{15}NO_2$ are observed starting from 260 s. The outlet concentrations of both ^{15}NO and $^{15}NO_2$ increase with time and tend to constant levels which are consistent with the constraints of the equilibrium of ^{15}NO oxidation to $^{15}NO_2$ in the presence of 3% v/v O_2 (^{15}NO = 590 ppm vs $^{15}NO_{eq}$ = 445 ppm and $^{15}NO_2$ = 410 ppm vs $^{15}NO_{2eq}$ = 555 ppm, at 350°C). After roughly 2000 s, the ^{15}NO feed is switched off and also in this case a tail is observed in the $^{15}NO_x$ concentration profile, due to the desorption of weakly adsorbed $^{15}NO_x$ species. At the end of the storage phase, nearly 0.34 mmol/g_{cat} of $^{15}NO_x$ have been stored on the catalyst surface.

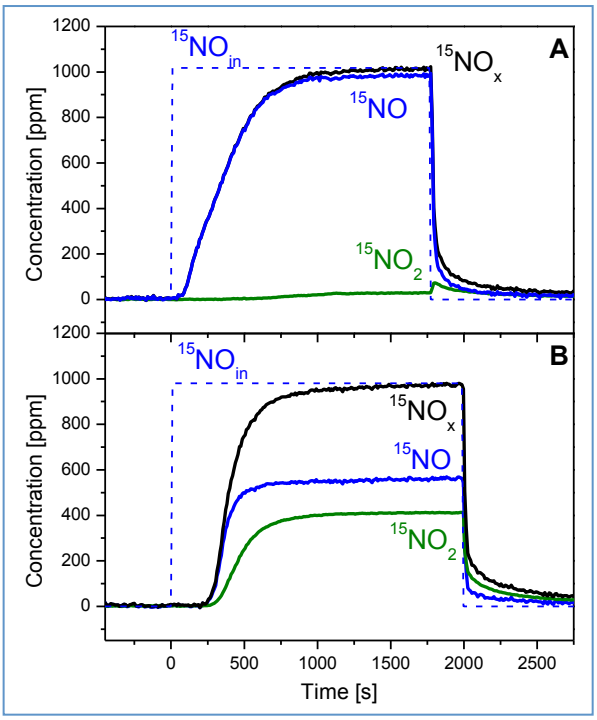

Fig.1 Adsorption of labeled NO at A) 150 and B) 350°C by imposing a rectangular step feed of ^{15}NO (1000 ppm) in flowing He + 3% v/v O_2 on Pt-Ba/Al_2O_3 catalyst

Reactivity of stored nitrites and nitrates with gas-phase NH_3. Figures 2 and 3 show the results of NH_3-TPSR and NH_3-ISC experiments carried out after $^{15}NO_x$ storage at 150 °C (labelled nitrites).

In the case of the TPSR experiment (Figure 2), the desorption of ammonia is observed at first; indeed ammonia is being stored on the catalyst upon admission at the beginning of the experiment, not shown in the Figure (t < 30500 s). From nearly 120°C a net consumption of ammonia is seen together with the formation of N_2O and N_2 due to the reaction of NH_3 with stored $^{15}NO_x$. Nitrogen is by far the most abundant product, with different isotopic composition.

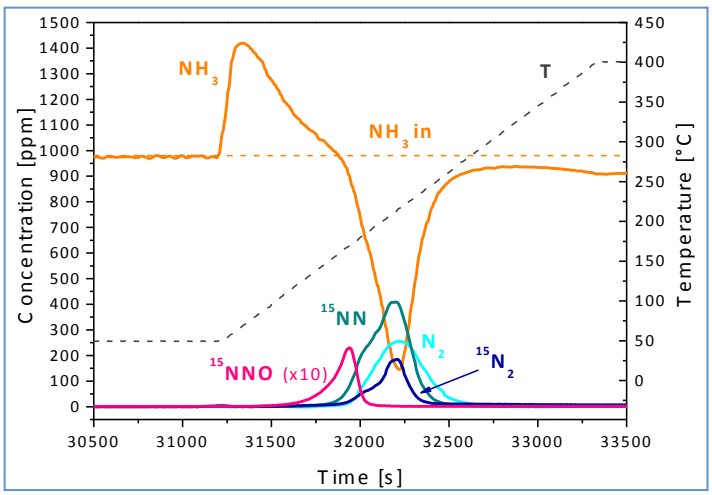

Fig.2 TPSR run with NH_3 (1000ppm) after $^{15}NO_x$ adsorption at 150°C (1000 ppm ^{15}NO + O_2 3% v/v in He) over Pt-Ba/Al_2O_3 catalyst

The single-labelled isotope (i.e. $^{15}N^{14}N$, m/z = 29) is initially observed in greater amounts whereas the unlabelled ($^{14}N_2$, m/z = 28) and double-labelled ($^{15}N_2$, m/z = 30) species are seen with a short delay. The single-labelled $^{15}N^{14}N$ molecule is the most abundant di-nitrogen species evolved during the experiment (49% of the total N_2 products), but the unlabelled ($^{14}N_2$) and double-labelled ($^{15}N_2$) di-nitrogen are also observed in significant amounts (35% and 16%, respectively). The evolution of very small amounts of single-labelled nitrous oxide ($^{15}N^{14}NO$, m/z = 47) is also observed at the onset of the reaction around 100°C (note that the concentration trace of $^{15}N^{14}NO$ is multiplied by a factor of 10).

Notably, the NH_3 consumption (0.3 mmol/g_{cat}, as estimated from the NH_3 uptake in Figure 2 in the temperature range 120-300°C) and the N_2 formation (0.29 mmol/g_{cat}) roughly obey the stoichiometry of reaction (1):

$$Ba(NO_2)_2 + 2\ NH_3 \rightarrow 2\ N_2 + BaO + 3\ H_2O \qquad (1)$$

Indeed nitrites are formed upon storage of NO/O_2 at 150°C and N_2 represents the major reaction product of NH_3-TPSR [25,26]. Above 300°C, ammonia is decomposed to a small extent into N_2 and H_2 (these species can be hardly detected due to the low concentrations).

Figure 3 shows the results obtained upon reduction of the stored nitrites at 150°C (NH_3-ISC). Upon admission, ammonia is completely consumed and nitrogen is formed as the major reaction product along with nitrous oxide in small amounts (its concentration trace is multiplied by a factor of 10). The NH_3 consumption is slightly higher than that expected from the stoichiometry of reaction (1) due to ammonia adsorption onto the catalyst surface.

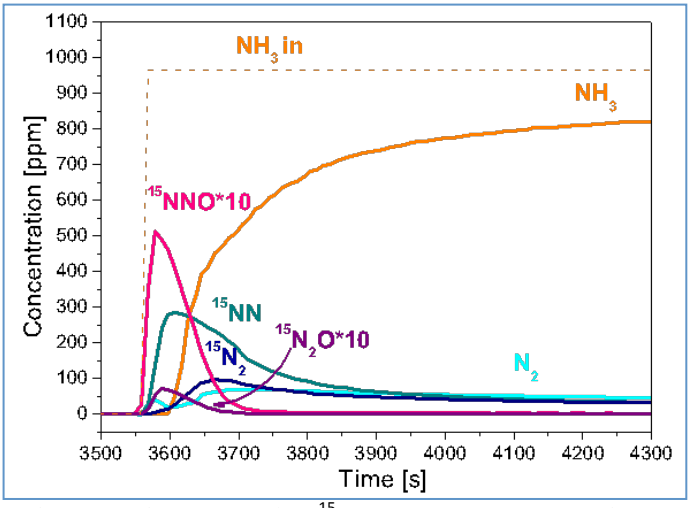

Fig.3 ISC-rich phase with NH_3 (1000ppm) at 150°C after $^{15}NO_x$ adsorption at 150°C (1000 ppm ^{15}NO + O_2 3% v/v in He) over Pt-Ba/Al_2O_3 catalyst

The temporal sequence and the distribution of products resemble those seen during the TPSR run (Figure 2). The single labeled $^{15}N^{14}N$ molecule represents the main di-nitrogen isotopic product (53%) and is seen before the other isotopes; $^{14}N_2$ and $^{15}N_2$ account for 23% and 24% of total N_2 respectively. Concerning N_2O,

the single-labeled molecule ($^{15}N^{14}NO$) is formed in significant amounts, along with traces (few ppm) of the double-labeled isotope ($^{15}N_2O$). The unlabeled molecule $^{14}N_2O$ is not observed.

The results obtained upon reaction of ammonia with the stored nitrates are shown in Figures 4 and 5. In the case of NH_3-TPSR experiment (Figure 4), the ammonia consumption is observed from near 150°C, and is accompanied by the evolution of N_2. The consumption of ammonia (0.6 mmol/g_{cat}) and the formation of N_2 (0.5 mmol/g_{cat}) are in line with the stoichiometry of reaction (2):

$$3\ Ba(NO_3)_2 + 10\ NH_3 \rightarrow 8\ N_2 + 3\ BaO + 15\ H_2O \qquad (2)$$

Indeed nitrates are formed upon storage of NO/O_2 at 350°C and N_2 represents the only reaction product in Figure 4. N_2O is not observed in this case, at variance with the NH_3-TPSR of nitrites (Figure 2) and in line with previous literature reports showing that the reduction of nitrates with ammonia is very selective towards N_2[13, 14, 17,18]. The dynamics of the evolution of the three di-nitrogen isotopes is the same; the unlabeled $^{14}N_2$ and the single labeled $^{15}N^{14}N$ species are most abundant (respectively 44% and 37%), while $^{15}N_2$ accounts for 19% of total N_2.

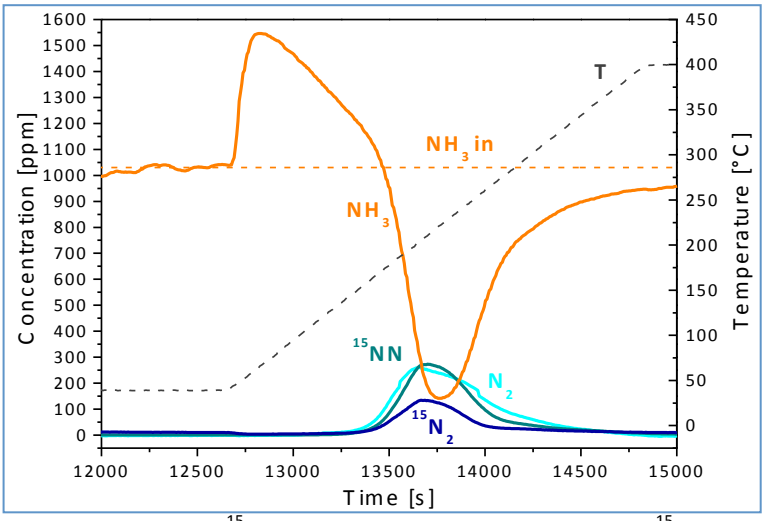

Fig.4 TPSR run with NH_3 (1000ppm) after $^{15}NO_x$ adsorption at 350°C (1000 ppm ^{15}NO + O_2 3% v/v in He) over Pt-Ba/Al_2O_3 catalyst

Similar results have been obtained in the case of NH_3-ISC carried out over the stored nitrates at 350°C (Figure 5). Ammonia is completely consumed upon admission and N_2 represents the only reaction product. At 350°C the adsorption of ammonia is negligible, so that the consumption of ammonia and the formation of N_2 obey the stoichiometry of reaction (2), as opposite to what observed in the case of nitrites where the NH_3-ISC experiment was carried out at much lower temperature (150°C, Figure 3). Unlabeled $^{14}N_2$ and single labeled $^{15}N^{14}N$ species represent the main products (50% and 35% respectively), while lower amounts of $^{15}N_2$ are observed (15%). As in the case of NH_3-TPSR of nitrates (Figure 4), N_2O is not observed and the reaction is fully selective towards nitrogen.

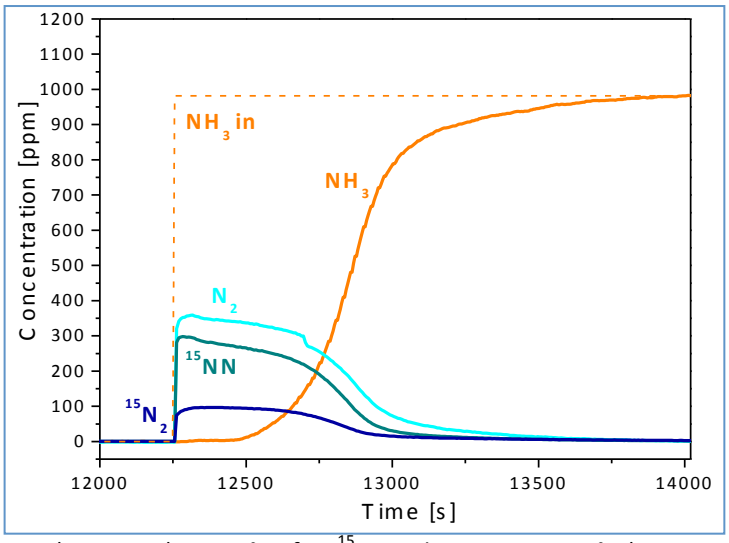

Fig.5 ISC-rich phase with NH_3 (1000ppm) at 350°C after $^{15}NO_x$ adsorption at 350°C (1000 ppm ^{15}NO + O_2 3% v/v in He) over Pt-Ba/Al_2O_3 catalyst

Reactivity of gas-phase NO and NH_3. The results of TPR of NH_3 with gas-phase ^{15}NO are shown in Figure 6. The onset of the reaction with formation of N_2O and N_2 in comparable amounts is observed at 100°C. Up to 180°C only labelled molecules are detected, i.e. $^{15}N_2O$ and $^{15}N^{14}NO$ for nitrous oxide and $^{15}N^{14}N$ for di-nitrogen. Above 180°C, where complete NO consumption is observed, the concentration of nitrous oxide species drops to zero and the formation of double labeled $^{15}N_2$ and of unlabeled $^{14}N_2$ is observed. Hence above 180°C the reaction is very selective towards N_2.

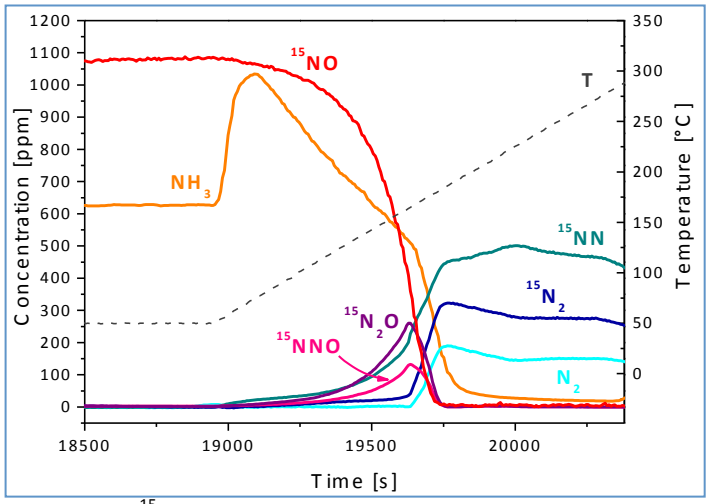

Fig.6 TPR run with NH_3 (660 ppm) and ^{15}NO (1000 ppm) in He over Pt-Ba/Al_2O_3 catalyst

Discussion

Mechanism of N_2 formation. The results show that the NO_x species stored onto PtBa/Al_2O_3 LNT catalyst, i.e. nitrites and nitrates, are selectively reduced by NH_3 to N_2, since no other products are observed if one neglects the formation of very small amounts of nitrous oxide in the reduction of nitrites. All di-nitrogen isotopes are formed but the abundance of single labeled $^{15}N^{14}N$ isotope is greater than those of unlabelled

$^{14}N_2$ and double labeled $^{15}N_2$ isotopes. Only in the case of nitrites the di-nitrogen isotopes show different temporal evolution; indeed the single labeled $^{15}N^{14}N$ isotope prevails at the beginning of both NH_3-TPSR and NH_3-ISC runs. Concerning nitrous oxide, only labelled species ($^{15}N^{14}NO$ and $^{15}N_2O$) are formed upon reaction of the stored NO_x with ammonia.

A different picture is apparent in the reaction of ammonia with gaseous ^{15}NO. In this case comparable amounts of N_2O and of N_2 are observed at low temperature (100-180°C), but the selectivity to di-nitrogen is complete above 180-200°C where NO is completely consumed. Like during NH_3-TPSR and NH_3-ISC runs of both nitrites and nitrates, only labeled species are observed in the case of nitrous oxide ($^{15}N^{14}NO$ and $^{15}N_2O$). On the other hand all types of di-nitrogen isotopes are observed among the products, but only the single labeled $^{15}N^{14}N$ isotope is detected at 100-180°C.

Mechanistic aspects involved in the formation of di-nitrogen during the reduction of NO_x by NH_3 have been the object of long debate in the scientific literature. In the case of the NH_3-SCR reaction over vanadia-based catalysts and transition metal exchanged zeolites (reaction (3)):

$$4\ NO + 4\ NH_3 + O_2 \rightarrow 4\ N_2 + 6\ H_2O \qquad (3)$$

it has been shown that the reaction between unlabeled ammonia ($^{14}NH_3$) and labeled NO (^{15}NO) leads to the selective formation of the single labeled nitrogen molecule ($^{15}N^{14}N$) [28,29,30], indicating that one N-atom comes from ammonia and the other from NO. Accordingly the formation of N_2 has been suggested to occur through the intermediacy of surface species like nitrosamide or ammonium nitrite[2931,32,29] formed via coupling of NH_3- with NO-derived species. In this pathway (SCR pathway) the self-coupling of N-species originated from ammonia and NO is ruled out due to the lack of significant amounts of $^{15}N_2$ and $^{14}N_2$ isotopes in the product mixture. The same conclusions have been reached in our labs where the reaction of stored $^{14}NH_3$ with ^{15}NO in the presence of excess O_2 has been accomplished over V_2O_5/TiO_2 and Fe-ZSM5 catalyst samples. In fact the very selective formation of $^{14}N^{15}N$ was observed (data not reported for the sake of brevity), in line with previous literature reports and with the mechanistic indications discussed above [28,30].

A different picture is apparent in the reduction of NO_x with ammonia in the case of the $PtBa/Al_2O_3$ catalyst sample investigated in this work. In the reduction of stored labeled nitrites by $^{14}NH_3$ (Figures 2 and 3) the formation of all di-nitrogen isotopes has been observed. The single labeled $^{14}N^{15}N$ species dominates (roughly 50% of total N_2), but relevant amounts of double labeled ($^{15}N_2$) and unlabeled ($^{14}N_2$) di-nitrogen are also observed. Worth to note that the stoichiometry of the reduction of stored nitrites with ammonia (reaction (1)) involves, like the NH_3-SCR reaction (3), a 1/1 molar ratio between $^{14}NH_3$ and nitrite group $^{15}NO_2^-$. Accordingly in this case the selective formation of only single labeled $^{14}N^{15}N$ molecule (via coupling of ^{14}N- and ^{15}N-containing species, as in the case of the SCR pathway) is possible. However the production

of $^{15}N_2$ and unlabeled $^{14}N_2$ has also been observed, in addition to $^{14}N^{15}N$, and this indicates that a SCR-like pathway does not represent the unique route of N_2 formation in the case of LNT catalysts.

Figure 7 sketches a possible pathway that can explain the formation of di-nitrogen (and of nitrous oxide, see below) during the reduction by NH_3 of $^{15}NO_x$ adsorbed over Pt-Ba/Al_2O_3. Stored $^{15}NO_x$ are located on Ba sites close to or far away from Pt; upon admission of ammonia the Pt sites are reduced and this drives the onset of the reduction process which involves the migration through surface diffusion of stored $^{15}NO_x$ towards reduced Pt sites, as suggested in the literature [33]. The $^{15}NO_x$ species are hence decomposed at the reduced Pt sites with formation of a pool of ^{15}N- and O- ad-atoms. These ad-species react with NH_3-derived species or fragments adsorbed onto the Pt sites, as suggested in the case of the NO-NH_3 reaction over Pt-based catalysts 6,[12, 34, 34, 35, 36, 37, 38]. In such a case there is a general consensus that di-nitrogen formation occurs via recombination of N-ad-atoms formed by dissociation of NO and NH_3 at the Pt site (*s*):

$$^{15}NO_{(g)} + s \rightarrow {}^{15}NO_{(a)} \quad (4)$$

$$^{15}NO_{(a)} + s \rightarrow {}^{15}N_{(a)} + O_{(a)} \quad (5)$$

$$^{14}NH_{3(g)} + s \rightarrow {}^{14}NH_{3(a)} \quad (6)$$

$$^{14}NH_{3(a)} + 3s \rightarrow {}^{14}N_{(a)} + 3H_{(a)} \quad (7)$$

$$^{15}N_{(a)} + {}^{15}N_{(a)} \rightarrow {}^{15}N_{2(g)} + 2s \quad (8a)$$

$$^{15}N_{(a)} + {}^{14}N_{(a)} \rightarrow {}^{15}N^{14}N_{(g)} + 2s \quad (8b)$$

$$^{14}N_{(a)} + {}^{14}N_{(a)} \rightarrow {}^{14}N_{2(g)} + 2s \quad (8c)$$

$$2H_{(a)} + O_{(a)} \rightarrow H_2O_{(g)} + 3s \quad (9)$$

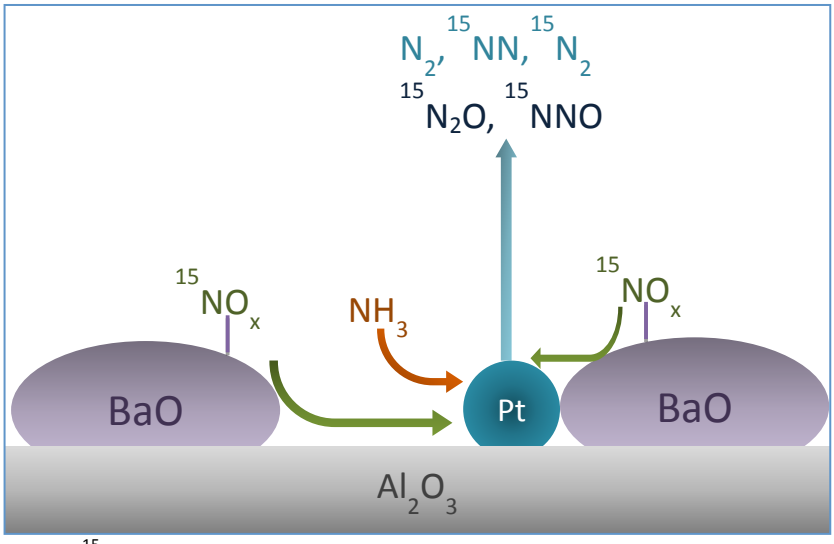

Fig.7 Reaction pathway for $^{15}NO_x$ reduction over Pt–Ba/Al_2O_3 catalyst

In the scheme depicted above, NO is decomposed at reduced Pt sites to form N- and O-ad-atoms (reaction (5)). Complete ammonia dehydrogenation (reaction (7)) leads to the formation of N- and H-ad-atoms, which in turn keep clean the Pt surface from O-ad-atoms via reaction (9). Eventually nitrogen formation

occurs through recombination of N-ad-atoms (reactions (8a)-(8c)), that produces all di-nitrogen isotopes with a distribution which depends on the surface concentration of ^{14}N- and ^{15}N-adatoms and can be derived on a statistical basis. At variance with the SCR pathway, this route does not result in the selective formation of only single labeled $^{14}N^{15}N$ species. The concentration of $^{14}N^{15}N$ is limited to a maximum of 50% of total di-nitrogen species and this occurs with equal coverage of ^{14}N- and ^{15}N-ad-species.

Figure 8 shows the concentration of the $^{14}N^{15}N$ isotope in % of total N_2 as function of time during NH_3-TPSR and NH_3-ISC experiments with nitrites and nitrates, calculated from the data of Figures 2-5. The abundance of the mixed $^{14}N^{15}N$ species is higher than 50% in the case of nitrites at the beginning of the experiments, up to 70% of total N_2 in the case of NH_3-TPSR (panel A) and up to 90% of total N_2 in the case of NH_3-ISC (panel B). This cannot be explained only with the statistical coupling of the N-ad-atoms formed upon adsorption/decomposition of stored $^{15}NO_x$ and of $^{14}NH_3$ but the occurrence of a SCR-like route involving the coupling of un-dissociated $^{15}NO_x$-derived species and of ammonia fragments (e.g. NH_2) must also be invoked (see Otto et al.[39]):

$$^{14}NH_{2(a)} + {}^{15}NO_{(a)} \rightarrow {}^{14}N^{15}N_{(g)} + H_2O_{(a)} + s \qquad (10)$$

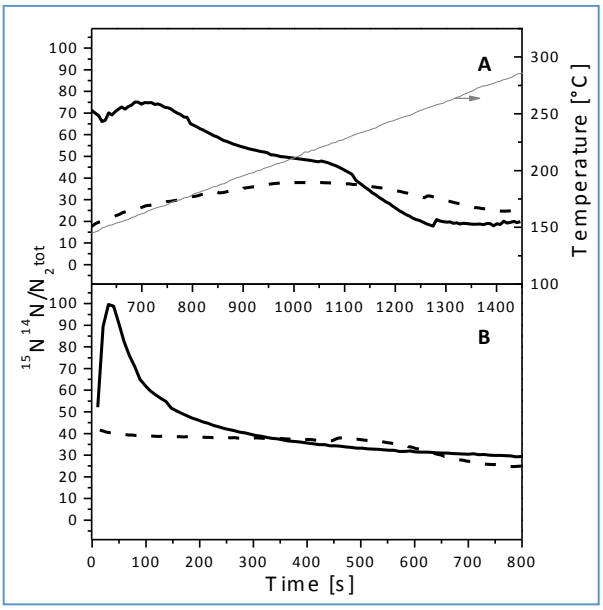

Fig. 8 $^{14}N^{15}N$ % concentration measured during TPSR (A) and ISC (B) experiments carried out after NO_x adsorption (1000 ppm ^{15}NO + O_2 3% v/v in He) at 150°C (solid lines) and at 350°C (dashed lines).

The occurrence of the SCR-like route is more favored in the case of nitrites possibly in view of the corresponding formal oxidation number of N in ammonia and nitrites (-3 and +3, respectively) which favors the formation of the NH_x-NO surface intermediate[31].

As pointed out by Kondratenko and Baerns [34], in the formation of N_2 over Pt the statistical coupling of N-ad-atoms and the SCR-like pathway may co-exist; the contribution of these routes in the formation of di-nitrogen depends on the relative coverage by adsorbed NO and NH_3, and on temperature [38]. Accordingly

changes in the concentration of the $^{14}N^{15}N$ species with time in Figure 8 are likely associated to changes in the surface concentration of NH_3- and nitrite- or NO-derived surface species.

The results obtained in the reduction of the stored nitrates show some distinct features. First of all the selective formation of only mixed $^{14}N^{15}N$ species is not possible in NH_3-TPSR and NH_3-ISC of nitrates. In fact the formation of the double labeled $^{14}N_2$ isotope is expected in view of the molar ratio $^{14}NH_3/^{15}NO_3^-$ = 10/6 > 1 dictated by the stoichiometry of reaction (2). Figures 4 and 5 show that all the possible N_2 isotopes are formed in the reduction of nitrates with ammonia and that the phase differences of the distribution of isotopic di-nitrogen species is limited. Figure 8 (panels C and D) also shows that the abundance of the $^{14}N^{15}N$ species is still high but less that 50% of total N_2 so that it is not necessary to invoke a SCR-like pathway in the case of nitrates although it cannot be excluded. On the other hand the formation of di-nitrogen isotopes originating from the self-coupling of $^{15}NO_x$-derived species (i.e. $^{15}N_2$) provides evidence for the occurrence of statistical coupling of the N-ad-species.

Finally, in the reduction of gas-phase ^{15}NO with NH_3 in the absence of oxygen according to reaction (11):

$$6\ ^{15}NO + 4\ NH_3 \rightarrow 5\ N_2 + 6\ H_2O \qquad (11)$$

the following statistical isotope distribution is expected for the pathway based on the statistical recombination of N-ad-atoms formed by dissociation of NO and NH_3 at Pt sites for the feed of Figure 6: $^{14}N^{15}N/\ ^{15}N_2/^{14}N_2$ = 48/36/16. The isotope distribution calculated from Figure 6 at T > 200°C where the N_2 selectivity is complete is $^{14}N^{15}N/\ ^{15}N_2/^{14}N_2 \approx$ 52/31/17. This distribution compares well with that listed above and is fully consistent with the recombination pathway of N-ad-atoms formed by decomposition of gas phase NO and NH_3 at Pt sites. However the SCR route, that might be involved in the formation of single labeled N_2, cannot be excluded.

Formation of N_2O – Small and almost negligible amounts of N_2O have been observed during NH_3-TPRS and NH_3-TPR of nitrites (Figures 2 and 3) and of nitrates (Figures 4 and 5) respectively, while relevant quantities of N_2O have been detected during the NH_3 + NO reaction (Figure 6). Notably only the formation of labeled nitrous oxide (i.e. $^{15}N_2O$ and $^{14}N^{15}NO$) has been observed during these experiments.

For comparison purposes, Figure 9 shows the N_2O concentration during NH_3-TPSR of nitrites (panel A) and during TPR of NH_3 and NO (panel B). The results obtained during the TPR of NH_3 and NO in the presence of O_2 (not presented previously) are also shown (panel C).

Inspection of Figure 9 shows that N_2O formation is poor during the reaction of stored NO_x with ammonia (TPSR of nitrites, Figure 9, panel A) but is noticeable when NO is present in the feed gas (NH_3 + NO reaction, Figure 9, panel B): in this last case N_2O concentration is greater by one order of magnitude. A further increase in N_2O concentration is seen when oxygen is present in the feed gas (Figure 9, panel C). These results and the fact that only labeled N_2O species are detected (if one neglects the small amounts of unlabeled N_2O observed at high temperature in Figure 9, panel C), indicate that adsorbed ^{15}NO takes part in

the formation of nitrous oxide. This is in line with literature proposals [34,40] where nitrous oxide is formed either by coupling of two adsorbed NO molecules (reaction (12)), or by recombination of an adsorbed NO molecule with an adsorbed NH_x fragment (reaction (13)):

$$2\ {}^{15}NO_{(a)} \rightarrow {}^{15}N_2O_{(g)} + O_{(a)} + s \qquad (12)$$

$${}^{14}NH_{x(a)} + {}^{15}NO_{(a)} \rightarrow {}^{14}N^{15}NO_{(g)} + x\ H_{(a)} \qquad (13)$$

These reactions are expected to occur during TPR of ^{15}NO + $^{14}NH_3$ (Figure 6 and Figure 9, panel B), and result in the formation of only double- and single-labeled N_2O species; the formation of unlabeled N_2O is not possible. On the other hand, during the reduction of stored nitrites $^{15}NO_2^-$ (Figure 9, panel A), the rate of nitrous oxide formation is limited by the low concentration of ^{15}NO-ad-species originated upon nitrite decomposition/reduction at Pt sites. Accordingly the reduction is very selective to di-nitrogen.

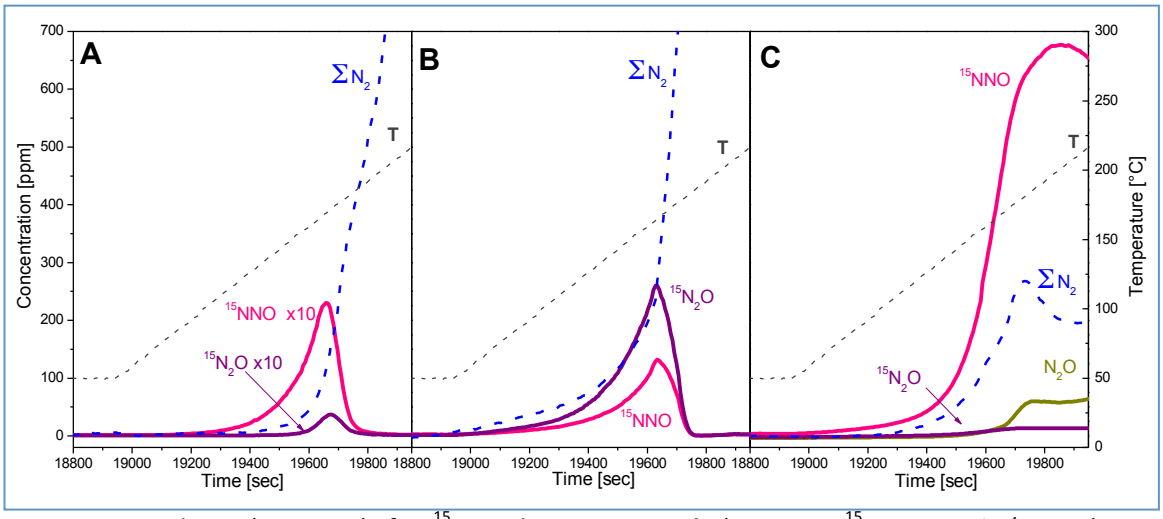

Fig. 9 A: TPSR run with NH_3 (1000ppm) after $^{15}NO_x$ adsorption at 150°C (1000 ppm ^{15}NO + O_2 3% v/v in He), B: TPR run with NH_3 (660 ppm) and ^{15}NO (1000 ppm) in He, C: TPR run with NH_3 (660 ppm), ^{15}NO (1000 ppm) and O_2 (3% v/v) in He over Pt-Ba/Al_2O_3 catalyst

Notably, nitrous oxide formation is strongly affected by temperature: in fact above 180 °C the N_2O concentration is always negligible in the absence of oxygen (Figure 9, panels A and B). It is suggested that at high temperature NO dissociation is favored because Pt is kept in a reduced state by ammonia, and this prevents N_2O formation due to the lack of molecularly adsorbed NO species. Along similar lines, the nitrous oxide concentration is markedly greater in the presence of oxygen in the feed stream (compare Figure 9, panels B and C) because NO dissociation is prevented over the oxygen-covered Pt surface and this increases the concentration of NO ad-species.

However, under reducing conditions the possibility that N_2O is reduced to N_2 cannot be excluded. In this light the decrease in N_2O concentration which is seen upon increasing the temperature in the absence of oxygen (Figures 9, panels A and B) might be due to the reduction of N_2O to give N_2[41] . This route may contribute only to the formation of single and double labeled N_2 molecules in the experiments of Figures 9

panel A (i.e. Figure 2) and panel B (i.e. Figure 6) but not in the formation of unlabeled N_2 because of the lack of $^{14}N_2O$ and of the fact that the reduction of N_2O does not involve the cleavage of the N-N bond[41].

Worth to note the presence of oxygen in the feed changes the nitrous oxide isotopic distribution during the TPR of NH_3+NO (compare Figure 9 panel B and panel C). In fact while in the absence of oxygen the double labeled nitrous oxide isotope ($^{15}N_2O$) prevails over the single labeled species ($^{14}N^{15}NO$) (Figure 9 panel B), in the presence of oxygen (Figure 9 panel C) the formation of the double labeled nitrous oxide molecule is negligible. Indeed the abundance of adsorbed oxygen drives reaction (12) from right to left so that the formation of $^{15}N_2O$ is less favored. On the other hand, since the overall nitrous oxide concentration is greater in the presence of oxygen, it turns out that reaction (13) must be favored by O_2 concentration. As a matter of fact, it has also reported that the presence of adsorbed oxygen species favors ammonia activation yielding reactive NH_x adsorbed intermediates [38]. This may result in the presence of a pool of unlabeled NH_x fragments whose reaction with molecularly adsorbed ^{15}NO results in the formation of single labeled nitrous oxide molecule (reaction (13)), as indeed observed. Notably, nitrous oxide formation due to ammonia oxidation, i.e. reaction (14):

$$2\ {}^{14}NH_{x(a)} + (x+1)\ O_{(a)} \rightarrow {}^{14}N_2O_{(g)} + x\ H_2O \qquad (14)$$

is limited compared to reaction (13) during the TPR of NH_3 + NO in the presence of oxygen (Figure 9, panel C) as pointed out by the relatively small amounts of unlabeled N_2O as compared to $^{15}N^{14}NO$.

Finally, it is noted that small amounts of N_2O are detected at low temperature during the TPSR of stored nitrites (Figures 2 and 3), whereas the reaction is very selective to nitrogen in the case of nitrates (Figures 4 and 5). As shown by dedicated TPD and H_2-TPSR experiments carried out over the stored nitrites and nitrates (not reported for the sake of brevity), the reduction/decomposition of nitrites onto the Pt sites occurs at lower temperatures than that of nitrates. This may lead, upon nitrite reduction, to the formation of NO-related intermediate ad-species that at low temperatures are involved in nitrous oxide formation. In fact these species are not readily decomposed to N- and O-ad-atoms due to the poor reducing capability of ammonia. At variance, the reduction/decomposition of nitrates is observed at slightly higher temperatures, and this would favor the decomposition of the NO-related adsorbed intermediates.

Conclusions.

In this paper mechanistic aspects involved in the formation of N_2 and N_2O during the reduction of NO_x stored over a model $PtBa/Al_2O_3$ NSR catalyst have been investigated by means of isotopic labeling experiments. The combined use of MS, UV-Vis and GC analysis has been adopted to allow a complete quantitative analysis of the reaction products.

The reduction of stored labeled NO_x species (nitrites and nitrates) with unlabeled NH_3 leads to the selective formation of N_2, since only very small amounts of nitrous oxide have been observed in the reduction of

nitrites only. The observed N_2 isotopic distribution includes all possible N_2 isotopes, i.e. $^{15}N_2$, $^{14}N_2$ and the mixed $^{15}N^{14}N$ species. Based on the pathway suggested for NO and NH_3 reaction on Pt-based catalysts, it has been found that the observed product distribution can be explained on the basis of the statistical coupling of ^{15}N- and ^{14}N-adatoms originated upon NH_3 and NO_x decomposition on Pt. However the simultaneous occurrence of a SCR-like pathway, involving the formation and decomposition of a NH_x-NO intermediate originating from ammonia and NO_x, and leading to the selective formation of the mixed $^{15}N^{14}N$ species is also likely. In fact at the early stages of the reduction of stored labeled nitrites with unlabeled ammonia the reduction process is selective towards the formation of the mixed $^{15}N^{14}N$ isotope, suggesting the occurrence of a SCR-like pathway.

Isotopic labeling experiments also provide indications on the pathways involved in the formation of N_2O. This species is formed in very limited amounts during the reduction by ammonia of stored NOx species (nitrites and nitrates); much higher quantities have been observed during the reduction of gaseous ^{15}NO with NH_3. Since no formation of unlabeled nitrous oxide has been observed, the participation of ^{15}NO is necessary for the formation of nitrous oxide. In line with literature proposals, it has been suggested that nitrous oxide formation involves (on the Pt sites) either the coupling of two adsorbed NO molecules or the recombination of an adsorbed NO molecule with an adsorbed NH_x fragment. Accordingly, N_2O formation is greatly enhanced in the presence of gas-phase NO.

Temperature also drives the selectivity to nitrous oxide. This product is favored at low temperature and is likely related to the oxidation state of Pt: at high temperatures Pt is kept in a reduced state by ammonia, and this would favor NO dissociation on the Pt sites thus preventing N_2O formation. Besides, N_2O could be reduced to N_2. The presence of oxygen in the feed stream favors N_2O formation, since it increases the concentration of molecularly adsorbed NO species and inhibits N_2O reduction. The route involving the coupling of NO-ad-species is however inhibited by the presence of oxygen, and hence nitrous oxide formation involves adsorbed NO and NH_x fragments.

References

([1]) Johnson, T. V. Diesel Emission Review. *SAE Int. J. of Eng.* **2011**, *4*, 143.

([2]) Granger, P.; Parvulescu, V. I. Catalytic NOx Abatement Systems for Mobile Sources: From Three-Way to Lean Burn after-Treatment Technologies. *Chem. Rev*. **2011**, *111*, 3155.

([3]) Baiker, R. S. NO_x Storage-reduction catalysis: From mechanism and materials properties to storage-reduction performance. *Chem. Rev*. **2009**, *109*, 4054.

([4]) Takahashi, N.; Shinjoh, H.; Iijima, T.; Suzuki, T.; Yamazaki, K.; Yokota, K.; Suzuki, H.; Miyoshi, N.; Matsumoto, S.; Tanizawa, T.; Tanaka, T.; Tateishi, S.; Kasahara K. The new concept 3-way catalyst for automotive lean-burn engine: NO_x storage and reduction catalyst. *Catal. Today* **1996**, *27*, 63.

([5]) Epling, W.; Campbell, L.; Yezerets, A.; Currier, N.; Parks, J. Overview of the Fundamental Reactions and Degradation Mechanism of NO_x Storage/Reduction Catalysts. *Catal. Rev. Sci. Eng.* **2004**, *46*, 163.

([6]) Miyoshi, N.; Matsumoto, S.; Katoh, K.; Tanaka, T.; Harada, J.; Takahashi, N.; Yokota, K.; Sugiura, M.; Kasahara, K. Development of New Concept Three-Way Catalyst for Automotive Lean-Burn Engines. *SAE Technical Paper* **1995**, 950809.

([7]) Johnson, T. Diesel Engine Emissions and Their Control. *Platinum Metals Rev.* **2008**, *52*, 23.

([8]) Castoldi, L.; Bonzi, R.; Lietti, L.; Forzatti, P. Catalytic behaviour of hybrid LNT/SCR systems: Reactivity and in situ FTIR study. *J. Catal*. **2011**, *1*, 128.

([9]) Toops, T. J.; Smith, D. B; Partridge, W. P.; NO_x adsorption on $Pt/K/Al_2O_3$. *Cat.Tod*. **2008,** *114*, 112.

([10]) Konsolakis, M.; Yentekakis, I. V. Strong Promotional effects of Li, K, Rb and Cs on the Pt-catalysed reduction of NO by propene. *Appl. Catal. B. Env.* **2001**, *29*, 103.

([11]) Nova, I.; Lietti, L.; Castoldi, L.; Tronconi, E.; Forzatti, P. New Insights in the NO_x Reduction Mechanism with H_2 over $Pt\text{-}Ba/\gamma\text{-}Al_2O_3$ Lean NO_x Trap Catalysts under near-isothermal Conditions. *J. Catal.* **2006**, *239*, 244.

([12]) Breen, J. P.; Burch, R.; Fontaine-Gautrelet, C.; Hardacre, C.; Rioche, C. Insight into the key aspects of the regeneration process in the NO_x storage reduction (NSR) reaction probed using fast transient kinetics coupled with isotopically labelled ^{15}NO over Pt and Rh-containing Ba/Al_2O_3 catalysts. *Appl. Catal. B Env*. **2008**, *81*, 150.

([13]) Lietti, L.; Nova, I.; Forzatti, P. Role of Ammonia in the Reduction by Hydrogen of NO_x Stored over $Pt\text{-}Ba/Al_2O_3$ Lean NO_x trap Catalysts. *J. Catal.* **2008**, *257*, 270.

([14]) Cumaranatunge, L.; Mulla, S. S.; Yezerets, A; Currier, N. W.; Delgass, W. N.; Ribeiro, F. H. Ammonia is a hydrogen carrier in the regeneration of $Pt/BaO/Al_2O_3$ NO_x traps with H_2. *J. Catal.* **2007**, *246*, 29.

([15]) Bhatia, D.; Harold, M. P.; Balakotaiah, V. Modeling the effect of Pt dispersion and temperature during anaerobic regeneration of a lean NO_x trap catalyst. *Catal. Today* **2010**, *151*, 314.

([16]) Castoldi, L.; Nova, I.; Lietti L.; Tronconi, E.; Forzatti, P. The NO_x reduction mechanism by H_2 under near isothermal conditions over Pt-Ba/Al_2O_3 Lean NO_x Trap systems. *Top. Catal*. **2007**,*42-43*, 189.

([17]) Nova, I.; Lietti, L.; Forzatti, P. Mechanistic Aspects of the Reduction of Stored NO_x over Pt-Ba/Al_2O_3 Lean NO_x Trap Systems. *Catal. Today* **2008**, *136*, 128.

([18]) Forzatti, P.; Lietti, L.; Nova, I. On Board Catalytic NO_x Control: Mechanistic Aspects of the Regeneration of Lean NO_x Traps with H_2. *Energy. Environ. Sci*. **2008,** *1*, 236.

([19]) Partridge, W. P.; Choi, J. S. NH_3 formation and utilization in regeneration of Pt/Ba/Al_2O_3 NO_x storage-reduction catalyst with H_2, *Appl. Catal. B Env*. **2009**, *91*, 144.

([20]) Forzatti, P; Lietti, L. ; Gabrielli N. A kinetic study of the reduction of NO_x stored on Pt-Ba/Al_2O_3 catalyst. *Appl. Catal. B Env* **2010**, 99, 145.

([21]) Mulla, S. S.; Chaugule, S. S.; Yezerets, A.; Currier, N. W.; Delgass, W. N.; Ribeiro, F. H. Regeneration Mechanism of Pt/BaO/Al_2O_3 Lean NO_x Trap Catalyst with H_2. *Catal. Today*. **2008**, *136*, 136.

([22]) Castoldi, L.; Nova, I.; Lietti, L.; Forzatti, P. Study of the Effect of Ba Loading for catalytic Activity of Pt-Ba/Al_2O_3 Model Catalysts. *Catal. Today* **2004**, *96*, 43.

([23]) Miyoshi, N.; Tanizawa, T.; Kasahara, K.; Tateishi, S. European Patent Application 0 669 157 A1, **1995.**

([24]) Nova, I.; Castoldi, L; Prinetto, F.; Dal Santo, V.; Lietti, L.; Tronconi, E.; Forzatti, P.; Ghiotti, G.;. Psaro, R.; Recchia, S. NO_x adsorption study over Pt-Ba/alumina catalysts: FT-IR and reactivity study. *Top. Catal.* **2004**, *30/31*, 181.

([25]) Prinetto, F.; Ghiotti, G.; Nova, I.; Castoldi, L.; Lietti, L.; tronconi, E.; Forzatti, P. In situ Ft-IR and reactivity study of NO_x storage over Pt–Ba/γ-Al_2O_3 catalysts. *Phys. Chem. Chem. Phys.* **2003**, *5*, 4428.

([26]) Nova, I.; Castoldi L.; Lietti L.; Tronconi, E.; Forzatti, P.; Prinetto, F.; Ghiotti, G. NO_X adsorption study over Pt-Ba/alumina catalysts: FT-IR and pulse experiments. *J. Catal* **2004**, *222*, 377.

([27]) Lietti, L.; Daturi, M.; Blasin-Aubé, V.; Ghiotti, G.; Prinetto, F.; Forzatti, P. Relevance of nitrite route in the NO_x adsorption mechanism over Pt-Ba/Al_2O_3, NSR catalysts investigated by FT-IR operando spectroscopy. *Chem Cat. Chem.* **2012**, *4*, 55.

([28]) Ozkan, U. S; Cai, Y.; Kumthehkar, M. W. Investigation of the Reaction Pathways in Selective Catalytic Reduction of NO with NH_3 over V_2O_5 Catalysts: Isotopic Labeling Studies Using $^{18}O_2$, $^{15}NH_3$, ^{15}NO, and $^{15}N^{18}O$. *J. Catal.* **1994**, *149*, 390

([29]) Chen, H.; Sun, Q. ; Wen, B.; Yeom, Y.; Weiz, E. ; Sachtler, W. M. Reduction over zeolite-based catalysts of nitrogen oxides in emissions containing excess oxygen: Unraveling the reaction mechanism. *Catal. Today* **2004**, *96* ,1.

([30]) Janssen, F .J J. G.; Van Den Kerkhof, F. M. G. ; Bosh, H. ; Ross, J. R. H. Mechanism of the Reaction of Nitric Oxide, Ammonia and Oxygen over Vanadia Catalysts 1. The Role of Oxygen Studied by Way of Isotopic Transient under Dilute Conditions. *J. Phys. Chem.* **1987**, *91*, 6633.

([31]) Busca, G.; Lietti, L.; Ramis G.; Berti, F. Chemical and mechanistic aspects of the selective catalytic reduction of NO_x by ammonia over oxide catalysts: a review. *Appl. Catal. B. Env.* **1998**, *18*, 1.

([32]) Yeom, Y.;. Li, M ; Savara, A.;. Sachtler, W; Weitz E. An overview of the mechanisms of NOx reduction with oxygenates over zeolite and γ-Al_2O_3 catalysts. *Catal. Today* **2008**, *136*, 55.

([33]) Kumar, A.; Harold, M. P.; Balakotaiah, V. Isotopic studies of NO_X storage and reduction on Pt/BaO/Al_2O_3 catalyst using temporal analysis of products. *J. Catal.* **2010**, *270*, 214.

([34]) Kondraratenko, V. A.; Baerns, M. Mechanistic insights into the formation of N_2O and N_2 in NO reduction by NH_3 over a polycrystalline platinum catalyst. *Appl. Catal. B. Env*. **2007**, *70*, 111.

([35]) Van Tol, M. F. H.; Siera, J.; Cobden, P. D.; Nieuwenhuys, B. E. Oscillatory behavior of the reduction of NO by H_2 over Rh. *Surface Sci.* **1992**, *274*, 63.

([36]) Nova, I.; Castoldi, L. ; Lietti, L.; Tronconi, E.; Forzatti, P.; Prinetto, F.; Ghiotti, G. The Pt-Ba interaction in Lean NO_x Trap systems. *SAE Technical Paper* **2005**, 2005-01-1085.

([37]) Nova, I.; Castoldi, L.; Lietti, L.; Tronconi, E.; Forzatti, P. A Low Temperature Pathway Operating the Reduction of Stored Nitrates in Pt-Ba/Al_2O_3 Lean NO_x Trap Systems. *SAE Technical Paper* **2006**, 2006-01-1368.

([38]) Perez-Ramirez, J.; Kondratenko, E. V.; Kondratenko, V. A.; Baerns, M. Selectivity-directing factors of ammonia oxidation over PGM gauzes in the Temporal Analysis of Products reactor: Secondary interactions of NH_3 and NO. *J. Catal.* **2005**, *229*, 303.

([39]) Otto, K.; Shelef, M.; Kummer J. T. Studies of surface reactions of nitric oxide by nitrogen-15 isotope labeling. I. Reaction between nitric oxide and ammonia over supported platinum at 200-250.deg. *J. Phys. Chem*. **1970**, *74*, 2690.

([40]) Burch, R.; Shestov, A. A.; Sullivan J. A. A Steady-State Isotopic Transient Kinetic Analysis of the $NO/O_2/H_2$ Reaction over Pt/SiO_2 Catalysts. *J. Catal.* **1999**, *188*, 69.

([41]) Cant, N. W; Chambers, D. C.; Liu, I. O. Y. The reduction of $^{15}N^{14}NO$ by CO and by H_2 over Rh/SiO_2: a test of a mechanistic proposal. *J. Catal.* **2011**, *278*, 162.

Paper VIII

Catalytic NO Oxidation Pathways and Redox Cycles on Dispersed Oxides of Rhodium and Cobalt

Brian M. Weiss, Nancy Artioli, and Enrique Iglesia
DOI: 10.1002/cctc.200

Catalytic NO Oxidation Pathways and Redox Cycles on Dispersed Oxides of Rhodium and Cobalt

Abstract

The elementary steps and site requirements of NO oxidation on Rh and Co catalysts and their respective oxidation states during catalysis were probed using isotopic tracer and chemisorption techniques combined with the measured kinetic consequences of NO, O_2, and NO_2 pressures on turnover rates. On both catalysts, NO oxidation rates were first-order in NO and O_2 and inversely proportional to NO_2 pressure, as also observed on Pt and PdO. These data suggest O_2 activation on isolated vacancies (*) on surfaces of Rh and Co oxides saturated with oxygen (O*) is the sole kinetically-relevant step.

Quasi-equilibrated NO-NO_2 interconversion steps establish oxygen chemical potentials (and O* and * coverages) on these oxides during catalysis. These chemical potentials determine the oxidation state of Rh and Co clusters and are rigorously described by the prevalent O_2 virtual pressures, which are estimated using the formalism of nonequilibrium thermodynamics. RhO_2 and Co_3O_4 are the prevalent phases present during NO oxidation catalysts at relevant conditions.

Turnover rates increased with increasing cluster size because vacancies, required for kinetically-relevant O_2 activation steps, are more abundant on large clusters, which delocalize electron density more effectively than small oxide clusters. NO oxidation turnover rates on RhO_2 and Co_3O_4 are higher than expected from the oxygen binding energy on Rh and Co metal surfaces or from the reduction potentials of Rh^{3+} and Co^{2+}. NO oxidation rates fall in line with those measured on Pt and PdO when one-electron reductions processes, accessible for Rh^{4+} and Co^{3+} but not for Pt^{2+} and Pd^{2+}, are used to describe the reactivity of RhO_2 and Co_3O_4. Such one-electron redox cycles also cause $^{16}O_2$-$^{18}O_2$ exchange rates to be much larger than NO oxidation rates, in contrast with their similar values on Pt and PdO, though O_2 activation on vacancies limits both NO oxidation and O_2 exchange on all catalysts. One-electron redox cycles allow electron sharing between metal cations and a more facile route for vacancy formation on RhO_2 and Co_3O_4, leading to high NO oxidation rates.

These data and their interpretation in terms of elementary steps, the role of vacancies in kinetically-relevant O2 activation steps, and the consequent higher reactivity of larger clusters provide a common framework to describe NO oxidation and the active species on catalysts of practical interest.

Keywords

Lean NOx traps • NOx storage and reduction • Structure sensitivity

Introduction

Nitrogen oxides must be removed from combustion exhaust to meet environmental regulations, which is challenging for streams that contain O_2 and low concentrations of CO and hydrocarbons. Catalyst sites are titrated by strongly-bound chemisorbed oxygen atoms (O*) during NO decomposition in the absence of reductants. As a result, open sites on O*-saturated surfaces, required for NO dissociation, are scarce [1,2]. Such conditions cause low NO conversions to N_2 and favor instead NO oxidation to NO_2. NO_2, however, adsorbs on metal oxides [3-5] and reduces to N_2 when soot or hydrocarbons are present in exhaust streams [6-9]. These reactions provide an alternate abatement strategy for NO removal from lean-burn effluent streams, but require effective catalysts for NO oxidation to NO_2.

NO oxidation on Pt [10-12] and PdO [13] clusters involves kinetically-relevant O_2 adsorption on vacant sites (*) at O*-saturated surfaces. O* coverages during NO oxidation are set by equilibrated NO-NO_2 interconversions [11-13]. The kinetic relevance of O_2 binding was confirmed by the identical rates of $^{16}O_2$-$^{18}O_2$ isotopic exchange and NO oxidation [12,13]. These studies showed that NO oxidation rates decrease as metal or oxide cluster size decreases because small clusters bind O* more strongly than larger clusters, leading to low vacancy concentrations.

NO oxidation is also catalyzed by Rh and Co clusters [14-16]. NO oxidation rates have been correlated with the reducibility of CoOx clusters [15], suggesting that O* binding and the availability of vacancies also determines turnover rates on Co-based catalysts. The rate data in previous studies were not attributed to specific elementary steps, which we do here using kinetic and isotopic methods for both RhO_2 and Co_3O_4 catalysts. We show that NO oxidation on these catalysts involves similar elementary steps and site requirements as those proposed on Pt and PdO catalysts.

The turnover rates for NO oxidation and isotopic oxygen exchange are higher on Rh and Co oxides than on PdO and small Pt clusters and also than rates expected from their metaloxygen bond energies. We attribute these findings to the ability of RhO_2 and Co_3O_4 to undergo facile one-electron oxidationreduction cycles during catalytic turnovers, which provides an alternate and more effective O_2 activation pathway than twoelectron reductions on Pt and Pd catalyst systems.

The turnover rates for NO oxidation and isotopic oxygen exchange are higher on Rh and Co oxides than on PdO and small Pt clusters and also than rates expected from their metaloxygen bond energies. We attribute these findings to the ability of RhO_2 and Co_3O_4 to undergo facile one-electron oxidationreduction cycles during catalytic turnovers, which provides an alternate and more effective O_2 activation pathway than twoelectron reductions on Pt and Pd catalyst systems.

Results and Discussion

1. NO Oxidation Kinetics on Rh and Co

NO oxidation rates were measured on Rh/Al_2O_3 and Co/SiO_2 as a function of the NO, NO_2, and O_2 pressures. The measured NO consumption rates reflect the dynamics of the forward ($\overset{f}{r}_{NO}$) and reverse ($\overset{s}{r}_{NO}$)directions of the stoichiometric chemical reaction:

$$2\ NO + O_2 \rightleftharpoons 2\ NO_2 \qquad (1)$$

which correspond to the rates of NO oxidation and NO_2 decomposition, respectively. The values of $\overset{f}{r}_{NO}$ and $\overset{s}{r}_{NO}$ are related by the approach-to-equilibrium factor (η) [18]:

$$\eta = \frac{\overset{s}{r}_{NO}}{\overset{f}{r}_{NO}} = \left([NO_2]^2\,[NO]^{-2}\,[O_2]^{-1}\,K_R^{-1} \right)^{\sigma} \qquad (2)$$

where σ is a constant derived from the stoichiometric number and reaction affinity for each elementary step [18] and K_R is the equilibrium constant for Eq. 1, estimated from tabulated thermodynamic data [17]. Forward NO oxidation turnover rates are obtained from measured NO conversion rates ($\overset{f}{r}_{NO}$) using:

$$r_{NO} = \overset{f}{r}_{NO} - \overset{s}{r}_{NO} = \overset{f}{r}_{NO}\left(1 - \eta\right) \qquad (3)$$

Figure 1 shows the effects of NO, NO_2 and O_2 pressures on forward NO oxidation turnover rates on Rh and Co catalysts. On all catalysts, forward NO oxidation rates increased linearly with NO and O_2 pressures and were strongly inhibited by NO_2. The dashed lines in Fig. 1 show that these data are consistent with the form of Eq. 4 and a value of η equal to one.

$$\overset{f}{r}_{NO} = 2k_{NO}[O_2][NO][NO_2]^{-1} \qquad (4)$$

as shown by the dashed curves in Figure 1.

This NO oxidation rate expression (Eq. 4) also describes all rate data on Pt and PdO catalysts and is consistent with the elementary steps proposed previously for NO oxidation on these catalysts [10-13]. These steps involve kinetically-relevant O_2 binding at unoccupied sites (*) (Scheme 1, step 1.1) on cluster surfaces nearly saturated with chemisorbed oxygen atoms (O*). Adsorbed O_2 molecules (O_2*) dissociate to form oxygen atoms (O*) in subsequent kinetically-irrelevant steps (Scheme 1, step 1.2). The surface coverages of O* and * are set by quasiequilibrated steps involving the interconversion of NO and NO_2 on cluster surfaces (Scheme 1, step 1.3). These steps, taken together with the steady-state approximation for all adsorbed species leads to the rate equation:

$$\overset{f}{r}_{NO} = \frac{2k_1[O_2]}{1 + K_3[NO_2][NO]^{-1}} \qquad (5)$$

in which the denominator terms reflect the relative concentrations of * and O* during steady-state catalysis. This expression (Eq. 5) accurately describes all kinetic data (Eq. 4) only when O* is the most abundant surface intermediate (MASI):

$$r_{NO} = \frac{2k_1}{K_3}\frac{[O_2][NO]}{[NO_2]} \qquad (6)$$

Measured rates therefore indicate that surfaces are nearly saturated with O* and that the measured rate constant (k_{NO}) (Eq. 4) is proportional to the ratio of k_1 and K_3.

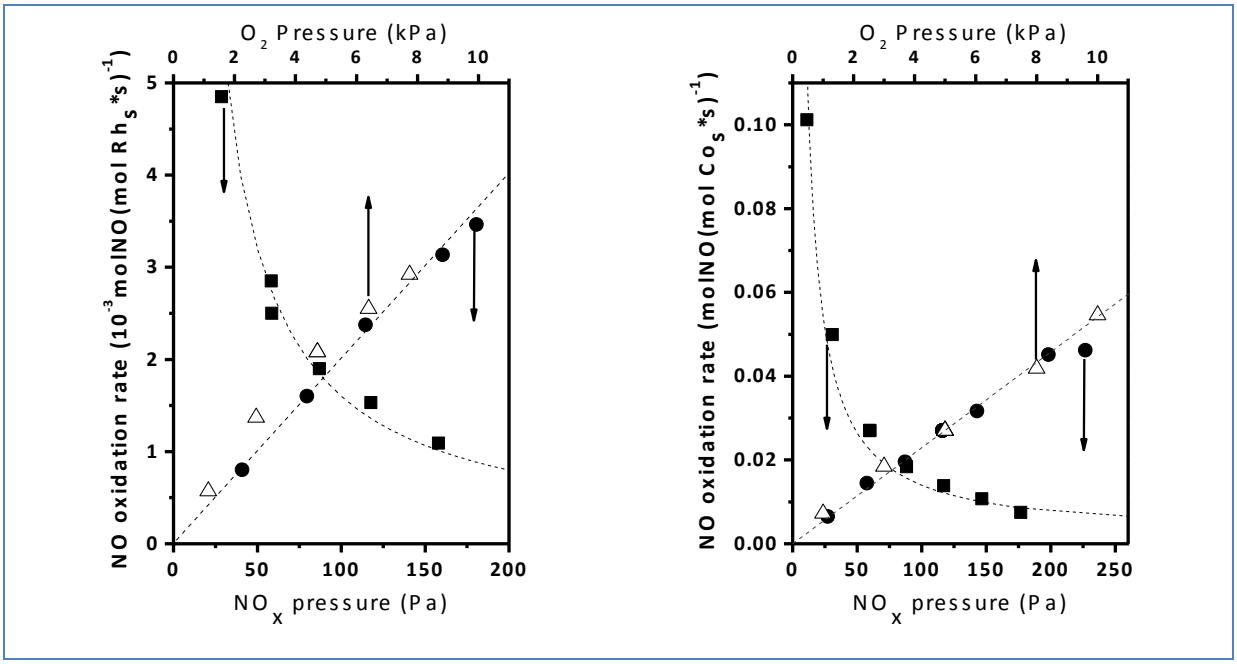

Figure 1. NO oxidation rates **(a)** on 2.4% wt. RhO_2/Al_2O_3 (573 K; 0.47 H / Rh) versus (●) NO pressure (at 0.055 kPa NO_2; 5 kPa O_2); (■) NO_2 pressure (at 0.11 kPa NO, 5 kPa O_2); and (△) O_2 pressure (at 0.11 kPa NO, 0.055 kPa NO_2) and **(b)** on 10% wt. Co_3O_4/SiO_2 (548 K; 0.02 H / Co_r) versus (●) NO pressure (at 0.060 kPa NO_2; 5 kPa O_2); (■) NO_2 pressure (at 0.12 kPa NO, 5 kPa O_2); and (△) O_2 pressure (at 0.12 kPa NO, 0.06 kPa NO_2).

Scheme 1. Proposed Elementary Steps for NO Oxidation

$$O_2 + * \overset{k_1}{\rightleftharpoons} O_2^* \qquad (1)$$

$$O_2^* + * \overset{k_2}{\rightleftharpoons} 2\,O^* \qquad (2)$$

$$NO + O^* \overset{K_3}{\rightleftharpoons} NO_2 + * \qquad (3)$$

O* coverages, as well as the driving force for the formation of Rh and Co oxides, depend on the oxygen chemical potentials at cluster surfaces. This oxygen chemical potential is rigorously given by a virtual oxygen pressure (O_2^v) during NO oxidation catalysis [12, 13]. O_2^v values are established by NO-NO_2 adsorption

equilibria, and its value is obtained by non-equilibrium thermodynamic treatments of chemical kinetics as [12, 13]:

$$[O_2^v] = [NO_2]^2 [NO]^{-2} K_R^{-1} \quad (7)$$

in which K_R is the equilibrium constant for Eq. 1 as written, which can be calculated from tabulated thermodynamic data. O_2^v equals the value of the O_2 pressure that gives the same O* coverage at equilibrium as the O* coverage during steady-state NO oxidation catalysis at a given NO_2/NO ratio.

The equilibrium constant for NO_2 dissociation (K_3, Scheme 1, Step 1.3) is related to the equilibrium constant for O_2 dissociation (K_O; Eq. 9) by [12, 13]:

$$K_3 = K_O^{1/2} / K_R^{1/2} \quad (8)$$

because the stoichiometry of step 1.3 corresponds to the difference between Eqs. 1 and 9:

$$2 * + O_2 \rightleftharpoons 2\ O* \quad (9)$$

Eqs. 5, 7, and 8 can be combined to show that NO oxidation rates depend only on the O_2(g) pressure and on the prevailing oxygen chemical potential, rigorously given by O_2^v:

$$r_{NO} = 2k_1[O_2][*] = \frac{2k_1[O_2]}{1+\left(K_O[O_2^v]\right)^{1/2}} \quad (10)$$

The assumption that O* is present at near saturation coverages leads to a simpler version of Eq. 10:

$$\frac{r_{O_2}}{[O_2]} = k_1[*] = \frac{k_1}{\left(K_O[O_2^v]\right)^{1/2}} \quad (11)$$

Thus, NO oxidation rates depend only on the O_2 pressure and on the chemical potential of oxygen at working catalytic surfaces. Eq. 11 is used in the sections that follow to probe any residual dependence of NO oxidation rate constants on O_2^v, indicative of structural or composition changes associated with phase transitions, and to compare NO oxidation rates with $^{16}O_2$-$^{18}O_2$ exchange rates at similar O* coverages.

2. Oxidation State of Rh and Co during NO Oxidation

The oxygen chemical potentials set by NO/NO_2 reactions on catalyst surfaces (Eq. 7) represent the rigorous thermodynamic driving force not only for the prevalent O* coverages but also for oxide-metal phase transitions during steady-state NO oxidation catalysis. Any changes in measured NO oxidation rate constants with O_2^v (Eq. 7) could reflect the occurrence of a phase transition consequential to catalysis, while rate constants that do not depend on O_2^v preclude phase transitions consequential for catalysis within the experimental range of conditions. The rearrangement of Eq. 11 given by:

$$\left(\frac{[O_2]}{r_{O_2}}\right)^2 = \frac{K_O}{k_1^2}[O_2^v] \quad (12)$$

describes all rate data, as shown by the linear dependence in Fig. 2. The consequent constant slope shows that NO oxidation rate constants on Rh and Co catalysts represent true constants unaffected by oxygen chemical potentials (0.01-0.4 and 0.001-0.15 kPa O_2^v for Rh and Co, respectively) or by any metal-oxide transitions. We conclude that the oxidation state of Rh and Co clusters remains unchanged throughout the conditions of this study and corresponds to the bulk phase dictated by these oxygen chemical potentials.

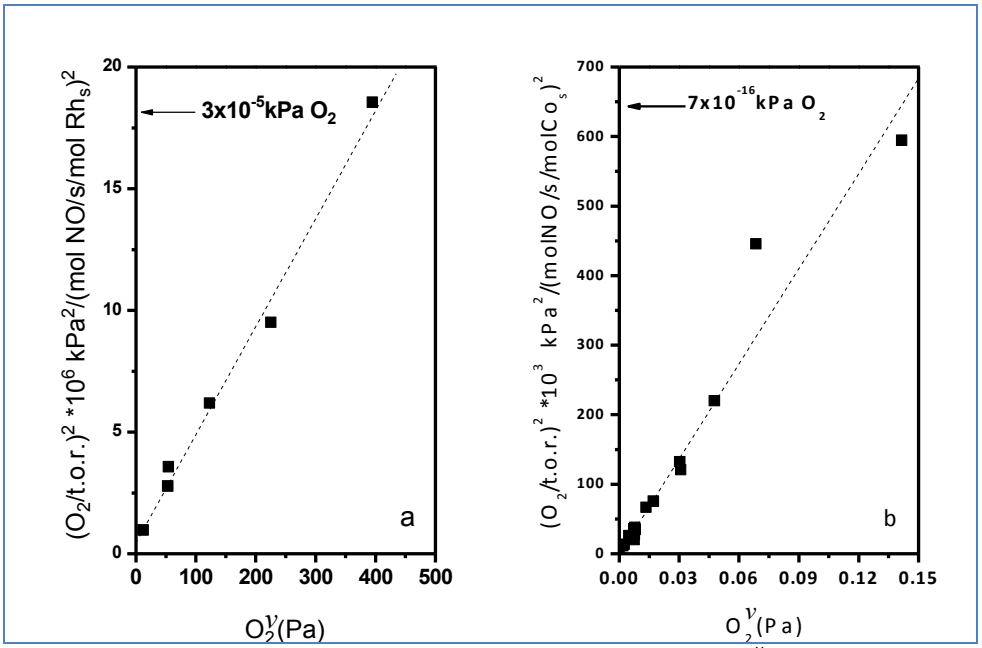

Figure 2. The NO oxidation kinetic response, $(O_2(g)/rNO)_2$, as a function of O_2^v (Eq. 7) on (a) RhO_2/Al_2O_3 (0.47 H/Rh; 573 K) and (b) Co_3O_4/SiO_2 (0.02 H/Cor; 548 K). The dashed line shows the fit to Eq. 11. The arrow indicates the O_2 pressure at the phase boundary between RhO_2/Rh_2O_3 [20] and Co_3O_4/CoO [17] in the respective plots

The phase diagram for bulk Rh oxides, [19] taken together with thermodynamic data for bulk Rh, Rh_2O_3 (ΔHf^o = -135 kJ (mol O)$^{-1}$), and RhO_2 (ΔHf^o = -122 kJ mol^{-1}) [20] and Co, CoO (ΔHf^o = -237 kJ (mol O)$^{-1}$), and Co_3O_4 (ΔHf^o = -223 kJ (mol O)$^{-1}$) [17] indicate that Rh and Co clusters exist as RhO_2 and Co_3O_4, respectively, at all conditions used in this study (573-673 K, 0.2-3.0 NO_2/NO, and 0.001-2 kPa O_2^v for Rh; 548-623 K, 0.25-2 NO_2/NO, and 0.0001-2 kPa O_2^v for Co). Rh and Co can form structures with lower oxidation states (Rh_2O_3 and CoO), but these oxides are stable only at significantly lower oxygen chemical potentials or higher temperatures than used here. For example, RhO_2/Rh_2O_3 and the Co_3O_4/CoO phase transitions occur at 10-6 and 10-14 kPa O_2, respectively, at 573 K. We conclude that the predominant phases of each catalyst are Co_3O_4 or RhO_2 during steady-state catalytic NO oxidation for clusters of all sizes.

The oxidation state of Co during catalysis was confirmed by O_2 uptakes in the temperature range of NO oxidation catalysis. The O_2 uptake at 548 K on Co/SiO_2 (0.02 H/Cor) was 0.57 mol O_2 (mol Co)$^{-1}$ (O/Co = 1.14) after the sample was treated in H_2 at 673 K for 1 h and remained unchanged between 5 and 60 kPa O_2 (Fig. 3). These data indicate that most Co atoms (85%) are present as Co3O4 upon contact with

O_2 and therefore with NO/NO_2 mixtures that provide equivalent oxygen chemical potentials during catalysis. The remaining Co atoms (15%) are present as Co silicates, which do not reduce during treatment in H_2 at 673 K [21] and therefore cannot uptake O_2. The constant uptakes with O_2 pressure (548 K, 5-60 kPa; Fig. 3) show that clusters do not change their oxidation state within this pressure range, as expected from thermodynamic data [17] and from measured rate constants that did not vary with O_2 pressure (Fig. 2b). Co^{3+} in Co_3O_4 and Rh^{4+} in RhO_2 can reduce to Co^{2+} in CoO and Rh^{3+} in RhO_2, respectively, via one-electron reductions. We infer in the next section that the availability of these one-electron oxidation-reduction cycles influence the pathways and dynamics of O_2 activation on RhO_2 and Co_3O_4 during both catalytic NO oxidation and $^{16}O_2$-$^{18}O_2$ isotopic exchange.

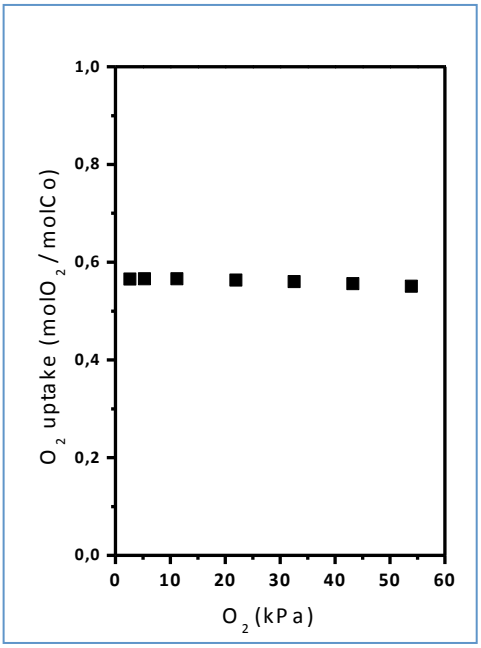

Figure 3. O_2 uptake at 548 K on 10% wt. Co/SiO_2 (0.02 dispersion) previously treated at 673 K with flowing 100 kPa H_2 for 1 h (0.1 cm^3 g^{-1} s^{-1}) and then under vacuum for 1 h.

3. $^{16}O_2$-$^{18}O_2$ Exchange and NO Oxidation Rates

$^{16}O_2$-$^{18}O_2$ isotopic exchange and NO oxidation (Scheme 1, step 1) share a common kinetically-relevant step (O_2 adsorption on vacant sites) on Pt and PdO clusters [12, 13]. On Pt and PdO, these two reactions occur at identical rates, irrespective of temperature or oxygen chemical potential, consistent with their common limiting elementary step. Similar experiments are used here to probe the kinetic relevance of O_2 activation during NO oxidation on RhO_2 and Co_3O_4 catalysts.

O_2 activation rates ($r_{O_2(ex)}$) were determined from measured $^{16}O_2$-$^{18}O_2$ isotopic exchange rates (r_{ex}) at 2 kPa O_2(g) in the absence of NOx using the equation:

$$r_{ex} = r_{O_2(ex)} \frac{[^{16}O_2][^{18}O_2]}{[O_2]^2}\left(1 - \frac{[^{16}O^{18}O]^2}{4[^{16}O_2][^{18}O_2]}\right) \qquad (13)$$

which describes measured steady-state exchange rates, irrespective of the mechanism of exchange [22]. In this equation, the terms in parenthesis account for the approach to isotopic equilibrium and the [O2] term denotes the sum of the pressures of all oxygen isotopologues ([$^{16}O_2$], [$^{18}O_2$], and [$^{16}O^{18}O$]). The $r_{O_2(ex)}$ term is the O_2 activation rate, which depends on the total O_2 pressure and on the coverage of vacancies (*) [22]. Previous rate data on Co_3O_4 and other Group VIII metal oxides indicate that O_2 exchange rates obey the equation [22]:

$$\frac{r_{O_2(ex)}}{[O_2]} = k_{ex}[*] = \frac{k_{ex}}{\left(K_O[O_2]\right)^{1/2}} \qquad (14)$$

in which k_{ex} is the rate constant for O_2 activation. Eq. 14 is consistent with a rate-determining step for exchange requiring isolated vacancies on surfaces nearly saturated with O*, as is also the case in NO oxidation reactions (Eq. 11). The density of vacancies (*) during exchange is given by the chemical equilibrium of Eq. 9 with KO as the equilibrium constant. Both Eq. 14, describing O_2 exchange rates, and Eq. 11, describing NO oxidation rates, probe O_2 activation rates on cluster, which depend only on the rate constant for O_2 activation and the availability of vacancies (*).

The rate constants of O_2 activation during exchange and during NO oxidation are shown in Fig. 4. NO oxidation rate constants were measured at $NO/NO_2/O_2$ pressures corresponding to O_2^v values of 2 kPa (Eq. 7) and compared with O_2 exchange rates measured at an actual total pressure of 2 kPa O_2(g).

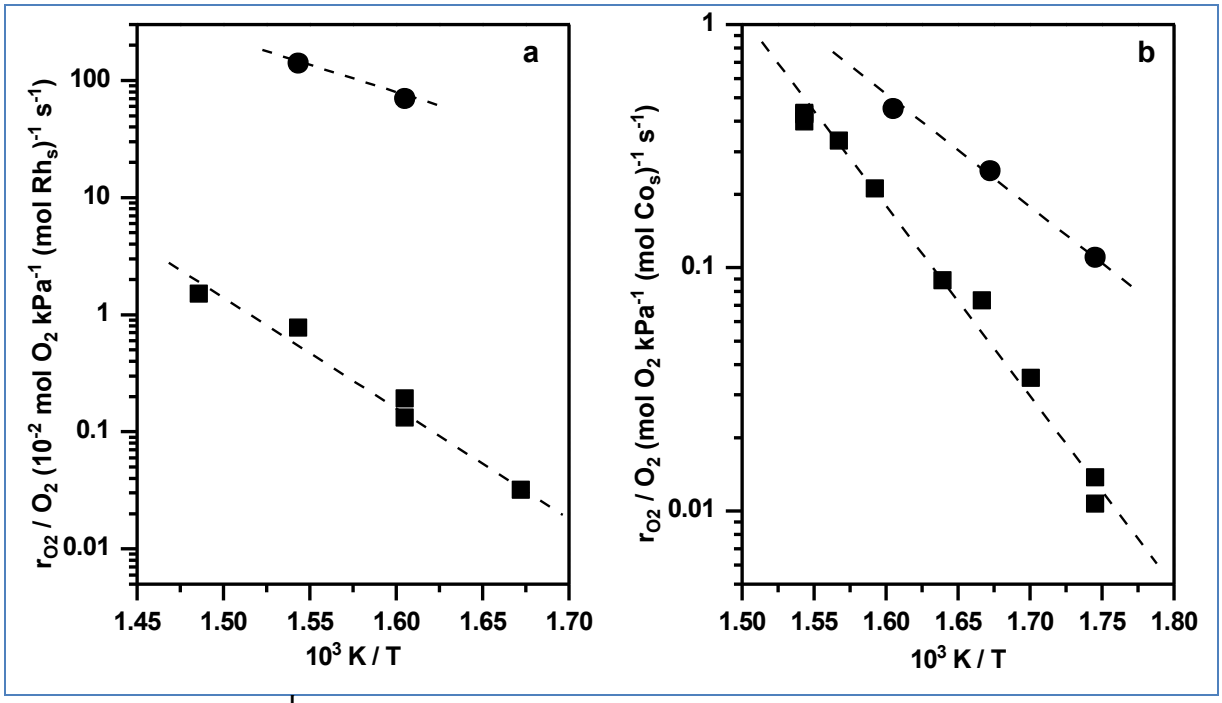

Figure 4. O_2 activation rates r_{O_2} divided by the prevalent O_2 pressure during (■) NO oxidation at 2 kPa O_2^v and during (●) O_2 exchange at 2 kPa O_2 on (a) 2.4% wt. Rh_2O_3/Al_2O_3 (0.47 dispersion) and (b) 10% wt. Co_3O_4/SiO_2 (0.01 dispersion).

Figure 4 shows that kex (Eq. 13) is larger than k1 (Eq. 11), by a factor of ~10 on Co_3O_4 and ~100 on RhO_2. Exchange rates depended more weakly on temperature than NO oxidation rates, suggesting that oxygen exchange has a lower activation energy than NO oxidation. These results contrast those reported previously on Pt and PdO clusters [12, 13], on which NO oxidation rate constants were the same within experimental accuracy.

The larger rate constants for exchange (k_{ex}) compared with those for NO oxidation (k_1) on RhO_2 and Co_3O_4 catalysts (Fig. 4) indicate that O_2 activation during $^{16}O_2$-$^{18}O_2$ exchange occurs via different kinetically-relevant steps than those required for O_2 activation in NO-O_2 reactions. $^{18}O_2$ exchange with lattice ^{16}O(^{16}O*) on some oxides [23] can occur via concerted three-atom transition states that mediate the O_2 activation and exchange elementary steps (Scheme 2). This step does not lead to O_2 dissociation and therefore it cannot contribute to NO oxidation turnovers, which require the ultimate dissociation of O_2* to form active O* species. The contributions of these three-atom transition states, in addition to those that can lead to both O_2 exchange and dissociation, is likely to contribute to O_2 exchange rates much larger than for O_2 activation during NO oxidation catalysis, even though both reactions are limited by elementary events that require the activation of O_2 via interactions with vacant sites on surfaces of clusters nearly saturated with oxygen.

Scheme 2. Proposed mechanism of $^{16}O_2$-$^{18}O_2$ exchange on Co_3O_4 and RhO_2

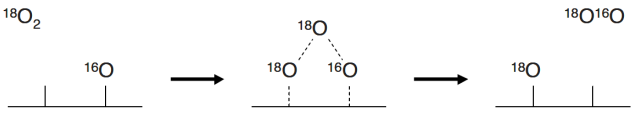

NO oxidation and O_2 exchange rates differ from each other on RhO_2 or Co_3O_4, but these two processes occur at similar rates on Pt [12] or PdO [13]. This different behavior of RhO_2 and Co_3O_4 compared with Pt and PdO may reflect the ability of each of these catalysts to transfer electrons into adsorbed dioxygen molecules, as previously proposed for O2 exchange [24]. Both Pd^{2+} [17] and Pt^{2+} [17] form Pd^0 or Pt^0 via direct two-electron reduction processes in aqueous electrochemical systems, but Co^{3+} [17] and Rh^{4+} [25,26] reduce sequentially via one-electron processes to Co^{2+} and Rh^{3+}, respectively, as is also the case for such cations in their respective bulk oxides. Co^{3+} in Co^3O^4 and Rh^{4+} in RhO_2 undergo one-electron reductions to form Co^{2+} centers in CoO and Rh^{3+} in Rh_2O_3, while Pd^{2+} in PdO and Pt^{2+} in PtO and Pt_3O_4 reduce directly to the respective metals. We infer from these differences between Pt^{2+}/Pd^{2+} and Co^{3+}/Rh^{4+} reduction paths that O_2 exchange may proceed via concerted reactions of O_2 with O* when metal centers at vacant sites can undergo a one-electron reduction processes. NO oxidation on Co_3O_4 and RhO_2 is slower than $^{16}O_2$-$^{18}O_2$ exchange apparently because more than one electron must be transferred to O_2 during the catalytic cycle for NO oxidation, but not during isotopic exchange.

In spite of these differences in O_2 activation modes on Co_3O_4, RhO_2, Pt and PdO, the kinetically-relevant step for NO oxidation on all catalytic systems is the activation of O_2 on scarce vacancies at surfaces nearly saturated with oxygen species, bound on Pt metal cluster surfaces and part of exposed planes in a bulk oxide for the others. This suggests that NO oxidation turnover rates on all materials depend on strength of surface metal-oxygen bonds, which determine the density of vacancies for any given oxygen chemical potential in the reacting mixture.

4. Site Requirements for NO Oxidation on Rh and Co Oxides

NO oxidation rates on Rh and Co oxides clusters were normalized by the H_2 uptake on the reduced catalyst to account for the fraction of sites on cluster surfaces. NO oxidation rates on dispersed RhO_2 clusters increased with increasing cluster size (Fig. 5), consistent with the trends reported on Pt [10, 12] and PdO [13] (Fig. 5). Oxide clusters become more difficult to reduce with decreasing size, as their valence electrons become confined within smaller domains and their HOMO-LUMO gaps become larger [27,28]. Consequently, vacancies become scarcer as oxide domains become less reducible with decreasing size, causing NO oxidation turnover rates to decrease with decreasing size because vacancies are required for kinetically-relevant elementary steps in NO oxidation catalytic sequences.

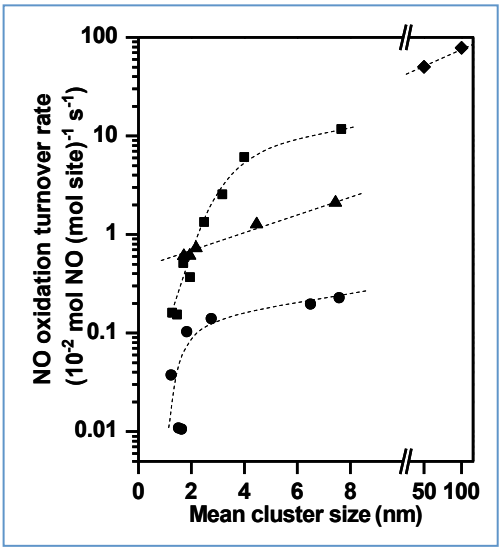

Figure 5. NO oxidation rates on (▲) RhO_2/Al_2O_3, (◆) Co_3O_4/Al_2O_3, (■) Pt/Al_2O_3 [12], and (●) PdO/Al_2O_3 [13] at 603 K, 5 kPa O_2, 120 Pa NO, 56 Pa NO_2.

NO oxidation turnover rates on large Co_3O_4 clusters (40-100 nm) were much higher than rates on all other catalysts examined (Fig. 5). NO oxidation rates on RhO2 were higher than those on PdO and similar in magnitude to those on Pt clusters similar in size (Fig. 4). The NO oxidation rate constant on each catalyst depends on the rate constant for O_2 activation (k_1) and the O* binding energy (via K_3 or K_O) (Eq. 6 or 11). O* binding energies account for these cluster size effects observed in NO oxidation (Fig. 5); as a result, they must also account for the trends in NO oxidation rates among these different catalytic elements.

Indeed, Pd(111) binds O* more strongly than Pt(111) by ~30 kJ mol-1 [29]. This difference in O* binding energies apparently persists on working catalysts (PdO and Pt surfaces saturated with O*), consistent with the lower NO oxidation rates on PdO catalysts (Fig. 5). In their metallic states, Rh(111) and Co(111), however, bind O* much more strongly than Pt(111) or Pd(111) by 100-200 kJ mol-1 [30]. Yet, NO oxidation turnover rates on Rh and Co oxides are much higher than on Pt or Pd and than expected from these high O* binding energies on Rh and Co metal (Fig. 5).

Clearly, O* binding energies on Rh and Co metal surfaces are not accurate descriptors of reactivity, because they are not inherently relevant to the stability and concentration of vacancies on catalysts that exist as oxides during NO oxidation catalysis.

Vacancy formation on clusters nearly saturated with oxygen occurs via the formal reduction of cations bound to chemisorbed or lattice oxygen atoms. The thermodynamics of such events should parallel those of electrochemical redox cycles. The standard reduction potential for Co^{3+}/Co^{2+} cycles (1.8 V) is significantly larger than for Pt^{2+}/Pt^{0} cycles (1.3 V), which is larger, in turn, than for Pd^{2+}/Pd^{0} cycles (0.9 V) [17] (Fig. 6). These reduction potentials indicate that Co^{3+} reduction to Co^{2+} is more facile than reduction of either Pt^{2+} or Pd^{2+} to the corresponding zero-valent state. For these systems, NO oxidation turnover rates and electrochemical reduction potentials appear to share common features that cause the correlation evident from the data in Fig. 6 for Co_3O_4, Pt, and PdO. The correlation in Fig. 6 suggest that the thermodynamics of electrochemical redox cycles parallels those relevant for vacancy formation on catalyst surfaces, which affect, in turn, O_2 adsorption rates for any given oxygen chemical potential during NO oxidation. The wide range of reduction potentials reported for Rh^{4+}/Rh^{3+} reduction cycles (0.8-1.7 V, for different coordinating ligands [25,26]) make any attempts at relating it to NO oxidation reactivity less precise than for the other metal systems. NO oxidation rate data suggest that the reduction tendency (and vacancy density) of RhO_2 clusters lies between that for Pt and PdO and is much greater than indicated by the reduction potential for Rh^{3+}/Rh^{0} cycles (Fig. 6).

The correlation between NO oxidation rates and redox potentials (Fig. 6) suggests that high NO oxidation turnover rates on RhO_2 and Co_3O_4 reflect the ability of Rh^{4+} and Co^{3+} to undergo one-electron reductions, which are more facile than reductions requiring the transfer of two electrons from a single cationic center. Such facile one-electron transitions in RhO_2 and Co_3O_4 lead to higher vacancy concentrations on these substrates than expected from the redox potentials for Rh^{3+}/Rh^{0} and Co^{2+}/Co^{0} transitions (Fig. 6) and from the strong binding of O* on Rh and Co metal. Moreover, the higher rates of $^{16}O_2$-$^{18}O_2$ exchange on RhO_2 and Co_3O_4 than NO oxidation appear to also reflect the ability of these substrates to undergo one-electron redox cycles.

These effects of one-electron cycles on NO oxidation rates (Fig. 6) and the much higher rates for $^{16}O_2$-$^{18}O_2$ exchange than for NO oxidation on RhO_2 and Co_3O_4 (but not on Pt or PdO) (Fig. 4) indicate that O_2

dissociation to form O* atoms involves multiple Co^{3+} or Rh^{4+} centers, whereas $^{16}O_2$-$^{18}O_2$ exchange occurs on only one Co^{3+} or Rh^{4+} center.

We note that Co oxides have been reported to exhibit high reactivity for electrochemical H_2O oxidation to O_2, a reaction that shares elementary steps with NO oxidation [31,32] in their common requirement for oxygen vacancies in their respective kineticallyrelevant steps. In H_2O oxidation, vacancies form via reduction of Co^{4+} to Co^{3+}, apparently by similar one-electron transitions that occur on Co^{3+} during NO oxidation.

These mechanistic connections between electrochemical reduction thermodynamics and NO oxidation turnover rates (Fig. 6) indicate a fundamental resemblance between electron transfer processes in solvated coordination complexes and inorganic oxides. For both, reduction tendencies reflect the energy levels of the frontier orbitals that accept electrons, which are set by metal-ligand and electron-electron interactions. Theoretical estimates of such energies remain uncertain, because DFT methods do not accurately describe the critical electron-electron interactions that influence the thermodynamics of electron transfer processes in inorganic solid oxides [33]. The connections inferred here between the reduction tendencies of aqueous metal complexes and solid oxides (and their consequences for reduction-oxidation catalysis) provide significant impetus for parallel efforts in the development and use of more exact theoretical approaches to describe the redox properties of solids, if so required by the use of coordination complexes as model systems more amenable to rigorous theoretical treatments to assess the accuracy of these theoretical methods.

Conclusion

The effects of NO, NO_2, and O_2 pressures on NO oxidation rates on RhO_2 and Co_3O_4 were consistent with a mechanism in which O_2 binding on oxygen atom vacancies is the kinetically-relevant step for NO oxidation, as also observed on Pt and PdO. Equilibrated reactions involving NO and NO2 establish vacancy concentrations and oxygen chemical potentials at catalyst surfaces. The oxygen chemical potentials prevalent during NO oxidation caused Rh and Co clusters to exist as RhO_2 and Co_3O_4 during catalysis. NO oxidation rates increased with increasing cluster size on RhO_2, as also observed for rates on Pt and PdO clusters because small oxide and metal clusters bind oxygen more strongly, resulting in lower concentrations of vacant sites that bind O_2 in kinetically-relevant steps. Both RhO_2 and Co_3O_4 have cations (Rh^{4+} and Co^{3+}) that reduce via one-electron redox cycles to form vacancies. This leads to $^{16}O_2$-$^{18}O_2$ exchange rates on RhO_2 and Co_3O_4 that are much larger than NO oxidation rates because exchange occurs by an O_2 activation pathway that requires only a one-electron transfer. NO oxidation, in contrast, requires that O_2 dissociates to oxygen atoms by two consecutive one-electron reductions of multiple Co^{3+} or Rh^{4+} centers in Co_3O_4 or RhO_2. NO oxidation rates on all catalysts correlated strongly

to the electrochemical redox potential when the one-electron transitions involving Co^{3+}/Co^{2+} and Rh^{4+}/Rh^{3+} were used to describe the reducibility of Co_3O_4 and RhO_2 catalysts. The presence of the one-electron pathways on Co_3O_4 and RhO_2 leads to NO oxidation rates that are higher than expected from the large O* binding energy on Rh and Co metal, causing both to be effective NO oxidation catalysts.

Experimental Section

Catalyst Synthesis and Characterization. γ-Al_2O_3 (Sasol, SBa-200, 180 m^2 g^{-1}) and SiO_2 (Davisil, Grade 646, 300 m^2 g^{-1}) supports were heated to 1023 K at 0.07 K s^{-1} in flowing dry air (Praxair, Extra Dry, 1 cm^3 s^{-1} g^{-1}) and held for 4 h. $Rh(NO_3)_3$•H_2O (Sigma Aldrich) or $Co(NO_3)_2$•$(H_2O)_6$ (Sigma-Aldrich) were added to de-ionized distilled water (Barnstead, Nanopure) and the solution was added dropwise to γ-Al_2O_3 or SiO_2 to the incipient wetness point (0.45 g solution (γ-Al_2O_3)-1, 0.9 g solution (g SiO_2)$^{-1}$) to prepare samples with 0.8% and 2.4% wt. Rh and 10% wt. Co. Impregnated supports were heated in ambient air at 393 K for 4 h and then in flowing dry air (Praxair, extra dry, 1 cm^3 s^{-1} g^{-1}) for 4 h by heating at 0.07 K s^{-1} to a temperature between 673-1148 K. Rh- or Co-containing samples were then heated to 873 K or 673 K, respectively, at 0.07 K s^{-1} and held in 9% H_2/He (Praxair, 99.999% purity, 1 cm^3 s^{-1} g^{-1}) for 5 h. Materials were treated with 0.5% O_2/He (Praxair, 99.999% purity, 1 cm^3 s^{-1} g^{-1}) at 295 K for 1 h before exposure to ambient air.

H_2 and O_2 uptakes were measured volumetrically (Autosorb-1; Quantachrome) to determine the number of Rh and Co atoms exposed at cluster surfaces (Rhs and Cos) and the number of reducible Co atoms (Cor). Samples (0.5-1.0 g) were heated to 673 K at 0.08 K s^{-1} and held at 673 K for 2 h in flowing H_2 (1 bar) and then evacuated for 1 h at 673 K before H_2 or O_2 uptake measurements at 313 K and 673 K, respectively, and 5-50 kPa titrant pressure. Uptake isotherms were extrapolated to zero pressure to exclude contributions from weakly-bound species. Mean cluster diameters were estimated from measured uptakes using the assumptions of one chemisorbed H atom per surface Rh or Co atom (denoted Rhs or Cos), 1.33 O atoms per reducible Cobalt atom, and hemispherical clusters with densities of bulk Rh or Co (12.4 g Rh cm^{-3}; 72 Rh nm^{-3}; 8.9 g Co cm^{-3}; 91 Co nm^{-3} [17]).

NO Oxidation Rate Measurements. NO oxidation rates were measured on 0.12-0.18 mm Rh/Al_2O_3 and Co/SiO_2 aggregates. Samples were held on a porous quartz frit within a tubular quartz reactor (10 mm). Reactants (15% O_2/He, 2% NO/He, 1% NO_2/He, and 5% CO_2/He) and He carrier (Praxair, 99.999% purity) were metered using electronic controllers (Porter Instruments) to achieve a broad range of reactant pressures (1-12 kPa O_2, 0.04-0.25 kPa NO, 0.02-0.25 kPa NO_2, 0-2 kPa CO_2). A resistively-heated furnace with a controller (Watlow, 96 series) and a K-type thermocouple were used to maintain constant temperatures (548-673 K). Inlet and outlet concentrations were measured using an infrared analyzer (MKS 2030; 2 cm^3 cell; 2 cm pathlength; 338 K). NO oxidation rates are reported as turnover

rates (TOR, mol NO converted (mol Rhs or Cos) - 1 s^{-1}) at NO conversions below 15%.

Isotopic Oxygen Exchange Measurements. $^{16}O_2$-$^{18}O_2$ exchange rates were measured using a gradientless batch reactor (498 cm^3 volume), in which reactants were circulated by a graphite gear pump (Micropump; 2 cm^3 s^{-1}). Gases (99.999% chemical purity) were obtained from Praxair (90% O_2/Ar, He) and Ikon Isotopes ($^{18}O_2$, 96% isotopic 18O purity). Catalysts were heated to 573-653 K at 0.07 K s^{-1} and held for 1 h in flowing 2 kPa $^{16}O_2$/Ar/He (30 cm^3 s^{-1} g^{-1}) before the reactor was evacuated and filled with an equimolar $^{16}O_2$-$^{18}O_2$ mixture and He as balance. Isotopomer concentrations were measured by pulses injected periodically into a mass spectrometer (MKS Mini-Lab).

Acknowledgements

We thank financial support from The Ford Motor Company, General Motors, the Chevron Corporation; and the Chemical Sciences, Geosciences, Biosciences Division, Office of Basic Energy Sciences, Office of Science US Department of Energy (grant number: DE-FG02-03ER15479).

Reference

[1] A. Amirnazmi, M. Boudart, J. Catal. 1973, 30, 55.

[2] A. Amirnazmi, M. Boudart, J. Catal. 1975, 39, 383.

[3] N. Takahashi, H. Shinjoh, T. Iijima, T. Suzuki, K. Yamazaki, K. Yokota, H. Suzuki, N. Miyoshi, S. Matsumoto, T. Tanizawa, T. Tanaka, S. Tateishi, K. Kasahara, Catal. Today 1996, 27, 63.

[4] N. W. Cant, M. J. Patterson, Catal. Today 2002, 73, 271.

[5] S. Roy, A. Baiker, Chem. Rev. 2009, 109, 4054.

[6] A. Kato, S. Matsuda, T. Kamo, F. Nakajima, H. Kuroda, T. Narita, J. Phys. Chem. 1981, 85, 4099.

[7] M. Koebel, M. Elsener, G. Madia, Ind. Eng. Chem. Res. 2001, 40, 52.

[8] B. R. Stanmore, J. F. Brilhac, P. Gilot, Carbon 2001, 39, 2247.

[9] F. Jacquot, V. Logie, J. F. Brilhac, P. Gilot, Carbon 2002, 40, 335.

[10] S. S. Mulla, N. Chen, L. Cumaranatunge, G. E. Blau, D. Y. Zemlyanov, W. N. Delgass, W. S. Epling, F. H. Ribeiro, J. Catal. 2006, 241, 389.

[11] S. S. Mulla, N. Chen, W. N. Delgass, W. S. Epling, F. H. Ribeiro, Catal. Lett. 2005, 100, 267.

[12] B. M. Weiss, E. Iglesia, J. Phys. Chem. C 2009, 113, 13331.

[13] B. M. Weiss, E. Iglesia, J. Catal. 2010, 272, 74.

[14] A. Amberntsson, E. Fridell, M. Skoglundh, Appl. Catal. B-Environ. 2003, 46, 429.

[15] M. M. Yung, E. M. Holmgreen, U. S. Ozkan, J. Catal. 2007, 246, 356.

[16] D. S. Kim, Y. H. Kim, J. E. Yie, E. D. Park, Korean J. Chem. Eng. 2010, 27, 49.

[17] W. M. Haynes, CRC Press/Taylor and Francis, Boca Raton, FL, 2011.

[18] W. L. Holstein, M. Boudart, J. Phys. Chem. B 1997, 101, 9991.

[19] O. Muller, R. Roy, J. Less-Common Metals 1968, 16, 129.

[20] K. T. Jacob, D. Prusty, J. Alloys Compd. 2010, 507, L17.

[21] K. Bakhmutsky, N. L. Wieder, T. Baldassare, M. A. Smith, R. J. Gorte, Appl. Catal. A 2011, 397, 266.

[22] S. L. Soled, E. Iglesia, R. A. Fiato, J. E. Baumgartner, H. Vroman, Topic. Catal. 2003, 26, 101.

[23] G. Boreskov, Adv. Catal. 1964, 15, 285.

[24] E. R. S. Winter, J. Chem. Soc. A 1968, 2889.

[25] E. R. S. Winter, Adv. Catal. 1958, 10, 196.

[26] C. Guharoy, R. J. Butcher, S. Bhattacharya, J. Organomet. Chem. 2008, 693, 3923.

[27] M. Maestri, D. Sandrini, V. Balzani, U. Maeder, A. Von Zelewsky, Inorg. Chem. 1987, 26, 1323.

[28] L. Brus, J. Chem. Phys. 1984, 80, 4403.

[29] Y. Wang, N. Herron, J. Phys. Chem. 1991, 95, 525.

[30] R. A. van Santen, M. N. Neurock, Molecular Heterogeneous Catalysis: A Conceptual and Computational Approach, John Wiley & Sons, Hoboken, NJ, 2006.

[31] J. B. Gerken, J. G. McAlpin, J. Y. C. Chen, M. L. Rigsby, W. H. Casey, R. D. Britt, S. S. Stahl, J. Am. Chem. Soc. 2011, 133, 14431.

[32] Y. Surendranath, M. W. Kanan, D. G. Nocera, J. Am. Chem. Soc. 2010, 132, 16501.

[33] A. T. Bell, M. Head-Gordon, Ann. Rev. Chem. Biomolec. Eng. 2011, 2, 453